HYDRATE PHASE EQUILIBRIUM STUDIES FOR Xe, Ar, Kr, AND CF_4 IN THE PRESENCE OF TBAB AQUEOUS SOLUTIONS

By

Saeideh Babaee

MSc (Chemical Engineering), Shiraz University of Technology, Iran

This thesis is submitted in fulfilment of the academic requirements for the degree of Doctor of Philosophy (PhD) in Chemical Engineering at the School of Engineering, University of KwaZulu-Natal.

Supervisor: Prof. Deresh Ramjugernath

Co-Supervisors: Prof. Amir H. Mohammadi, and Prof. Paramespri Naidoo

September 2015

DECLARATION 1 – PLAGIARISM

I, Saeideh Babaee, declare that:

(i) The research reported in this thesis, except where otherwise indicated, is my original work.

(ii) This thesis has not been submitted for any degree or examination at any other university.

(iii) This thesis does not contain other persons' data, pictures, graphs or other information, unless specifically acknowledged as being sourced from other persons.

(iv) This thesis does not contain other persons' writing, unless specifically acknowledged as being sourced from other researchers. Where other written sources have been quoted, then: a) their words have been re-written but the general information attributed to them has been referenced; b) where their exact words have been used, their writing has been placed inside quotation marks, and referenced.

(v) Where I have reproduced a publication of which I am an author, co-author or editor, I have indicated in detail which part of the publication was actually written by myself alone and have fully referenced such publications.

(vi) This thesis does not contain text, graphics or tables copied and pasted from the internet, unless specifically acknowledged, and the source being detailed in the thesis and in the References sections.

Saeideh Babaee Date

_____ _____

As the candidate's supervisor I agree/do not agree to the submission of this thesis.

Prof. Deresh Ramjugernath Date

_____ _____

Prof. Amir H. Mohammadi Date

_____ _____

Prof. Paramespri Naidoo Date

_____ _____

DECLARATION 2 - PUBLICATIONS

DETAILS OF CONTRIBUTION TO PUBLICATIONS that form part and/or include research presented in this thesis (include publications in preparation, submitted, *in press* and published and give details of the contributions of each author to the experimental work and writing of each publication)

Publication 1: Journal of Chemical Thermodynamics 81 (2015) 52–59.
Journal Title: Kinetic and thermodynamic behaviour of CF_4 clathrate hydrates.
Authors: S. Babaee, H. Hashemi, A. H. Mohammadi, P. Naidoo, D. Ramjugernath

Publication 2: Journal of Chemical and Engineering Data 2014, *59* (11), 3900–3906.
Journal Title: Experimental Measurement and Thermodynamic Modeling of Hydrate Dissociation Conditions for the Argon + TBAB + Water System.

Authors: S. Babaee, H. Hashemi, A. H. Mohammadi, P. Naidoo, D. Ramjugernath

Publication 3: Journal of Chemical Engineering Data 2015, 60 (5), 1324–1330.

Journal Title: Experimental Measurements and Thermodynamic Modeling of Hydrate Dissociation Conditions for the Xenon + TBAB + Water System.
Authors: S. Babaee, H. Hashemi, A. H. Mohammadi, P. Naidoo, D. Ramjugernath

Publication 4: The Journal of Supercritical Fluids 2016, 107, 676–681.

Journal Title: Experimental Measurements and Thermodynamic Modelling of Hydrate Dissociation Conditions for the Krypton + TBAB + Water System.

Authors: S. Babaee, H. Hashemi, A. H. Mohammadi, P. Naidoo, D. Ramjugernath

Publication 5: Journal of Chemical Engineering (*Manuscript in preparation*).

Journal Title: Hydrate Kinetic Behavior for the System of Argon and Aqueous Solution of TBAB + SDS

Authors: S. Babaee, H. Hashemi, A. H. Mohammadi, P. Naidoo, D. Ramjugernath

Publication 6: Journal of Chemical Thermodynamics (*Manuscript in preparation*).
Journal Title: Experimental Measurement and Thermodynamic Modelling of Hydrate Phase Equilibrium Condition for CF_4 + TBAB Aqueous Solution
Authors: S. Babaee, H. Hashemi, A. H. Mohammadi, P. Naidoo, D. Ramjugernath

Additional Journals

Publication 1: The Journal of Chemical Thermodynamics 2015, 90, 193-198.

Journal Title: Clathrate Hydrate Dissociation Conditions of Refrigerants R404A, R406A, R408A and R427A: Experimental Measurements and Thermodynamic Modeling.

Authors: H. Hashemi, S. Babaee, P. Naidoo, A.H. Mohammadi, and D. Ramjugernath

Publication 2: The Journal of Chemical Thermodynamics 2015, 80, 30-40.

Journal Title: Experimental measurements and thermodynamic modeling of refrigerant hydrates dissociation conditions

Authors: H. Hashemi, S. Babaee, P. Naidoo, A.H. Mohammadi, and D. Ramjugernath

Publication 3: The Journal of Chemical Thermodynamics 2015, 82, 47-52.

Journal Title: Experimental study and Modeling of the Kinetics of Refrigerant Hydrate Formation.

Authors: H. Hashemi, S. Babaee, P. Naidoo, A.H. Mohammadi, and D. Ramjugernath

Publication 4: Journal of Chemical and Engineering Data 2014, 59, 3907–3911.

Journal Title: Experimental Measurements and Thermodynamic Modeling of Clathrate Hydrate Dissociation Conditions for Refrigerants R116, R23, and Their Mixture R508B.

Authors: H. Hashemi, S. Babaee, P. Naidoo, A.H. Mohammadi, and D. Ramjugernath

Publication 5: Fluid Phase Equilibria 2015, 388, 182-187.

Journal Title: A Thermodynamic Consistency Test for Experimental Isobaric Data of Wax Solubility in Gaseous Systems.

Authors: J. Kondori, H. Hashemi, S.Babaee, P. Naidoo, A. H. Mohammadi, and D. Ramjugernath

Publication 6: Fluid Phase Equilibria 2013, 360, 161-168.

Journal Title: Gas hydrate phase equilibrium in porous media: An assessment test for experimental data.

Authors: P. Ilani-Kashkouli, H. Hashemi, F. Gharagheizi, S. Babaee, A. H. Mohammadi, and D.Ramjugernath

Publication 7: Fluid Phase Equilibria 2013, 360, 68-76.

Journal Title: An assessment test for phase equilibrium data of water soluble and insoluble clathrate hydrate formers.

Authors: P. Ilani-Kashkouli, S. Babaee, F. Gharagheizi, H. Hashemi, A. H. Mohammadi, and D. Ramjugernath

Publication 8: Journal of Chemical Engineering Data 2014, 59 (9), 2914–2919.

Journal Title: Phase Equilibria of Clathrate Hydrates of Ethyne + Propane.

Authors: K. Tumba, S. Babaee, P. Naidoo, A. H. Mohammadi, and D. Ramjugernath

Publication 9: Fluid Phase Equilibria 2013, 349, 71-82.

Journal Title: Assessment of Clathrate Hydrate Phase Equilibrium Data for CO_2 + CH_4/N_2 + Water System.

Authors: A. Eslamimanesh, S. Babaee, F. Gharagheizi, J. Javanmardi, A. H. Mohammadi, and D. Richon

Publication 10: Journal of Chemical Engineering Data, (to be submitted)

Journal Title: Kinetics of the hydrate formation of Acethyene, Ethyne, Propene, propylene, ethane, ethylene.

Authors: H. Hashemi, S. Babaee, P. Naidoo, A.H. Mohammadi, and D. Ramjugernath

Publication 11: The Journal of Chemical Thermodynamics, (to be submitted).

Journal Title: Application of clathrate hydrate in energy systems: A review**.**

Authors: H. Hashemi, S. Babaee, P. Naidoo, A.H. Mohammadi, and D. Ramjugernath

Publication 12: The Journal of Chemical Thermodynamics, (to be submitted)

Journal Title: Kinetics of the hydrate formation of the refrigerants R404A, R406A, R408A and R427A.

Authors: H. Hashemi, S. Babaee, P. Naidoo, A.H. Mohammadi, and D. Ramjugernath

Publication 13: Fluid Phase Equilibria Journal 2016, 413, 99-109.

Title: Clathrate Hydrate Dissociation Conditions for Refrigerant + Sucrose Aqueous Solutions: Experimental Measurement and Thermodynamic Modelling.

Authors: A. Smith, S. Babaee, A. H. Mohammadi, P. Naidoo, D. Ramjugernath

Book chapters

Publication 1: Advances in Chemistry Research (Volume 25); 2015; Nova Science Publishers, Inc., NY, USA, Editors: James C. Taylor, pp.177-198.

Chapter Title: A Thermodynamic Consistency Test for Experimental Data of Salt Deposition in Saline Water.

Authors: S. Babaee, H. Hashemi, J. Kondori, A. H. Mohammadi, and D. Ramjugernath

Publication 2: Advances in Chemistry Research (Volume 24), 2014; Nova Science Publishers, Inc., NY, USA, Editors: James C. Taylor. pp.73-78.

Chapter Title: Evaluation of the Experimental data for Gas Solubility in Liquid Water in Equilibrium with the Gas Hydrates. **Authors:**P. Ilani-Kashkouli, S. Babaee, F. Gharagheizi, H. Hashemi, A. H. Mohammadi, and D. Ramjugernath

ACKNOWLEDGEMENTS

All praises and thanks to **God**, the most gracious the most merciful, for all his apparent and unapparent graces and helps.

I would like to express my deepest gratitude to **my parents,** Mr. Azad Babaee and Mrs. Shirin Ghayour, for their continuous and unconditional support, patience, love and dedication. It was really impossible to go for this whole PhD study without their support.

I would like to express my sincere gratitude to my supervisors: **Prof. Deresh Ramjugernath, Prof. Amir H. Mohammadi and Prof. Paramespri Naidoo** for their non-stop support of my research, for their patience, inspiration, enthusiasm, and broad knowledge. It was truly an honour and a great experience to work with such talented, skilled experimentalists.

I want to express my wholehearted appreciation to my husband, **Mr. Hamed Hashemi**, for his love and his care in my life and in my PhD study. He was always around encouraging and supporting me during all difficult moments.

I would like to express my deepest gratitude to **Prof. Giancarlo Contrafatto** and **Mrs. Elaine Contrafatto** for their admirable support, patience, and providing me with a calm atmosphere to perform my study in South Africa.

I would like to express my sincere appreciation to **Mr Leon Augustyn, Dr. Wayne Nelson** and **Mr Ayanda Khanyile** for their valuable assistant and care in the chemical engineering laboratory, during my PhD study.

ABSTRACT

The separation of xenon from a mixture of xenon, krypton and argon is an important industrial problem. Cryogenic distillation, zeolite adsorbent, metal - organic framework (MOF) and membranes are the well-established methods for the separation of these gases. A large amount of energy is consumed for the gas separation using the cryogenic distillation method during the gas liquefaction. Zeolite adsorbents can select xenon over krypton at conditions close to room temperature. The capacity of MOFs is 20 percent of the total pore volume for the separation of Xe from a mixture of Xe, Kr and Ar. In a comparison of these methods, cryogenic distillation is a costly and energy intensive and other separation methods such as membranes and adsorbents have not been proven to be economical. Hence the purification of noble gas mixtures remains a challenge with researchers investigating alternate separation techniques. One of the newest methods for gas separation is the use of gas/clathrate hydrates. The basic idea is to take advantage of selective encapsulation of gas molecules inside a gas hydrate crystal at the specific conditions of temperature and pressure.

Gas hydrates or clathrate hydrates, are non-stoichiometric crystals of guest molecules with an appropriate molecular diameter recognised as hydrate formers which can be trapped inside the cavities of water molecules by hydrogen bonds at suitable temperature and pressure conditions. It is well established that gas hydrates can be utilized for separating mixtures of expensive gases consisting of Ar, Kr, Xe and CF_4 instead of using the conventional methods such as cryogenic distillations which is costly and quite energy intensive. Hence, accurate information of the hydrate formation/dissociation conditions of Ar, Kr, Xe and CF_4 hydrate formation is vital to develop such hydrate based procedures. The major problem in the implementation of gas hydrate technology for applications in gas separation is their conditions for dissociation, which occur at high pressures. One solution to this problem is the application of Quaternary Ammonium Salts or QAS semi-clathrate hydrates such as tetra-n-butyl ammonium bromide (TBAB) which can moderate the hydrate formation and dissociation conditions. The addition of the salt to the solution enables a shift in the *P-T* diagrams to lower pressures and higher temperatures.

The aim of this study was to measure the hydrate dissociation conditions in the system of Xe/Ar/Kr and CF_4 in the presence of aqueous TBAB solutions. For this purpose, the isochoric pressure search method was applied to measure the hydrate (H) - liquid (L) - vapour (V) phase equilibrium. For this purpose, the hydrate phase dissociation conditions for the systems of Ar + water + TBAB (0, 5, 10, 20, and 30 wt% TBAB), Kr + water + TBAB (0, 5,

10, and 20 wt% TBAB), Xe + water + TBAB (0, 10, 20, and 30 wt% TBAB) and CF_4 + water + TBAB (0, 5, 10, 20, and 30wt % TBAB) were measured.

The results indicate that TBAB has a significant promotion effect on the hydrate formation of Ar and Kr. In addition, with an increase in the TBAB concentration, a promotion effect of TBAB is observed. The hydrate dissociation measurements using a mass fraction of 0.1, 0.2 and 0.3 promotes the Xe hydrate dissociation conditions at pressures lower than 0.73 MPa, 1.40 MPa and 1.57 MPa, respectively. At the higher pressures the TBAB aqueous solution showed no effect on the Xe hydrate phase equilibrium. Results also show that TBAB aqueous solution with the mass fractions of 0.05, 0.1, and 0.2 has no promotion effect on the hydrate formation of CF_4. However, the aqueous TBAB solution with 0.30 mass fraction showed a significant promotion effect on the CF_4 hydrate formation.

Three thermodynamic models namely the fugacity approach, the Chen and Guo approach (1998) and a simple method based on fugacity approach and vapour pressure calculations were applied to estimate the hydrate equilibrium data for the system of Ar/Kr/Xe and CF_4 + water. The results show a good agreement between the experimental measurements and modelling calculations. Additionally, a thermodynamic model based on the models of Chen and Guo (1998) and Joshi et al. (2012) was developed to correlate the hydrate dissociation conditions for the systems of Xe + water + TBAB, Ar + water + TBAB, Kr + water + TBAB and CF_4 + water + TBAB. The Langmuir and Antoine constants for the Xe / Kr / Ar and CF_4 hydrate as well as the constants for water activity in the system of semi-clathrate hydrates of Xe / Ar / Ke and CF_4 + aqueous solutions of TBAB were optimized. The results indicate a reasonably good agreement between the experimental measurements and modelling calculations.

This study also presents an experimental kinetic study for CF_4 clathrate hydrates to investigate the effect of initial temperature and initial pressure on the rate of hydrate formation. The results display that an increase in the initial pressure at constant temperature decreases the induction time, while the CF_4 hydrate formation rate, water to hydrate conversion, the apparent rate constant of reaction and storage capacity increase. The similar behaviours are detected with a decrease in the initial temperature at constant pressure. A thermodynamic model based on van der Waals and Platteeuw (vdW-P) solid solution theory (van der Waals and Platteeuw, 1959) was used for the representation of hydrate dissociation conditions. The Langmuir constants for CF_4 based on the equation by Parrish and Prausnitz is also reported.

In this study, the effect of initial temperature, initial pressure, aqueous TBAB solution concentration, and sodium dodecyl benzene sulfonate (SDS) concentration on the kinetic of the semi-clathrate hydrate of Ar + aqueous TBAB solutions was also investigated. The results indicated that with an increase in the initial pressure at a constant temperature, the induction time decreases significantly. The same trends were detected with a decrease in the initial temperature at a constant pressure. In addition, with an increase in the TBAB concentration from 0.1 to 0.3 mass fraction TBAB, the rate of semi-clathrate hydrate nucleation increases and the induction time decreases, significantly. The results show the positive kinetic and thermodynamic effect of TBAB on Ar hydrate which makes TBAB as a reliable promoter to decrease the pressure of argon hydrate formation and increase the rate of argon hydrate formation. The results for the addition of SDS (in the concentration of 100, 200, 400 ppm) indicated that SDS increases the induction time of the semi-clathrate hydrate formation for the system of Ar + TBAB + water.

TABLE OF CONTENTS

LIST OF FIGURES

LIST OF TABLES

NOMENCLATURE

Symbol	Description	Units
a_w	Activity of water	--
A, B, C	Antoine constants	Pa, K, K (respectively)
a_{ij}	Cross parameters for the terms a_m	Pa. $(m^3/mol)^2$
a_m	EOS parameter for the mixture	Pa. $(m^3/mol)^2$
b_{ij}	Cross parameters for the terms b_m	m^3 / mol
b_m	EOS parameter for the mixture	m^3 / mol
C	Langmuir constant	Pa^{-1}
f	Fugacity	Pa
k_{app}	apparent rate constant	mol / (min. Pa)
k_{ij} *and* l_{ij}	Binary interaction parameters for NDD mixing rule	--
L_w	The liquid phase	--
L_H	Liquid phase containing mainly hydrocarbons	--
M	hydration number	--
N	Number of experimental data	--
n	Number of moles	mol
n_{w_0}	Initial number of moles of water in the liquid phase	mol
OF	Objective function	--
P	Pressure	Pa
r	Radial coordinate	m
R	Universal gas constant	m^3.Pa / (mol.K)
r (t)	Rate at time equal t	mol / min
s	Structure of gas hydrate	--
T	Temperature	K
t	Time	s
V_{H_t}	Volume of the hydrate at time = *t*	m^3
V_{cell}	Cell volume	m^3
V_{RW_t}	Volume of reacted water	m^3
V_{S_0}	Initial volume	m^3
v_i'	Number of cavities of type I per water molecule in a unit hydrate	--
v	Partial molar volume	m^3 / mol
x	Mole fraction in liquid phase	--
X, Y, Z	Langmuir parameters	Pa^{-1}, K, K (respectively)
y	Mole fraction in vapour phase	--
Z	Compressibility factor	--

Greek symbol

Symbol	Description	Units
Δ	Change in a property	--
μ	Chemical potential	J / mol
γ	Activity coefficient	--
λ_1	Number of linked cavities per water molecule and	--
λ_2	Number of gas hydrate former per water molecule	--
ϕ	Fugacity coefficient	--
$\Delta H_{sol.}$	Enthalpy of solution	J / mol
ΔC_{pw}	Specific heat capacity differences	J / (mol. K)
K_H^{θ}	Henry's constant at $T_0 = 298.15$	Pa
θ	Cage occupancy	--
α'	Number of linked cavities per number of gas molecules.	--
α	EOS temperature dependent parameter	--
ω	Acentric factor	--
$\omega(r)$	Spherically symmetric cell potential in the cavity	J / mol
v	Molar volume	m^3 / mol
ν_{ki}	Number of groups of kind *k* in molecule *i*	--
σ	Collision diameter	m
ε	Depth of energy well	J / mol

Superscripts

Symbol	Description
Exp	Experimental
Cal	Calculated
g	Gas phase
H	Hydrate phase
L	Liquid water phase
MT	Empty hydrate
sat	Saturation
v	Vapour phase
β	Empty hydrate phase
α	Ice phase
∞	Infinite dilution condition

Subscripts

Symbol	Description
Equib.	Equilibrium condition
I	Ice
i,j	Component
l	Large cavity
m	Cavity type *m*
s	Small cavity
w	Water

ABBREVIATIONS

Symbol	Description
AAD	Average Absolute Deviation
AE	Absolut Error
Ar	Argon
CB	Cyclobutane
CF	Cold finger
CF_4	Tetrafluoromethane
CH	Cyclohexane
CO	Cyclooctane
CP	Cyclopentane
CHP	Cycloheptane
DAS	Data acquisition system
EC	Equilibrium cell
EOS	Equation of state
GC	Gas chromatograph
GH	Gas hydrate
HBGS	Hydrate Base Gas Separation
H-L_w-V	Hydrate – liquid water –vapour
IT	Induction time
Kr	Krypton
LB	Liquid bath
LV	Loading valve
MCH	Methylcyclohexane
MCP	Methylcyclopentane
MJ	Mechanical jack
MR	Magnetic rod
MS	Mechanical stirrer
NDD	Non-Density-Dependent (NDD) mixing rules
PP	Platinum probe
PR	Peng-Robinson
PT	Pressure transducer
QAS	quaternary ammonium salts
QCM	Quartz Crystal Microbalance
QS	Quaternary salts

PCM	Phase change material
SC	Storage Capacity
SD	Stirring device
SDS	Sodium dodecyl sulfate
sI	structures I
sII	structures II
sH	structure H
STS	Sodium tetradecyl sulfate
STP	Standard temperature and pressure
TBAB	Tetra-n-butylammonium bromide
TBAC	Tetra-n-butylammonium chloride
TBAF	Tetra-n-butylammonium fluoride
TBPB	Tetra-n-phosphonium bromide
THF	Tetrahydrofuran
TR	Temperature controller
V	Valve
VLE	Vapour-liquid equilibrium
VPT EoS	Valderrama modification of Patel–Teja Equation of State
vdWP	van der Waals and Platteeuw
Xe	Xenon

1

CHAPTER ONE: INTRODUCTION

Noble or inert gases such as argon, krypton and xenon, have a diverse range of applications in industries such as gas laser, space exploration, welding, metallurgy, quartz lamps and fluoroscopic examinations of the brain. Krypton and xenon have high atomic weights which promote their use in the applications of multi-pane windows and light bulbs with longer suitable operating life (Vorotyntsev and Malyshev, 2011). Liquid xenon has been reported to be used in the detection of particles and astroparticle physics (Abe et al., 2009, Bernabei et al., 1998, Collaboration et al., 2008), and in the reduction of the γ and β rays emitted from uranium (U) and thorium (Th) pollutants by self-shielding. The short lived radioactive isotopes of liquid xenon can be used in rare phenomena experiments such as double beta decay searches and dark matter experiments (Abe et al., 2009).

The separation of xenon from a mixture of xenon, krypton and argon is an important industrial problem. Current technologies for separating these gases consist of cryogenic distillation (Abe et al., 2009), zeolite adsorbent (Alagappan, 2013), methal-organic framework (MOF) (Sikora et al., 2012, Liu et al., 2012) and membranes (Ohno et al., 1977). A mixture of xenon and krypton can be separated to a ratio of 80 / 20 (molar basis) of krypton to xenon via cryogenic distillation of air (Ryan and Hills, 2012). With using additional cryogenic distillation steps, greater purification of krypton and xenon would be achieved. Due to gas liquefaction in the cryogenic distillation process, a large amount of energy is consumed during the gas separation with this method. Separation of the noble gases can be performed using selective adsorbents such as zeolites at conditions close to room temperature (Alagappan, 2013). Zeolites are suitable for these applications because these adsorbents are selective of xenon over krypton.

Furthermore zeolites can eliminate the radioactive krypton 85 from the xenon rich phase. Methal-Organic Framework (MOF) is another method for the separation of noble gases mixtures (Sikora et al., 2012, Liu et al., 2012). MOFs can selectivity adsorb xenon from a mixture of xenon, krypton and argon. Due to the small pore volume of MOFs, such materials can acommodate one Xe atom per one pore. It is reported that the capacity of such materials is 20 percent of the total pore volume in achieving the separation of Xe from a mixture of noble gases (Ryan and Hills, 2012).

In a comparison of the separation methods mentioned above for the purification and separation of noble gases, cryogenic distillation is a costly and energy intensive process owing to the required low temperature for gas liquefaction and other separation methods such as membranes and adsorbents have not been proven to be economical (Hnatow M.A. and Happel, 1995). Hence the purification and separation of noble gas mixtures remains a challenge with researchers investigating alternate separation techniques. One of the newest methods for gas separation is the use of gas/clathrate hydrates which has captured the attentions of scientists in recent decades (Vorotyntsev and Malyshev, 2011). Since gas and water molecules can form gas hydrates at room temperature conditions, the gas hydrate method has lower cost in comparison to the cryogenic distillation which is based on gas liquefaction at very low temperatures. One of the other advantages of the gas/ clathrate hydrate method is its simplicity because gas hydrate can form and dissociate easily with cooling and heating of the system (Eslamimanesh et al., 2012b).

The major problems in the implementation of gas hydrate technology for applications in gas industries are their slow formation rate and the high pressure dissociation conditions (Ilani-Kashkouli et al., 2013). In gas hydrate formation processes, one of the usual ways to moderate the gas hydrate equilibrium conditions is using gas hydrate promoters such as Quaternary Ammonium Salts (QAS). QAS such as tetra-n-butyl ammonium bromide (TBAB) produce semi-clathrate hydrates and can moderate the hydrate formation and dissociation conditions. The addition of salt to the aqueous solution enables a shift in the *P-T* diagrams to lower pressures and higher temperatures conditions. The properties of the hydrate promoters as well as semi-clathrate hydrate structures will be discussed in later chapters.

Prior to the design of a hydrate based gas separation process it is essential to be aware of the dissociation conditions of the pure constituents of the considered mixture. Consequently, the main objective of this study is to provide the hydrate phase equilibrium of noble gases such as Xe, Ar and Kr. To study the effect of TBAB on the hydrate phase equilibrium, the experiments were performed in the presence of pure water and TBAB aqueous solution with

different concentrations. It has been proved that the highest stabilization effect of TBAB is at the stoichiometric concentrations of 0.40 mass fraction (Lee et al., 2010). For this purpose, in this dissertation, gas hydrate dissociation experimental data for the systems of argon / xenon/ krypton + aqueous TBAB solutions were measured below the stoichiometric TBAB concentration with a TBAB range of 0 to 0.30 mass fraction (0, 0.05, 0.10, 0.20 and 0.30 mass fraction).The other aim for the selection of this range of TBAB concentration was to develop a comprehensive thermodynamic model for the system of of argon / xenon/ krypton + aqueous TBAB solutions.

In addition to the work focused on noble gases, the separation of carbon tetrafluoride (CF_4) and nitrogen trifluoride (NF_3) is of considerable significance in the electronic industries. Nitrogen trifluoride (NF_3) is used in the electronics industries as a dry etchant through plasma assisted etching of silicon wafers, or through the plasma cleaning of chemical vapour deposition chambers (Branken et al., 2014). With the contamination of NF_3 with CF_4, it is crucial to remove CF_4 from NF_3. The high purity of NF_3 in electronic manufacturing industry desires in which the impurity content (CF_4 content in the mixture of NF_3 + CF_4) must not exceed 20 ppm. The chemical and physical properties of NF_3 and CF_4 are quite similar which makes it difficult to separate these gases (Branken et al., 2014). As the difference in boiling point of NF_3 (-129 ^{o}C) and CF_4 (-127.8 ^{o}C) is too small, the separation of these gases using cryogenic distillation needs a large number of theoretical trays which makes it financially not feasible (Branken et al., 2014). Another method for purification of NF_3 and removal of CF_4 is using zeolite adsorbents which selectively adsorbs NF_3 as the major component (because of the zeolite pore volume). As mentioned earlier, adsorbents can adsorb approximately 20% of their pore volumes. As a result, for the adsorption of the main component (NF_3) in the mixture of NF_3 and CF_4, a large amount of zeolite is needed (Branken et al., 2014). According to Branken et al., (Branken et al., 2014) amorphous glassy perfluoro polymer Teflon AF and Hyflon AD60 membranes are suitable adsorbents for separation of NF_3 and CF_4 in which the CF_4 content would be near 11 ppm. The gas hydrate method is an alternative technique/technology which can be applied for the separation of NF_3 and CF_4. Prior to the design of a hydrate based gas separation process, it is essential to be aware of the exact information of the CF_4 hydrate formation/ decompositions temperature and pressure and the kinetics of CF_4 hydrate formation. For this purpose in this study, the experimental measurements on the phase equilibria of CF_4 hydrate in the presence of pure water and aqueous solution of TBAB were performed. Furthermore, the effect of initial temperature and initial pressure on the rate of CF_4 hydrate formation was studied.

In this thesis, the gas hydrate concept is introduced in chapter 2 which includes a history of research performed to date on gas hydrates. In addition, the molecular structures of gas hydrates, the application of gas hydrates in industries, gas hydrate promoters and the structure and properties of semi- clathrate hydrate are explained.

In chapter three, the theory of the thermodynamic methods for modelling of the gas hydrate and semi- clathrate hydrate dissociation conditions is discussed. In addition, a kinetic model to investigate the gas hydrate rates and the related parameter such as the apparent rate constant of reaction, converting water into hydrate, gas consuming and storage capacity are presented.

In chapter four, the experimental method for measuring gas hydrate dissociation conditions consisting of the visual isobaric temperature search method, visual isothermal pressure search and isochoric pressure search method is explained.

In chapter five, the experimental setup and procedure developed in this study which was based on the isochoric pressure search method is explained. In addition the calibration results and the vapour pressure measurements for testing the reliability of the used experimental method is presented.

The experimental and model results are reported in chapter six and are categorised in three sections:

1. Experimental measurements of hydrate dissociation conditions for the system of Ar + water + TBAB (0 to 30 wt %), Xe + water + TBAB (0 to 30 wt %), Kr + water + TBAB (0 to 20 wt %) and CF_4 + water + TBAB (0 to 30 wt %).
2. Representation of a thermodynamic model of the hydrate phase equilibria for the system of Ar + water + TBAB (0 to 30 wt %), Xe + water + TBAB (0 to 30 wt %), Kr + water + TBAB (0 to 20 wt %) and CF_4 + water + TBAB (0 to 30 wt %).
3. Kinetic behaviour of CF_4 hydrate and the semi-clathrate hydrate for the system of Ar + TBAB + water.

The results obtained in this study showed that TBAB aqueous solutions with 0.05 to 0.30 mass fractions has a drastic promotion effect on the argon and krypton hydrate and shift the three

phase equilibrium curve to higher temperatures and lower pressures conditions. The results show that the effect of TBAB on the xenon hydrate is influenced by the pressure conditions. So that, a 0.1 mass fraction of TBAB aqueous solution has a promoting effect on the xenon hydrate dissociation conditions at pressures lower than 0.73 MPa. In addition, 0.2 and 0.3 mass fraction of TBAB has a promoting effect on the xenon hydrate at pressures lower than 1.4 MPa and 1.57 MPa, respectively. The results for the effect of TBAB aqueous solution on the CF_4 hydrate showed that 0 to 0.20 mass fraction of TBAB aqueous solution has no promotion effect on the CF_4 hydrate. However, the aqueous TBAB solution with 0.30 mass fraction showed a significant promotion effect on the CF_4 hydrate formation.

A good agreement between the experimental measurements in this study and those reported in the literature as well as the model results for all investigated systems were observed. In the kinetic study, the effects of initial pressure and initial temperature on the kinetics of CF_4 hydrate formation were investigated. The results demonstrated that the induction time of hydrate formation decreases with an increase in the initial pressure. However, other kinetics parameters such as the rate of CF_4 hydrate formation, the apparent rate constant, storage capacity, and ratio of water to hydrate conversion increase. The decrease in the initial temperature shows a similar behaviour on the kinetics of CF_4 hydrate formation. The results obtained in this study reveals the promoting effect of aqueous TBAB solution on the aforementioned gas hydrates as well as a kinetic study on the CF_4 hydrate formation which will be helpful in the application of the gas hydrate in the separation.

The effect of the initial temperature, initial pressure, concentration of aqueous TBAB solution, and concentration of SDS on the kinetics of the semi-clathrate hydrate of Ar + aqueous TBAB solutions was determined experimentally in chapter six. A kinetic model based on the work of Tajima et al. (2010) was used to calculate the rate of hydrate formation and the number of gas consumed during the hydrate formation (Tajima et al., 2010). The results indicate that with an increase in the initial pressure, the induction time decreases significantly however the kinetic constant and moles of Ar consumed during the semi-clathrate hydrate formation increases. The same trends were detected with a decrease in the initial temperature. In addition, with an increase in the TBAB concentration from 0.1 to 0.3 mass fraction TBAB, the rate of semi-clathrate hydrate formation and consumption of Ar during the hydrate formation increases however the induction time decreases, significantly. The results show the positive kinetic and thermodynamic effect of TBAB on Ar hydrate which makes TBAB as a reliable promoter to decrease the pressure of argon hydrate formation and increase the rate of argon hydrate formation. The results for the addition of SDS (in the concentration of 100, 200,

400 ppm) indicated that SDS increases the induction time of the semi-clathrate hydrate formation for the system of Ar + TBAB + water.

2

CHAPTER TWO: GAS HYDRATES

Gas hydrates or clathrate hydrates, are known as non-stoichiometric crystals of water and guest molecules with an appropriate molecular diameter recognised as hydrate formers. In these structures, guest molecules can be trapped inside the cavities of water molecules which are formed by hydrogen bonds at suitable temperature and pressure conditions. The favourable conditions for the formation of gas/clathrate hydrates are high pressures and low temperatures (Sloan and Koh, 2008). Different well-known structures of clathrate hydrates include structures I (sI), structures II (sII), and structure H (sH). Typical hydrate formers include methane, ethane, propane, and carbon dioxide. It has been discovered lately that the use of heavy hydrocarbons with a help gas (a small sized gas like hydrogen and nitrogen) can form gas hydrates of structure H (Sloan and Koh, 2008).

The appearance of ice and clathrate hydrates are hardly distinguishable. Nevertheless, at the microscopic level, the structure of ice and clathrate hydrates are different from each other. Ice has a normal hexagonal structure while nonstoichiometric clathrate hydrates are compounds with complicated structures. These microscopic differences lead to differences in the behaviour and properties of ice and clathrate hydrates. Previously, in order to identify clathrate hydrate from ice, polarized light was used. Unlike clathrate hydrates which do not have any effect on the polarized light, the effect of ice is clear (Sloan and Koh, 2008).

2.1. Historical background

Sir Humphery Davy in 1810 observed that dissolved chlorine gas in cold water at a temperature of 9° C formed a solid ice-like structure; this led to the discovery of chlorine hydrates (Sloan

and Koh, 2008). In 1832, Faraday gave the first chemical formula for gas hydrates in which one gas molecule can be surrounded by ten water molecules. From 1810 to 1934 several attempts were made to identify the nature of gas hydrates and some studies on the bromine hydrate and hydrates of inorganic compounds containing sulfur, chlorine, phospor and carbon dioxide were performed (Sloan and Koh, 2008). de La Rive discovered sulphur dioxide hydrates in 1829. Then Wroblewski in 1888 discovered carbon dioxide hydrates. Villard (Villard, 1888) in 1888 discovered gas hydrates of methane (CH_4), ethane (C_2H_6) and propane (C_3H_8). He reported that in a unit hydrate structure, one guest molecule can be surrounded by six water molecules. However, it is well established now that there are many exceptions for the theory of Villard about the ratio of gas to water in a hydrate structure. He then discovered argon hydrate in 1896. de Forcrand et al (de Forcrand, 1902) measured the hydrate dissociation conditions for fifteen hydrate formers at atmospheric pressure (Sloan and Koh, 2008). The results obtained by the researchers from the discovery of gas hydrate in 1810 to 1930 revealed that three conditions are necessary for the gas hydrate formation which consist of the presence of water, the existence of a gas molecule with small size like methane (CH_4), ethane (C_2H_6), propane (C_3H_8), argon (Ar) and finally the apropriate conditions (high pressure and low temperature) (Sloan and Koh, 2008).

In 1934, the phenomenon of blockages of gas pipelines in America by solid particles of gas hydrate were reported by Hammerschmidt (Hammerschmidt, 1934). The researchers revealed serious economic and operational problems which was made by the formation of gas hydrates in the gas transportation organizations and blockage the pipelines in the petroleum industries (Sloan and Koh, 2008). Following this phenomenon different techniques were investigated to try to avoid the formation of gas hydrates in the gas and oil pipelines. The methods for prevention of gas hydrate formation in the gas and petroleum pipelines include: 1) injection of methanol and ethylene glycol in the gas pipelines as a suitable thermodynamic inhibitors, 2) dehydration of natural gas, and 3) to maintain the conditions in the gas pipelines far from the hydrate formation conditions (such as heating the pipeline and decreasing the operating pressures) (Sloan and Koh, 2008).

Clathrate hydrates also have many positive applications in industries such as gas storage and transportation, carbon dioxide capturing, gas separation, air-conditioning systems, desalination of water and concentration of dilute aqueous solutions (Eslamimanesh et al., 2012b, Mohammadi et al., 2012). The details of some applications will be discussed in this chapter.

2.2. Gas hydrates structures

Three well known gas-hydrate structures, namely: structure I (sI), structure II (sII), and structure H (sH) are recognized based on the capability of the water molecules to form the unstable lattice cavities as well as the size and properties of the guest molecules. Structure H is less common and is formed with a small molecule such as methane, hydrogen or nitrogen (as a help gas) and a larger hydrate former such as cyclohexane, cycloheptene, dimethylbutane, and methylcyclohexane (Sloan and Koh, 2008). Figure 2-1 shows a schematic diagram of the three types of gas hydrate structures (Sloan and Koh, 2008).

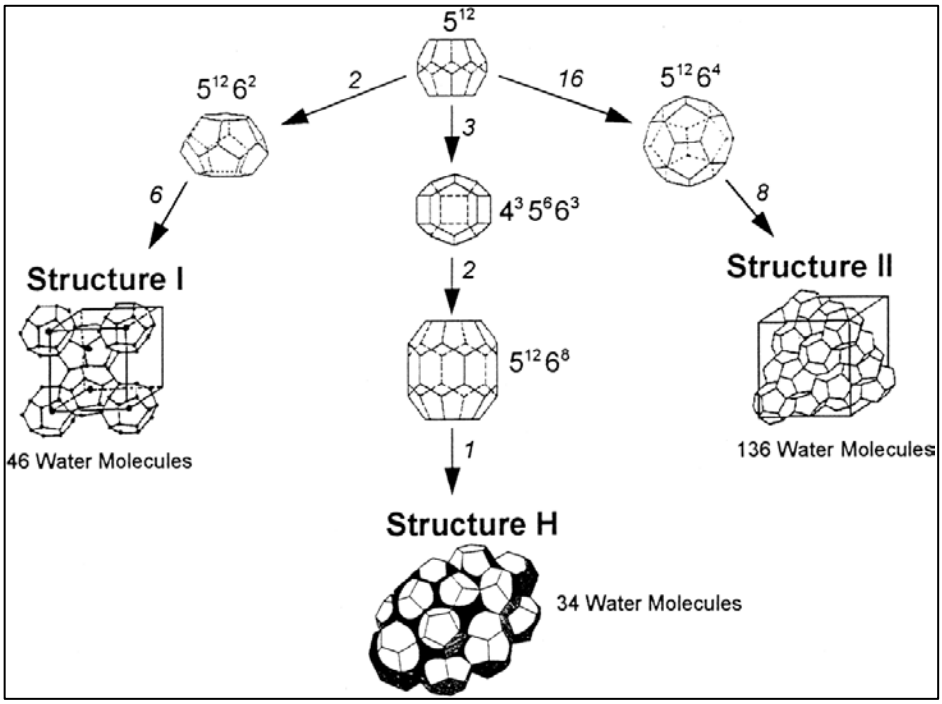

Figure 2-1. Typical gas hydrate structures with the cavity arrangements (Khokhar et al., 1998).

2.2.1. Structure I (sI)

The simplest hydrate structure is structure I, which is in a cubic shape with a side length of 1200 pm. Each unit cell of structure I contains 46 water molecules which are linked to each other by hydrogen bonding creating two small dodecahedron cavities and six large tetrakaidecahedron cavities (Sloan and Koh, 2008). As the size of dodecahedron cavities are less than the tetrakaidecahedron cavities, they are denoted as “small cavities”, while the

tetrakaidecahedron are considered as “large cavities”. Dodecahedron cavities are composed of a polyhedron with twelve pentagonal faces and are labelled as 5^{12} cavities. A diagram of a dodecahedron cavity is shown in Figure 2-2.

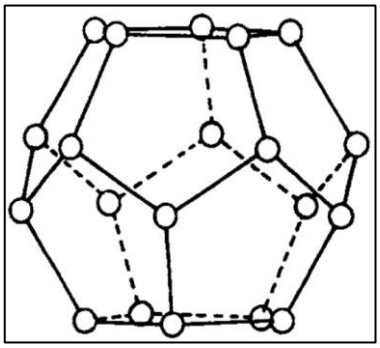

Figure 2-2. A schematic of the dodecahedron or 5^{12} cavity (a polyhedron with twelve pentagonal faces) (Sloan and Koh, 2008).

Due to the large tetrakaidecahedron cavities consisting of a polyhedron with fourteen-sided, twelve pentagonal faces (5^{12}) and two hexagonal faces (6^2), they are normally labelled as ($5^{12}6^2$) cavities (Sloan and Koh, 2008). A graphic of a tetrakaidecahedron cavity is presented in Figure 2-3.

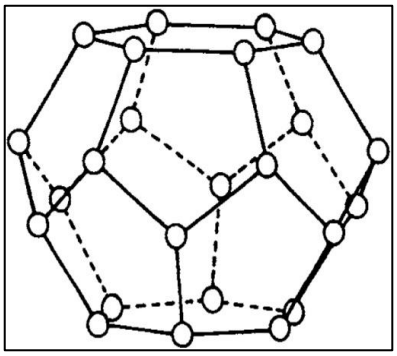

Figure 2-3. A schematic of the tetrakaidecahedron or $5^{12}6^2$ cavity (Sloan and Koh, 2008).

The structure I can be occupied by the guest molecules with a molecular diameter smaller than 6 angstrom such as methane, ethane, propane, carbon dioxide and hydrogen sulphide. The later gas molecules can indwell tetrakaidecahedron and dodecahedron cavities together but ethane molecule has the ability to fill only the tetrakaidecahedron cavities.

2.2.2. Structure II (sII)

A unit cell of structure II consists of 16 small cavities (dodecahedron or 5^{12} cavity) and 8 large cavities (hexakaidecahedron or $5^{12}6^4$ cavity which is a polyhedron consisting of twelve pentagonal faces (5^{12}) and four hexagonal faces (6^2)). Nitrogen, propane, isobutene and the natural gas are common guest molecules which have the ability to occupy structure II. Nitrogen and natural gas can occupy both small and large cavities, however, propane and isobutene fill the large cavities only (Sloan and Koh, 2008). A diagram of a hexakaidecahedron or $5^{12}6^4$ cavity is presented in Figure 2-4.

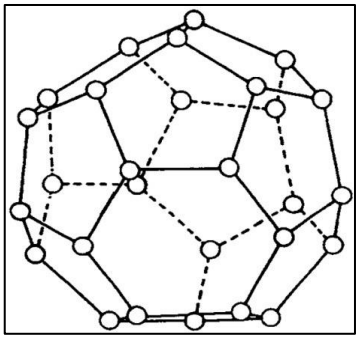

Figure 2-4. Hexakaidecahedron or $5^{12}6^4$ cavity (Sloan and Koh, 2008).

2.2.3. Structure H (sH)

Ripmeester et al. in 1990 revealed a new hexagonal structure named structure H which is much less common compared to structures I and II (Ripmeester and Ratcliffe, 1990). Structure H contains 34 water molecules which are connected by hydrogen bonds and creates three small (dodecahedral (5^{12})), two medium (irregular dodecahedral ($4^3 5^6 6^3$)) and one large (icosahedral ($5^{12}6^8$)) cavities. In structure H, small guest molecules such as methane occupy the small cavities as a help gas, however, large cavities are filled by heavy guest molecules such as 2-methylbutane, 2-2 dimethylbutane,, 2-3 dimethylbutane, 3-2-2 three-methylbutane, 2-2 dimethylpentane, 3-3 dimethylpentane, cyclohexane, methylpentane, cyclohexane, ethylpentane, methylcyclohexane, cyclohexane, heptane, cyclohexane, and octane (Sloan and Koh, 2008). Figure 2-5 presents the medium and large cavities for structure H. Table 2-1 reports the properties and characteristics of the different hydrate structures (Sloan and Koh, 2008).

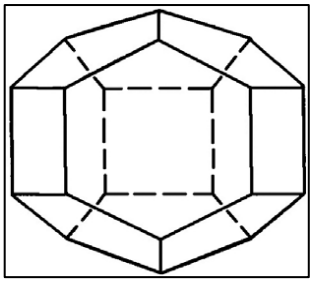
(a)

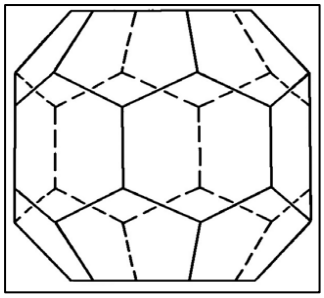
(b)

Figure 2-5. (a) Medium cavity ($4^3 5^6 6^3$) and (b) large cavity ($5^{12} 6^8$) for structure H (Sloan and Koh, 2008).

Table 2-1. Molecular characteristics of the different hydrate structures (Sloan and Koh, 2008).

Hydrate Structure	Structure (I)		Structure (II)		Structure (H)		
Cavity type	Small 5^{12}	Large $5^{12}6^2$	Small 5^{12}	Large $5^{12}6^4$	Small 5^{12}	Medium $4^3 5^6 6^3$	Large $5^{12}6^8$
Number of cavities per unit cell	2	6	16	8	3	2	1
Cavity diameter (A^o)	7.9	8.6	7.8	9.5	7.8	8.1	11.2
Coordination number	20	24	20	28	20	20	36
Cavity number per water molecule number	1/23	3/23	2/17	1/17	3/34	2/34	1/34
Water molecules for a unit cell	46		136		34		
Volume of unit cell (m^3)	1.728×10^{-27}		5.178×10^{-27}		---		
Crystal structure	Cubic		Cubic		Hexagonal		
Typical former	CH_4, C_2H_4, H_2S, CO_2		N_2, C_3H_8, i-C_4H_{10}		Methylcyclohexane, cyclopentane, etc.		

2.3. Cages occupancies

Only molecules with suitable size and shape can be occupied in the cavities of gas hydrates. Table 2-2 shows the components which form gas hydrates and the related structures.

Table 2-2. Guest molecules as well as their cage occupancies for natural gas hydrates (Sloan and Koh, 2008).

Gas component	Structure I		Structure II	
	Small cavity	Large cavity	Small cavity	Large cavity
Methane	+	+	+	+
Ethane	-	+	-	+
Propane	-	-	-	+
n- butane	-	-	-	+
i-butane	-	-	-	+
Carbon dioxide	+	+	+	+
Nitrogen	+	+	+	+

The ratios of the hydrate former molecular diameter to the cavity diameter are presented in Table 2-3. The sign "*a*" in this table is referred to as the normal cage occupancy by a gas hydrate former. As it can be seen in Table 2-3, methane can be occupied in the small and large cavities of structure I while propane occupies only the large cavities of structure II. If the ratio of guest molecule diameter per cell cavity diameter is less than 0.78 (such as He, Ne and H_2 in Table 2-3), the attraction forces between the water and guest molecules is too small which damages the network stability. As a result, these hydrate formers (He, Ne and H_2) can form gas hydrates only at high pressures. If the ratio of guest molecule diameter per cell cavity diameter is more than 1, the hydrate former does not fit inside the cell cavity and gas hydrate formation cannot be formed. As it can be observed in Table 2-3, methane can be trapped inside the small and large cavities of structure I and small cavities of structure II. Ethane gas can occupy the large cavities in structure I and structure II. Iso-butane and propane can occupy the large cavities of structure II. If the diameter of the guest molecule is less than 2.4 Å, structure II hydrates can be formed. Gaseous molecules with diameters between 2.4 and 6 Å such as methane, ethane, carbon dioxide and hydrogen sulfide, can form structure I. Large molecules such as propane, iso-butane with molecular diameters between 6 and 7 Å can form structure II. Larger molecules with molecular diameters between 7 and 9 Å, such as methyl cyclohexane and iso-pentane, can form structure H with a small molecule such as hydrogen, as a help gas (Sloan and Koh, 2008).

Table 2-3. The ratio of the molecular diameter to cavity diameter for gas hydrate formers (Sloan and Koh, 2008).

Hydrate former		The ratio of the molecular diameter of hydrate former to the cell diameter for each cavity			
Molecule	Diameter (°A)	Structure I		Structure II	
		Small cavity	Large cavity	Small cavity	Large cavity
He	2.28	0.447	0.389	0.454 [a, b]	0.342 [a, b]
H_2	2.72	0.533	0.464	0.542 [a, b]	0.408 [a, b]
Ne	2.97	0.582	0.507	0.592 [a, b]	0.446 [a, b]
N_2	4.10	0.804	0.700	0.817[a]	0.616[a]
H_2S	4.58	0.898[a]	0.782[a]	0.912	0.687
CO_2	4.58	1.00 [a]	0.834[a]	1.02	0.769
CH_4	4.36	0.855[a]	0.744 [a]	0.868	0.655
C_2H_6	5.50	1.08	0.939[a]	1.10	0.826
C_3H_8	6.28	1.23	1.07	1.25	0.943[a]
i-C_4H_{10}	6.50	1.27	1.11	1.29	0.976[a]
n-C_4H_{10}	7.10	1.39	1.21	1.41	1.07

[a] normal cavity occupancy by a gas hydrate former.

[b] Hydrate formation at the high pressures.

To identify the type of gas hydrate structure, some techniques such as H-NMR, Raman Spectrometry, C13-NMR and X-Ray Diffraction can be used. Figure 2-6 shows the size of the guest gas molecule and their cavities occupied at various hydrate structures. This result was obtained by Von Stackelberg in 1949 using X-Ray diffraction (Sloan and Koh, 2008). As can be seen in Figure 2-6, the small guest molecules with diameters less than 3.8 Å cannot be included in the hydrate structures. In addition, molecules with a diameter bigger than 7.5 Å cannot form structure I and II, however they are able to form structure H (Sloan and Koh, 2008).

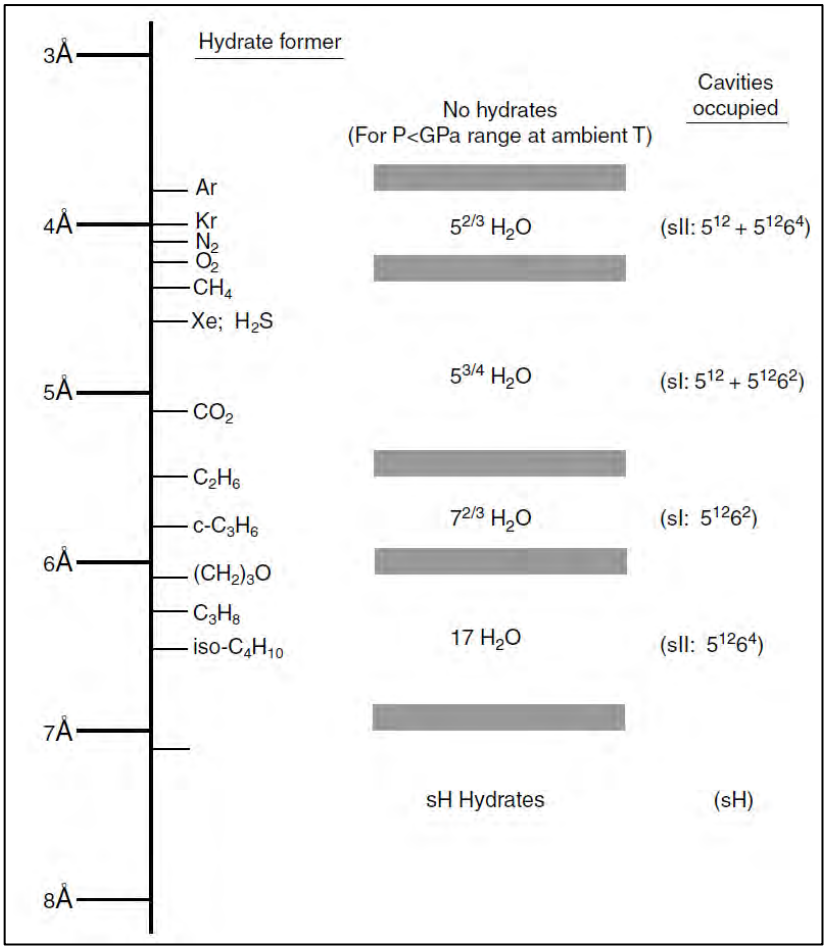

Figure 2-6. Comparison between the size of hydrate formers and cage occupancies in different structures (Sloan and Koh, 2008).

2.4. Gas hydrate applications

As mentioned previously, gas hydrates can form within petroleum pipelines and related facilities causing some serious economic problems. Alternatively, this phenomenon has many positive aspects which have recently attracted many researcher's attention. Gas hydrates can be used in several applications such as gas storage and transportation (Khokhar et al., 1998, Javanmardi et al., 2005, Pang et al., 2007), seawater desalination/treatment technology (Chatti et al., 2005), gas separation (Kamata et al., 2004, Kamata et al., 2005), carbon dioxide capture and sequestration (Kang and Lee, 2000, Herslund et al., 2012), cool storage systems (Martinez et al., 2008, Delahaye et al., 2008), concentration of dilute aqueous solutions and many new applications which have been published in recent decades (Eslamimanesh et al., 2012b, Chatti et al., 2005).

2.4.1. Future energy source

The existence of methane gas hydrate in sea-floor sediments and arctic permafrost may be considered as a new energy supply. Researchers found that the amount of gas in the gas hydrate reservoirs (in sea-floor sediments and arctic permafrost) is approximately twice the energy of the entire fossil fuel reserves (Kvenvolden, 1988, Makogon, 1998). According to estimations by Collett and Kuuskraa , the amount of gas supply in the permafrost areas and oceanic sediments are about 1.4 to 3.4 × 10^4 and 3.1 to 7.6 × 10^6 trillion cubic meters respectively (Collett and Kuuskraa, 1998). Thus, achieving a small percentage of this huge amount of gas source supply could provide for the gas energy of the world for many years.

The techniques that can be used for achieving this kind of energy supply consists of reducing pressure and increasing temperature of the gas hydrate reservoir (to dissociate the gas hydrate), and injection of carbon dioxide or methanol as an alternative to methane gas hydrate (Eslamimanesh et al., 2012b).

2.4.2. Gas storage and transportation

Gas hydrates have been proposed as a new method for the storage of gas molecules such as hydrogen, methane and carbon dioxide. The use of the gas hydrate method as a mean for natural gas storage and transportation was first determined by Benesh in 1942 (Benesh, 1942). The amount of methane which is kept in a cubic meter of methane hydrate under the standard conditions (at a temperature of 273.15 K and a pressure of 0.1 MPa) is about 172 cubic meters (Sloan and Koh, 2008). A low storage space and the safety of the hydrate natural gas (HNG) method are advantages of employing gas hydrate for storage and transportation compared to other methods such as liquid natural gas (LNG) (Byk and Fomina, 1968, Davidson, 1973). Due to high storage capacity of the HNG method at atmospheric pressure and not very low temperature, this method could be favourable in the industrial locations where the gas wells in that area are not available (Sloan and Koh, 2008).

2.4.3. Water desalination

One of the other possible applications of gas hydrates is their usage in desalination/treatment of water when a gas hydrate former (with low equilibrium pressure such as a refrigerant) and brine are mixed at appropriate conditions of temperature and pressure to form the gas hydrate. In this case, the hydrate former and pure water combine to form the gas hydrate structures while the

salts cannot be included in the hydrate structures. With increasing temperature, the gas hydrate dissociates and pure water produces while the released gas could be recycled in the gas hydrate formation unit (Eslamimanesh et al., 2012b, Chun et al., 2000, Seo and Lee, 2001, Javanmardi and Moshfeghian, 2003). Javanmardi and Moshfeghian in 2003 performed an economic study to estimate the costs of operational, maintenance and total capital investment in a gas hydrate formation unit to produce pure water from brine. This economical study revealed that the price for the production of 1 ton of pure water through the propane hydrate process is about 2.8 to 4.2 US$ which depends on the yield of procedure (the ratio of the number of moles of the produced pure water to the number of mole of seawater through a procedure) and temperature of the seawater (Javanmardi and Moshfeghian, 2003). The most important reason for the high price of the gas hydrate method is its high pressure conditions. Gas hydrate promoters such as THF and TBAB can decrease the pressure of hydrate formation. The results reveal that water desalination using the gas hydrate formation process in the absence of any hydrate promoters (such as THF and TBAB) may not be as economical compared with the traditional methods for water desalination (Eslamimanesh et al., 2012b).

2.4.4. Gas separation

Gases released from combustion of the fossil fuels such as coal, oil and natural gas have a significant contribution to global warming (Bacher, 2002, Hall et al., 2003, Chatti et al., 2005). Decreasing the emission amount of greenhouses gases such as carbon dioxide (CO_2), methane (CH_4), hydrogen, sulfide (H_2S) and sulfur hexafluoride (SF_6) into the atmosphere is a most important environmental challenge (Chatti et al., 2005, Eslamimanesh et al., 2012b).

Since, approximately sixty four percent of the released greenhouse gases are related to CO_2, many efforts have been made to remove this gas from the atmosphere (Bryant, 1997). To reduce the CO_2 emitted into the atmosphere, commonly employed methods include chemical absorption such as alkanolamines (MEA, DEA, TEA) (Peng and Zhuang, 2012, Belandria et al., 2012, Eslamimanesh et al., 2012b), pre-combustion or CO_2 removal before the fuel combustion (Peng and Zhuang, 2012, Belandria et al., 2012, Eslamimanesh et al., 2012b), CO_2 injection to the depth of oceans (Kojima et al., 2002, Chatti et al., 2005), fuel burning using pure oxygen instead of air (Peng and Zhuang, 2012), and finally replacing methane with carbon dioxide during the extraction of methane from the methane hydrate reservoirs (Komai et al., 2000).

Separation of other greenhouse gases from the atmosphere such as methane (which has a global warming effect of 21 times that of carbon dioxide), hydrogen sulphide, sulphur hexafluoride, and CFCs or chlorofluorocarbons such as R11, R12 are the major environmental challenge in the last few decades. Sulphur deposition during the sour gas productions in well bores and related facilities is a serious problem in the sour gases producing (Hyne, 1983, Mohammadi and Richon, 2008a, Eslamimanesh et al., 2011b). As the natural gas flows upwards from the bottom of the well to the tubing string near the wellbore, the temperature and pressure decrease and the solubility of sulphur in sour gas decreases rapidly which leads to sulphur precipitations. This deposition causes serious reduction in the permeability of the sour gas formation. Sulphur deposition can also occur through natural gas transporting pipelines and cause some economic problems (Hyne, 1983, Mohammadi and Richon, 2008a, Eslamimanesh et al., 2011b). The effect of sulphur decomposition on the natural gas transportation equipment as well as the most common places which is affected by sulphur precipitation is explained elsewhere (Pack, 2003).

Apart from the aforementioned methods for the separation of emitted greenhouse gases (CO_2, CH_4, H_2S, etc.) into the atmosphere, the gas hydrate crystallization method is considered as a new method for these separations. The hydrate method for gas separation is based on the difference between the affinities of gases to be trapped in the hydrate cavities. For instance, for the binary mixture of CO_2 and N_2, the attraction of CO_2 for gas hydrate formation is more than N_2 which leads to enrichment of the hydrate phase with CO_2 while the gas phase enriched with N_2 (the concentration of N_2 increases in the gas phase). Thereafter, by increasing the temperature or decreasing the pressure, the hydrate phase dissociates and the CO_2 concentration improves. For further purification of CO_2, more steps of hydrate formation / dissociation are needed (Eslamimanesh et al., 2012b).

The gas hydrate process was used by the US Department of Energy (DOE) for the separation of CO_2 from the other gases such as H_2 (Chatti et al., 2005). In this process, using the combination between a synthesis gas flow (consisting of CO_2, H_2 and other gases) and pre-cooled water in a reactor, CO_2 hydrate was formed. The output steams included a CO_2 hydrate slurry, while a H_2-rich product gas stream (containing other gases) were sent to a gas separator.

In other hydrate base gas separation (HBGS) processes, the gas hydrate crystallizes in the presence of gas hydrate promoters such as tetrahydrofuran (THF) and tetra-*n*-butylammonium bromide (TBAB) as in the separation of CO_2 from other gases (Kang and Lee, 2000). Results show that using HBGS processes, the equilibrium pressure of the gas hydrate is moderated in the presence of these promoters and about 99 mol% of CO_2 is recovered from the flue gas. Low

pressure conditions, moderate temperature conditions (273– 283 K) and continuous operations are the advantages of this method compared to applying the gas hydrate process in the presence of pure water (Chatti et al., 2005).

In order to effectively design a CO_2 separation approach using the gas hydrate method, reliable experimental hydrate dissociation data are required. For this purpose, there are a lot of experimental studies on the gas hydrate equilibrium conditions for the system (CO_2 + other gases (N_2/H_2/CH_4) + water) in the open literature (Ohgaki et al., 1996, Tajima et al., 2004, Sugahara et al., 2005, Bruusgaard et al., 2010).

2.4.4.1. The separation of noble gases

In spite of the advantage of the gas hydrate method for gas separation, extraction of noble gas mixtures such as Ar, Kr and Xe using the gas hydrate method as well as investigation of the equilibrium conditions of noble gas hydrates have scarcely been studied. Nikitin et al. (Nikitin, 1956) in Russia used the gas hydrate method for the separation of mixed noble gas with sulfur dioxide (SO_2). The separation was performed by the static method using multiple hydrate formation/ dissociation stages (up to 180) with a low output of the separated substances. In 1963, an apparatus was designed by Kinney and Kahre (Kinney and Kahre, 1963) for the separation of helium from natural gas using the gas hydrate method. Barrer and Ruzikha (Barrer and Ruzicka, 1962) applied the gas hydrate crystallization method for the separation of binary mixtures of chloroform with argon, krypton, oxygen, nitrogen, benzene, carbon tetrachloride, and obtained a high separation coefficient for these mixtures. Byk et al. in 1980 proposed that mixed gas hydrates crystallizing from gas mixtures differ in composition from the gas phase. With using this property of gas hydrates, separation and concentration of noble gases and other components in natural gas is possible (Byk et al., 1980).

Vorotyntsev and Malyshev (Vorotyntsev and Malyshev, 2011, Vorotyntsev and Malyshev, 1998) obtained the separation coefficients for argon, krypton and xenon with different initial feed compositions. According to their work, the separation coefficient for xenon is almost 65 times greater than the separation coefficient for krypton and 400 times greater than the separation coefficient for argon for a mixture of 30% each of argon, krypton, xenon with 10% sulfur dioxide. Their calculations were performed with and without booster gas and the results showed that the distribution coefficients are less dependent on the mixture's pressure than on the concentration of the booster gas. According to their calculations, even without the use of a booster gas, xenon can be extracted almost completely from the mixture using two stages of gas

hydrate crystallization. Gas hydrate crystallization also allowed them to extract xenon more efficiently (Vorotyntsev and Malyshev, 2011, Vorotyntsev and Malyshev, 1998). A schematic diagram of the separation of xenon from the mixture of Ar, Kr, Xe using gas hydrate method is presented in Figure 2-7.

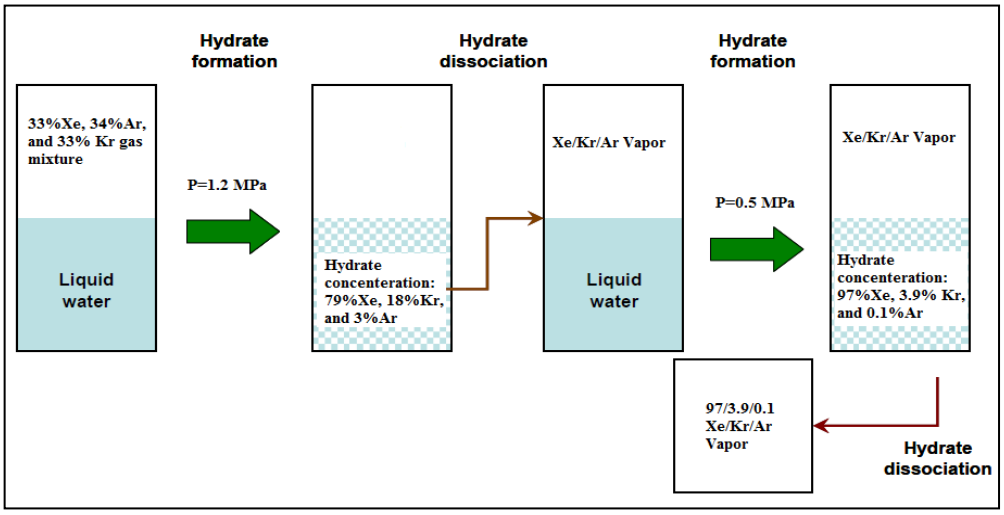

Figure 2-7. A schematic diagram of the xenon separation from the mixture of Ar, Kr, Xe using gas hydrate method (Vorotyntsev and Malyshev, 2011).

As seen in Figure 2-7, at the first step of gas hydrate formation, the concentration of xenon increases from 33 mol % to 79 mol % in the mixture of Xe + Kr + Ar over the first hydrate stage. This concentration improves to 97 mol % over the second hydrate step (Vorotyntsev and Malyshev, 2011, Vorotyntsev and Malyshev, 1998). A distillation system can remove Kr from Xe down to a concentration of 10^{-12} Kr/Xe (mol/mol) which means a complete purification of Xe from the mixture of Xe and Kr (Abe et al., 2009). It is expected that the gas separation using the hydrate method provides comparable degree of purification to that of distillation method using additional stages of hydrate formation and dissociation. To estimate the number of separation stages for the complete purification of Xe from the mixture of noble gases, the mole fractions of the compounds in the liquid, vapour and hydrate phases are required which has not been performed yet.

In order to efficiently design the separation process for the purification of Xe from the mixture of Xe, Ar, and Kr using the gas hydrate method, reliable experimental hydrate dissociation data of the mentioned gases are needed. Table 2-4 reports the available experimental studies for gas hydrate equilibrium condition of pure noble gases of Ar/ Kr/ Xe in the presence of pure water and the aqueous solutions of TBAB.

Table 2-4. The experimental studies for gas hydrate equilibrium conditions of noble gases of Ar/ Kr/ Xe in the presence of pure water and TBAB aqueous solution.

systems	Temperature range (K)	Pressure range (MPa)	Reference
Ar + H_2O	304.6, 348.2	720,1540	(Dyadin et al., 1997c)
Ar + H_2O	274.3-304.1	10.65-378.11	(Marshall et al., 1964)
Xe+ H_2O	273.1-285.1	0.15-0.49	(Ewing and Ionescu, 1974)
Xe + H_2O	299.8, 308.15	2.5 , 6.0	(Dyadin et al., 1996)
Xe + H_2O	273.1-288.1	0.15-0.70	(Makogon et al., 1996)
Xe+ H_2O	286.5-316.6	0.6-37.5	(Dyadin et al., 1997c)
Xe + H_2O	290.5-314.0	0.93-25.58	(Ohgaki et al., 2000)
Xe+ H_2O + TBAB	275.7-287.2	0.11-0.26	(Jin et al., 2012)
Kr+ H_2O	273-347.9	1.43-1540.00	(Dyadin et al., 1997c)
Kr+ H_2O	164.9-202.9	0.01- 0.11	(Barrer and Edge, 1967)
Kr+ H_2O	273.2,283.2	1.47, 3.70	(Holder et al., 1980)
Kr+ H_2O	245.4, 273.2	0.10, 1.47	(Stackelberg, 1970)

2.5. Gas hydrate promoters

The major problems in the implementation of gas hydrate technology for applications in gas industries are their slow formation rate and the high pressure dissociation conditions (Eslamimanesh et al., 2011a, Babaee et al., 2012, Ilani-Kashkouli et al., 2013). In gas hydrate formation processes, one of the common ways to moderate the gas hydrate equilibrium conditions is using gas hydrate promoters. The usual hydrate promoters are categorized in two groups of water soluble and water insoluble promoters. Water insoluble promoters including heavy hydrocarbons (alkanes, alkenes and alkynes) such as cyclobutane (CB), cyclopentane (CP), cyclohexane (CH), methylcyclopentane (MCP), methylcyclohexane (MCH), cyclooctane (CO), cycloheptane (CHP), 1,4-dimethylcyclohexane, and 2,2- dimethylbutane which when placed in the large cavities of structure H and structure II, creates a shift in the equilibrium conditions to the lower pressures (Sloan and Koh, 2008, Eslamimanesh et al., 2012a, Ilani-Kashkouli et al., 2013). These promoters however suffer from disadvantages such as toxicity,

volatility and flammability in a hydrate based process (Mohammadi et al., 2013, Manteghian et al., 2013).

Water soluble promoters are classified into two groups of kinetic and thermodynamic promoters (Ilani-Kashkouli et al., 2013). Sodium dodecyl sulfates (SDS) or kinetic promoters which were introduced by Zhong and Rogers (Zhong and Rogers, 2000) have no effect on gas hydrate equilibrium phase data (*T-P*) and promote the rate of hydrate formation depending on their concentrations. Zhong and Rogers (Zhong and Rogers, 2000) reported that a SDS solution with the concentration of 284 ppm could enhance the ethane hydrate formation rate about 700 times faster than that of the pure water (Zhong and Rogers, 2000).

Water soluble thermodynamic promoters are additives that change the phase equilibria of hydrate formation to lower pressures and higher temperatures. These types of promoters are also classified as: chemical additives (e.g. 1,3-dioxalane, 1,4-dioxane, acetone and tetrahydrofuran (THF)) (Papadimitriou et al., 2011, Sabil et al., 2010, Mooijer-van den Heuvel et al., 2001, Strobel et al., 2009a, Strobel et al., 2009b, Illbeigi et al., 2011) which do not contribute in the cavities of hydrate, rather affect the activity of water and, the group of environmental friendly quaternary ammonium salts (QAS) which produce semi-clathrate hydrates and change the structure of water cages in the traditional clathrate hydrates (Sloan and Koh, 2008, Eslamimanesh et al., 2012a, Ilani-Kashkouli et al., 2013).

Gas hydrate formation in the presence of QASs such as TBAB leads to more storage capacity than those in the presence of THF. In addition, although THF can considerably reduce the hydrate formation pressure conditions, these types of promoters suffer from the volatility which leads to loss in their amount during the gas hydrate processes such as separation, storage and transportation (Eslamimanesh et al., 2012b). The promoter TBAB is environmental friendly which can have a drastic (decreasing) effect on the dissociation hydrate pressure conditions which is beneficial in gas hydrate separation. For the aforementioned reasons, hydrate dissociation conditions of noble gases such as Xe, Ar and Kr in the presence of various aqueous solution of TBAB have been measured in this study.

2.6. Semi-clathrate hydrates

Quaternary ammonium salts such as tetra-n-butyl ammonium bromide (TBAB), tetra-n-butyl ammonium chloride (TBAC), tetra-n-butyl ammonium fluoride (TBAF), and tetra-n-butyl phosphonium bromide (TBPB) which were discovered by Fowler et al. (Fowler et al., 1940),

can form semi-clathrates hydrate crystals without any guest molecule at atmospheric pressure (Jeffrey and McMullan, 1967, Dyadin and Udachin, 1984). Due to the low equilibrium pressure conditions of the semi-clathrate hydrates of QASs, these additives can be used in processes such as storage and transportation of natural gas and cold storage application in air conditioning systems (McMullan R. and G.A., 1959, Bouchemoua et al., 2011a, Bouchemoua et al., 2011b). For instance, there are some studies on the application of pure semi-clathrate hydrates of QAS (water + QAS hydrate system) in air conditioning systems as a Phase Change Material (PCM) (Arjmandi et al., 2007). Semi-clathrate hydrates have the same properties as conventional clathrate hydrates however the difference lies in their structures; for semi-clathrate hydrates the guest molecule not only occupies the hydrate cage but contributes to the water lattice structure (Bouchemoua et al., 2011a, McMullan and Jeffrey, 2004). A diagram of a typical semi-clathrate hydrate for the system of small gas hydrate former + TBAB + water is presented in Figure 2-8. (Shimada et al., 2005). As observed in Figure 2-8, in the TBAB semi-clathrate hydrates, the positive/ cation section of the TBAB salt, can be found in the centre of four cavities (two tetrakaidecahedra and two pentakaidecahedra) while the bromide anion, Br^-, forms hydrogen bonds with the water molecules and hence participates in the water lattice (Shimada et al., 2005). When low molecular weight gases such as nitrogen, methane, carbon dioxide and hydrogen sulphide are present in the system, the empty dodecahedral cavities are filled by these small molecules. This kind of structure leads to stronger hydrogen bonding and as a result of higher stability when compared with the conventional clathrate hydrate structures (Shimada et al., 2005). Gas molecules in the presence of an aqueous solution of TBAB can form hydrate at lower pressures compared to those hydrates in the presence of pure water (Shimada et al., 2005).

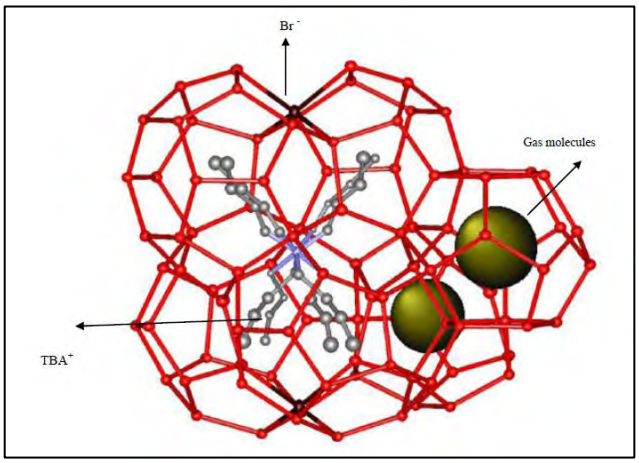

Figure 2-8. A schematic diagram of a typical semi-clathrate hydrate of small gas hydrate former + TBAB + water (Shimada et al., 2005).

The tetra butyl ammonium bromide salt can form five different clathrate hydrate structures with 24, 26, 32, 36, and 38 different hydration numbers (McMullan R. and G.A., 1959, Gaponenko et al., 1984, Shimada et al., 2005). Semi-clathrate hydrates of TBAB with hydration numbers of 38 and 26 (TBAB·26H_2O and TBAB·38H_2O) are more well-known compared to those with hydration numbers 24, 26, and 32. A three-dimensional vision of semi-clathrate hydrate of aqueous solution of TBAB with hydration number of 38 ($C_{16}H_{36}N^+ \cdot Br^- \cdot 38H_2O$) is presented in Figure 2-9 (Shimada et al., 2005).

It has been recognized that the promotion effect of TBAB salt on the argon hydrate is more than TBAC salts at two mass fractions of 0.05 and 0.2 (Garcia and Clarke, 2014a). Li et al. (2010) showed that the promotion effect of TBAF on CO_2 hydrate is more than TBAB and TBAC which makes the three-phase equilibrium pressure of the system of CO_2 + TBAF aqueous solution shift to lower pressures compared to TBAB and TBAC at the same temperature (Li et al., 2010). The problem of using the TBAF aqueous solution is that at high concentrations (more than 0.3 mass fraction), this salt forms gas hydrate at room temperature and block the related lines to the equilibrium cell. In this study Ar, Kr, Xe and CF_4 gas hydrates equilibrium phase in the presence of TBAB aqueous solutions were measured. The investigations of the effect of other promoters such as THF, TBAC, TBAF and TBPB as well as mixture of these promoters on the aforementioned hydrate system are suggested for future work.

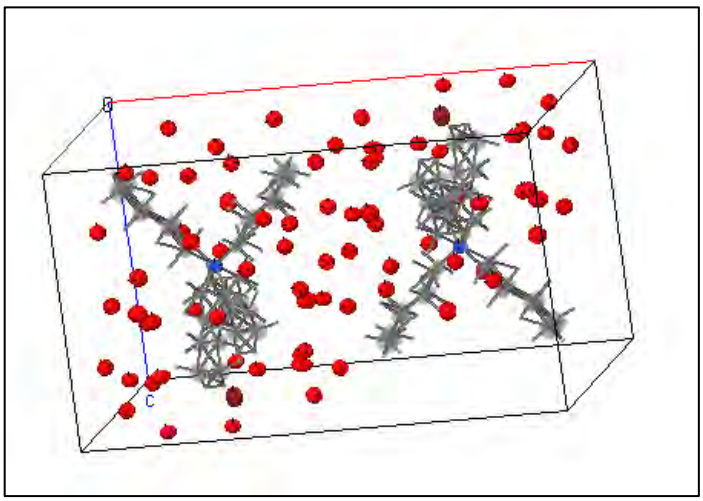

Figure 2-9. A three-dimensional vision of semi- clathrate hydrate of aqueous solution of TBAB with hydration number of 38 ($C_{16}H_{36}N^+ \cdot Br^- \cdot 38H_2O$) (Shimada et al., 2005).

3

CHAPTER THREE: THERMODYNAMIC AND KINETIC MODELLING

Following the discovery that gas hydrates can plug oil and gas transmission lines by Hammerschmidt (1934) (Hammerschmidt, 1934), extensive research was initiated to propose a predictive model for estimation of the gas hydrate equilibrium conditions. Graphical methods, empirical correlations and thermodynamic models are the available models in the literature for predicting gas hydrate equilibrium conditions. The diagram methods and empirical correlations are known as the simplest methods for predicting the gas hydrate equilibrium conditions. However, their results are limited to hydrocarbon hydrate forming systems which are suitable for rapid estimation in industry. Thermodynamic models are the reliable approaches for the estimation of the gas hydrate equilibrium conditions which are based on the solid solution theory of van der Waals and Platteeuw (vdW-P) (van der Waals and Platteeuw, 1959). These models include the activity approach which is established on the equality of water chemical potential in liquid/ice and hydrate phase (Holder et al., 1980), the fugacity approach which is based on the equality of water fugacity in liquid/ice and hydrate phase (Avlonitis and Varotsis, 1996, Klauda and Sandler, 2000) and finally the Chen and Guo model (Chen and Guo, 1998) which is based on the equality of the fugacity of the hydrate former in vapour and hydrate phases for predicting the gas hydrate equilibrium conditions. The thermodynamic model and kinetic behaviour of gas hydrates will be presented briefly in this chapter.

3.1. Modelling of gas hydrate dissociation conditions

3.1.1. K-values and gravity diagram method

To predict the hydrate formation conditions, several empirical correlations are available in the literature. One of the primary methods for estimating the hydrate equilibrium conditions is the K-values method or diffusion coefficient method. In this method for modelling of hydrate dissociation conditions, the solid-vapour phase equilibria is used and the *K* value is defined as follows:

$$K_{vs,i} = \frac{y_i}{x_i} \qquad (3\text{-}1)$$

where, y_i and x_i are the mole fraction of i^{th} hydrocarbon in the gas and solid phases, respectively. In this method, the hydrate equilibrium condition is established by the following equation:

$$\sum_{i=1}^{n} \frac{y_i}{K_{vs,\mathrm{i}}} = 1 \qquad (3\text{-}2)$$

The diagram of the K value for the various hydrocarbons such as methane, carbon dioxide, ethane, nitrogen over wide range of temperature and pressure are available in the literature. For instance, Figure 3-1 shows the diagram of the K value for predicting methane hydrate equilibrium condition (Sloan and Koh, 2008, Carroll, 2009).

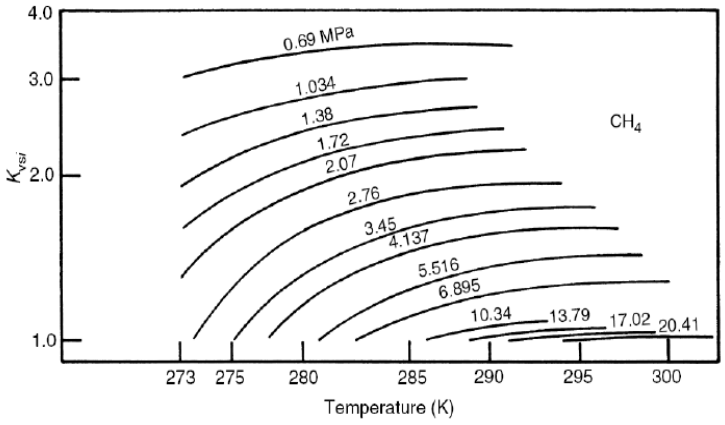

Figure 3-1. K values diagram for predicting methane hydrate equilibrium condition (Sloan and Koh, 2008, Carroll, 2009).

As it can be seen in Figure 3-1, using the *K* value at a given pressure, the gas hydrate dissociation temperature can be easily determined. In this method, large group of diagrams proposed by Carson and Katz (1942) are suggested for predicting gas hydrate dissociation conditions for various hydrocarbons such as methane, carbon dioxide, ethane, nitrogen (Carson and Katz, 1942). The temperature of gas hydrate dissociation conditions is achieved using *K* values diagram, and at a given gas composition and pressure condition. The other graphical method for representation of gas hydrate equilibrium conditions is the gas gravity method which was presented by Katz in 1945 (Katz, 1945). The gas gravity is introduced as the ratio of the molecular weight of gas to the molecular weight of air. The gas gravity diagram proposed by Katz (1945) and reproduced by and Sloan and Koh (2008), is shown in Figure 3-2 (Carroll, 2009, Katz, 1945). As it can be seen in Figure 3-2 using the gas gravity at given pressure, the gas hydrate dissociation temperature can be uncomplicatedly determined.

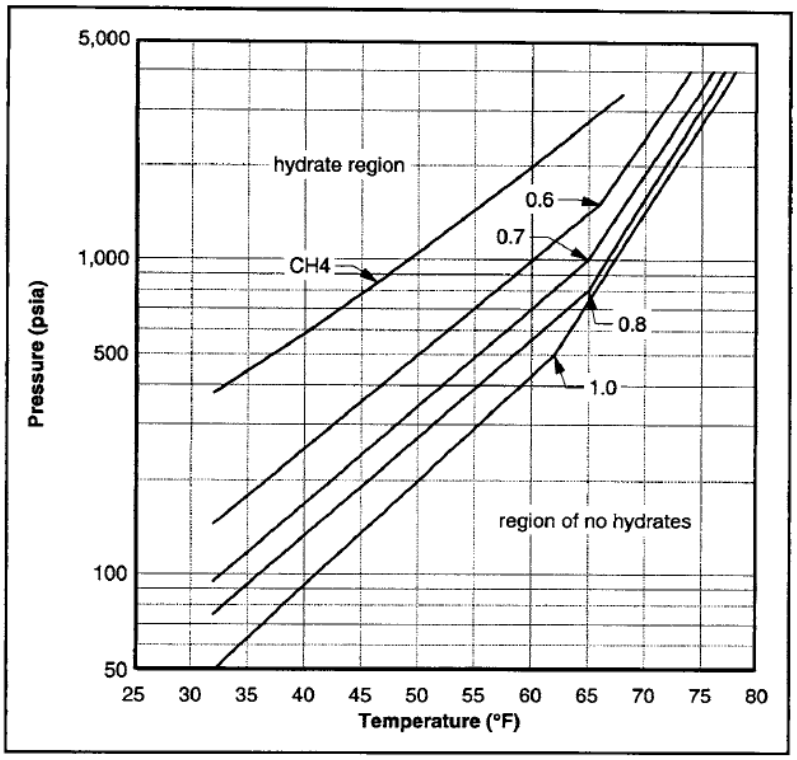

Figure 3-2. Gas gravity diagram for the predicting natural gas hydrate dissociation conditions (Carroll, 2009).

3.1.2. Fugacity approach (equality of water fugacity in the neighbouring phases)

The probable equilibrium phases during gas hydrate formation include (Sloan and Koh, 2008):

Gas phase (*G*): This phase mainly contains gases which can form hydrate crystal (maybe some of them are not able to form crystal hydrate). Depending on the equilibrium conditions, this phase may include a small amount of water vapour.
The liquid phase (L_w): This phase contains mainly water. In addition, other components in the system which have been dissolved in water can exist in this phase.
Liquid phase containing mainly hydrocarbons (L_H): This phase consists mainly of hydrocarbons and small amount of water which can be dissolved in this phase.
Solid hydrate phase (*H*): This phase consists of crystalline hydrates which contain water molecules and gas molecules which can be trapped inside the hydrate crystal lattice. Different types of hydrate crystals may be simultaneously formed in certain conditions (such as crystals, type I and II).
Ice-phase (*I*): This is the phase consists of water molecules which have been frozen.

Note that depending on the system and the related equilibrium conditions, some of the aforementioned phases may not exist. The existence of the available equilibrium phases can be determined using the Gibbs free energy theory (Sloan and Koh, 2008). The thermodynamic models for the representation of gas hydrate dissociation conditions are based on the solid solution theory of van der Waals and Platteeuw (1959) or vdWP theory (van der Waals and Platteeuw, 1959). The fundamental assumptions in the vdWP theory are summarized as follows (Sloan and Koh, 2008):

1) Each cavity in the crystal lattice comprises at most one molecule of hydrate former.
2) Ideal gas partition function for guest molecule is applicable.
3) A potential function is applied for expressing the intermolecular forces between guest and water molecules in a spherical cavity.
4) Interaction between the encaged guest molecules is negligible.
5) The interaction forces are considered between a surrounding guest molecule and water molecules in the same cavity.
6) The host molecules' contribution to the free energy is independent of the occupation of the cavity.

According to the solid solution theory of van der Waals and Platteeuw (vdWP) (1959) (van der Waals and Platteeuw, 1959), at the equilibrium conditions the equality of the fugacity of water in the liquid, vapour and hydrate phases is applied as a criterion for hydrate dissociation conditions as the following equation (Mohammadi et al., 2005, Javanmardi et al., 2012):

$$f_w^L(P,T) = f_w^V(P,T) = f_w^H(P,T) \qquad \text{ß-3}$$

where, f_w^L, f_w^V and f_w^H present the fugacity of water in the liquid, vapour and hydrate phases, respectively. The fugacity of water in the vapour and liquid phases can be determined using an EoS (Equation of State) and an appropriate mixing rule. It is believed that Valderrama's modification of Patel–Teja equation of state (VPT EoS) (Valderrama, 1990) together with the non-density-dependent (NDD) mixing rules (Avlonitis et al., 1994) are the strong tools for the modelling of the phase equilibria for the systems containing water and polar molecules. In this thesis, the VPT EoS (Valderrama, 1990) and the NDD mixing rules (Avlonitis et al., 1994) along with the flash calculations was used for predicting the fugacity of water in the vapour and liquid phases. The reader is referred to Appendix A for the details of the VPT EoS (Valderrama, 1990) and the NDD mixing rules (Avlonitis et al., 1994). More details regarding the calculation of the fugacity of water in the hydrate phase, f_w^H, in Equation 3-3, are given in Appendix B. Figure 3-3 represents the algorithm which was used in this study for calculating the hydrate dissociation temperature in the fugacity approach. Since the fugacity approach is based on the flash calculations, it is useful for high soluble hydrate forming systems such as CO_2 hydrates.

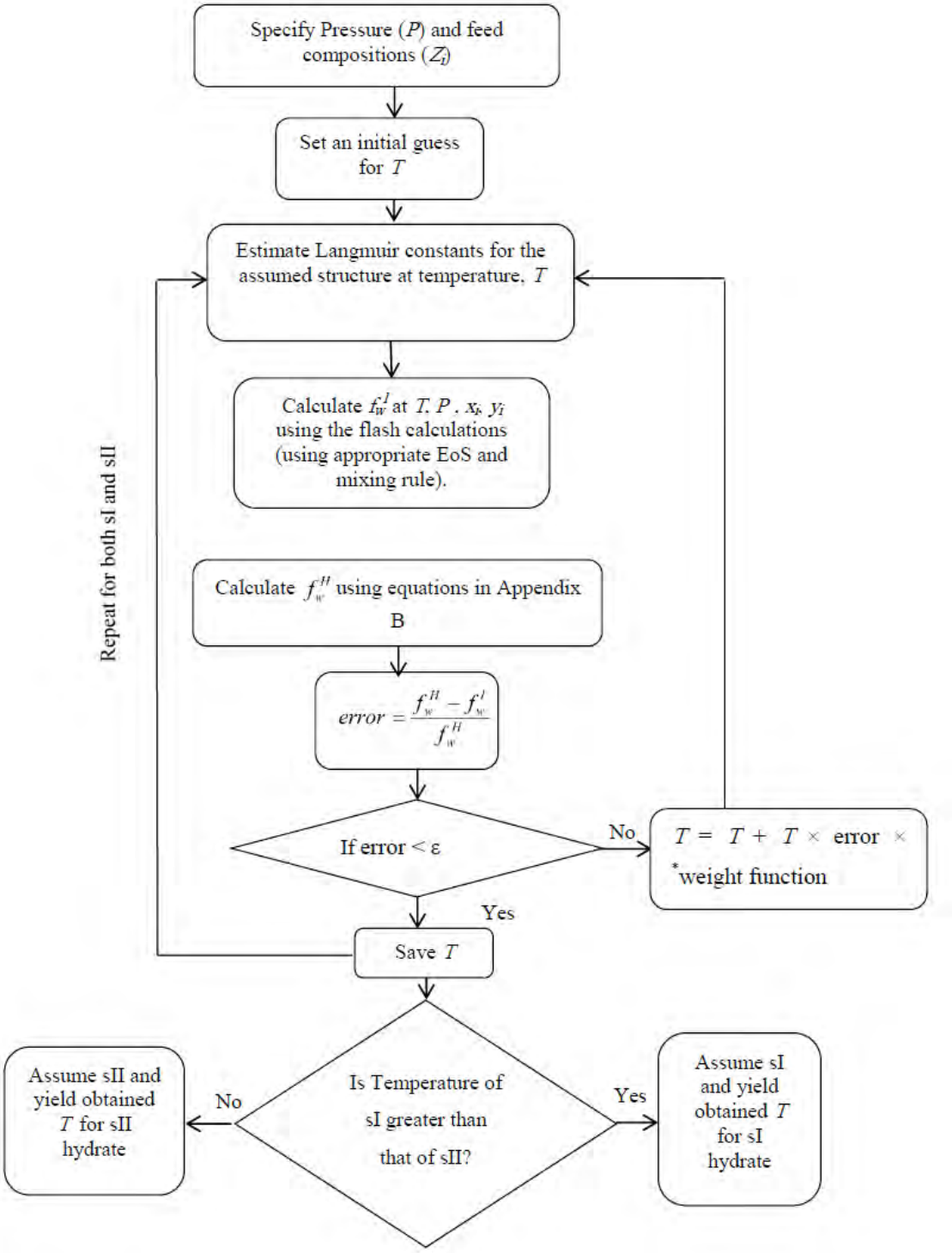

Figure 3-3. The algorithm used in this study based on fugacity approach (Li et al., 2008, Abbott et al., 2001) for calculating the hydrate dissociation temperature (Newton- Raphson method (Ben-Israel, 1966) was used in the flash calculations). The weight fraction value was 0.001 in these calculations.

3.1.3 Chemical potential approach

Holder et al. (1980) presented a model using van der Waals and Platteeuw (1959), the (vdWP) theory (van der Waals and Platteeuw, 1959), and based on the equality of the chemical potential of water in the hydrate phase (μ_w^H) and in liquid/ ice phase ($\mu_w^{l/\alpha}$) as a criteria for the phases equilibria (Holder et al., 1980):

$$\mu_w^H = \mu_w^{l/\alpha} \qquad 3\text{-}4$$

Subtracting the chemical potential of water in the empty hydrate lattice (μ_w^β) from the both sides of Equation 3-4, the following equation is derived:

$$\Delta\mu_w^{\beta-H} = \Delta\mu_w^{\beta-l/\alpha} \qquad 3\text{-}5$$

in which, $\Delta\mu_w^{\beta-H}$ represents the water potential difference between the hydrate phase and the hypothetical empty hydrate lattice phase. In addition, $\Delta\mu_w^{\beta-l/\alpha}$ in Equation 3-5 shows the water potential difference between the hypothetical empty hydrate lattice phase and the liquid or ice phase. The details of the parameters in equation 3-5 are given in Appendix B. The final equation for calculating the hydrate dissociation temperature in the activity approach is presented as follows (Holder et al., 1980):

$$\frac{\Delta\mu_w^{\beta-l/\alpha}}{RT} = \frac{\Delta\mu_w^0}{RT} - \int_{T_0}^{T} \frac{\Delta h_w^{\beta-l/\alpha}}{RT} dT + \int_{P_0}^{P} \frac{\Delta v_w^{\beta-l/\alpha}}{RT} dP - \ln(a_w) \qquad 3\text{-}6$$

All the parameters in the above equation are given in Appendix B. The activity of water (a_w) in Equation 3-6 is considered to be unity for the gas hydrates in the presence of pure water.

Li et al. (2008) used the fugacity and the activity approach for the hydrate dissociation conditions of the single and mixed gas hydrates (Li et al., 2008). In many cases, they obtained more accurate results using the fugacity approach.

3.1.4. A simple method based on fugacity approach

Another method to predict the hydrate phase equilibrium conditions is a simple method based on the equality of the fugacity of water in the liquid and hydrate phases as follow (Eslamimanesh et al., 2011c):

$$f_w^L(P,T) = f_w^H(P,T) \qquad 3\text{-}7$$

where, f_w^L and f_w^H represent the fugacity of water in the liquid and hydrate phase, respectively. This method can predict the gas hydrate dissociation conditions for the systems with low water content and gas solubility. In this method it is assumed that the vapour phase is a pure gas during to its low water content. Hence, due to the simplification, the flash calculations are not necessary. The model has poor results at higher pressures (> 1 MPa) because with increasing pressure, the gas solubility and water content increase.

In this study, this method is used for estimating the hydrate phase equilibrium conditions. For the calculation of the water fugacity in the liquid phase (f_w^L) the equation below is applied (Eslamimanesh et al., 2011c, Eslamimanesh et al., 2012a, Mohammadi and Richon, 2008b, Mohammadi and Richon, 2009, Sloan and Koh, 2008):

$$f_w^L = x_w^L \gamma_w P_w^{sat} \exp\left(\frac{v_w^L\left(P - P_w^{sat}\right)}{RT}\right) \qquad 3\text{-}8$$

where, $x_w^L, \text{and}\, \gamma_w$ represent the mole fraction of water in the liquid phase and the activity coefficient of water, respectively. In addition, P_w^{sat} in Equation 3-8 indicates the saturated vapour pressure of water. According to the UNIFAC model (Fredenslund et al., 1975), the water activity coefficient (γ_w) in the liquid phase for the mixture of water and gas, is equal to unity. The mole fraction of water in the liquid phase, x_w^L, is calculated as follow:

$$x_w^L = 1 - x_{gas} \qquad 3\text{-}9$$

The following equation can be used for calculating the mole fraction of gas molecule in the liquid phase, x_g , (Eslamimanesh et al., 2012a):

$$x_g = \frac{f_g}{K_H \exp\left(\frac{v_g^\infty}{RT}\left(P - P_w^{sat}\right)\right)} \qquad 3\text{-}10$$

where f_g is the fugacity of pure gas in the gas phase and v_g^∞ is described as the molar volume of gas at the infinite dilution condition which can be calculated using the following equation (Javanmardi et al., 2011):

$$v_g^{\infty} = -\left[\frac{\left(\partial P/\partial n_2\right)_{T,V,n_1}}{\left(\partial P/\partial V\right)_{T,n_1,n_2}}\right]_{n_2=0} \qquad \text{3-11}$$

where n_1 and n_2 denote the number of molecule of water and gas respectively. According to Stryjek and Vera (1986) the following equations can be used for estimating the terms in Equation 3-11 (Stryjek and Vera, 1986):

$$\left[\left(\partial P/\partial n_2\right)_{T,V,n_1}\right]_{n_2=0} = \frac{RT}{v_1-b_1} + \frac{RTb_2}{\left(v_1-b_1\right)^2} - \frac{2\sqrt{a_1a_2}}{\left(v_1^2+2v_1b_1-b_1^2\right)} - \frac{2a_1b_2\left(v_1-b_1\right)}{\left(v_1^2+2v_1b_1-b_1^2\right)^2} \qquad \text{3-12}$$

$$\left[\left(\partial P/\partial V\right)_{T,n_1,n_2}\right]_{n_2=0} = -\frac{RT}{\left(v_1-b_1\right)^2} + \frac{2a_1\left(v_1+b_1\right)}{\left(v_1^2+2v_1b_1-b_1^2\right)^2} \qquad \text{3-13}$$

The parameters used in the above equations are defined in Appendix A. In this study the equation below is used for the estimation of the Henry's constant , K_H , (Sander, 1999):

$$K_H\left(\mathrm{Pa}\right) = \frac{55.3}{K_H^{\theta}\exp\left(\frac{-\Delta H_{sol.}}{R}\left(\frac{1}{T}-\frac{1}{T_0}\right)\right)} \qquad \text{3-14}$$

where, $\Delta H_{sol.}$ is the enthalpy of solution and K_H^{θ} indicates the Henry's constant at temperature of 298.15 K. The saturated vapour pressure of water in Equation 3-10, P_w^{sat}, is defined as follows (Eslamimanesh et al., 2011c):

$$P_w^{sat} = 10^{-6}\exp\left(73.649 - \frac{7258.2}{T} - 7.3037\ln\left(T\right) + 4.1653\times10^{-6}T^2\right) \qquad \text{3-15}$$

The temperature and pressure in Equation 3-15 are in K and Pa, respectively. The molar volume of water is calculated using the equation below (Mohammadi et al., 2014):

$$v_w^L\left(m^3/mol\right) = 18.015\times\left[\begin{matrix}1-1.0001\times10^{-2}+1.33391\times10^{-4}\left(1.8\left(T-273.15\right)+32\right)+\\ 5.50654\times10^{-7}\left(1.8\left(T-273.15\right)+32\right)^2\end{matrix}\right]\times10^{-3} \qquad \text{3-16}$$

where, T is in K.

Equation 3-17 is used for estimating the fugacity of water in the hydrate phase (f_w^H):

$$f_w^H = f_w^{\beta}\exp\left(\frac{-\Delta\mu_w^{\beta-H}}{RT}\right) \qquad \text{3-17}$$

The details of the parameters in Equation 3-17 were explained earlier in Appendix B. In this model, the vapour pressure calculation is used for estimating the fugacity of water in the empty hydrate lattice, f_w^{β}. More details regarding the calculation of the fugacity of water in the empty hydrate lattice in Equation 3-17, are given in Appendix C. In this method the correlation suggested by Parrish and Prausnitz (Parrish and Prausnitz, 1972) which is explained in Appendix B, is used for the calculation of the Langmuir constants. Compared to the other models, this model is simple since Henry's law was used to estimate the solubility of the gas in the liquid phase. In addition, this model does not require flash calculations.

3.1.5. Equality of hydrate former fugacity in the neighbour phases (Chen and Guo, 1998) model

In this study, the model based on Chen and Guo in 1998 was used to calculate the gas hydrate equilibrium conditions. In the approach of Chen and Guo (Chen and Guo, 1998), hydrate formation consists of two steps. Firstly, a stoichiometric basic hydrate is formed through a quasi-chemical reaction where the dissolved gas molecules in water form unstable clusters with a number of water molecules surrounding the guest molecule. Secondly, the low molecular weight gas molecules such as Ar, N_2, O_2, CH_4 which are dissolved in water, are trapped into the linked cavities. As explained earlier most of the available thermodynamic models for the representation of the hydrate phase equilibria are based on the vdWP solid solution theory (van der Waals and Platteeuw, 1959) which was improved for the hydrate phase equilibria by Parish and Prausnitz in 1972 (Parrish and Prausnitz, 1972). These theoretical methods are based on the equality of the fugacity (or chemical potential) of water in the vapour/ liquid and hydrate phases and Langmuir adsorption theory. The model used by Chen and Guo in 1998 was based on the equality of the fugacity of the hydrate former in the hydrate and vapour phases. In this method a correlation was used to calculate the Langmuir constant which has made it as an easy approach for the engineering applications in order to estimate the gas hydrate equilibrium conditions.

According to Chen and Guo, the equation below is applied for the modelling of gas hydrate phase equilibria (Chen and Guo, 1998):

$$f = f^0(1-\theta)^{\alpha'} \qquad (3\text{-}18)$$

$$\alpha' = \frac{\lambda_1}{\lambda_2} \qquad (3\text{-}19)$$

where f and f^0 denote the fugacity of a gas species in the vapour phase and in equilibrium with the unfilled basic hydrate respectively. λ_1 and λ_2 represent the number of related cavities per water molecule and number of gas hydrate former per water molecule, respectively. With these assumptions the α' values in Equation 3-18 for structure I and II are 1/3 and 2 respectively (Chen and Guo, 1998). According to the Langmuir adsorption theory θ parameter , cage occupancy , in Equation 3-18 is defined as (Chen and Guo, 1998):

$$\theta = \frac{Cf}{1+Cf} \qquad (3\text{-}20)$$

where f and C are the fugacity of the hydrate former in the gas phase and the Langmuir constant respectively. In this study, the Valderrama modification of the Patel and Teja equation of state (VPT EoS) (Valderrama, 1990) is used to calculate the fugacity of the hydrate former in the gas phase. Details of the EoS used are include in Appendix A. The following correlation is applied to calculate the Langmuir constant as shown in Equation 3-20 (Chen and Guo, 1998):

$$C = X\exp\left(\frac{Y}{T-Z}\right) \qquad (3\text{-}21)$$

where, T is the temperature and X, Y, and Z parameters are the Langmuir constants for the hydrate formers. Equation 3-22 is applied to calculate the fugacity of a gas molecule in equilibrium with the unfilled basic hydrate (f^0) (Chen and Guo, 1998):

$$f^0 = f^0(T)f^0(P)f^0(a_w) \qquad (3\text{-}22)$$

where,

$$f^0(T) = A\exp\left(\frac{B}{T-C}\right) \qquad 3\text{-}23$$

$$f^0(P) = \exp\left(\frac{\beta' P}{T}\right) \qquad (3\text{-}24)$$

$$\beta' = \frac{\Delta V}{\lambda_2 R} \qquad (3\text{-}25)$$

$$f^0(a_w) = 1 \qquad (3\text{-}26)$$

In the equations above, T and P are in Kelvin and Pascal, respectively. The A, B and C parameters in Equation 3-23 are the Antoine constants for the hydrate former (Chen and Guo, 1998). The β' parameter in Equation 3-25 is equal to 0.4242×10^{-5} (K/Pa) and 1.0224×10^{-5} (K/Pa) for structure I and II, respectively (Chen and Guo, 1998).

3.2. Modelling of semi-clathrate hydrate dissociation conditions

The phase equilibria of semi-clathrate hydrates of Ar + water + TBAB, Xe + water + TBAB, and Kr + water + TBAB were predicted using the approach proposed by Joshi et al (Joshi et al., 2012) which was based on the model of Chen and Guo (Chen and Guo, 1998). The following equation is used as an equilibrium condition for the modelling of semi-clathrate hydrate dissociation conditions:

$$f = f^{0}(1-\theta)^{\alpha'} \qquad \text{Ɜ-27}$$

The VPT EoS (Valderrama, 1990) was used to predict the fugacity of the hydrate former in the vapour phase (f parameter in Equation 3-27). The α' parameter in Equation 3-27, in the case of semi-clathrate hydrate, is defined as:

$$\alpha' = \frac{\lambda_1}{\lambda_2} \qquad \text{Ɜ-28}$$

where λ_1 indicates the number of inter-connected cavities per number of water molecule and λ_2 shows the number of gas molecules per number of water molecule in the basic hydrate. Depends on the concentration of the TBAB aqueous solution, two kinds of semi-clathrate structures known as type A and type B exist (Oyama et al., 2005, Shimada et al., 2003). In these structures, the hydration numbers for type A and B are 26 and 38, respectively (Oyama et al., 2005, Shimada et al., 2003). In addition, for systems with a concentration of TBAB above 18 wt%, type A is more stable and has a higher melting point than type B and vice versa. At concentrations below 18 wt% of TBAB, type B is more stable compared to type A (Oyama et al., 2005, Shimada et al., 2003). The properties of type A and B include the hydrate number, number of linked cavity, number of gas molecules, as well as λ_1, λ_2 and α' for a unit cell of TBAB semi-clathrate hydrate are summarized in Table 3-1 (Joshi et al., 2012). The following equation is used for estimating the fugacity of gas species in equilibrium with the unfilled basic hydrate (f^0):

$$f^{0} = f^{0}(T) f^{0}(P) f^{0}(a_w) \qquad \text{Ɜ-29}$$

The following equations were used for calculating $f^{0}(T)$, $f^{0}(P)$ and $f^{0}(a_w)$ parameters in Equation 3-29:

$$f^{0}(T) = A\exp\left(\frac{B}{T-C}\right) \qquad \text{Ɜ-30}$$

$$f^0(P) = \exp\left(\frac{\beta' P}{T}\right) \qquad (3\text{-}31)$$

$$f^0(a_w) = a_w^{-1/\lambda_2} \qquad (3\text{-}32)$$

Table 3-1. The properties of type A and B for a unit cell of TBAB semi-clathrate hydrate (Joshi et al., 2012).

	Type B	**Type A**
hydrate number	38	26
number of linked cavity	1.75	1.65
number of gas molecule	3	3
[a] λ_1	1.75/38	1.65/26
[b] λ_2	3/38	3/26
[c] α'	1.75/3	1.65/3

[a] number of linked cavities per water molecule.

[b] number of gas molecules per water molecule.

[c] number of linked cavities per number of gas molecules.

where, *A*, *B* and *C* in Equation 3-30 are the Antoine constants for the gas spaces as explained in the previous section. The β' structural constant in Equation 3-31 which depends on the weight fraction of TBAB, has been reported for all the TBAB concentrations ranges in Table 3-2 (Joshi et al., 2012). The structural parameters (α and β') are dependent on the TBAB concentration and independent of the guest molecule type (Joshi et al., 2012). a_w in Equation 3-32 denotes the water activity in the presence of TBAB which is dependent on the TBAB concentration and the type of guest molecule. The following equation was used for estimating the water activity (Joshi et al., 2012):

$$a_w = \frac{1}{1 - x_{TBAB}} \exp\left(\frac{k_1}{T} - k_2\right) \qquad (3\text{-}33)$$

where x_{TBAB} is the TBAB mole fraction and, k_1 and k_2 are the guest dependent parameters.

Table 3-2. Structural parameter β for semi-clathrate of TBAB (Joshi et al., 2012).

TBAB Concentration (*wt.* fraction)	Structural Parameter β' (K/bar)
0.05	0.697
0.10	0.450
0.20	0.350
0.30	0.300

3.3. Kinetic study

Prior the design of a hydrate based process such as gas separation, gas storage and transportation, it is crucial to be aware of the kinetics of the hydrate formation. The initial temperature, initial pressure, interfacial area, water history and degree of subcooling are the parameters which can affect the kinetics of hydrate formation (Vysniauskas and Bishnoi, 1983). Using the kinetic parameters, Vysniauskas and Bishnoi developed a semi-empirical kinetic model and revealed that the the water history increases the induction time (Vysniauskas and Bishnoi, 1983). In this study, the renowned kinetic models developed by Englezos et al. was used to calculate the kinetics constant and the rate of hydrate formation (Englezos et al., 1987). Englezos et al. (1983) using the crystallization and mass transport theories indicated that the rate of gas consumption during hydrate formation is dependent on the crystal growth rate (Englezos et al., 1987). This crystallization theory (Englezos et al., 1987) was based on the difference between the fugacity of gas molecule in the vapour and hydrate equilibrium phases. Skovborg and Rasmussen (1994) (Skovborg and Rasmussen, 1994) examined the model proposed by Englezos et al. (1987) (Englezos et al., 1987) and revealed that the rate of hydrate formation was dependent on the mass transport between the water and guest molecule and independent of the total particle surface area. Subsequently, there is no need to know the particle size distribution in the hydrate formation processes. Investigations on the influence of various additives on the kinetics of hydrate formation is a different feature of kinetic study which is undertaken by numerous researchers (Mohammadi et al., 2014, Manteghian et al., 2013, Fazlali et al., 2013, Arjang et al., 2013, Partoon and Javanmardi, 2013, Kelland et al., 2013). Happel et al. (1994) (Happel et al., 1994) investigated the rate of hydrate formation of methane and a mixture of methane and nitrogen in a one liter continues stirrer tank reactor (CSTR) and discovered that the hydrate formation rate in the CSTR reactor is much higher than those in a semi-batch reactor which was reported by Vysniauskas and Bishnoi (1983) (Vysniauskas and Bishnoi, 1983). Hence, the results obtained from a semi-batch reactor may cause problems in designing of the continuous hydrate formation reactor. According to

Englezos et al.'s work (Englezos et al., 1987), it is well established that hydrate formation contains three steps. Both the first and second steps involve dispersion of the hydrate former from the interface of vapour-liquid phases to the liquid phase and the latter from the liquid to the interface of hydrate phase. The physical reaction of water molecules and hydrate former at the interface of hydrate phase is the final step of hydrate formation. Some models (Englezos et al., 1987) include all three steps, while others consider only the first two diffusion processes (Mork and Gudmundsson, 2002) or even only the transfer at the vapour-liquid water interface (Skovborg and Rasmussen, 1994). The physical reaction between a gas and water in order to form gas hydrates is defined as below (Sloan and Koh, 2008):

$$Gas + MH_2O \longrightarrow Gas \bullet MH_2O \qquad (3\text{-}34)$$

M in the above equation is the hydration number which is represented as the ratio of number of water molecule to number of gas molecule. In the case of single cage occupancy, the hydration number for sI, sII and sH are 23/4, 17/3 and 17/3 respectively. The hydrate number, M, for sI is calculated using the following equation (Sloan and Koh, 2008):

$$M = \frac{46}{6\theta_L + 2\theta_S} \qquad (3\text{-}35)$$

where θ indicates the cage occupancy and subscripts S and L show the small and large cavities, respectively. The θ parameter can be defined as:

$$\theta_i = \frac{C_i f_g}{1 + C_i f_g} \qquad (3\text{-}36)$$

where f_g is the fugacity of gas in the vapour phase and C_i indicates the Langmuir constant defined previously.

The real gas law is used for estimation of the gas consumed through the formation of clathrate hydrates is (Smith et al., 2001):

$$\Delta n_g = \frac{P_0 V_0}{Z_0 R T_0} - \frac{P_t V_t}{Z_t R T_t} \qquad (3\text{-}37)$$

where P, T and V signify pressure, temperature and volume of gas inside the equilibrium cell respectively. Subscripts '0' and 't' specify the equilibrium conditions at time equal to 0 and t, respectively. The compressibility factor of guest molecule, Z, in Equation 3-37 is estimated by

VPT EoS. (Valderrama, 1990). The gas volume inside the cell, (V_t), at time equals *t* is estimated using the following equation (Mohammadi et al., 2014):

$$V_t = V_{cell} - V_{S_0} + V_{RW_t} - V_{H_t} \qquad 3\text{-}38$$

where V_{cell} is the volume of the cell and V_{S_0} denote the initial volume of the injected water. In this study, the amount of cell volume is approximately 40 cm^3 and the initial volume of water which is injected in the cell at the start of an experiment is about 16 cm^3. In Equation 3-38, V_{RW_t} and V_{H_t} show the volume of reacted water and volume of the hydrate at time = *t*.

The amount of reacted water at time= *t* is calculated using the equation below (Mohammadi et al., 2014):

$$V_{RW_t} = M \times \Delta n_g \times v_w^L \qquad 3\text{-}39$$

where v_w^L indicates the molar volume of water defined earlier in Equation 3-16. The molar volume of the hydrate is estimated as follows (Mohammadi et al., 2014):

$$V_{H_t} = M \times \Delta n_g \times v_w^{MT} \qquad 3\text{-}40$$

The rate of gas consumption through the formation of gas hydrate is estimated by the following equation (Mohammadi et al., 2014):

$$r(t) = \frac{n_{g,i-1} - n_{g,i+1}}{(t_{i+1} - t_{i-1}) n_{w_0}} \qquad 3\text{-}41$$

where n_{w_0} shows the initial number of water mlecules in the liquid phase which is estimated using the initial volume of water (16 cm^3 in this study) and molecular volume of water. In Equation 3-41, $n_{g,i-1}$ and $n_{g,i+1}$ describe the number of gas molecules in the vapour phase at time equal to t_{i-1} and t_{i+1}, respectively.

Another parameter which is described in this work is k_{app} (the apparent rate constant of reaction during hydrate formation) which is estimated using the following equation (Englezos et al., 1987):

$$k_{app} = \frac{r(t)}{f_g - f_{equib.}} \qquad 3\text{-}42$$

In Equation 3-42, $f_{equib.}$ is described as the fugacity of gas at the hydrate equilibrium pressure ($P_{equib.}$) and initial temperature conditions. f_{equib} can be calculated using the thermodynamic model for calculation of gas hydrate equilibrium conditions which was explained in the previous sections. The storage capacity (SC) of gas hydrates is the volume of gas stored in the standard condition per a volume of hydrate and can be described as below:

$$SC = \frac{V_{STP}}{V_H} = \frac{\Delta n_g R T_{STP} / P_{STP}}{V_H} \qquad \text{ß-43}$$

where subscript *STP* symbolizes standard temperature pressure conditions. And finally, the conversion of water to hydrate which is estimated in this study, is described as the number of moles of water converted to hydrate per mole of initial water as below (Mohammadi et al., 2014):

$$\text{water - to - hydrate conversion} = \frac{\mathrm{M} \times \Delta n_g}{n_{W_0}} \qquad \text{ß-44}$$

A flowchart used for kinetic modelling in this study is presented in Figure 3-4. The results for the kinetic study will be reported in Chapter 6.

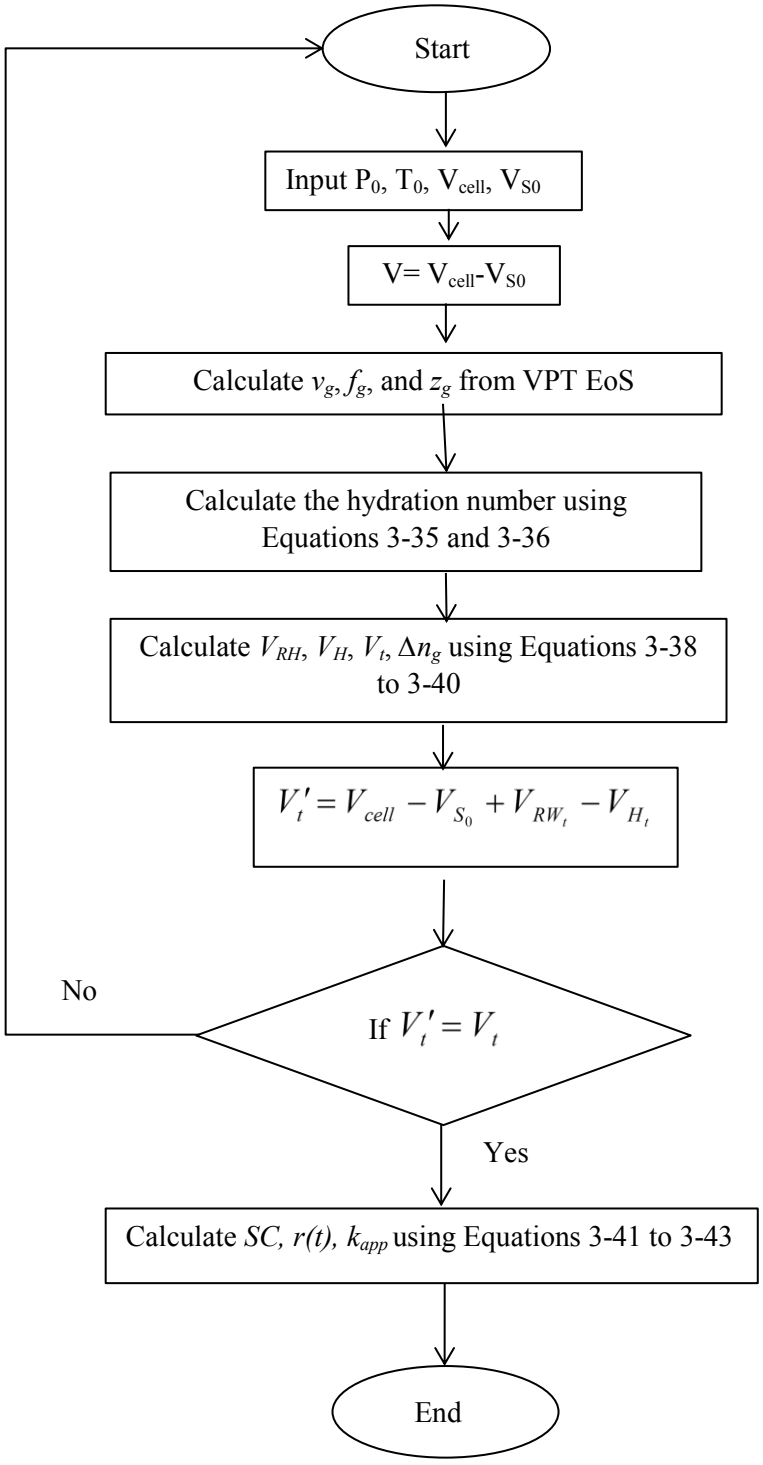

Figure 3-4. A flowchart used for kinetic modelling in this study (Mohammadi et al., 2014).

4

CHAPTER FOUR: REVIEW OF THE EXPERIMENTAL METHODS AND EQUIPMENT

Since the discovery of gas hydrates, numerous types of equipment with varying experiment procedures have been developed for the measurement of hydrate phase equilibria. The most common equipment for measuring gas hydrate equilibrium conditions have been reviewed and are explained in this chapter. In addition, the significant parameters for designing equipment will be discussed. This chapter concludes with a discussion of the different experimental procedures used for acquiring hydrate equilibrium data. The methods used to measure the gas hydrate phase equilibrium data (temperature and pressure condition of gas hydrate formation/ dissociation) are divided into two categories, viz., direct and indirect procedures. The visual observation method is the only way to determine the hydrate phase equilibria data directly, while the non-visual method, based on the increase in pressure during hydrate dissociation, is more common, and highly accurate. As it is difficult to distinguish between the ice crystals and the gas hydrate, the visual method is not recommended for the situations below the freezing point of water; this method is applied at conditions above the freezing point of water (Schroeter et al., 1983). In addition, there is a difference between the experimental data obtained visually in macroscopic and microscopic scale. For instance, macroscopic phase equilibrium data may specify a homogenous hydrate formation, while microscopic measurements express a heterogeneous hydrate composition, visually (Sloan and Koh, 2008).

The apparatus used during the discovery period of hydrates between 1810 to 1900 were equipped with hand-blown glass and used at low pressure conditions. These glasses were expensive and fragile without the ability to measure the high pressure conditions of gas

hydrates (Sloan and Koh, 2008). Villard in 1888 and 1890 changed the glass container with a round metal container for the measurement of methane and ethane hydrate dissociation conditions at high pressures (Villard, 1888, Villard, 1890).

Developing an experimental apparatus depends on various features such as the chemical and physical properties of the compounds used, the pressure and temperature equilibrium conditions, and the type of experimental equilibrium data (Richon, 1996). Richon et al. in 1996 categorised the methods for measuring phase equilibrium data in to two groups, viz., dynamic (open circuit) and static methods (closed circuit). In the dynamic method, the sample of gas and liquid phases are flashed at specific temperature and pressure conditions resulting in forced circulation of the corresponding phases. In the static method, a mechanical or magnetic agitator is used to agitate the neighbouring phases in order to reach equilibrium conditions (Raal and Mu̇h bauer, 1998). The static method is a more convenient technique for measuring phase equilibrium experimental data compared to the dynamic method; this is due to the following reasons: wide ranges of temperature and pressure, simplicity of the method, applicable for a variety of single and multi-component systems, operating with small quantities of compounds, appropriate for high pressure conditions and low cost of method (Oellrich, 2004).

4.1. Significant parameters for the development of a gas hydrate apparatus.

The significant parameters for designing an apparatus for the measurement of the gas hydrate phase equilibria include the following:

1. The apparatus must have strong agitation (using mechanical or magnetic agitators) for complete water transformation. Hammerschmidt in 1934 stated that agitation is essential to initiate hydrate formation and reduce the gas hydrate metastability zone (Hammerschmidt, 1934). Increasing the agitation of the neighbour phases (gas, liquid and hydrate phase) in an equilibrium cell, decreased the number of water molecule in the hydrate phase. In addition, water occlusion is avoided and surface renewal of gas and liquid phase at the interface will be improved by the cell agitation. Villard in 1896 stated that formation of nitrous oxide hydrate may take up to fifteen days without agitation in the system (Sloan and Koh, 2008).

2. The final hydrate dissociation point is more reproducible than the hydrate formation curve. Therefore it is more reliable to select the final hydrate dissociation point as the equilibrium data point. To avoid the occurrence of the metastable pressure, the hydrate must be heated slowly as well as in a step by step manner to the final dissociation point. In other words, metastability cannot happen if a slow heating rate around the final dissociation point is applied (Tohidi et al., 2001, Sloan and Koh, 2008). The hydrate equilibrium point is considered as a point when all crystal hydrates have dissociated in the visual method and/or a point at which a significant change in the slope of the pressure versus temperature plot is occurred which is more accurate compared to visual methods (Sloan and Koh, 2008).

3. During hydrate measurements in a constant volume cell, a rapid decrease in pressure or a sudden increase in temperature indicate the hydrate formation. The gas encapsulation inside the hydrate cavities is the main reason for the decrease in pressure during hydrate formation. In addition, as hydrate formation is an exothermic reaction and the translation energy of the encapsulated molecules in the hydrate phase is lower than those in the vapour and liquid phase, the temperature is increased during hydrate nucleation (Sloan and Koh, 2008).

4. The most important part of the hydrate apparatus is an equilibrium cell, usually enclosed within a thermostatted bath.

5. The temperature and pressure during the hydrate formation and dissociation are measured using a thermometer and a pressure transducer (or a Bourdon tube gauge) which are placed inside the cell.

6. In the visual or direct method, the main part of the equilibrium cell is a sight glass for viewing the gas hydrate formation and decomposition, inside the equilibrium cell.

4.2. Equipment review

4.2.1. The apparatus of Deaton and Frost (1937)

Deaton and Frost in 1937 developed a static apparatus for measuring the gas hydrate equilibria, which was in use for many years. Figure 4.1 presents the rocking hydrate equilibrium cell (Sloan and Koh, 2008).

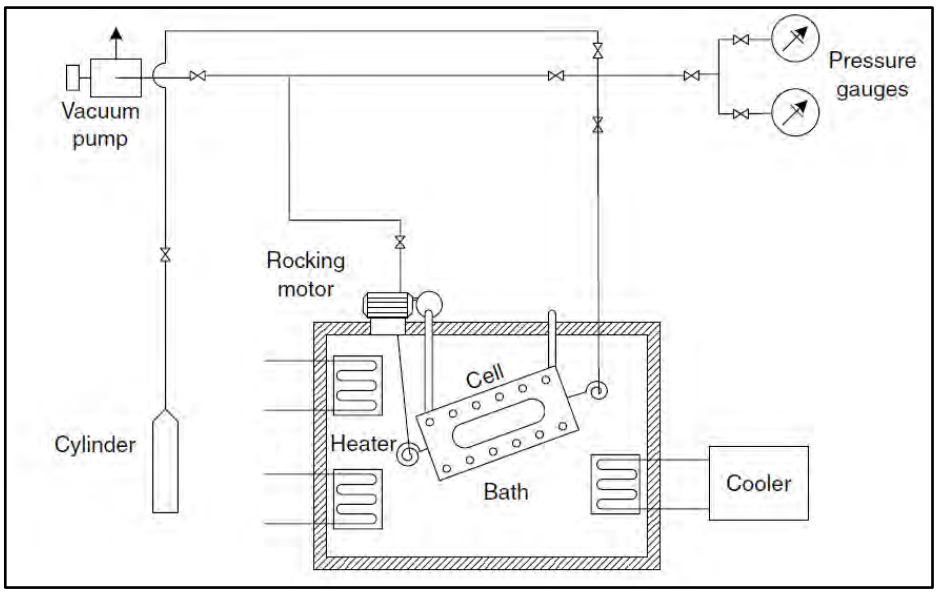

Figure 4-1. A diagram of the rocking hydrate equilibrium cell developed by Deaton and Frost in 1937 (Sloan and Koh, 2008).

In this apparatus, an equilibrium cell, equipped with a sight glass for viewing the formation and dissociation of gas hydrate, is placed inside a thermostatted bath. The agitation of the surrounding phases (gas, liquid and hydrate) is performed via rocking the cell on a horizontal axle inside the thermostatted bath for complete water transformation during experiments. In this apparatus, the gas can enter the chamber via a port located above the liquid phase or it can be sprayed through the liquid phase which increases the mixing (Sloan and Koh, 2008). As seen in Figure 4.1, a heater and cooler are placed in the bath to increase or decrease the temperature, hence enabling the formation or dissociation of the hydrate phase. In this equipment, the pressure of the equilibrium cell is measured by a pressure gauge. Hydrate phase dissociation data is achieved using the visual observation of the decomposition of the final hydrate crystals.

4.2.2. Quartz crystal microbalance (QCM)

Mohammadi et al. in 2003 developed a new technique for measuring the phase equilibria of gas hydrate using a Quartz Crystal Microbalance (QCM) (Sloan and Koh, 2008, Mohammadi et al., 2003). Figure 4-2 presents a schematic diagram of the QCM equipment.

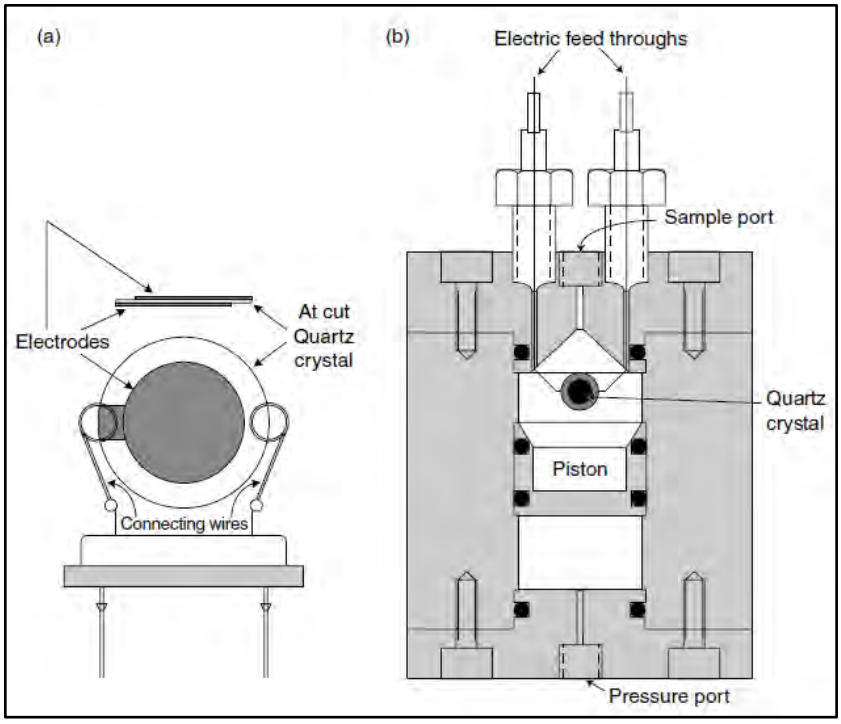

Figure 4-2 (a) Quartz crystal microbalance (QCM) apparatus. (b) QCM placed inside a high pressure equilibrium cell (Sloan and Koh, 2008, Mohammadi et al., 2003).

The QCM contains a thin disk made from quartz which is pressed between two electrodes. In this apparatus when an electric current passes through the electrodes, the quartz disk starts to oscillate at a certain resonant frequency. The frequency is dependent on the crystal properties of the disk. During hydrate formation, the amount of hydrate mass which is attached to the surface of the disk is changed. This mass change can cause a change in the resonant frequency. Hence, hydrate formation and hydrate dissociation can be detected by the change in frequency and disk oscillations. The QCM apparatus is very sensitive and can measure very small amounts of mass which results in a reduction in the time for experiments. In this apparatus, the time taken to reach equilibrium at each temperature step is fifteen minutes, which is significantly lower than several hours in the conventional methods. Phase data with pressures up to 6000 psi, can be

measured with this apparatus. The temperature and pressure of the system were measured using a pressure transducer and a thermocouple, respectively.

4.2.3. Cailletet Apparatus

A diagram of the Cailletet apparatus (Shariati and Peters, 2003, Kroon et al., 2005, Raeissi and Peters, 2001) is shown in Figure 4-3.

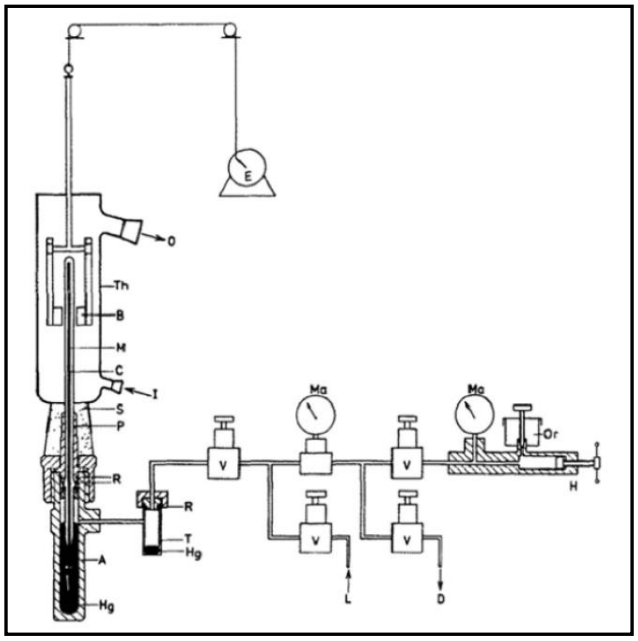

Figure 4-3. A schematic diagram of Cailletet apparatus. A, autoclave; B, magnets; C, Cailletet tube; D, drain; E, stirring motor; H, hydraulic pump; Hg, mercury; I, inlet tube; L, connection with dead-weight pressure gauge; M, sample of mercury; Ma, manometer; O, outlet thermostat liquid; Or, oil reservoir; P, closing plug; R, O' rings; S, silicone rubber stopper; T, mercury trap; Th, glass thermostat; V, valve (Sabil, 2009).

This apparatus is used for measuring the hydrate phase equilibrium data over a pressure range of 0.35 to 15 MPa and over a wide temperature range of 255 to 470 K. At the start of each experiment, a desired sample with fixed composition is prepared and the Cailletet tube is placed at the top of the Cailletet apparatus. The Cailletet tube is sealed using a mercury column which can also act as a part of the pressure transferring medium. The system is pressurized by the

injection of the hydraulic oil into the system using a hand pump. The Cailletet tube is immersed inside the thermostat bath to keep the temperature of the system constant. A dead-weight pressure gauge with an accuracy of 0.0025 MPa and a platinum resistance temperature probe (placed at the top of the Cailletet tube) with an accuracy of 0.01 K were used to measure the pressure and temperature of the system, respectively. The agitation of the system is performed using a stainless ball with moving magnets. In order to improve visibility of the cell contents in the glass tubes, a microscope is placed in front of the Cailletet tube to modify the light source. In this apparatus, visual observation which is not a very accurate technique, is used to obtain the hydrate phase equilibrium data (Sabil, 2009).

4.2.4. High Pressure autoclave

The high pressure autoclave is the most common equipment for measuring the gas hydrate equilibrium conditions in recent decades (Zhang et al., 2004, Duc et al., 2007, Herri et al., 2011, Mohammadi et al., 2011, Javanmardi et al., 2012). The most important part of this apparatus contains a high-pressure cylindrical cell which is immersed inside a thermostat liquid bath. The aqueous solution of ethylene glycol is usually used as the cooling/heating fluid. The equilibrium cell may consist of a sapphire sight glass for visual observation of the gas hydrate formation and dissociation. The system agitation is commonly performed using magnetic stirrers in order to agitate the surrounding phases (vapour- liquid- hydrate). A diagram of the high equilibrium cell is shown in Figure 4-4.

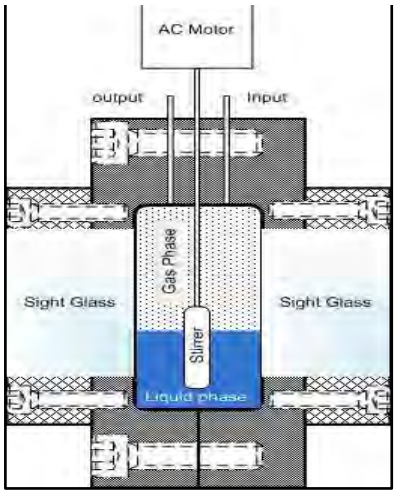

Figure 4-4. A schematic diagram of a high equilibrium cell equipped with two sight glasses/ windows (Javanmardi et al., 2012).

The equilibrium cell is pressurised by introducing the hydrate former from a capsule container. The temperature and pressure of the apparatus are monitored using the temperature probe and high pressure transducer, respectively. Figure 4-5 shows the high pressure apparatus which was developed by Mohammadi et al. (Mohammadi et al., 2011).

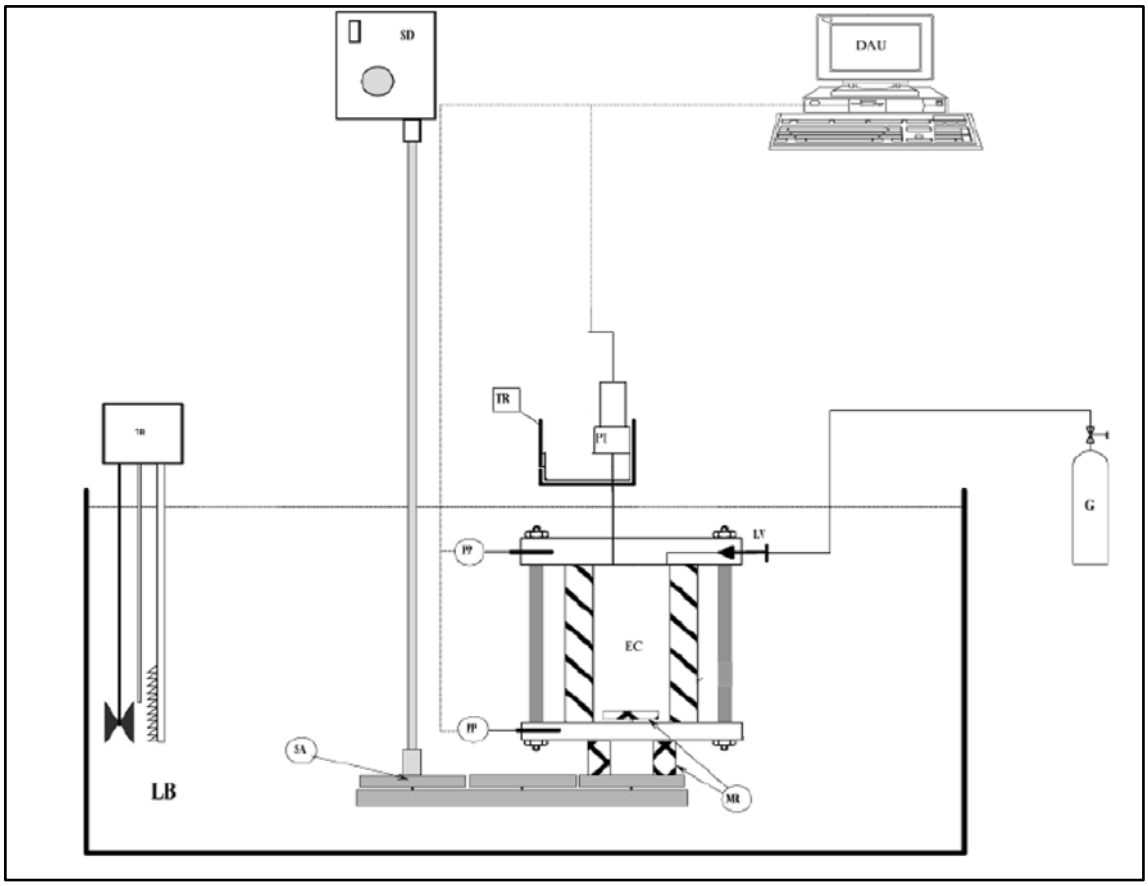

Figure 4-5. A schematic diagram of high pressure apparatus (Mohammadi et al., 2011). DAU, data acquisition unit; EC, equilibrium cell; G, gas cylinder; LB, liquid bath; LV, loading valve; MR, magnetic rod; PP, platinum probe; PT, pressure transducer; SA, stirring assembly; SD, stirring device with variable speed motor; TR, temperature controller.

4.2.5. Calorimetric approaches

Dalmazzone et al. developed a Differential Scanning Calorimetry (DSC) device equipped with special high-pressure vessels to measure the enthalpy and temperature dissociation of semi-clathrate hydrate for the system of hydrogen + TBAB/ TBAC/ TBPB + water (Deschamps and Dalmazzone, 2010). Figure 4-6 shows a schematic diagram of this apparatus. As observed in

Figure 4-6, a micro DSC VII device is used to measure the difference in heat flow between the sample and the reference. The apparatus works in the temperature and pressure range of (228.15 to 393.15 K) and (0.1 – 40 MPa), respectively. The high pressure cell in this apparatus is not equipped with the stirring device. In this method, a motorcycle technique of the hydrate crystallisation is applied to accelerate the rate of hydrate formation. In this process, at each cycle, the temperature of the system decreases to 258.15 K with a rate of 3 kelvin per minutes and then after 10 minutes, the temperature of the system increases to a temperature which is lower than the gas + semiclathrate hydrate dissociation temperature and higher than the semi-clathrate hydrate dissociation temperature. In this experimental method, the semi-clathrate hydrate can form and dissociate while the quantity of the gas + semi-clathrate hydrate growths during the each cycle. At the end of cycle the temperature of the equipment increases to the ambient temperature. With dissociation of the semi- clathrate hydrate, the surface of the picks of crystallization decreases. The surface of the last peak of DSC device is used to determine the dissociation enthalpy of the gas + semi-clathrate hydrate (Deschamps and Dalmazzone, 2010). The advantages of this method consist of high rate of measurements (compared with PVT methods), small amount of sample, and measuring thermodynamic and thermal experimental data, simultaneously (Le Parlouër et al., 2004). However, the differences in the hydrate dissociation temperature using this kind of calorimetric apparatus is larger than the experimental uncertainties (Suginaka et al., 2012).

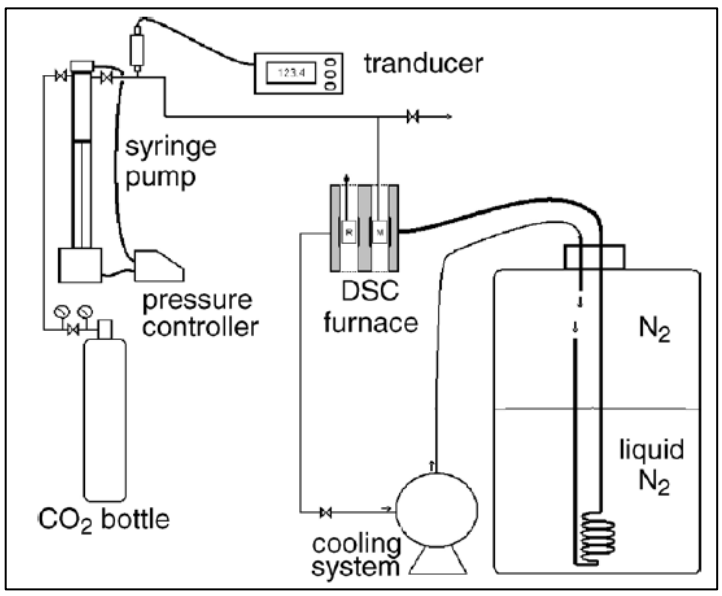

Figure 4-6. A schematic diagram of the high-pressure micro Differential Scanning Calorimetry (DSC) device (Marinhas et al., 2006, Deschamps and Dalmazzone, 2010).

4.3. Available experimental methods for the determination of hydrate dissociation

There are two methods, namely, direct (visual) and indirect (nonvisual) using a static apparatus, to measure the gas hydrate phase equilibria. Isobaric (constant pressure) and isothermal (constant temperature) methods are based on visual observation and, the isochoric method (volume constant) is based on the non- visual method. In these methods (isothermal, isobaric and isochoric), one of the three parameters of temperature, pressure and volume is set constant and the other two parameters are changed through the gas hydrate formation and dissociation (Ye and Liu, 2012). As mentioned previously, the visual methods (isobaric and isothermal) are not suitable for conditions below the freezing point of water, since it is difficult to distinguish between the ice crystals and the gas hydrate clusters (Schroeter et al., 1983). The isochoric method is accurate, and does not require the observation of the gas hydrate formation and dissociation. In this method, the hydrate dissociation conditions are determined using the significant change in the slope of the heating curves in the *P-T* diagram. The basic properties of three methods, isobaric, isothermal and isochoric, are presented briefly in Table 4-1.

Table 4-1. Three methods of isobaric, isothermal and isochoric for the determination of gas hydrate dissociation conditions (Sloan and Koh, 2008).

Method	Characteristic	Hydrate formation detection	Hydrate dissociation
Isothermal	Constant temperature	Temperature is increased at the start of hydrate nucleation because the gas hydrate formation is an exothermal reaction.	Visual observation of decomposition of hydrate crystal is used.
Isobaric	Constant pressure	Addition or withdraw fluids (gas or liquid) from an external reservoir is used for maintaining pressure on a constant amount.	Visual observation of decomposition of hydrate crystal is used.
Isochoric	Constant volume	Because of trapping gas molecules inside the hydrate structures, pressure is decreasing sharply	Sharp changing in *P-T* diagram's slope in the heating curve is used.

In this section the aforementioned experimental methods for the determination of gas hydrate phase equilibrium conditions are explained.

4.3.1. Visual isothermal pressure search method

At the start of the experimental measurement by the isothermal pressure search method, the temperature of the system is set at the constant value. After the evacuation of the cell to eliminate any contamination, the pressure of the system is set at a pressure above the estimated region of hydrate formation by introducing hydrate former inside the equilibrium cell (approximately 20-30 kPa above the estimated pressure). Then the agitation of the system is initiated and the system is allowed to reach to equilibrium conditions at that temperature. At the start of hydrate nucleation, the temperature at the hydrate interface increases because of the translational energy output due to the movement of the molecules from the gas and liquid phases to the hydrate phase. However, it is necessary to discharge this kind of energy from the system to the bath and neighbouring phases using agitation or conduction/ convection. During hydrate formation, the system pressure decreases because of gas encapsulation. The pressure during the experiment is controlled by the exchange of a gas or liquid such as mercury from an external reservoir. After the formation of gas hydrates, the pressure is decreased gradually by withdrawing fluids (gas or liquid) from the external reservoir until the disappearance of the last crystal of hydrate. This procedure is valid only for pure liquid or gas. This point is considered as the visual equilibrium pressure point of hydrate at a constant temperature. In order to reduce the inaccuracy when using the visual effect, the experimental procedure for hydrate formation and dissociation should be performed twice (Sloan and Koh, 2008, Englezos and Bishnoi, 1991).

4.3.2. Visual isobaric temperature search method

In the isobaric temperature search method, addition or withdrawal of fluid (gas or liquid) from an external reservoir is used to maintain a constant pressure. After the evacuation of the cell to remove any impurities in the cell, the equilibrium cell is pressurised by introducing the hydrate former to reach to the desired and constant pressure. The temperature of the system is then decreased about 5 K below the expected temperature of the hydrate equilibrium conditions. After the temperature of the system reached a constant value, the stirrer is switched on and the formation of gas hydrate begins. Hydrate formation is determined by the addition of a

significant fluid (gas or liquid) from an external reservoir in to the cell. After hydrate formation is complete and the pressure of the system has reached to constant value, the temperature of the cell is increased slowly to dissociate the gas hydrate. In order to maintain the pressure at the constant value in this step, some fluid must be withdrawn from the cell. This procedure is valid only for pure liquid or gas. The decrease in the temperature continues until the last hydrate crystal disappears. This point is considered as the visual equilibrium temperature point of hydrate at a constant pressure. In order to reduce the inaccuracy using the visual effect, the experimental procedure for hydrate formation and dissociation should be performed twice (Sloan and Koh, 2008).

4.3.3. Isochoric pressure search method

The isochoric or constant volume method is appropriate for gas hydrate measurements at high pressure conditions. As the isochoric method does not require viewing of the cell contents to distinguish the final hydrate dissociation point, this procedure can be used as an alternative to the visual isothermal and isobaric methods. This method was applied in the experiments conducted in this study. A pressure- temperature diagram generated during the hydrate formation and dissociation conditions in the isochoric procedure is presented in Figure 4-7. As seen in this figure, measurements commence with a mixture of water and gas and conditions of pressure and temperature outside the hydrate stability zone, point A. Then the gradual cooling to the point B provides the system to reach to the hydrate formation conditions. After point B, crystals of gas hydrate start to form and consequently the pressure of the system is decreased until the system reaches point C, owing to gas encapsulation. The amount of the pressure reduction in this step depends on the amount of gas molecules filling the hydrate cavities and other thermodynamic restrictions. Once the gas hydrate formation is complete and the system has reached a constant pressure, point C, the temperature is increased slowly to dissociate the gas hydrate crystals. Heating of the system continues until all of the encapsulated gas is released from the crystals and the pressure and temperature of the system reaches an equilibrium, known as the dissociation condition, at point D. After complete decomposition of the hydrate crystals, with temperature increasing, the pressure is altered by considering the relationship between temperature, volume and pressure change. According to Sloan and Koh in 2008, the hydrate equilibrium point is considered as the intersection between the hydrate dissociation curve and the initial cooling curve (point D) (Sloan and Koh, 2008).

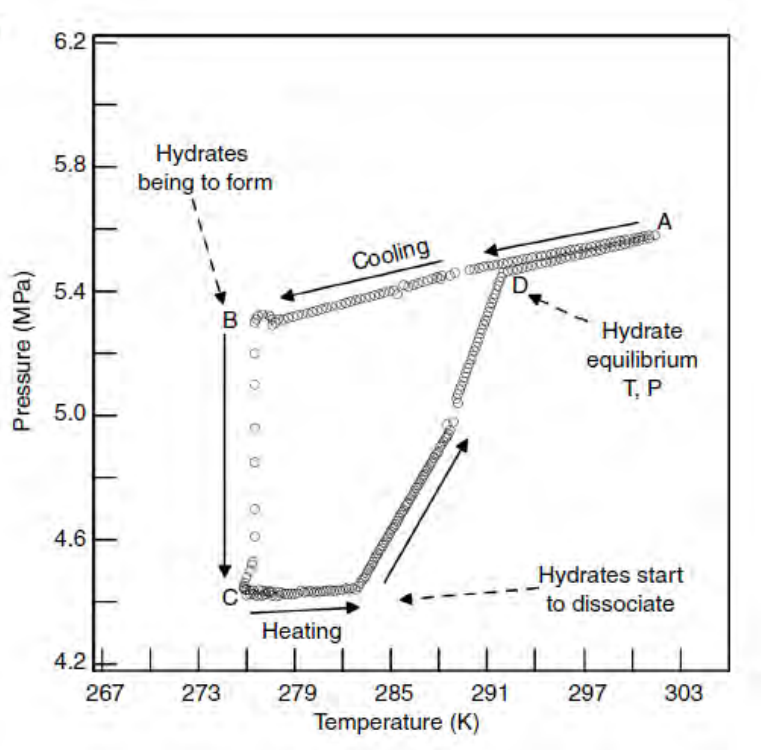

Figure 4-7. Primary cooling and heating curve for formation and dissociation of simple hydrate in the isochoric method (Sloan and Koh, 2008).

5

CHAPTER FIVE: DESCRIPTION OF THE EXPERIMENTAL APPARATUS AND PROCEDURE

Reliable gas hydrate equilibrium experimental data plays an essential role in the design of a hydrate based process. Furthermore, such data is vital for the development and testing of predictive thermodynamic models. In order to produce precise hydrate equilibrium data, a reliable apparatus and an accurate as well as reproducible experimental method is essential.

The static non-visual isochoric method, discussed extensively in Chapter 4 is a more reliable procedure with a higher accuracy compared to the isobaric and isothermal methods which are based on the visual observation to detect the gas hydrate formation and dissociation conditions. In this study gas hydrate/semi-clathrate equilibrium data were measured via a non-visual isochoric method using a static high pressure equilibrium apparatus designed and built in-house. The advantages of this non visual apparatus and the technique adopted include higher accuracy, stronger agitation, and an automated process compared to techniques reported in literature and discussion in Chapter 4. The opportunities to employ corrosive solutions such as salt aqueous solutions and to be able to perform measurements overnight are among other benefits.

The main part of the experimental set-up comprises a high pressure equilibrium cell which is placed inside a thermo-statted bath. An agitator, temperature probe, pressure transducer, vacuum pump, and data acquisition system are the other devices which are used in this apparatus. In this chapter, the accuracies and limitations of these measuring devices are also described. In addition, details of materials used, purities and suppliers of the chemicals used are presented. In order to achieve accurate data, temperature and pressure calibrations, leak test and vapour pressure tests are performed before the experimental measurements which are explained in the sections which follow.

5.1. Materials

The purities and suppliers of the chemicals used in this study are reported in Table 5-1. Ultrapure Millipore Q water with an electrical resistivity of 18 MΩ·cm was used in all measurements. The TBAB aqueous solutions were prepared gravimetrically using an analytical balance (Mettler Toledo Balance, model no. AB204-S) with an uncertainty of ± 0.0001 g.

Table 5-1. Details of the purities and the suppliers of the materials used in this study [a].

Chemical	Formula	Supplier	Purity
Argon	Ar	AIR LIQUIDE	0.999 mole fraction
Krypton	Kr	AIR LIQUIDE	0.999 mole fraction
Xenon	Xe	AIR LIQUIDE	0.999 mole fraction
Tetrafluoromethane	CF_4	AIR LIQUIDE	0.999 mole fraction
Tetra Butyl Ammonium Bromide	$C_{16}H_{36}BrN$	SIGMA-ALDRICH	> 0.99 mass fraction
SDS	$CH_3(CH_2)_{11}OSO_3Na$	0.990	Sigma-Aldrich

[a] Ultrapure Millipore Q water with an electrical resistivity of 18 MΩ·cm was used in all experiments.

5.2. Experimental apparatus

The schematic diagram of the apparatus is presented in Figure 5-1, and as shown in the figure, the set-up consists of the following devices listed below. A photograph of the experimental set-up is also shown in Figure 5-2.

1. A high pressure stainless-steel equilibrium cell with an internal volume of approximately 40 cm^3 (the most important part of set-up).
2. A mechanical agitator.
3. A liquid thermo-statted bath with dimensions 43 cm × 35 cm × 26 cm.
4. A temperature controller Model TXF200 supplied by PolyScience®, with an operating temperature range of 228 to 397 K.
5. A cold finger supplied by PolyScience®.
6. A Pt-100 temperature probe.
7. A WIKA pressure transducer (0-16 MPa) with an accuracy of 0.05% stated by the manufacturer.
8. An Agilent data acquisition system.
9. A mechanical jack.
10. An Edwards vacuum pump.

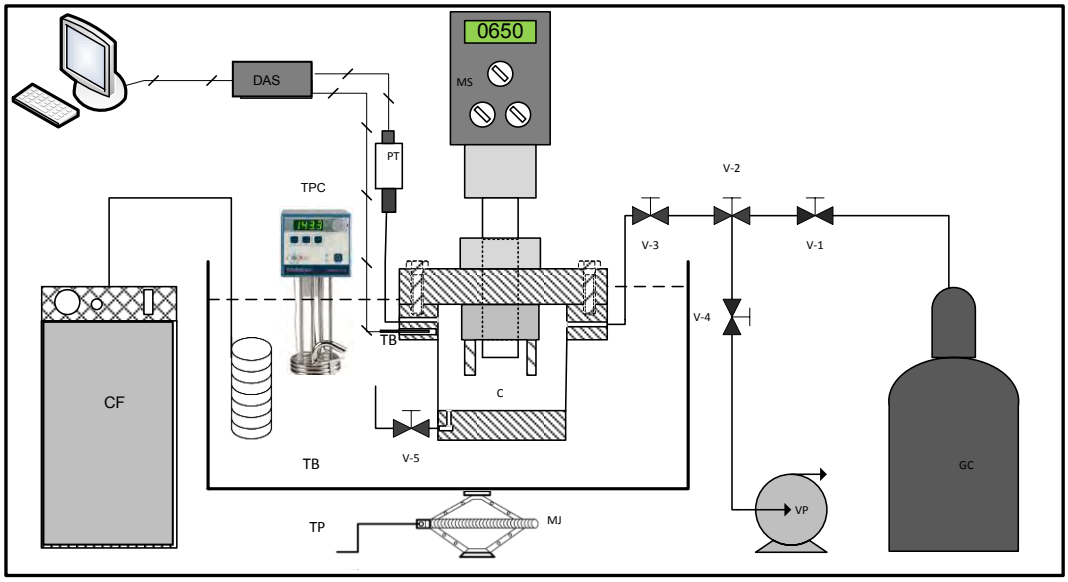

Figure 5-1. A schematic diagram of the apparatus developed in this study. C, cell; CF, cold finger; DAS, data acquisition system; GC, gas cylinder; MJ, mechanical jack; MS, mechanical stirrer; PT, pressure transmitter; TB, thermos-statted bath; TP, temperature probe; TPC, temperature programmable circulator; VP, vacuum pump; V, valve.

Figure 5-2. A photograph of the experimental setup.

5.2.1. The high pressure equilibrium cell

A high-pressure equilibrium cell, constructed from 316 stainless steel, with the internal volume of approximately 40 cm^3 constitutes the main part of the experimental setup. The equilibrium cell can withstand pressures up to 20 MPa. Since the dissociation pressure of the hydrate dissociation conditions for Ar, Kr, and CF_4 at the temperature above the ice point (273.15 K) is more than 10 MPa, the equilibrium cell required to tolerate the pressure up to 20 MPa. The thickness of the cell body and the top flange, and the height of the cell were calculated and designed according to this limitation of pressure (Sinnott, 2005). Figure 5-3, and 5-4 show a schematic of the high pressure equilibrium cell which was used in this study.

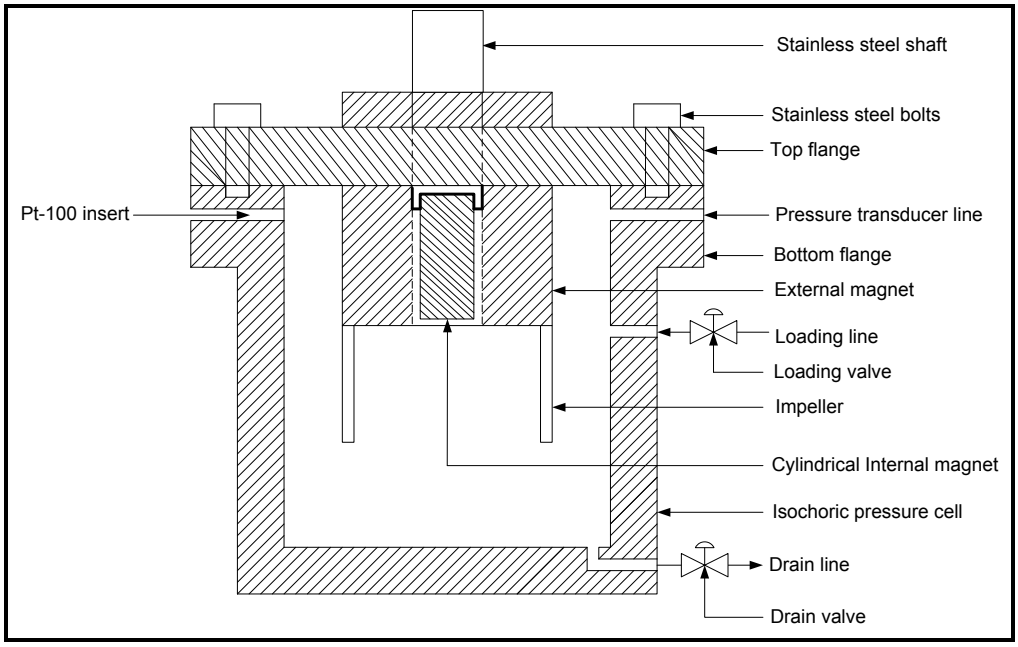

Figure 5-3. A schematic of the equilibrium cell.

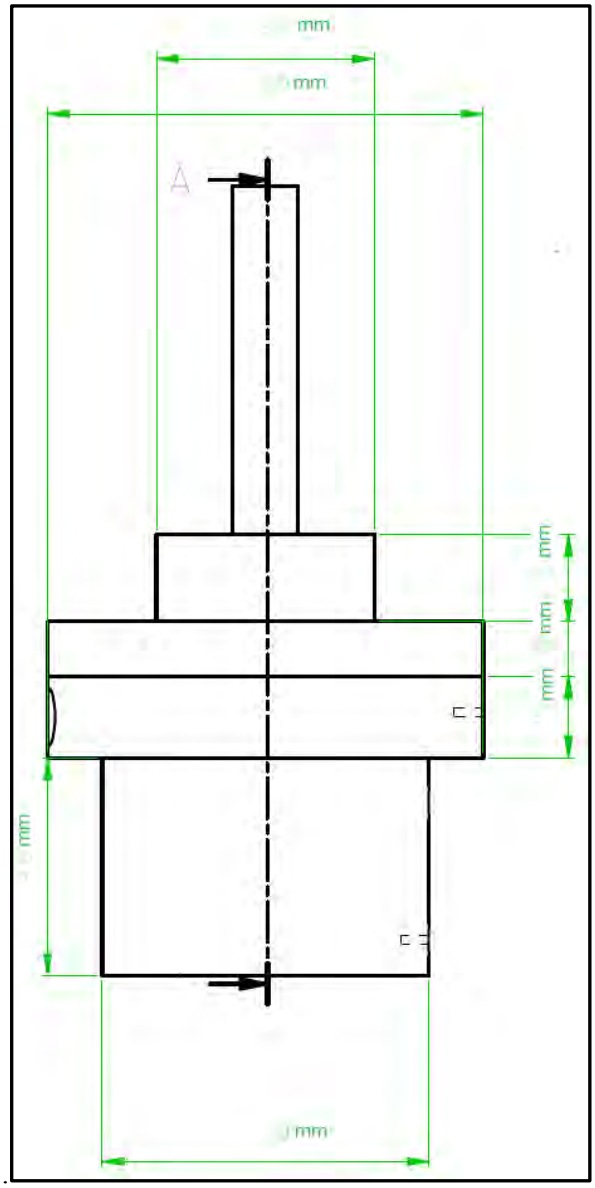

Figure 5-4. Exterior view of the equilibrium cell (sizes are in mm).

Three holes were drilled into the equilibrium cell body. The first hole, placed on the top, connects the cell to the pressure transducer via a 1/16' inch 316 stainless steel tubing. The second hole with a diameter of 8 mm is located at the middle of the cell and is used for filling/ evacuation of the cell for gas chemicals. The third hole with a diameter of 8 mm located at the bottom of the equilibrium cell is used for charging and withdrawing liquids. Two valves supplied by Swagelok are used to control the input/output of gas and liquid to/from the cell. In addition there is an 1/8' inch hole drilled into the cell body to house the Pt-100 temperature probe to record the equilibrium temperature. An O-ring inserted into a groove in the flange aids

in the sealing of the flange and the cell body. These two fittings are joined to seal the cell using 6 × 10 mm stainless steel bolts. Figure 5-5 to Figure 5-7 presents photographs of the cell body and the top flange.

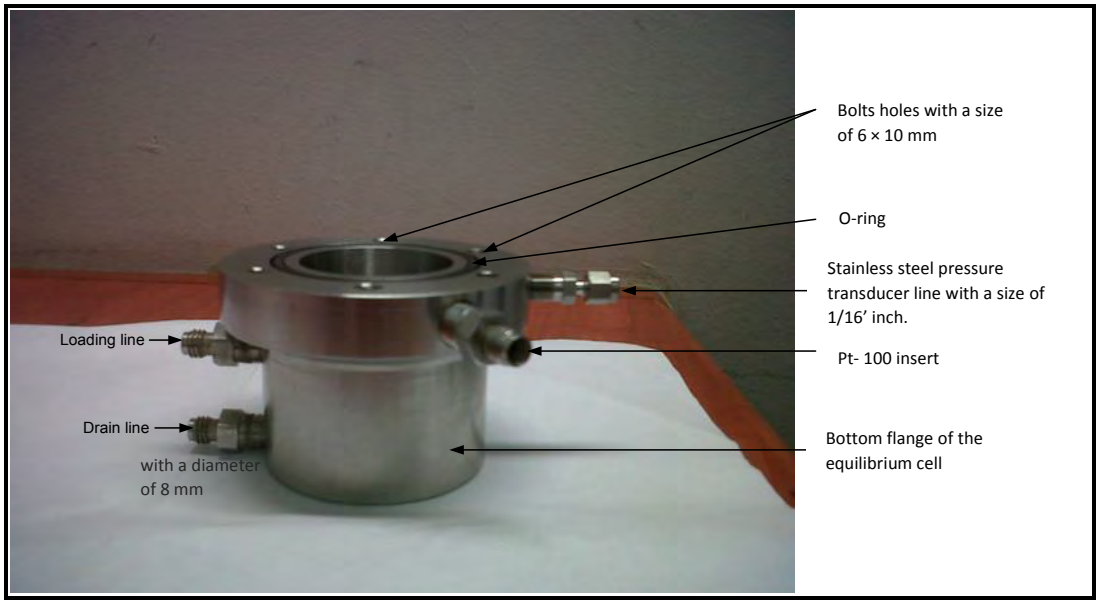

Figure 5-5. A photograph of the bottom flange of the equilibrium cell.

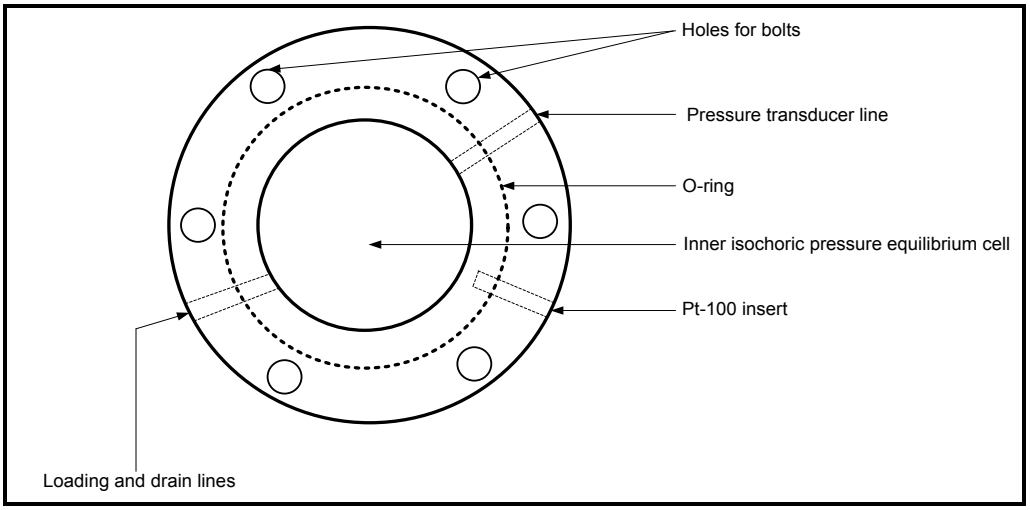

Figure 5-6. Top view of the equilibrium cell.

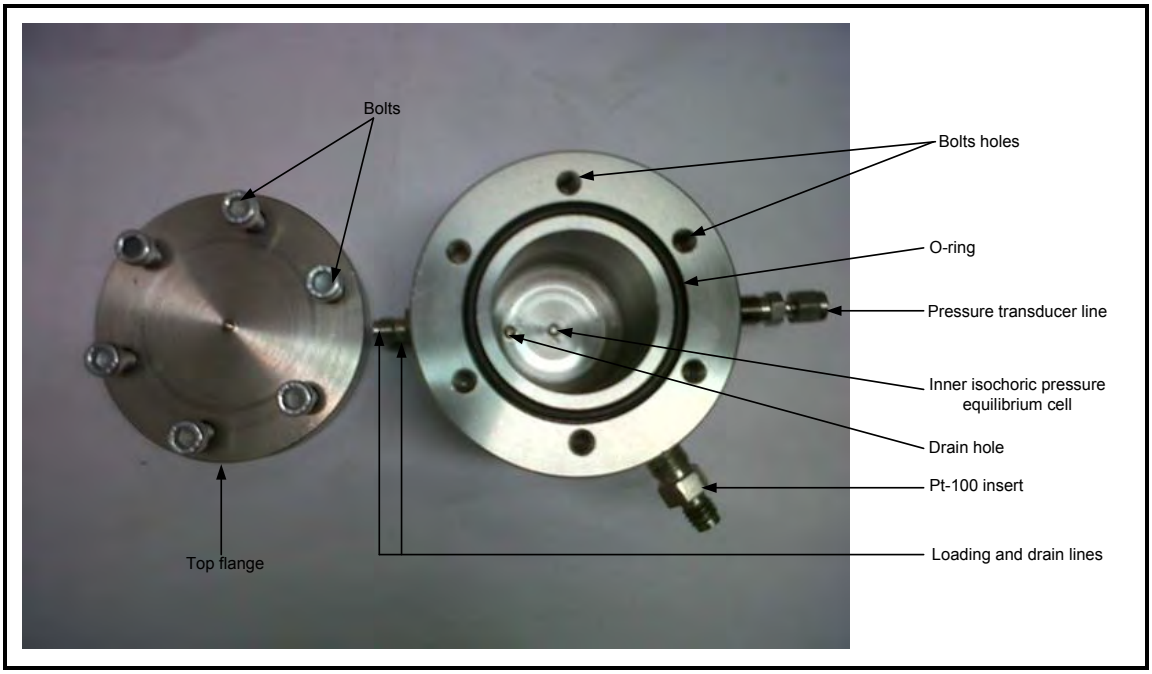

Figure 5-7. Top view of the equilibrium cell.

5.2.2. Agitation system

As mentioned before, to reduce the gas hydrate metastability zone and increase water transformation, a strong agitation system is required. The agitation system in this work consists of a Heidolph RZR 2041 motor, a small magnet which is situated inside the stainless steel shaft and a stirrer device with four blades and an external strong magnet. The magnets are constructed from neodymium with an extremely strong magnetic field which can operate at high temperatures of 353.15 K. Compared to other types of permanent magnets, neodymium magnetite provides superior strength, higher resistance to becoming demagnetized, and lower Curie temperature (Gorman, 2009).

The Heidolph stirrer motor is placed at the top of the cell in order to rotate the shaft. This motor is equipped with two gear speeds of 40 - 400 rpm and 200 - 2000 rpm. A speed of 600 rpm is suitable for complete agitation of the phases inside the cell.

The stirrer shaft is connected to the Heidolph motor at the top and the stirring mechanism is connected at the bottom of the top flange of the cell body. Figure 5-8 shows the agitation system used in this study.

Figure 5-8. Photograph of the Heidolph motor with the shaft connected to the top flange of the cell.

As observed in Figures 5-9 and 5-10, the stirring device consists of a neodymium magnet and four removable blades to mix the equilibrium phases inside the cell. The length, height and width of each blade are 5, 13, and 1 mm, respectively. As shown in Figure 5-10, the four blades are attached to an external magnet which has an external diameter of 28 mm, internal diameter of 17 mm and a height of 10 mm. A gold plate is used to cover the surface of the stirrer device to decrease the friction which is created from the high magnetic field between the stainless steel shaft and neodymium magnet inside the stirrer device. This agitation system is highly effective especially with the high stirring speed and power to mix the gas, liquid and hydrate phases inside the cell. This leads to reduced time for gas hydrate formation / dissociation compared to agitation with magnetic stirrer bars.

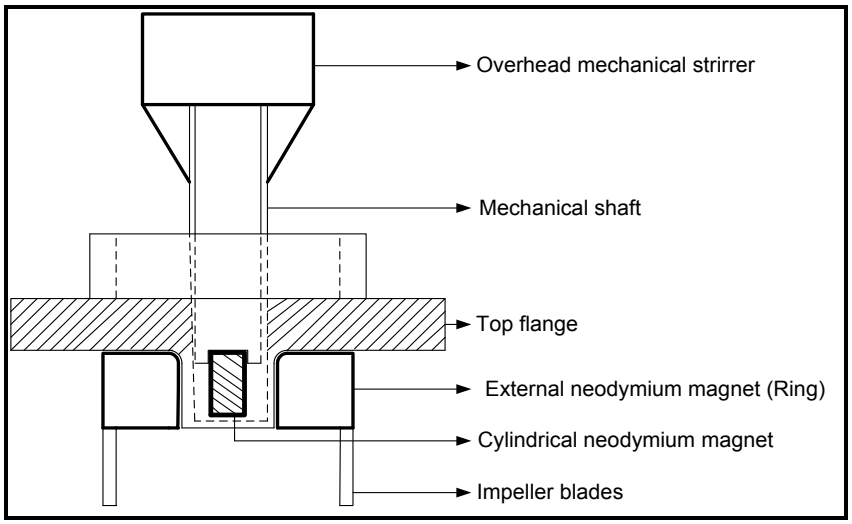

Figure 5-9. A schematic diagram of the stirring mechanism.

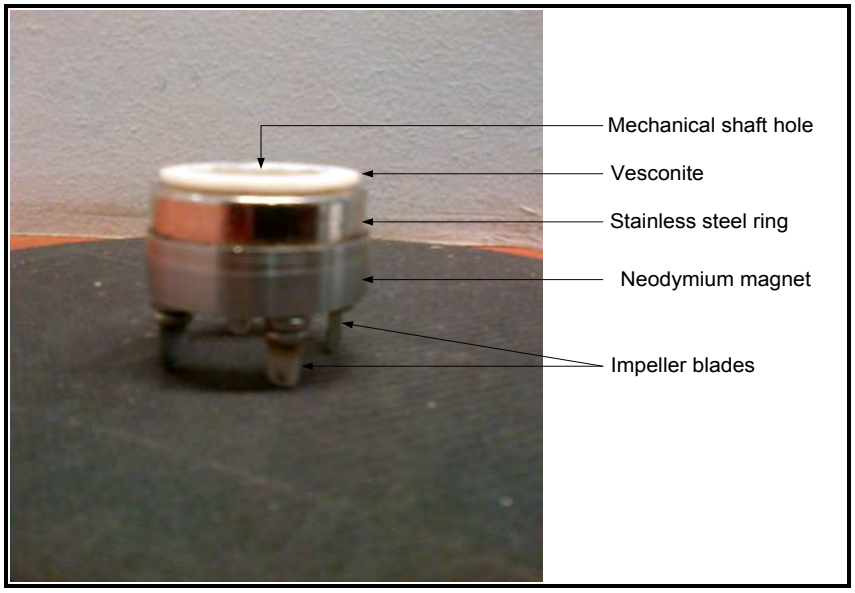

Figure 5-10. Photograph of the agitation device (with neodymium magnets).

5.2.3. The liquid thermostated bath

The cell is maintained at a constant temperature using a thermostated bath which is constructed from 316 stainless steel. The bath with dimensions of 43 cm length, 35 cm width and 26 cm height is filled with 50/50 mass ratio of ethylene glycol and water solution which is suitable to

operate in the temperature ranges of 228 to 397 K. The cell is immersed in the bath to prevent the heat from transferring from the environment to the cell. The top surface of the water bath is covered using polystyrene foam to avoid heat loss or gain from the surroundings. A 1.5 ton mechanical jack is used to lift and lower the water bath which is housed in a steel frame.

5.2.4. Temperature Controllers

Temperature of the bath is controlled using a Model TXF200 programmable controller supplied by PolyScience®. This temperature controller includes an immersion circulator pump with an internal temperature probe to heat or cool the bath liquid with an operating temperature range of 243.15 K to 323.15 K. The data software supplied by Labwise® was used to provide stepwise heating/cooling programs or specified rates of cooling/heating during hydrate formation/dissociation.

An immersion cooler or cold finger supplied by PolyScience® which consists of an evapourator, condenser, compressor and throttling valve is used to cool the liquid bath. This chilling unit can decrease the bath temperature down to 173.15 K.

In order to compensate for temperature fluctuations, the temperature of the pressure transducer is maintained at the maximum estimated environmental temperature, 313.15 K, using a heated stainless block. A heating cartridge (with a 7 mm diameter and 40 mm length) is placed in a heating block housing the pressure transducer.

5.2.5. Temperature Probe

The WIKA model REB Pt-100 temperature probe with an accuracy of 0.05 K is used to measure the equilibrium temperature in the equilibrium cell. The temperature probe is placed at top of the bottom stainless steel flange and is connected to a 34972A LX Agilent data acquisition system. The temperature is monitored along with the time and the data is logged every 2 minutes using the data acquisition system.

5.2.6. Pressure Transducer

A WIKA pressure transducer (0-16 MPa) with an accuracy of 0.05%, stated by the manufacture, is used to measure the pressure of the cell. The pressure transmitter is connected to the cell via a 1/16 inch stainless steel line. The pressure is monitored along with the time and the data is logged every 2 minutes using the 34972A LXI Agilent data acquisition system.

5.3. Preparation of the set-up before hydrate measurements

In order to produce accurate and reliable experimental data, the set-up must be prepared for hydrate measurements. The preparation consists of the following: cleaning the equilibrium cell, leak testing the equilibrium cell and the adjoining lines, calibration of the temperature and pressure sensors, and vapour pressure checks.

5.3.1. Cleaning the equilibrium cell

Before performing experiments, the equilibrium cell and all connecting lines should be cleaned and washed to decrease the effect of any contamination on the measurement results. For this purpose, the cell was washed using double-distilled and deionised water from Direct-Q5 Ultrapure Water Systems (Millipore^{TM}) with an electrical resistivity of 18 MΩ·cm to remove the effect of any impurity. Then using high pressure nitrogen, the water inside the cell was drained from the bottom of the cell by opening the drain valve. The cell and the connecting lines were then evacuated using an Edwards vacuum pump to 0.00039 MPa for thirty minutes to eliminate air and any volatile substances in the cell. After cleaning of the cell, the apparatus was deemed ready to start measurements.

5.3.2. Leak test

Before performing any calibration or measurement, it is important to ensure that there is no leak in the system. The leak test was performed after connecting all lines and fittings in the set-up.

To start the leak test, the equilibrium cell was filled with nitrogen to 13 MPa. Then, the temperature was kept constant at 298.15 K to eliminate the effect of temperature fluctuations on the pressure reading. The effect of a leak was determined by a decrease in the pressure reading over 15 hours. To find the leak, a leak detecting fluid (SNOOP®) was used on the all the connections and fittings. The leak was determined by the existence of bubbles around a fitting as a result of gas exiting from that connection point. The fitting was tightened or covered with thread tape or sealed using Loctite to eliminate the problem. If using Loctite on the fitting, the equilibrium cell and all fittings were evacuated to confirm that the Loctite on the mentioned fitting had dried. An additional test was also performed in order to identify any leakage in the system in which the equilibrium cell was left under vacuum for 15 minutes at the pressure of 0.00039 MPa. Any increase in the pressure of the cell would show a possible leakage in the system.

5.3.3. Pressure calibration

A standard pressure calibration device, model CPH 6000 supplied by WIKA was used to calibrate the pressure transducer. The standard pressure transducer was suitable in the range 0 to 25 MPa with an uncertainty of ±0.006 MPa. As mentioned before, the pressure transducer was kept at the temperature of 313.15 K to eliminate the effect of environmental temperature fluctuations on the pressure reading. During the pressure calibration, the temperature of the equilibrium cell was kept at a constant temperature of 298.15 K. Pressure calibrations were performed in the pressure range of 0.35 to 14.5 MPa. For this purpose, after stabilizing the temperature to 298.15 K, nitrogen was loaded into the cell and left to stabilise. After stabilization of the pressure, the pressure readings from the pressure transducer and the standard pressure transducer were recorded. For each point, data was collected for three minutes and then averaged. Pressure calibrations were executed step by step from low to high pressures initially and then vice versa. Finally, the pressure transducer measurements were plotted against the standard pressure measurements and a first order polynomial was fitted to the data points. A first order relation between the reading of the standard device and pressure transmitter on the apparatus is presented in Figure 5-11. In addition the deviation of the sensor from the standard pressure is plotted in Figure 5-12. As observed in this figure, the maximum pressure deviation from the standard pressure is about 1.8 kPa.

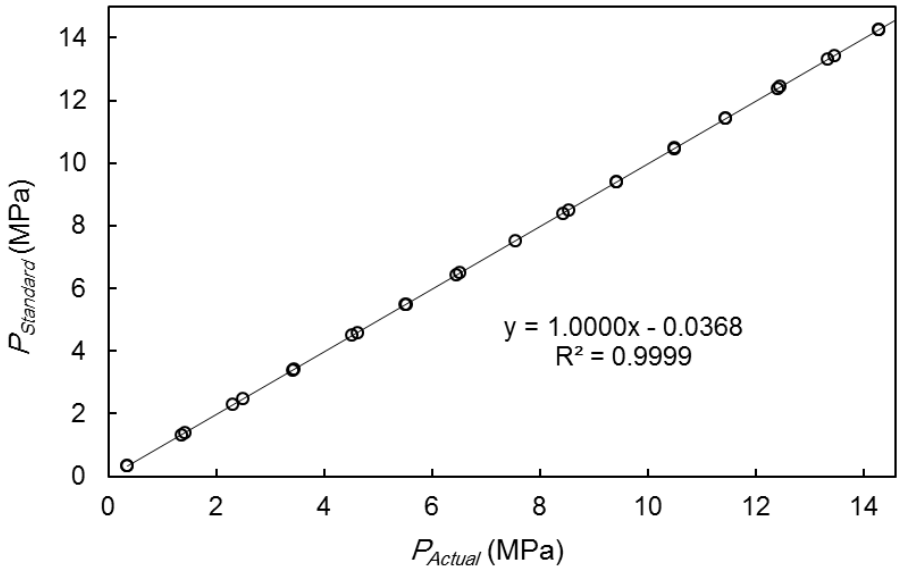

Figure 5-11. Calibration of the WIKA pressure transducer (0-16 MPa) used in this study. A first order relation between standard and transducer pressure was achieved. These results were performed in June 2013 and verified in February 2014.

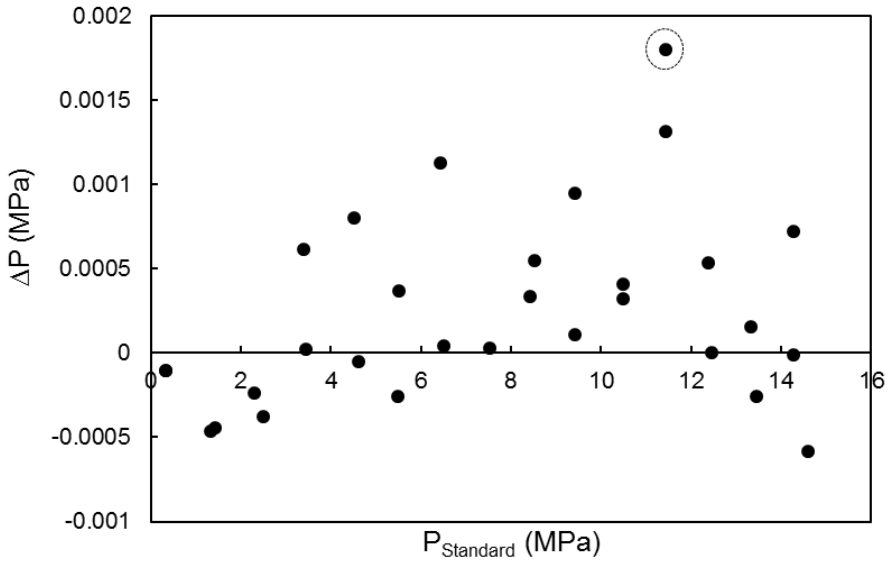

Figure 5-12. Deviations from the standard pressure due to first order relation with the maximum deviation of ±1.8 kPa.

5.3.4. Temperature calibration

A standard temperature calibration unit, model CTH 6500 supplied by WIKA was used to perform the temperature calibrations. The accuracy of the standard temperature probe is 0.03 K, as stated by the manufacture, over the temperature range of 73.15 K to 473.15 K. During the temperature calibration, the temperature readings were recorded from the temperature probe and the standard temperature probe at specified temperatures. Temperature calibrations were executed in the temperature range of 269 K to 315 K, over three times from low to high temperature and vice versa, step by step. For each point, the temperature was read 10 times from the standard calibration device and temperature probe (Pt100 probe) for two minutes and the values were thereafter averaged. Finally, the actual temperature measurements were plotted against the standard temperature measurements and a first order polynomial was fitted to the data points, which are shown in Figure 5-13. Deviations from the standard temperature due to first order relation are plotted in Figure 5-14. As can be observed in this figure, the maximum temperature deviation from the standard temperature probe is about 0.03 K.

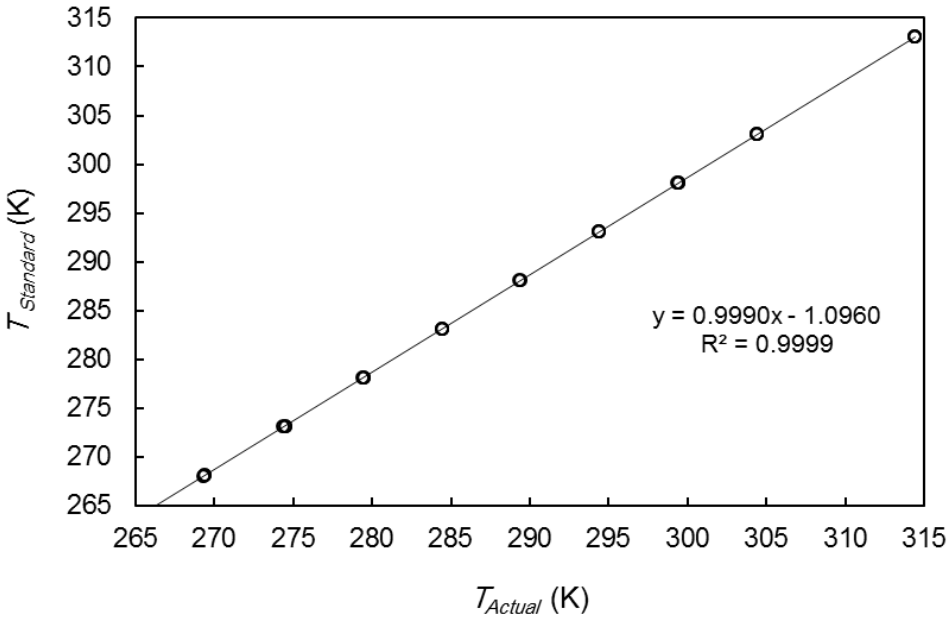

Figure 5-13. Calibration of the Pt-100 temperature probe used in this study. A first order relation between standard and used temperature probe was achieved. These results were performed in June 2013 and verified in February 2014.

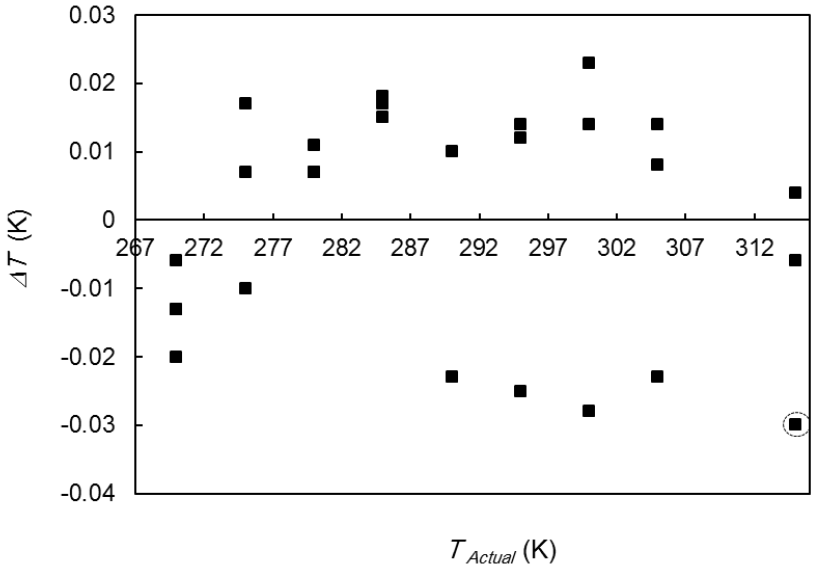

Figure 5-14. Deviations from the standard temperature due to first order relation, with maximum deviation of ±0.03 K.

5.3.5. Vapour Pressure Measurement Test

In this study, to test the reliability of the experimental set up, vapour pressure measurements for carbon dioxide were performed. At the start of the vapour pressure measurement, the cell was evacuated using a vacuum pump to the pressure of 0.00039 MPa for nearly 30 minutes to eliminate the air and any contamination inside the cell. The cell was thereafter immersed in the temperature controlled bath and the temperature of the system was fixed to a constant value. Then the pressure of the cell was increased by introducing CO_2 into the cell until the pressure reached a desired value. The stirrer was switched on, at a speed of 600 rpm to agitate the equilibrium phases inside the cell. To check if the equilibrium cell enclosed both liquid and gas phases of CO_2 at the specified conditions of temperature and pressure, the top valve of the cell was opened to release a little amount of CO_2 gas and then closed immediately. If the pressure of the cell was raised back to its original value, it meant that the two phase equilibrium condition had been achieved; else more gas should be injected into the cell. The equilibrium vapour pressure conditions were obtained when the pressure was stabilized at the constant temperature. Figure 5-15 and Table 5-2 show the results for the CO_2 vapour pressure measurements obtained in this study. The deviation in pressures between the experimental data obtained in this work and those reported in the literatures (Yarym-Agaev, 1999, Yucelen and Kidnay, 1999, Roebuck

et al., 1942) is about 35.34 kPa. As seen in this Figure 5-5, there is a reasonable agreement between the experimental data obtained in this study and those reported in the literature.

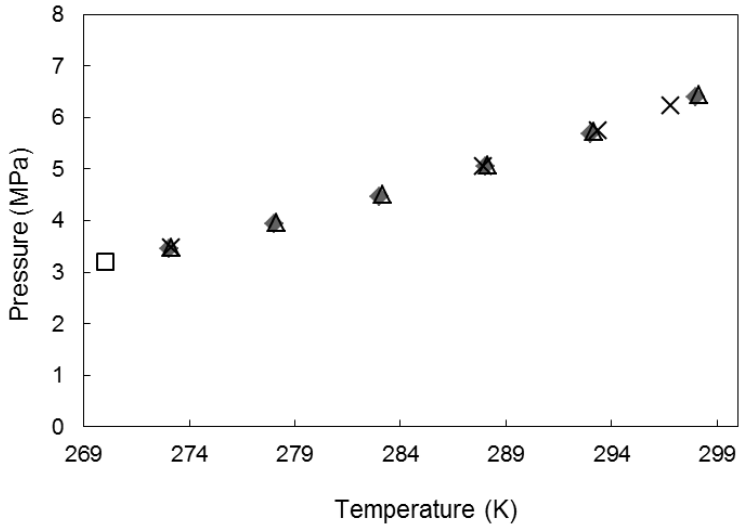

Figure 5-15. Carbon dioxide vapour pressure measurement: ♦, this study; ×, Roebuck et al. (1942) (Roebuck et al., 1942); □, Yucelen and Kidnay (1999) (Yucelen and Kidnay, 1999); Δ, Yarym-Agaev (1999) (Yarym-Agaev, 1999);

Table 5-2. Vapour pressure data for CO_2.

This study		[a] Literature data	
T/K	P/MPa	P/MPa	[b] ΔP/MPa
298.0	6.41	6.44	0.03
293.0	5.70	5.73	0.03
288.0	5.05	5.08	0.03
283.0	4.47	4.50	0.03
278.0	3.94	3.97	0.03
273.0	3.46	3.49	0.03

[a] References: (Yucelen and Kidnay, 1999, Yarym-Agaev, 1999, Roebuck et al., 1942) [b] To compare the vapour pressure data obtain in this study with the literature, a line was fitted to the literature data which makes the Δ P more than the accuracy. In addition mistake in the calibrations and low-accuracy of measurements in literature may have caused increasing the ΔP.

[c] $\Delta P = |P_{experimental} - P_{literature}|$

5.4. Experimental procedure for gas hydrate measurements

The experimental measurements in this study are classified in two groups: measurement of hydrate dissociation points and the kinetic measurement of gas hydrate formation. In this section, the procedures for these measurements are explained.

5.4.1. Experimental procedures for measurements of hydrate dissociation points

At the start of the measurements, the cell was evacuated to a pressure of 0.00039 MPa using an Edwards vacuum pump for approximately 30 minutes to eliminate air and any impurities from previous experiments. Thereafter, approximately 16 cm^3 of the aqueous solution (pure water or TBAB aqueous solutions) was introduced to the cell using the injection line which was installed at the bottom of the cell. The cell was evacuated again to eliminate any trace of air. Then the equilibrium cell was immersed inside the bath and the initial temperature fixed to a value far from the hydrate stability region. The pressure of the cell was thereafter increased by introducing the hydrate former (Xe, Kr, Ar, or CF_4) into the cell. Once the pressure and temperature of the cell had stabilised, the stirrer was then switched on at a speed of 600 rpm to agitate the phases inside the cell. After the pressure was stabilized during the solubility of gas in water, the temperature controller was set to 6-7 K below the estimated hydrate dissociation temperature. This process is known as the cooling curve. Hydrate / semi-clathrate hydrate formation was determined by the sharp drop in the pressure due to the encapsulation of the gas molecules inside the hydrate cavities. After the hydrate was formed and the pressure was stabilized, the temperature of the equilibrium cell was then increased in a step-wise manner, known as the heating curve. With an increase in the temperature, the hydrate dissociates and the encapsulated gas is released from the cavities which lead to an increased pressure reading. From the beginning of the heating curve and proceeding closer to the dissociation point, the temperature steps are approximately 1 K per each hour. A step-change of 0.1 K per hour was used in the vicinity of the dissociation point. Figure 5-16 shows an example of a primary cooling and heating curve for the semi-clathrate hydrate of argon with 0.2 mass fraction of aqueous TBAB solution. It can be seen in this figure, that the point corresponding to the sharp change of the slope of the pressure−temperature plot is determined as the final dissociation

point (Javanmardi et al., 2012, Chapoy et al., 2004, Mohammadi et al., 2005, Tumba et al., 2013). In other words, before the final dissociation point, with an increase in the temperature, the slope of pressure-temperature diagram will change to a greater value due to hydrate dissociation. However after the final dissociation point, with an increase in the temperature, pressure does not change too much; it is only a function of temperature. This slope change specifies the final dissociation point. Changes in the temperature and pressure during the hydrate formation and dissociation are shown in Figures 5-17 and 5-18, respectively.

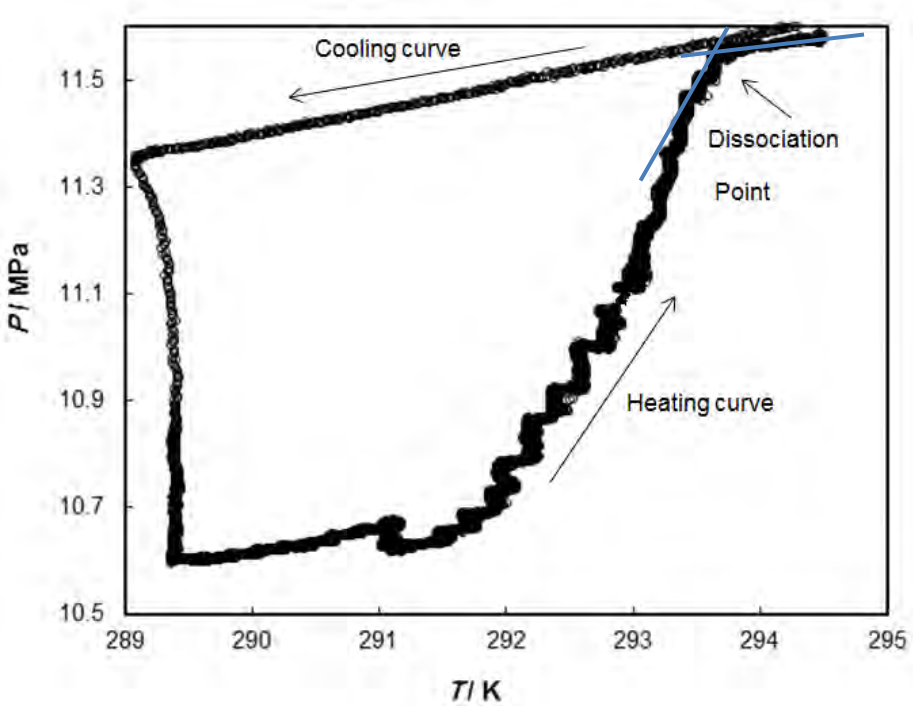

Figure 5-16. An example of the primary cooling and heating curve for the semi-clathrate hydrate of argon and 0.20 mass fraction of TBAB aqueous solution.

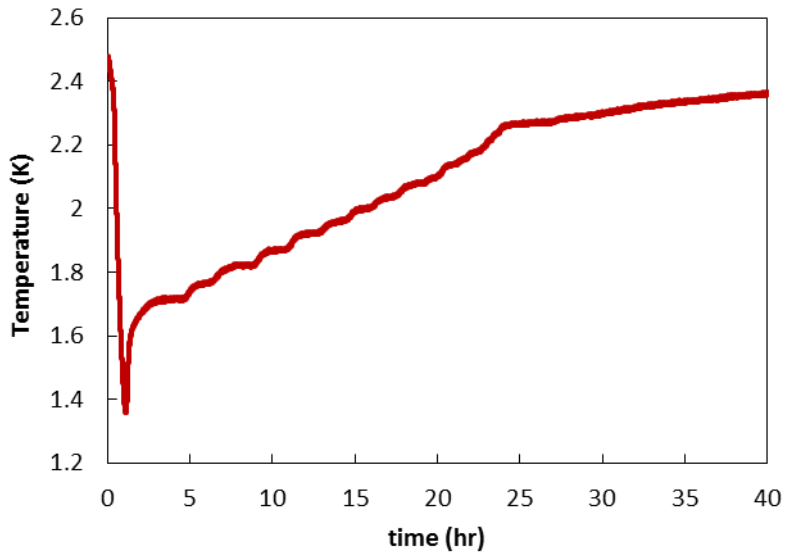

Figure 5-17. Change in the temperature during hydrate formation and dissociation for the semi-clathrate hydrate of xenon and 0.20 mass fraction of TBAB aqueous solution.

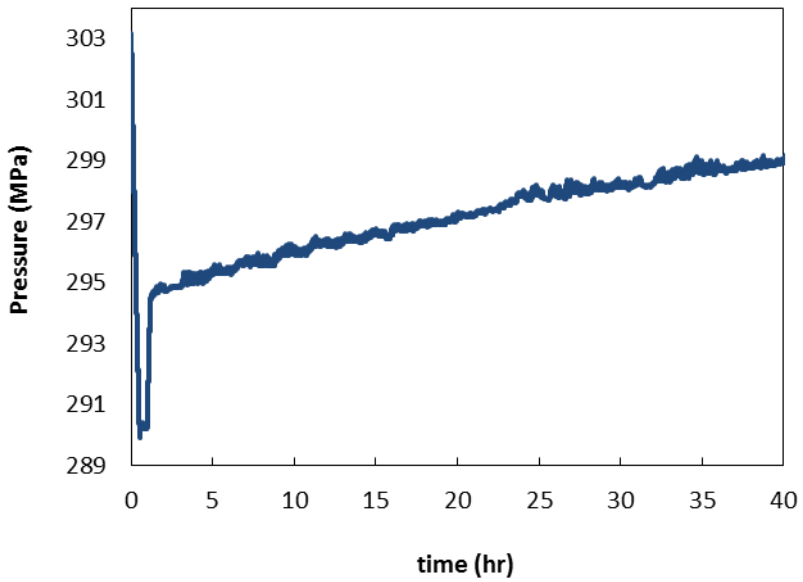

Figure 5-18. Change in the pressure during hydrate formation and dissociation for the semi-clathrate hydrate of xenon and 0.20 mass fraction of TBAB aqueous solution.

5.4.2. Experimental procedures to assess the kinetic behaviour of gas hydrate formation

The kinetics of gas hydrate formation was studied in this work. For this purpose the effect of the initial temperature and initial pressure on the rate of gas hydrate formation, the apparent rate constant of hydrate reaction, water to hydrate conversion, gas consumption and storage capacity were studied. Many factors can affect the kinetics of hydrate formation which consists of: cell volume, shape of equilibrium cell, the amount of aqueous solution, water history, stirrer speed, initial pressure and initial temperature. To study the effect of the initial pressure and temperature on the kinetics of hydrate formation, all the aforementioned parameters were kept constant except the initial temperature and pressure conditions. At the start of the measurements, the cell was washed using double-distilled and deionised water from Direct-Q5 Ultrapure Water Systems (Millipore^{TM}). Then the cell was evacuated to a pressure of 0.00039 MPa using an Edwards vacuum pump for approximately 30 minutes to eliminate air and any impurities. Thereafter, approximately 16 cm^3 of the pure water was introduced to the cell using the injection line installed on the bottom of the cell. In order to eliminate the effect of the history of the water used in the kinetic measurements, new and fresh water was used in each experiment. Hence water from previous experimental runs could not be used. The cell was then evacuated again for a short time (about 1 minute) to remove any air and contaminants. Thereafter, the cell was immersed inside the thermostated bath and the temperature was set to the desired temperature inside the hydrate stability region at the expected hydrate pressure. After the temperature of the cell had stabilized, the hydrate former was introduced slowly into the cell to pressurize the cell to the desired pressure. It is important that the initial pressure and temperature were within the hydrate stability region. After the cell was pressurized, the valve for loading the gas was closed and the stirrer was switched on at a speed of 520 rpm for the kinetic measurements of CF_4 and 430 rpm for the kinetic measurements of semi-clathrate hydrate of Ar + TBAB + water. Due to hydrate formation inside the cell and the encapsulation of gas molecules inside the hydrate cavities, the pressure decreases continuously until it reaches a steady state condition. The gas consumption through the hydrate formation is estimated using the VPT EoS (Valderrama, 1990).

5.4.3. Shutdown the procedure

Once the hydrate measurements were complete, the devices used in the experiments, such as the stirrer, the cold finger, the temperature controller and the data acquisition system were switched off. Thereafter, the drain line was opened to remove the aqueous solution from the cell and then closed. Afterwards, the system was vented and then evacuated by opening the valve to exit the cell to the suction device was opened to empty the cell. Lastly, the cleaning method which was explained earlier in Section 5.3.1 was performed for cleaning and preparation of the set-up for the next measurement.

5.5. NIST uncertainty analysis for the measurement of the hydrate dissociation experimental data.

Systematic and random errors are the restriction of the measuring device and the skill of the experimenter making the measurements, respectively. These two factors can affect the uncertainty of the experimental measurements. The uncertainty of the experimental measurement is defined as the interval around an experimental data point which related to the accuracy of that point (Taylor, 2009). Hence, if the measurement of the data point was repeated at the same condition, the result should lie within the stated interval. Expressing the uncertainties of the experimental measurements presents a good comparison between the results obtained from different researchers and laboratories in the same area of measurements as well as comparison of the obtained result with the standard reference values. This comparison allows the user/s to judge the accuracy of the experimental data and select those with higher accuracy to produce a more reliable thermodynamic model and avoid repetition in uncertainties of experiments if differences are not significant (Birch, 2003). The difference between the experimental test result and the stated value for the specific property should lie inside the uncertainty range (Birch, 2003).

5.5.1. Estimation of Uncertainties

In experimental measurements, prior to reporting the measured data, it is significant to identify and report the effect of all sources of uncertainties on the measurements. Based on the NIST guidelines, to estimate the uncertainty of measurements, two methods of type A and type B exist. In type A, the standard deviation of the mean of a series of independent observations can be calculated using a statistical method such as least squares to fit a curve to data in order to evaluate the parameters of the curve and their standard deviations. For instance, in the case of an input quantity (X_i) which depends on n independent parameters of $X_{i,k}$, the uncertainty is calculated using the standard deviation as shown below:

$$u\ (x_i) = \left(\frac{1}{n(n-1)} \sum_{k=1}^{n} \left(X_{i,k} - \overline{X}_i \right)^2 \right)^{1/2} \qquad (5\text{-}1)$$

where:

$$\overline{X}_i = \frac{1}{n} \sum_{k=1}^{n} \left(X_{i,k} \right) \qquad (5\text{-}2)$$

Uncertainties in the repeatability of temperature and pressure in type A come from the instrument manufacturer error. From temperature and pressure recordings taken every 30 seconds for 30 minutes at a steady state condition and using the equations above, the repeatability of the temperature and pressure can be estimated. In Type B, estimation of the uncertainty is based on all the available information related to the measurements such as previous measurement data, manufacturer's specification, and results from calibrations and uncertainties assigned to reference data taken from handbooks. Evaluation of the uncertainty for temperature and pressure, using type B method, comes from the polynomial used in the calibrations as well as the manufacturer's specifications. The overall uncertainty of the pressure and temperature in this study is including the uncertainty of standard calibration device as well as the uncertainty of the measuring devices (temperature probe or pressure transducer). Based on the NIST guide, the following equation should be taken for estimation of the overall uncertainty:

$$u_c(x) = \pm \sqrt{\sum_i u_i(x)^2} \qquad (5\text{-}3)$$

According to above equation, the following equation was applied in this study for evaluation of temperature and pressure uncertainties:

$$u_c(x) = \pm\sqrt{u_{instrument}(x)^2 + u_{calibration}(x)^2 + u_{repeatability}(x)^2} \quad (5\text{-}4)$$

where, $u_{intrument}$ shows the standard uncertainty of the temperature probe or pressure transmitter, and $u_{calibration}$ indicate the uncertainty of calibration. In addition, $u_{repeatibility}$ and $u_{reproducibility}$ in Equation 5-4 are the standard uncertainty come from repeatability and reproducibility, respectively in type A. The rectangular distribution was used for the estimation of instrument and calibration uncertainties by the following equation:

$$u_{calibration}(x) = \frac{b}{\sqrt{3}} \quad (5\text{-}5)$$

$$u_{instrument}(x) = \frac{b}{\sqrt{3}} \quad (5\text{-}6)$$

$$b = \left(\frac{a_+ \pm a_-}{2}\right) \quad (5\text{-}7)$$

As observed in Figure 5-12, the uncertainty for the pressure calibration was ± 0.002 MPa. In addition, in Figure 5-14 the uncertainty for temperature calibration was ± 0.03 K. Table 5-3 presents the calibration uncertainties and combined uncertainty for temperature and pressure in this study.

Table 5-3. The uncertainties in the pressure and temperature.

Calibration	a	b	$u_{calibration}$	[a] u_c (x)
Pressure transducer (0-25 MPa)	0.002	0.002	0.001 MPa	±0.01 MPa
Temperature probe	0.03	0.03	0.02 K	±0.05 K

[a] combined uncertainty in Equation 5-4

5.5.2. Reporting uncertainty

All standard uncertainty components using Type A and Type B methods, generate a combined standard uncertainty. Depending on the application of experimental data, it is usually necessary

to expand the combined standard uncertainty, $u_c(x)$, by multiplying the combined standard uncertainty by a coverage factor, k, to produce expended uncertainty, U(x), as in the following equation: (Birch, 2003)

$$U(x) = k u_c(x) \qquad 5\text{-}7$$

A greater interval for the experimental measurement is provided using the expanded uncertainty instead of the combined standard uncertainty. In this report, a coverage factor of unity (k=1) was used in order to produce more accurate experimental data.

6

CHAPTER SIX: RESULTS AND DISCUSSION

The aim of this chapter is to provide the main results from the research carried out in this study. The results are categorised into two groups of experimental measurements and thermodynamic modelling. The major aim of this study was to investigate the effect of aqueous TBAB solution as a promoter on the argon (Ar)/ krypton (Kr)/ xenon (Xe) or tetrafluoromethane (CF_4) hydrate phase equilibria. In the experimental measurement section, experimental hydrate dissociation data for Ar /Kr /Xe/ CF_4+ aqueous TBAB solution are reported followed by the kinetic studies on CF_4 and Ar hydrate formation. The kinetic study included estimation of the apparent rate constant, rate of hydrate formation, mole consumption, storage capacity, and water to hydrate conversion during the hydrate formation. The effect of initial temperature, initial pressure, and concentrations of aqueous TBAB solutions and SDS solutions on the semi-clathrate hydrate of Ar + TBAB + water are investigated. In the thermodynamic modelling section, measured hydrate/semi-clathrate hydrate phase equilibria for the system of Ar /Kr /Xe/ CF_4+ TBAB + water were regressed using the aforementioned methods explained in Chapter three.

6.1. Experimental measurements of the hydrate/semi-clathrate hydrates dissociation conditions

In this thesis, experimental hydrate/semi-clathrate hydrate dissociation data for the system of (TBAB + H_2O), (CF_4 + H_2O + TBAB), (Ar + H_2O + TBAB), (Kr + H_2O + TBAB), and (Xe + H_2O + TBAB) with varying concentrations of aqueous TBAB solutions were measured.

Table 6-1. Hydrate/ semi-clathrate hydrate systems along with temperature and pressure ranges.

System [a]	Temperature ranges (K)	Pressure ranges (MPa)	NDP[b]
TBAB + H_2O	276.7 to 285.6	0.0998 [c]	4
Ar + H_2O	274.0 to 276	10.66 to 12.08	4
Kr + H_2O	274.1 to 294.2	1.44 to 11.97	7
Xe + H_2O	296.9 to 310.6	1.70 to 10.09	11
CF_4 + H_2O	273.8 to 278.3	4.55 to 11.57	12
Ar + (0.05 TBAB + 0.95 H_2O)	275.8 to 287.6	0.34 to 11.56	7
Ar + (0.10 TBAB + 0.90 H_2O)	280.4 to 290.7	0.51 to 12.32	7
Ar + (0.20 TBAB + 0.80 H_2O)	283.0 to 293.6	0.51 to 11.55	8
Ar + (0.30 TBAB + 0.70 H_2O)	285.9 to 293.1	1.09 to 9.82	8
Kr + (0.05 TBAB + 0.95 H_2O)	279.0 to 292.1	0.24 to 6.05	7
Kr + (0.10 TBAB + 0.90 H_2O)	280.8 to 296.0	0.22 to 8.43	9
Kr + (0.20 TBAB + 0.80 H_2O)	284.6 to 297.1	0.22 to 8.34	8
Xe + (0.10 TBAB + 0.90 H_2O)	282.9 to 304.9	0.15 to 4.73	10
Xe + (0.20 TBAB + 0.80 H_2O)	284.7 to 302.3	0.12 to 3. 86	9
Xe + (0.30 TBAB + 0.70 H_2O)	285.9 to 303.1	0.13 to 3. 87	10
CF_4 + (0.05 TBAB + 0.95 H_2O)	274.6 to 277.6	5.00 to 9.55	5
CF_4+ (0.10 TBAB + 0.90 H_2O)	274.1 to 275.3	4.86 to 6.51	4
CF_4+ (0.20 TBAB + 0.80 H_2O)	275.4 to 277.7	6.14 to 10.18	5
CF_4+ (0.30 TBAB + 0.70 H_2O)	284.7 to 285.4	1.03 to 6.24	7

[a] mass fractions stated; [b] Number of Data Points; [c] Atmospheric pressure

The aim of this study was to investigate the effect of TBAB as a promoter on the hydrate phase equilibrium conditions. Table 6.1 summarizes the investigated hydrate/ semi-clathrate hydrate systems and their temperature and pressure ranges.

6.1.1. Test system

In order to test the reliability of the experimental procedure used in this study, four dissociation data points for carbon dioxide hydrate were measured. Table 6.2 and Figure 6.1 show the experimental carbon dioxide hydrate dissociation conditions in the temperature range of 274.2 to 281.4 K and pressure range of 1.31 to 3.34 MPa.

Table 6-2. Experimental CO_2 hydrate dissociation conditions.

T_{exp} (K)	P_{exp} (MPa)
274.2	1.31
278.2	2.22
280.2	2.87
281.4	3.34

[a] Combined standard uncertainty, u_c, in T, P are u_c (T_{exp}) = ±0.1 K and u_c (P) = ±0.01 MPa, respectively.

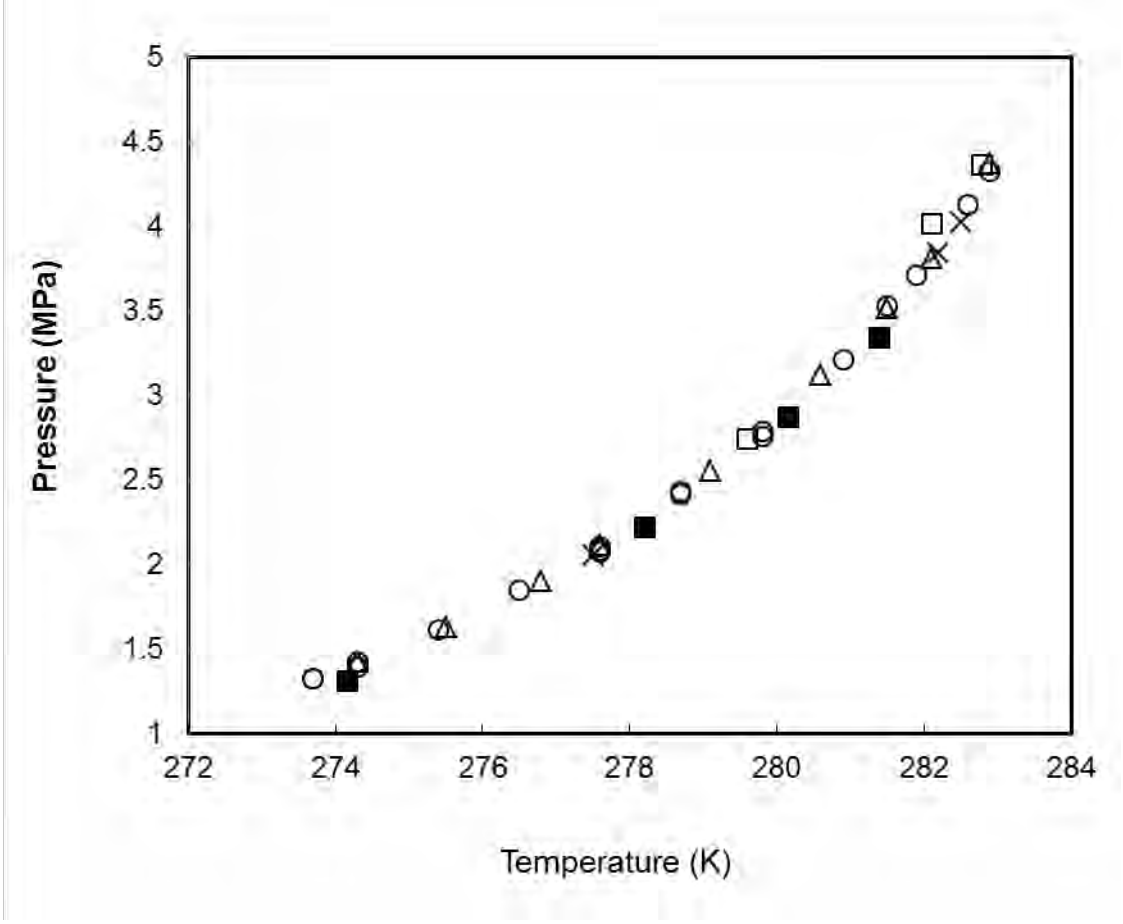

Figure 6-1. Experimental hydrate dissociation conditions for the carbon dioxide + water system. The symbols represent the experimental data: ■, this work; ○, (Frost and Deaton, 1946); □, (Ng and Robinson, 1985); Δ, (Adisasmito et al., 1991); ×, (Mohammadi et al., 2005).

As shown in Figure 6-1, there is reasonable agreement between the measurements in this study and those from the literature (Frost and Deaton, 1946) which confirms the reliability of the experimental apparatus and the procedure in this study.

6.1.2. TBAB + H_2O system

As mentioned earlier, semi-clathrate hydrates can form with the addition of additives such as tetrabutylammonium bromide (TBAB) to water even without any gas molecule. The semi-

clathrate hydrate formation at low pressure conditions (near atmospheric pressure) makes them attractive alternatives to conventional clathrate hydrates (Oyama et al., 2005, Shimada et al., 2003). It should be noted that at low pressure conditions near the atmospheric pressure, gas molecules cannot be trapped inside the semi-clathrate cavities and only semi-clathrate hydrate of TBAB + water (without the gas molecule) is formed. Consequently, the gas mixtures can not be separated at such conditions and then higher pressure conditions are required for this purpose. In this study, semi-clathrate hydrate dissociation conditions for the system of TBAB + H_2O were measured in order to distinguish the equilibrium temperatures in which semi-clathrate hydrate of water + TBAB can be formed. At this pressure and temperature condition, the gas molecules cannot be trapped inside the semi-clathrate hydrate of Table 6-3 reports the experimental semi-clathrate hydrate dissociation conditions for the system of TBAB + H_2O measured in this study.

Table 6-3. Experimental semi-clathrate hydrate dissociation conditions for the system TBAB + H_2O at the pressure of 0.1 MPa.

[a] TBAB Concentration (mass fraction)	T_{exp} (K)
0.05	276.7
0.1	280.1
0.2	282.5
0.3	285.2

[a] Combined standard uncertainty, u_c, in T, P, x_{TBAB} in mass fraction are u_c (T_{exp}) = ±0.1 K, u_c (P) = ±0.01 MPa, and u_c (x_{TBAB}) = 0.0002, respectively.

Figure 6-2 represents the experimental semi-clathrate hydrate dissociation conditions for the system of TBAB + H_2O, at the pressure of 0.1 MPa measured in this work and those from literature (Lipkowski et al., 2002, Oyama et al., 2005, Deschamps and Dalmazzone, 2009, Darbouret et al., 2005). As seen in Figure 6-2, there is a good agreement between the experimental and literature data. Depending on the temperature conditions and the initial concentration of TBAB in aqueous solution, TBAB can form different hydrate crystal structures (Lipkowski et al., 2002). Due to its complexity, the structure of TBAB is not yet well understood. In fact, it is still addressed by on-going scientific investigations.

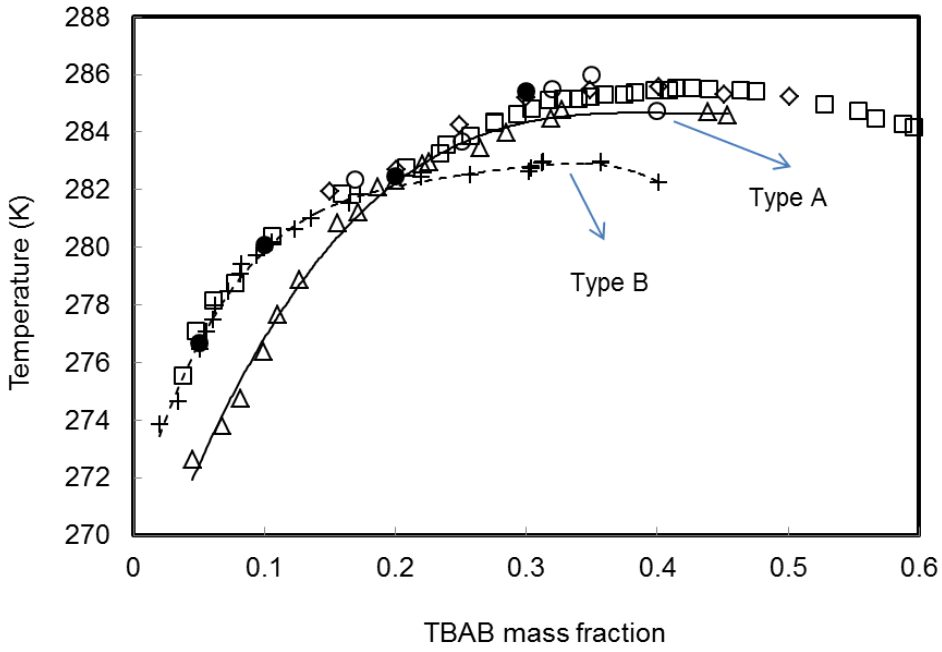

Figure 6-2. Semi-clathrate hydrate phase diagram for the system of TBAB + H_2O at the pressure of 0.1 MPa. The symbols represent the experimental data: ●, This work; Δ, (Oyama et al., 2005) (with the hydration number of 26); +, (Oyama et al., 2005) (with the hydration number of 38); □, (Lipkowski et al., 2002); ○, (Deschamps and Dalmazzone, 2009); ◊, (Darbouret et al., 2005), ▬, Trend line for type A, ----, Trend line for type B.

As shown in Figure 6-2, two types of crystalline structures of TBAB exist, type A and type B, both able to form at atmospheric pressure. Crystals of type A have been described to have a columnar (tetragonal) shape with higher hydrate equilibrium temperature compared to type B with an undefined (orthorhombic) form composed of thin crystals (Dyadin and Udachin, 1984, Oyama et al., 2005). As shown in Figure 6-2, the intersection between the semi-clathrate hydrate equilibrium curves for the two crystals of type A and type B can be seen at the concentration of 0.18 mass fraction of TBAB (Oyama et al., 2005). A maximum equilibrium temperature of 286 K and pressure of 0.1 MPa for the semi-clathrate hydrate curve is observed at approximately 0.40 mass fraction of TBAB for type A (Shimada et al., 2003) and approximately 0.32 mass fraction of TBAB for type B (Oyama et al., 2005).

6.1.3. Ar + TBAB + Water system

Hydrate dissociation data for the system of Ar + H_2O + TBAB were measured at 0.05, 0.10, 0.20 and 0.30 mass fraction of aqueous solution of TBAB. The measured hydrate dissociation data are summarized in Table 6-4 and presented graphically in Figure 6-3. As shown in Figure 6-3, the argon hydrate dissociation data measured in this study were compared to those reported by Marshal et al. (Marshall et al., 1964). There is a good agreement between the experimental data generated in this study and the data reported by Marshal et al. (Marshall et al., 1964). As can be seen in Figure 6-3, TBAB has a drastic promotion effect on the argon hydrates. This promotion effect on the argon hydrate formation is an advantage for the practical application of gas hydrate in gas separation technologies compared with processes using only the conventional clathrate hydrate method which is in the presence of pure water. Also, evident in Figure 6-3 is that an increase in the concentration of TBAB from (0.05 to 0.20) mass fraction, increases the promotion effects of TBAB on the argon hydrate formation significantly. Furthermore, as seen in Figure 6-3, the effect of the addition or use of the TBAB solution on the promotion of the argon hydrate at the TBAB concentrations of (0.20 and 0.30) mass fractions at high pressures is almost identical. However, at pressures lower than 7.5 MPa, a solution of 0.30 mass fraction of TBAB has a greater promoting effect on the argon hydrate compared to 0.20 mass fraction of TBAB. In order to obtain the optimal concentration of TBAB for a separation process based on semi-clathrate hydrates, some economic studies are essential.

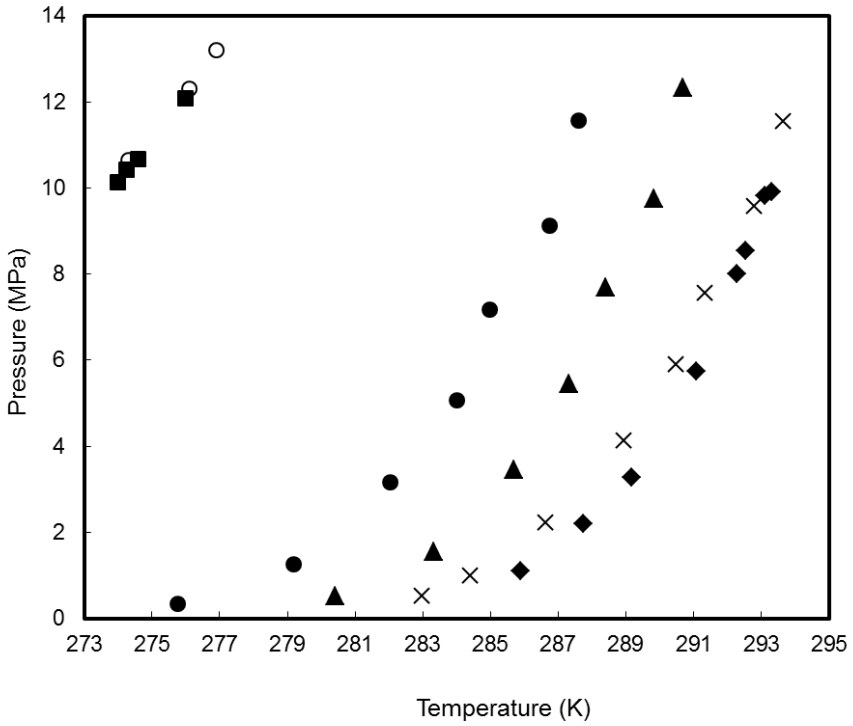

Figure 6-3. Hydrate dissociation conditions measurements for the system of argon + TBAB + water. Symbols signify experimental data: ●, This work, 0.05 mass fraction aqueous TBAB solution; ▲, This work, 0.10 mass fraction aqueous TBAB solution; ×, This work, 0.20 mass fraction aqueous TBAB solution; ♦, This work, 0.30 mass fraction aqueous TBAB solution; ■, This work, 0 mass fraction of TBAB (argon hydrate); ○, (Marshall et al., 1964), 0 mass fraction of TBAB (argon hydrate).

In addition, the experimental results show that a small increase in the hydrate equilibrium temperature causes a large increase in the hydrate equilibrium pressure. Therefore, the measurement of the hydrate dissociation conditions should be done very slowly and carefully in order to prevent the generation of erroneous experimental data. For this reason, a step-change of 0.1 K per hour was used to increase the temperature of the cell and an adequate interval time (about five hours) at each temperature step was taken during the heating procedure.

Table 6-4. Experimental hydrate dissociation conditions for the system of argon + TBAB + water.

[a] TBAB Concentration (mass fraction)	T_{exp}/K	P_{exp}/ MPa	[a] TBAB Concentration (mass fraction)	T_{exp}/K	P_{exp}/ MPa
0.00	276.0	12.08	0.20	293.6	11.55
	274.6	10.66		292.8	9.57
	274.2	10.42		291.3	7.55
	274.0	10.12		290.5	5.90
				288.9	4.11
0.05	287.6	11.56		286.6	2.22
	286.8	9.12		284.4	0.98
	285.0	7.17		283.0	0.51
	284.0	5.06			
	282.0	3.16	0.30	293.1	9.82
	279.2	1.27		292.5	8.54
	275.8	0.34		292.3	8.00
				293.3	9.91
0.10	290.7	12.32		291.1	5.74
	289.8	9.76		289.2	3.27
	288.4	7.68		287.8	2.19
	287.3	5.43		285.9	1.09
	285.7	3.44			
	283.3	1.56			
	280.4	0.51			

[a] Combined standard uncertainty, u_c, in T, P, x_{TBAB} in mass fraction are u_c (T_{exp}) = ±0.1 K, u_c (P) = ±0.01 MPa, and u_c (x_{TBAB}) = 0.0002 respectively.

6.1.4. Kr + TBAB + Water system

New experimental dissociation data for the krypton + aqueous solution of TBAB with concentrations of 0.05, 0.10 and 0.20 mass fraction of TBAB, are reported in Table 6-5 and plotted in Figure 6-4. Figure 6-4 and Table 6-5 report the krypton hydrate dissociation data in the temperature range of (274.1 to 294.2) K and pressures ranging from (0.22 to 11.97) MPa. As shown in Figure 6-4, there is a reasonable agreement between the krypton hydrate data measured in this study and those reported in the literature (Stackelberg and Meuthen, 1958, Holder et al., 1980, Dyadin et al., 1997a, Sugahara et al., 2005).

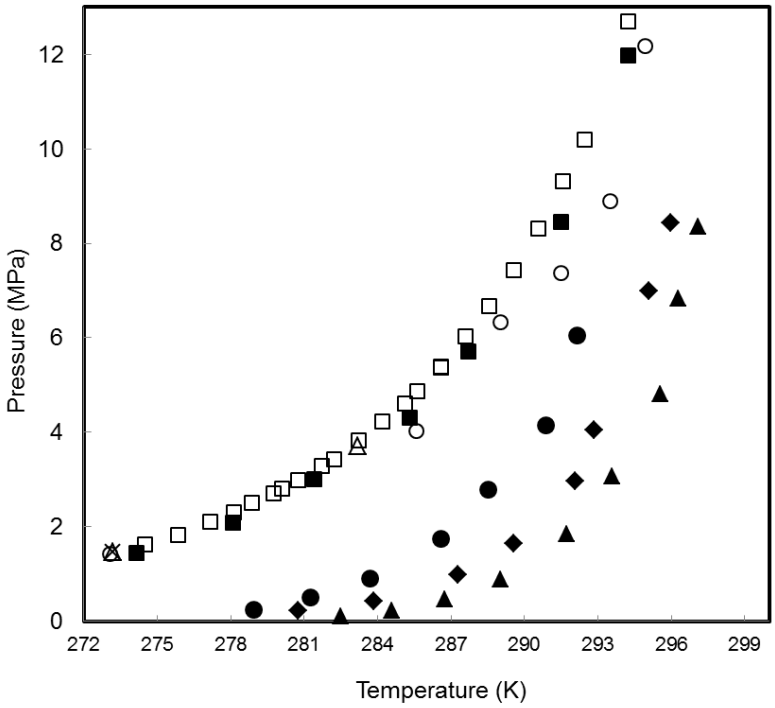

Figure 6-4. Hydrate dissociation data for the system krypton + TBAB + water. Symbols represent experimental data. 0.0 mass fraction of TBAB (krypton hydrate): ■, This work, □, (Sugahara et al., 2005), ○, (Dyadin et al., 1997a), Δ, (Holder et al., 1980), ×, (Stackelberg and Meuthen, 1958); 0.05 mass fraction of TBAB: ●, This work; 0.10 mass fraction of TBAB: ♦, This work; 0.20 mass fraction of TBAB: ▲, This work,

Table 6-5. Experimental hydrate dissociation conditions for the system of krypton + water + TBAB.

[a] TBAB Concentration (mass fraction)	T_{exp} /K	P_{exp} / MPa
0.00	294.2	11.97
	291.5	8.44
	287.7	5.70
	285.3	4.30
	281.4	3.01
	278.1	2.10
	274.1	1.44
0.05	292.1	6.05
	290.9	4.16
	288.5	2.79
	286.6	1.74
	283.7	0.91
	281.3	0.50
	279.0	0.24
0.10	296.0	8.43
	295.1	6.99
	294.1	5.41
	292.8	4.05
	292.1	2.97
	289.6	1.65
	287.3	0.98
	283.8	0.41
	280.8	0.22
0.20	297.1	8.34
	296.3	6.82
	295.6	4.81
	293.6	3.06
	291.7	1.84
	289.0	0.89
	286.7	0.46
	284.6	0.22

[a] Combined standard uncertainty, u_c, in T, P, x_{TBAB} in mass fraction are u_c (T_{exp}) = ±0.1 K, u_c (P) = ±0.01 MPa, and u_c (x_{TBAB}) = 0.0002, respectively.

As shown in Table 6-5, the experimental data are reported in the temperature range of (279 to 297.1) K and pressures ranging from (0.12 to 4.73) MPa. As shown in Figure 6-4, aqueous TBAB solutions with concentrations of 0.05, 0.10, and 0.2 mass fractions, showed a promotion

effect for krypton hydrate dissociation conditions causing a shift of the equilibrium pressure-temperature curve to lower pressures and higher temperatures. The difference between the dissociation temperature of krypton hydrate and krypton + TBAB semi-clathrate hydrate (ΔT) at the constant pressure of 1.8 MPa and at TBAB concentrations of 0.05, 0.1 and 0.2 mass fractions are 10.8 K, 13.8 K, and 15.9 K, respectively. These results indicate that with an increase in the TBAB concentration from 0.05 to 0.20 mass fractions, the promotion effect of TBAB on the dissociation condition of the krypton semi-clathrate hydrate increases. This promotion effect of TBAB is beneficial in the application of semi-clathrate hydrates for the storage of krypton as well as the separation of noble gases such as krypton, compared to the use of conventional clathrate hydrate method.

6.1.5. Xe + TBAB + Water system

In this study, xenon hydrate dissociation data were measured and compared to available experimental data in the literature (Ewing and Ionescu, 1974, Makogon et al., 1996, Dyadin et al., 1997a, Ohgaki et al., 2000) in order to examine the reliability of the experimental procedure and the experimental setup used in this study. The xenon hydrate dissociation data were measured in the temperature range of (282.9 to 310.6) K and pressures ranging from (0.12 to 10.09) MPa and are reported in Table 6-6 and Figure 6-5. There is good agreement between the data measured in this study and the data from literature (Ewing and Ionescu, 1974, Makogon et al., 1996, Dyadin et al., 1997a, Ohgaki et al., 2000).

There is good agreement between the results reported in this study and the experimental data reported by Jin et al. (Jin et al., 2012) and Garcia and Clarke (Garcia and Clarke, 2014) for the semi-clathrate hydrate dissociation conditions for the system of xenon + 0.1 and 0.20 mass fraction of aqueous TBAB solution. The results of this study show that aqueous TBAB solutions, depending on the pressure range, have a twofold effect on the xenon gas hydrate phase equilibria. As shown in Figure 6-5, at pressures below 0.73 MPa, the aqueous TBAB solution with a concentration of 0.1 mass fraction, has a drastic promotion effect on the xenon hydrate dissociation conditions. The results indicate that the difference between the dissociation temperature of xenon hydrate and xenon + TBAB semi-clathrate hydrate at the TBAB concentration of 0.1 mass fraction and the pressure of 0.34 MPa is 4.5 K. Conversely, at pressures higher than 0.73 MPa, there is no promotion effect on the xenon hydrate phase equilibria and in some cases, an inhibition effect on the xenon hydrate dissociation conditions is observed.

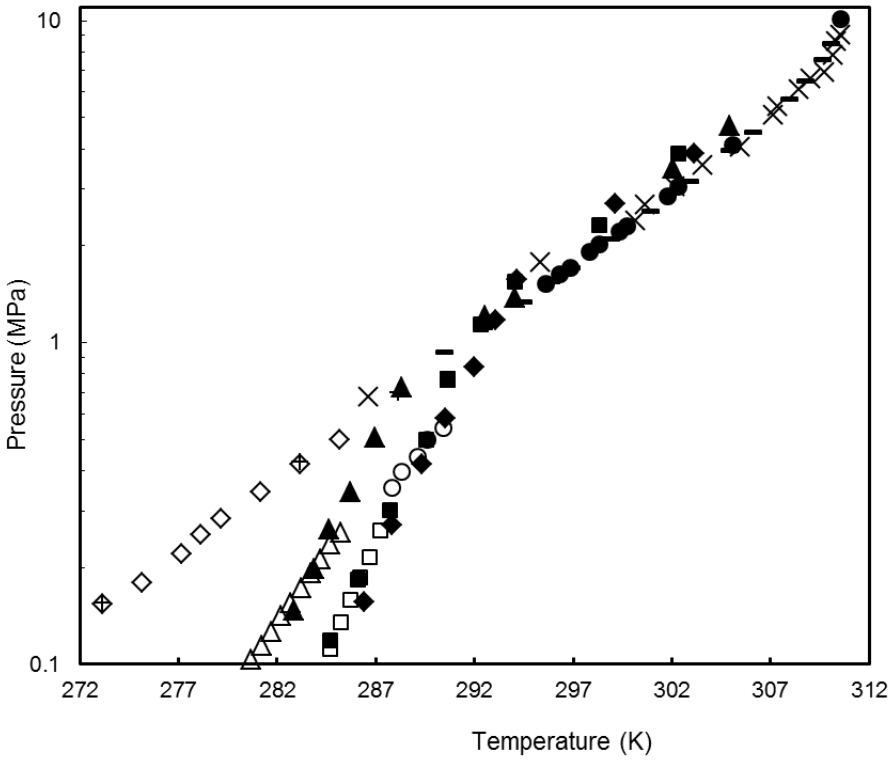

Figure 6-5. Experimental measurements of hydrate dissociation conditions for the system of xenon + TBAB + water. Symbols represent experimental data. 0.0 mass fraction of TBAB (Xe hydrate): ●, This work, ◊, (Ewing and Ionescu, 1974), +, (Makogon et al., 1996), ×, (Dyadin et al., 1997a), -, (Ohgaki et al., 2000); 0.10 mass fraction of TBAB: ▲, This work, Δ, (Jin et al., 2012); 0.20 mass fraction of TBAB: ■, This work, □, (Jin et al., 2012), ○,(Garcia and Clarke, 2014); 0.30 mass fraction of TBAB: ♦, This work.

As seen in Figure 6-5, a similar behaviour was observed for the semi-clathrate hydrate dissociation conditions for the system of xenon + 0.2 and 0.3 mass fraction of aqueous TBAB solution in which, aqueous TBAB solutions with concentrations of 0.2 and 0.3 mass fraction, showed a promotion effect for xenon hydrate dissociation conditions at pressures below (1.4 and 1.57) MPa respectively. The difference between the dissociation temperature of xenon hydrate and xenon + TBAB semi-clathrate hydrate, ΔT, at the constant pressure of 1.8 MPa and at TBAB concentrations of 0.2 and 0.3 mass fractions are 7 K, and 7.7 K, respectively. At the higher pressures, the 0.2 and 0.3 mass fraction aqueous TBAB solutions had no promotion effect on the xenon hydrate phase equilibria. The results indicate that with an increase in the

TBAB concentration from 0.1 to 0.3 mass fraction, the promotion effect of TBAB on the xenon semi-clathrate hydrate dissociation condition increases.

Table 6-6. Experimental hydrate dissociation conditions for the system of xenon + aqueous solutions of TBAB.

[a] TBAB Concentration (mass fraction)	T_{exp}/K	P_{exp}/ MPa	[a] TBAB Concentration (mass fraction)	T_{exp}/K	P_{exp}/ MPa
0.00	310.6	10.09	0.20	302.3	3.86
	305.1	4.11		298.3	2.32
	302.4	3.04		294.0	1.55
	301.8	2.86		292.3	1.14
	299.7	2.30		290.6	0.77
	299.4	2.21		289.5	0.50
	298.3	2.01		287.7	0.30
	297.9	1.92		286.1	0.18
	296.9	1.70		284.7	0.12
	296.3	1.63			
	295.6	1.52			
0.10	304.9	4.73	0.30	303.1	3.87
	302.1	3.47		299.1	2.70
	294.0	1.38		294.2	1.58
	292.5	1.21		293.1	1.18
	288.3	0.73		292.0	0.84
	286.9	0.51		290.5	0.58
	285.7	0.34		289.4	0.42
	284.6	0.26		287.8	0.27
	283.9	0.20		286.4	0.16
	282.9	0.15		285.9	0.13

[a] Combined standard uncertainty, u_c, in T, P, x_{TBAB} in mass fraction are u_c (T_{exp}) = ±0.05 K, u_c (P) = ±0.01 MPa, and u_c (x_{TBAB}) = 0.0002 respectively.

6.1.6. CF_4 + TBAB + Water system

CF_4 hydrate dissociation data are reported in Table 6-7 and compared to available experimental data in the literature (Mooijer-van den Heuvel et al., 2006, Sugahara et al., 2004, Garg et al., 1975) in Figure 6-6. The dissociation conditions for CF_4 hydrate were measured in the temperature range of (273.8 to 285.6) K and pressure ranging from (1.03 to 11.57) MPa. As can be seen in Figure 6-6, there is a good agreement between the measured CF_4 hydrate data in this study and those reported in the literature (Garg et al., 1975, Sugahara et al., 2004). However, some discrepancies are observed between data measured in this study and those reported by Mooijer van den Heuvel et al. (Mooijer-van den Heuvel et al., 2006). With increasing temperature, this discrepancy increases to approximately a 2 K temperature difference at high pressures. Such erroneous measurements may have occurred due to some parameters such as leakage in set-up, fast heating, mistake in calibration and low-accuracy of measurements. The accuracies of temperature and pressure of the measurements by Mooijer van den Heuvel et al. were 0.02 K and 0.005 MPa, respectively (Mooijer-van den Heuvel et al., 2006).

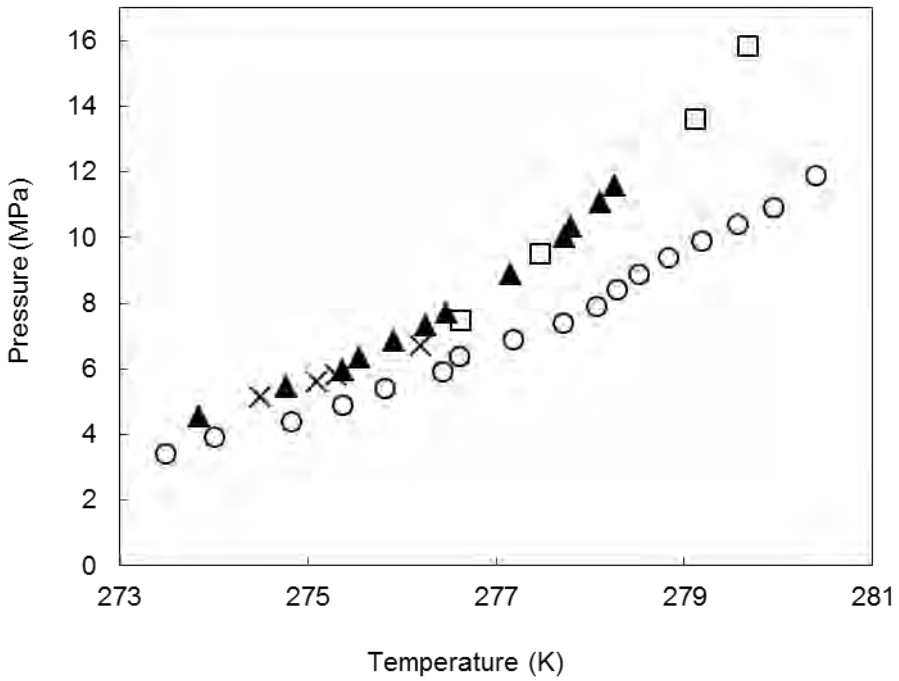

Figure 6-6. Experimental CF_4 hydrate dissociation data. Symbols represent experimental data: ▲, This work; ×, (Garg et al., 1975); □, (Sugahara et al., 2004); ○, (Mooijer-van den Heuvel et al., 2006).

Hydrate dissociation conditions for the system of CF_4+ TBAB + water at varying TBAB concentrations of 0.05, 0.10, 0.20 and 0.30 mass fractions are reported in Table 6-7 and compared to the CF_4 hydrate dissociation conditions in Figure 6-7.

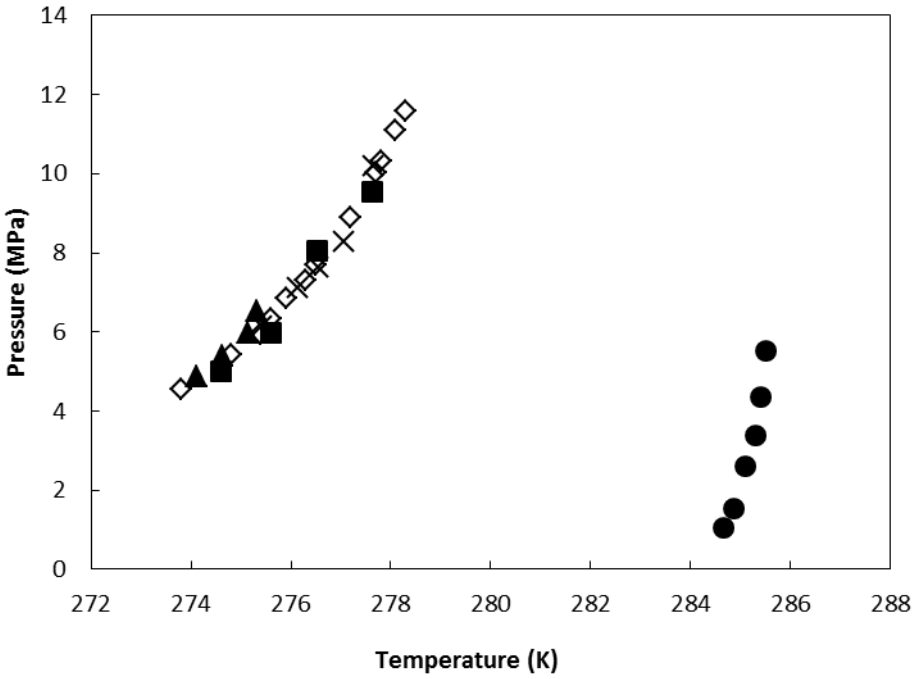

Figure 6-7. Experimental measurements of hydrate dissociation conditions for the system of CF_4 + TBAB + water. Symbols represent experimental data. ◊, 0.0 mass fraction of TBAB (CF_4 hydrate); ■, 0.05 mass fraction of TBAB; ▲, 0.10 mass fraction of TBAB; ×, 0.20 mass fraction of TBAB; ●, 0.30 mass fraction of TBAB.

As shown in Figure 6-7, aqueous TBAB solutions with 0.05, 0.10, and 0.20 mass fractions showed no promotion effect on the CF_4 hydrate phase equilibrium. However, the aqueous TBAB solution with 0.30 mass fraction showed a significant promotion effect on the CF_4 hydrate formation with a temperature difference, ΔT, approximately equal to 10 K. Some crystallographic studies such as H-NMR, Raman Spectrometry, C13-NMR or X-Ray Diffraction are needed to explain the strange behaviour of this hydrate system. Figure 6-8 shows an example of the cooling-heating curve obtained for the hydrate system of CF_4 + 0.30 mass fraction of aqueous TBAB solution.

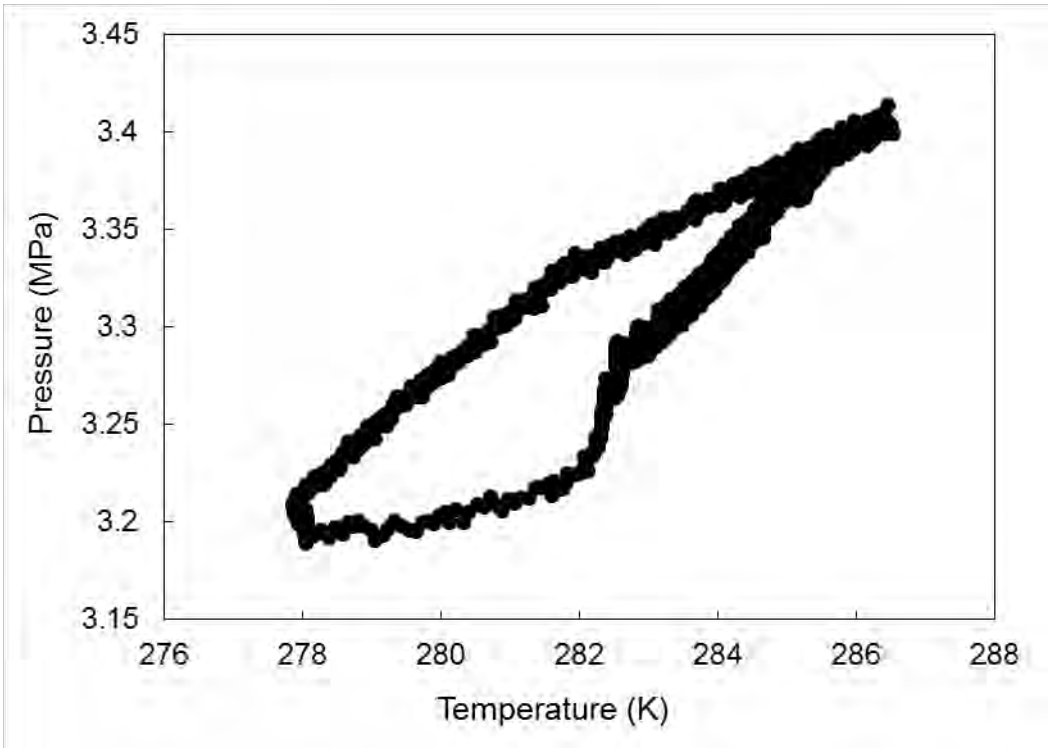

Figure 6-8. Cooling and heating curve for formation and dissociation of semi-clathrate hydrate of CF_4 + 0.30 mass fraction of aqueous TBAB solution.

As observed in Figure 6-8, the pressure drop of the system during the cooling process, confirms the formation of semi-clathrate hydrate of CF_4 + 0.30 mass fraction TBAB (CF_4 encapsulation inside the TBAB + water hydrate cavities). However, further specifications of the structure of the resultant clathrate using some techniques such as H-NMR, Raman Spectrometry, C13-NMR or X-Ray Diffraction are needed since the temperature of the clathrate hydrate dissociation data are close to that of the TBAB + water hydrate at 0.30 mass fraction TBAB.

Table 6-7. Experimental hydrate dissociation conditions for the system of CF_4 + TBAB + water.

[a] TBAB Concentration (mass fraction)	$P_{exp.}$/ MPa	$T_{exp.}$/K	[a] TBAB Concentration (mass fraction)	$P_{exp.}$/ MPa	$T_{exp.}$/K
0	4.55	273.8	0.10	4.86	274.1
	5.43	274.8		5.39	274.6
	5.95	275.4		5.98	275.2
	6.34	275.6		6.51	275.3
	6.84	275.9			
	7.31	276.3	0.20	6.14	275.4
	7.702	276.5		7.11	276.2
	8.89	277.2		7.64	276.6
	10.02	277.7		8.28	277.1
	10.33	277.8		10.18	277.7
	11.09	278.1			
	11.57	278.3	0.30	1.03	284.7
				1.54	284.9
0.05	5.00	274.6		2.62	285.1
	5.96	275.6		3.38	285.3
	8.06	276.7		4.35	285.4
	9.55	277.6		5.52	285.5
				6.24	285.6

[a] Combined standard uncertainty, u_c, in T, P, x_{TBAB} in mass fraction are u_c (T_{exp}) = ±0.1 K, u_c (P) = ±0.01 MPa, and u_c (x_{TBAB}) = 0.0002 respectively.

6.2. Thermodynamic modelling

For the thermodynamic modelling applied in this study, two groups of models were used, i.e., modelling of simple gas hydrate of Ar, Kr, Xe and CF_4 and modelling of semi-clathrate hydrate for the systems of Ar/Kr/Xe or CF_4 + water + TBAB at different TBAB concentrations. In this section, the models are described and the model results are presented.

6.2.1. Modelling of simple hydrate of Ar, Kr, Xe and CF_4

As mentioned earlier in chapter three, three thermodynamic models based on the fugacity approach (Approach 1) (Mohammadi et al., 2005, Javanmardi et al., 2012), the model proposed by Chen and Guo (Approach 2) (Chen and Guo, 1998) and finally a simple method based on the fugacity approach, and vapour pressure calculations (Approach 3) (Parrish and Prausnitz, 1972, Eslamimanesh et al., 2011c) were used in this study to predict the hydrate phase equilibria for the argon, krypton, xenon and CF_4 simple hydrates.

The fugacity approach (Approach 1) which is based on the equality of fugacity of water in the liquid, vapour and hydrate phases, is the most suitable model for the representation of the phase equilibria for the systems containing water, polar compounds in equilibrium with the gases with high solubilities in water. The advantage of this method is its good results at high pressure conditions due to the incorporation of the flash calculations. Approach 2 which is based on Chen and Guo's work (Chen and Guo, 1998) relies on the equality of the fugacity of the hydrate former in the hydrate and vapour phases. The advantage of this method is the use of the fugacity of hydrate former instead of the fugacity of water as an equilibrium criteria which is useful for polar and complicated liquid phase equilibria such as water + TBAB. In this method a correlation was used to calculate the Langmuir constant which has made it as an easy approach for the engineering applications in order to estimate the gas hydrate equilibrium conditions. Approach 3 can predict the gas hydrate dissociation conditions for the systems with low water content and gas solubility. In this method it is assumed that the water content in the vapour phase is small and consequently the vapour phase is consisted of pure gas. Hence, in this model the flash calculations is not used, simplifying the model. The model has poor results at high pressures because with increasing the pressure, the gas solubility and water content increase.

The aim of the selection of these thermodynamic models was to optimize the new binary interaction parameters (BIPs) of the VPT EoS (Valderrama, 1990) combined with the NDD mixing rules (Avlonitis et al., 1994) for Ar/Ke/Xe/ or CF_4 + water, new Kihara parameters, Antonine constants, and Langmuir constants for Ar, Kr, Xe and CF_4. In addition the results of these thermodynamic models is compared to each other. In this section, the optimized parameters produced in this study as well as the results of the mentioned models are presented.

6.2.1.1. The optimized parameters for fugacity approach (Approach 1)

The VPT EoS (Valderrama, 1990) along with NDD mixing rule (Avlonitis et al., 1994) were used for estimation of the water and gas fugacities in the liquid and vapour phases. The binary interaction parameters (BIPs) of the VPT EoS combined with the NDD mixing rules, i.e. k_{ij}, l^0_{ij}, l^l_{ij} were estimated using experimental data for gas solubilities in water in the literature (Braibanti et al., 1994, Scharlin and Battino, 1995) and minimization of the following objective function:

$$F_{obj} = \left(\frac{1}{NDP}\right)\sum_{k=1}^{NDP}\left(\frac{\left|x_{\exp} - x_{cal}\right|}{x_{\exp}}\right)_k \qquad 6\text{-}1$$

in which NDP is the number of data points, and x_{exp} and x_{cal} indicate the experimental and calculated gas solubility in water, respectively. Flash calculations was used to predict the gas solubilities in water. Table 6-8 represents the optimized binary interaction parameters (BIPs) of the VPT equation of state combined with the NDD mixing rules. The solubility of Kr in water has been neglected in this study, due to the lack of Kr solubility experimental data.

Table 6-8. The optimal binary interaction parameters between water (i) and guest molecule (j) for the VPT-EoS and NDD mixing rules.

System	k_{ij}	l_{ij}^0	$l^l_{ij}\times10^4$	References for solubility data
H_2O (i) + Ar (j)	0.3860	1.7024	62.7165	(Braibanti et al., 1994)
H_2O (i) + Xe (j)	0.6379	1.6811	43.1417	(Braibanti et al., 1994)
H_2O (i) + CF_4 (j)	0.6198	2.9459	47.2500	(Scharlin and Battino, 1995)

The following objective function was minimised using the HLV (Hydrate-Vapour-Liquid) equilibrium data for Ar, Kr, Xe and CF_4 in order to obtain the Kihara potential parameters (Kihara, 1953):

$$F_{obj} = \left(\frac{1}{NDP}\right)\sum_{k=1}^{NDP}\left(\frac{\left|T_{\exp} - T_{cal}\right|}{T_{\exp}}\right)_k \qquad 6\text{-}2$$

where, *NDP* is the number of data points, and T_{exp} and T_{cal} show the experimental and calculated hydrate dissociation temperature. Table 6-9 reportes the obtained Kihara parameters for Ar, Kr, Xe and CF_4 hydrate.

Table 6-9. *Kihara potential parameters for Ar, Kr, Xe and CF_4 hydrates.

Compound	α /Å	σ /Å	$(\varepsilon/k)/K$
Ar	0.226	2.770	170.500
Kr	0.170	2.961	185.185
Xe	0.236	3.310	191.500
CF_4	0.710	2.965	161.630

* The hydrate dissociation data obtained in this study were used to calculate Kihara parameters.

6.2.1.2. The optimized parameters for Chen and Guo model (Approach 2)

An objective function similar to Equation 6-2 was used to obtain the Antoine and Langmuir constants for Ar, Kr, Xe and CF_4 in the Chen and Guo model (Chen and Guo, 1998). Table 6-10 and 6-11 reports the values for Antoine and Langmuir constants in the Chen and Guo model.

Table 6-10. Antoine constants for calculating $^a f^0(T)$ in the Chen and Guo model.

Gas	$^b A \times 10^{-10}$	B (K)	C (K)	Temperature Range (K)	Ref.
Ar	7.368e13	-12889	-2.610	274.3 to 296.7	(Chen and Guo, 1998)
Kr	3.153e13	-12943	4.232	274.1 to 294.2	This work
Xe	1968.773	-7383.463	27.888	295.6 to 310.6	This work
CF_4	2293.481	-62379.703	45.213	273.8 to 278.3	This work

^{a} $f^0(T) = A\exp\left(\frac{B}{T-C}\right)$, T in K. ^{b} A is a dimensionless quantity.

Table 6-11. [a] The parameters of Equation (3-21) for calculation of the Langmuir constant.

Gas	$X \times 10^5$ (MPa^{-1})	Y (K)	Z (K)	Ref.
Ar	5.6026	2657.94	-3.42	(Chen and Guo, 1998)
Kr	4.5684	3016.70	6.24	(Chen and Guo, 1998)
Xe	1.8762	3138.04	23.04	This work
CF_4	3.290	2150.853	27.856	This work

[a] $C = X \exp\left(\frac{Y}{T-Z}\right)$, T in K. [b] Y and Z constants are dimensionless quantities.

6.2.1.3. Optimized Langmuir constants in the Parrish and Prausnitz equations for Approach 3

The objective function which was introduced in Equation 6-2 was applied to obtain the Langmuir constants in the Parrish and Prausnitz equations (Parrish and Prausnitz, 1972) using Approach 3 which is based on the fugacity approach and vapour pressure calculations. The parameters obtained for the Langmuir constants for Ar, Kr, Xe and CF_4 are summarized in Table 6-12.

Table 6-12. The parameters for calculation of the Langmuir constant based on the equations of Parrish and Prausnitz [*] (Parrish and Prausnitz, 1972).

Gas	Small cavity	Large cavity	Small cavity	Large cavity
	$a_{small} \times 1000\ [K/MPa]$	$b_{small}\ [K]$	$a_{large} \times 1000\ [K/MPa]$	$b_{large}\ [K]$
Ar	235.799	1800.0	18416.412	1100.0
Kr	138.096	2888.0	15269.894	2909.0
Xe	31.858	3786.7	824.900	1799.2
CF_4	0.056	0.035	5.441	3813.1

[*] $C = \frac{a}{T} \exp\left[\frac{b}{T}\right]$

6.2.1.4. Modelling results

Table 6-13 as well as Figures 6-9 through 6-12 indicate that the results of the mentioned three approaches are in good agreement with the newly reported data and the literature data. The average absolute deviation (AAD%) between the experimental and predicted temperature is defined as follow:

$$AAD\% = \frac{\left|T_{\exp} - T_{cal}\right|}{T_{\exp}} \times 100 \qquad 6\text{-}3$$

In which T_{exp} and T_{cal} present the experimental and calculated temperature, respectively.

Table 6-13. Comparisons between three approaches: Approach 1, Approach 2 and approach 3 for modelling of Ar, Kr, Xe, and CF_4 simple hydrates.

			AAD%		
System	P_{exp}	T_{exp}	Approach 1	Approach 2	Approach 3
Ar + H_2O	12.08	276.0	0.1	0.1	0.1
	10.66	274.6	0.2	0.3	0.2
	10.42	274.2	0.1	0.1	0.0
	10.12	274.0	0.1	0.1	0.2
Kr + H_2O	11.97	294.2	0.3	0.3	0.1
	8.44	291.5	0.1	0.1	0.0
	5.70	287.7	0.1	0.1	0.0
	4.30	285.3	0.0	0.0	0.2
	3.01	281.4	0.0	0.1	0.2
	2.10	278.1	0.2	0.1	0.4
	1.44	274.1	0.2	0.1	0.5
Xe + H_2O	10.09	310.6	0.1	0.0	0.1
	4.11	305.1	0.0	0.0	0.1
	2.86	301.8	0.0	0.0	0.0
	3.04	302.4	0.0	0.0	0.1
	1.92	297.9	0.1	0.0	0.0
	2.01	298.3	0.0	0.0	0.0
	2.21	299.4	0.0	0.0	0.0
	2.30	299.7	0.0	0.0	0.0
	1.52	295.6	0.0	0.0	0.0
	1.63	296.3	0.0	0.0	0.0

Table 6-13 continued…

	1.70	296.9	0.0	0.0	0.1
$CF_4 + H_2O$	4.55	273.8	0.1	0.0	0.1
	5.43	274.8	0.1	0.0	0.0
	5.95	275.4	0.1	0.0	0.1
	6.34	275.6	0.0	0.0	0.0
	6.84	275.9	0.0	0.0	0.0
	7.31	276.3	0.0	0.0	0.0
	7.702	276.5	0.0	0.0	0.0
	8.89	277.2	0.0	0.0	0.0
	10.02	277.7	0.0	0.0	0.0
	10.33	277.8	0.0	0.0	0.0
	11.09	278.1	0.0	0.0	0.0
	11.57	278.3	0.0	0.0	0.0

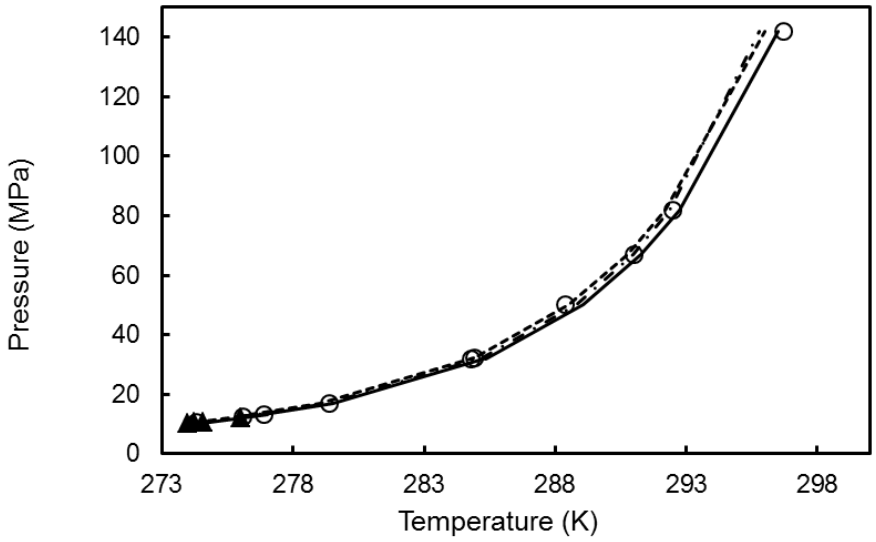

Figure 6-9. Plot of Ar hydrate dissociation data and comparison with experimental, literature data and model results. Symbols represent experimental data: ▲, This work; ○, (Marshall et al., 1964); Model results: •••••••, Approach 1, — • —, Approach 2, —, Approach 3.

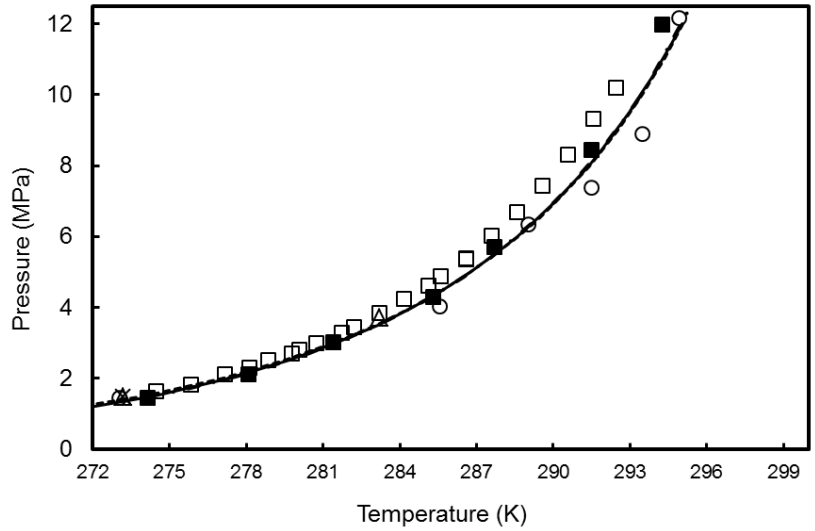

Figure 6-10. Plot of Kr hydrate dissociation data and comparison with experimental, literature data and model results. Symbols represent experimental data: ■, This work, □, (Sugahara et al., 2005), ○, (Dyadin et al., 1997b), Δ, (Holder et al., 1980), ×, (Stackelberg and Meuthen, 1958); Model results: •••••••, Approach 1, — • —, Approach 2, —, Approach 3.

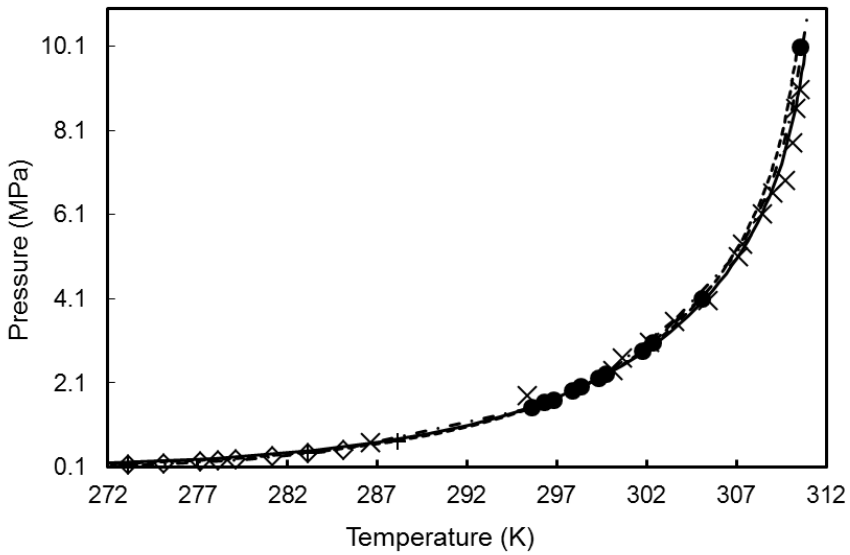

Figure 6-11. Plot of Xe hydrate dissociation data and comparison with experimental, literature data and model results. Symbols represent experimental data: ●, This work, ◊, (Ewing and Ionescu, 1974), +, (Makogon et al., 1996), ×, (Dyadin et al., 1997a), -, (Ohgaki et al., 2000); Model results: •••••••, Approach 1, — • —, Approach 2, —, Approach 3.

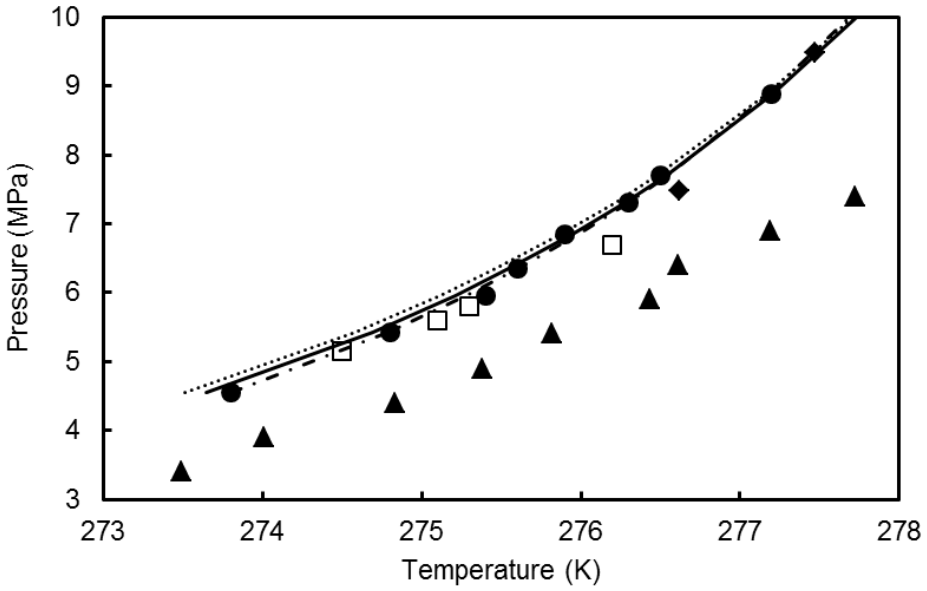

Figure 6-12. Plot of CF_4 hydrate dissociation data and comparison with experimental, literature data and model results. Symbols represent experimental data: ●, This work; ▲, (Mooijer-van den Heuvel et al., 2006); □, (Garg et al., 1975), ♦, (Sugahara et al., 2004); Model results: •••••••, Approach 1, ——•——, Approach 2, ——, Approach 3.

As can be seen in Table 6-13 and Figures 6-9 through 6-12, there is a reasonable agreement between the experimental data and the model results. As observed in Table 6-13, the maximum value for AAD% is about 0.3% which indicates these three methods can predict the hydrate dissociation conditions for Ar, Kr, Xe, CF_4, fairly well. As can be seen in Figure 6-12, there is some discrepancies between CF_4 hydrate dissociation data reported by Mooijer van den Heuvel et al. (Mooijer-van den Heuvel et al., 2006) to the data measured in this study as well as the model results. As mentioned earlier, some factors such as leakage in set-up, high heating rate, mistake in calibration and low-accuracy of measurements could have caused such erroneous data.

6.2.2. Modelling of semi-clathrate hydrates for the systems of Ar/ Kr/ Xe/ CF_4 + TBAB + water

As mentioned earlier, the model proposed by Joshi et al. (Joshi et al., 2012) was extended in this work for representation of semi-clathrate hydrates for the systems of Ar/ Kr and Xe in the presence of aqueous TBAB solutions. The objective function as shown in Equation 6-2 was

used to optimize the water activity constants *(k_1* and k_2 in Equation 3-33), using the measured experimental data of Ar, Kr, Xe and CF_4 semi-clathrate hydrate in the presence of aqueous TBAB solutions. Table 6-14 provides the optimized constants (k_1 and k_2) in Equation 3-33 for each TBAB concentration and temperature range.

Table 6-14. *Constants (k_1 and k_2) for the water activity calculations in the system of semi-clathrate hydrates of Ar/Kr/Xe or CF_4 + aqueous solutions of TBAB.

System	TBAB Concentration (mass fraction)	Temperature Ranges (K)	k_1	k_2
Ar + TBAB + water	0.05	$275.8 \le T \le 287.6$	1599.00	5.568
	0.10	$280.4 \le T \le 290.7$	2179.00	7.511
	0.20	$283.0 \le T \le 293.6$	3025.80	10.303
	0.30	$285.9 \le T \le 293.1$	3029.60	10.291
Kr + TBAB + water	0.05	$278.9 \le T \le 292.1$	762.72	2.293
	0.10	$280.76 \le T \le 296.0$	962.59	2.921
	0.20	$284.6 \le T \le 297.1$	1908.07	5.923
Xe + TBAB + water	0.10	$282.7 \le T \le 288.3$	1521.51	5.301
		$288.3 \le T \le 304.9$	79.53	0.307
	0.20	$284.7 \le T \le 292.3$	2293.23	7.892
		$292.3 \le T \le 302.3$	291.03	1.046
	0.30	$285.9 \le T \le 293.0$	2457.23	8.439
		$293.0 \le T \le 303.1$	20.03	0.150
CF_4 + TBAB + water	0.05	$274.6 \le T \le 277.6$	-66.97	-0.248
	0.10	$274.1 \le T \le 275.3$	79.61	0.296
	0.20	$275.4 \le T \le 277.7$	-77.29	-0.266
	0.30	$284.7 \le T \le 285.6$	15140.97	52.926

* $a_w = \frac{1}{1 - x_{TBAB}} \exp\left(\frac{k_1}{T} - k_2\right)$

A comparison between the experimental data and the model results for the semi-clathrate hydrates of Ar/ Kr/ Xe or CF_4 in the presence of various TBAB concentrations are presented in Figures 6-13 through 6-16 and Tables 6-15 to 6-18. As can be seen in Figures 6-13 through 6-16 and Tables 6-15 to 6-18, there is good agreement between the measured data and the model results for the semi-clathrate hydrates dissociation conditions for the system of Ar + TBAB + water, Kr + TBAB + water, Xe + TBAB + water and CF_4 + TBAB + water. The average absolute deviation (*AAD%*) between the measurements and the model results are reported in Tables 6-15 to 6-18. As can be observed in these tables, the *ARD%* between the measurements and the model results are lower than 0.3 % except for the data point with 0.7 *AAD%* which was observed for Ar + TBAB + water hydrate phase equilibria at the temperature and pressure conditions of 275.8 K and 0.34 MPa, respectively. These results confirm the accuracy of the model.

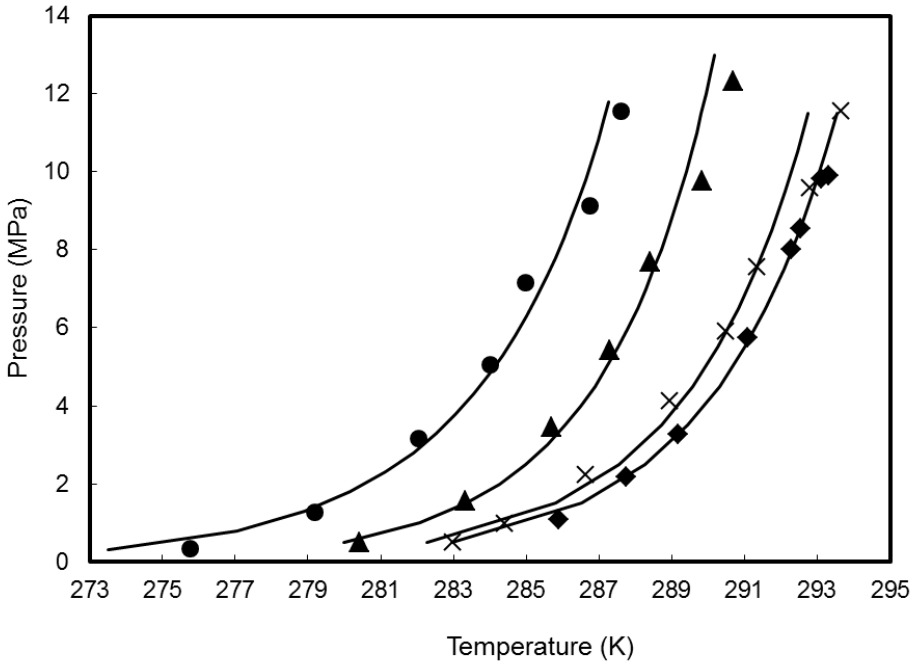

Figure 6-13. Experimental data and modelling of semi-clathrate hydrate dissociation conditions for the system of Ar + TBAB + water. Symbols represent experimental data: ●, This work, 0.05 mass fraction aqueous TBAB solution; ▲, This work, 0.10 mass fraction aqueous TBAB solution; ×, This work, 0.20 mass fraction aqueous TBAB solution; ♦, This work, 0.30 mass fraction aqueous TBAB; ___, This work, model results.

Table 6-15. Experimental and calculated semi-clathrate hydrate dissociation conditions for the system of Ar + aqueous TBAB solution.

[a] TBAB Concentration (mass fraction)	T_{exp}/K	P_{exp}/ MPa	T_{cal}/ K	[b] AD/K	[c] ARD%
0.05	287.6	11.56	287.2	0.4	0.1
	286.8	9.12	286.4	0.4	0.1
	285.0	7.17	285.5	0.5	0.2
	284.0	5.06	284.2	0.2	0.1
	282.0	3.16	282.4	0.4	0.1
	279.2	1.27	278.8	0.4	0.1
	275.8	0.34	273.9	1.9	0.7
0.10	290.7	12.32	290.0	0.7	0.2
	289.8	9.76	289.3	0.5	0.2
	288.4	7.68	288.6	0.2	0.1
	287.3	5.43	287.5	0.2	0.1
	285.7	3.44	286.0	0.3	0.1
	283.3	1.56	283.5	0.2	0.1
	280.4	0.51	280.0	0.4	0.1
0.20	293.6	11.55	292.8	0.8	0.3
	292.8	9.57	292.1	0.7	0.2
	291.3	7.55	291.3	0	0.0
	290.5	5.90	290.5	0	0.0
	288.9	4.11	289.3	0.4	0.1
	286.6	2.22	287.1	0.5	0.2
	284.4	0.98	284.4	0	0.0
	283.0	0.51	282.3	0.7	0.2
0.30	293.1	9.82	293.0	0.1	0.0
	292.5	8.54	293.0	0.5	0.2
	292.3	8.00	292.5	0.2	0.1
	293.3	9.91	292.3	1	0.3
	291.1	5.74	291.2	0.1	0.0
	289.2	3.27	289.2	0	0.0
	287.8	2.19	287.8	0	0.0
	285.9	1.09	285.5	0.4	0.1

[a] Combined standard uncertainty, u_c, in T, P, x_{TBAB} in mass fraction are u_c (T_{exp}) = ±0.1 K, u_c (P) = ±0.01 MPa, and u_c (x_{TBAB}) = 0.0002 respectively. [b] $AD = |T_{exp} - T_{cal}|$. [c] $ARD\% = (|T_{exp} - T_{cal}|/ T_{exp}) \times 100$, absolute relative deviation.

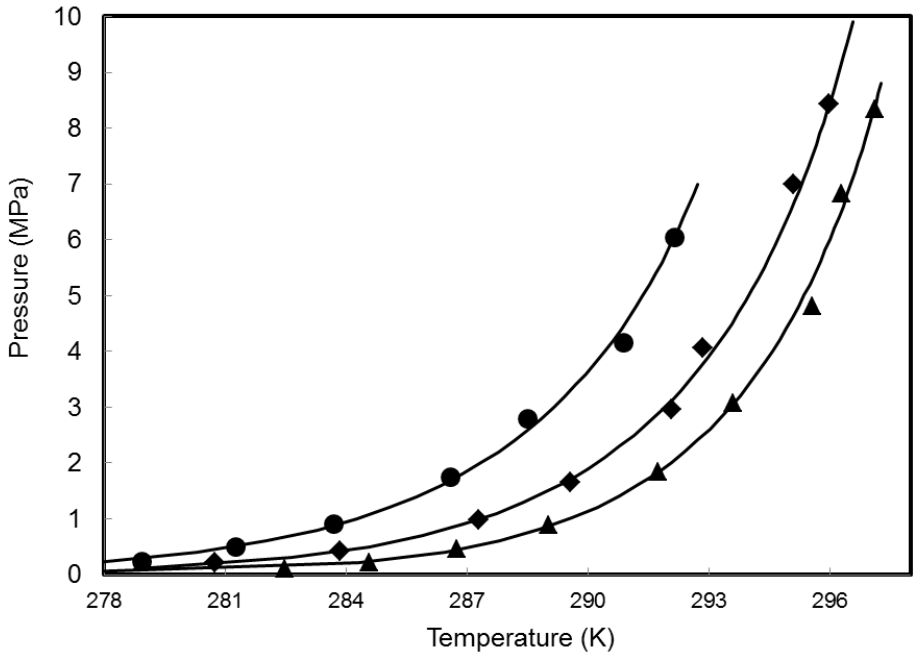

Figure 6-14 Experimental data and modelling of semi-clathrate hydrate dissociation conditions for the system of Kr + TBAB + water. Symbols represent experimental data. ●, This work, 0.05 mass fraction aqueous TBAB solution; ♦, This work, 0.10 mass fraction aqueous TBAB solution; ▲, This work, 0.20 mass fraction aqueous TBAB solution; ___, This work, model results.

Table 6-16. Experimental and calculated hydrate dissociation conditions for the system of Kr + aqueous TBAB solutions.

[a] TBAB Concentration (mass fraction)	T_{exp}/K	P_{exp} / MPa	T_{cal}/ K	[b] AD/K	[c] ARD%
0.05	292.1	6.05	292.1	0	0.0
	290.9	4.16	290.6	0.3	0.1
	288.5	2.79	288.8	0.3	0.1
	286.6	1.74	286.7	0.1	0.0
	283.7	0.91	283.8	0.1	0.0
	281.3	0.50	281.3	0	0.0
	279.0	0.24	278.2	0.8	0.3
0.10	296.0	8.43	296.0	0	0.0
	295.1	6.99	295.3	0.2	0.1
	294.1	5.41	294.3	0.2	0.1
	292.8	4.05	293.1	0.3	0.1
	292.1	2.97	291.9	0.2	0.1
	289.6	1.65	289.4	0.2	0.1
	287.3	0.98	287.3	0	0.0
	283.8	0.41	283.8	0	0.0
	280.8	0.22	281.5	0.7	0.2
0.20	297.1	8.34	297.1	0	0.0
	296.3	6.82	296.4	0.1	0.0
	295.6	4.81	295.2	0.4	0.1
	293.6	3.06	293.6	0	0.0
	291.7	1.84	291.7	0	0.0
	289.0	0.89	289.1	0.1	0.0
	286.7	0.46	286.8	0.1	0.0
	284.6	0.22	284.4	0.2	0.1

[a] Combined standard uncertainty, u_c, in T, P, x_{TBAB} in mass fraction are u_c ($T_{\exp}$) = ±0.1 K, u_c (P) = ±0.01 MPa, and u_c (x_{TBAB}) = 0.0002 respectively. [b] $AD = |T_{exp} - T_{cal}|$. [c] $ARD\% = (|T_{exp} - T_{cal}| / T_{exp}) \times 100$, absolute relative deviation.

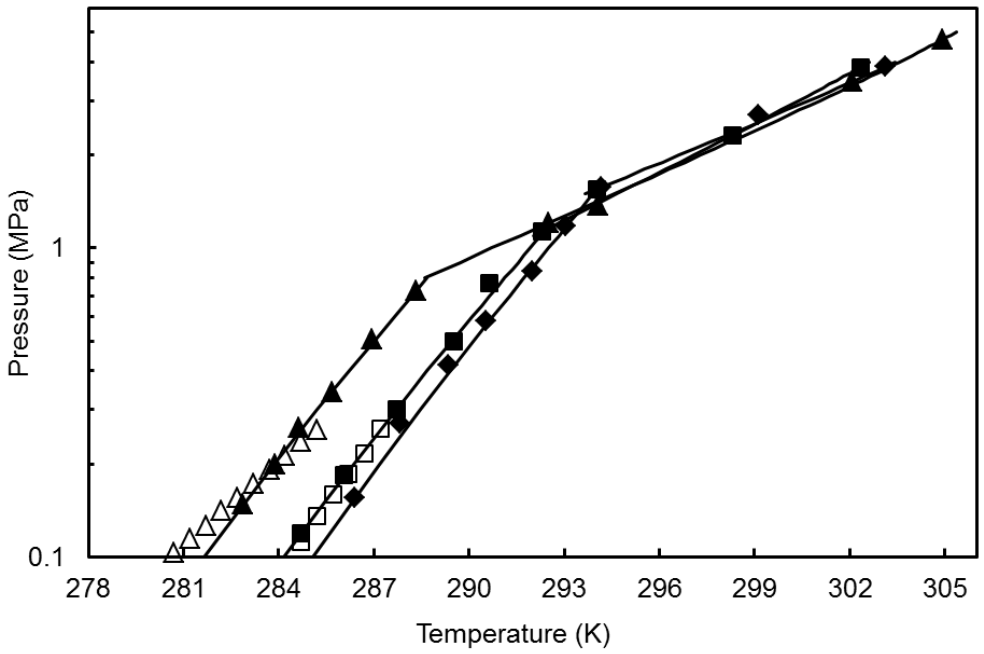

Figure 6-15. Experimental data and modelling of semi-clathrate hydrate dissociation conditions for the system of Xe + TBAB + water. Symbols represent experimental data. 0.10 mass fraction of TBAB: ▲, This work, Δ, (Jin et al., 2012); 0.20 mass fraction of TBAB: ■, This work, □, (Jin et al., 2012), ○, (Garcia and Clarke, 2014); 0.30 mass fraction of TBAB: ♦, This work; ___, model results, This work.

As mentioned earlier, the aqueous TBAB solutions have a twofold effect on the Xe hydrate, depending on the temperature and pressure range. As shown in Figure 6-15, TBAB aqueous solutions with mass fractions of 0.1, 0.2 and 0.3 TBAB show a promotion effect with regard to the xenon hydrate equilibrium dissociation conditions at pressures lower than 0.73 MPa, 1.40 MPa, and 1.57 MPa, respectively. At higher pressures, the TBAB aqueous solutions show no promotion effect on the xenon hydrate phase equilibrium. As shown in Figure 6-15, the model was able to predict this double behaviour with a good accuracy.

Table 6-17. Experimental and calculated semi-clathrate hydrate dissociation conditions for the system of Xe + TBAB aqueous solution.

[a] TBAB Concentration (mass fraction)	T_{exp}/K	P_{exp}/ MPa	T_{cal}/ K	[b] AD/K	[c] ARD%
0.10	304.9	4.73	304.9	0.0	0.0
	302.1	3.47	302.3	0.2	0.1
	294.0	1.38	293.8	0.2	0.1
	292.5	1.21	292.5	0.0	0.0
	288.3	0.73	288.3	0.0	0.0
	286.9	0.51	287.0	0.1	0.0
	285.7	0.34	285.7	0.0	0.0
	284.6	0.26	284.8	0.2	0.1
	283.9	0.20	283.8	0.1	0.0
	282.9	0.15	282.9	0.0	0.0
0.20	302.3	3.86	302.3	0.0	0.0
	298.3	2.32	298.3	0.0	0.0
	294.0	1.55	294.9	0.9	0.3
	292.3	1.14	292.3	0.0	0.0
	290.6	0.77	291.0	0.4	0.1
	289.5	0.50	289.4	0.1	0.0
	287.7	0.30	287.7	0.0	0.0
	286.1	0.18	286.1	0.0	0.0
	284.7	0.12	284.7	0.0	0.0
0.30	303.1	3.87	303.1	0.0	0.0
	299.1	2.70	299.6	0.5	0.2
	294.2	1.58	294.2	0.0	0.0
	293.1	1.18	293.1	0.0	0.0
	292.0	0.84	291.9	0.1	0.0
	290.5	0.58	290.6	0.1	0.0
	289.4	0.42	289.5	0.1	0.0
	287.8	0.27	288.1	0.3	0.1
	286.4	0.16	286.4	0.0	0.0
	285.9	0.13	285.9	0.0	0.0

[a] Combined standard uncertainty, u_c, in T, P, x_{TBAB} in mass fraction are u_c (T_{exp}) = ±0.1 K, u_c (P) = ±0.01 MPa, and u_c (x_{TBAB}) = 0.0002 respectively. [b] $AD = |T_{exp} - T_{cal}|$. [c] $ARD\% = (|T_{exp} - T_{cal}| / T_{exp}) \times 100$, absolute relative deviation.

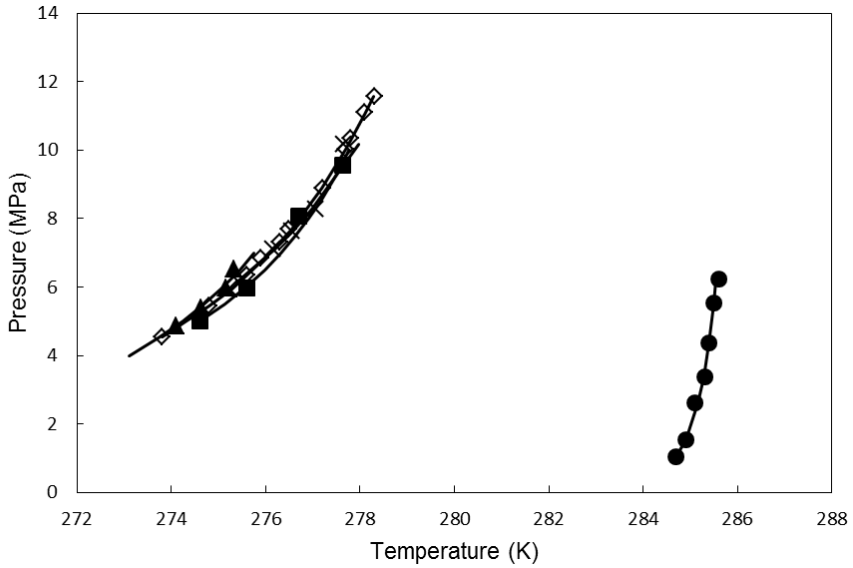

Figure 6-16. Experimental data and modelling results of semi-clathrate hydrate dissociation conditions for the system of CF_4 + TBAB + water at various TBAB concentrations. Symbols represent experimental data. 0.0 mass fraction of TBAB (pure CF_4 hydrate): ◊, This work; 0.05 mass fraction of TBAB: ■, This work; 0.10 mass fraction of TBAB: ▲, This work; 0.20 mass fraction of TBAB: ×, This work; 0.30 mass fraction of TBAB: ●, This work; Solid lines, This work, model results. The maximum ΔT between the measured data and the model results is equal 0.1 K.

Table 6-18. Experimental and calculated semi-clathrate hydrate dissociation conditions for the system CF_4 + aqueous TBAB solutions.

[a] TBAB Concentration (wt. fraction)	T_{exp}/K	P_{exp}/ MPa	T_{cal}/ K	[b] AD/K	[c] ARD%
0.05	5.00	274.6	274.6	0	0.0
	5.96	275.6	275.5	0.1	0.0
	8.06	276.7	276.9	0.2	0.1
	9.55	277.6	277.6	0	0.0
0.10	4.86	274.1	274.1	0	0.0
	5.39	274.6	274.6	0	0.0
	5.98	275.2	275.1	0.1	0.0
	6.51	275.3	275.4	0.1	0.0
0.20	6.14	275.4	275.4	0	0.0
	7.11	276.2	276.2	0	0.0
	7.64	276.6	276.6	0	0.0
	8.28	277.1	277.0	0.1	0.0
	10.18	277.7	278.0	0.3	0.1
0.30	1.03	284.7	284.7	0	0.0
	1.54	284.9	284.9	0	0.0
	2.62	285.1	285.2	0.1	0.0
	3.38	285.3	285.3	0	0.0
	4.35	285.4	285.4	0	0.0
	5.52	285.5	285.5	0	0.0
	6.24	285.6	285.5	0.1	0.0

[a] Combined standard uncertainty, u_c, in T, P, x_{TBAB} in mass fraction are u_c ($T_{\exp}$) = ±0.1 K, u_c (P) = ±0.01 MPa, and u_c (x_{TBAB}) = 0.0002 respectively. [b] $AD = |T_{exp} - T_{cal}|$. [c] $ARD\% = (|T_{exp} - T_{cal}| / T_{exp}) \times 100$, absolute relative deviation.

As can be seen in Figure 6-16, 0.3 mass fraction of aqueous TBAB solution has a promotion effect on the CF_4 hydrate. The model was able to predict this promotion effect accurately in which the maximum ΔT between the measured data and the model results was equal to 0.1 K, within the experimental uncertainty of 0.1 K. The temperature ranges for the measurements were 274.1 – 285.6 K, over a 11.5 K range. It should be mentioned that TBAB aqueous solutions with the concentrations of 0.05, 0.10, and 0.20 mass fractions showed no significant promotion effect on the CF_4 hydrate phase equilibrium.

6.3. Kinetics results for CF_4 hydrate formation

Experiments performed in this study on the kinetics of hydrate formation involved estimation of the apparent rate constant, rate of hydrate formation and mole consumption plot, storage capacity plot, and water to hydrate conversion plot, where the amount of gas consumed and water to hydrate conversion during the hydrate formation were plotted as a function of time. To produce the aforementioned kinetic parameters during the hydrate formation, the model proposed by Englesos and Bishnoi and other researchers are available in the literature (Englezos et al., 1987, Clarke and Bishnoi, 2001a, Clarke and Bishnoi, 2001b, Clarke and Bishnoi, 2004). One of the well-known kinetic models which was used in this study for estimating the kinetic parameters of the hydrate formation such as rate of hydrate formation, apparent rate constant, gas consumption and storage capacity, is that proposed by Englezos et al. (Englezos et al., 1987). This crystallization theory (Englezos et al., 1987) is based on calculating the difference between the fugacity of gas species in the vapour phase and hydrate phase, which is a driving force for the gas hydrate formation. The details of this model as well as the equations used were explained in Chapter 3.

6.3.1. Initial temperature and pressure, and driving force of growth

In this study, the effects of initial temperature and pressure on the kinetic of CF_4 hydrate formation were investigated. For investigation of the effect of initial pressure, experimental measurements were performed at a constant temperature of 275.3 K and four initial pressures of 7.08, 7.92, 9.11 and 11.83 MPa. The initial temperature and pressures were selected inside the hydrate stability zone to examine the effect of degree of subcooling on the hydrate formation rate. The change in the initial pressure influences the driving force of hydrate formation. In

addition, the experiments were conducted at a constant pressure of 11.47 MPa and two temperatures of 276.1 and 276.6 K to investigate the effect of initial temperature. Table 6-19 reports the initial temperatures and pressures on the kinetics of CF_4 hydrate formation. Numerous researchers defined several driving forces such as temperature, pressure, fugacity (chemical potential), and concentration (mole fraction) for the kinetics of gas hydrate (Bergeron et al., 2010). For instance, Englezos et al. (Englezos et al., 1987) defined the driving force as the difference between the fugacity of the dissolved gas in the vapour phase and that in the hydrate phase at a constant temperature.

Table 6-19. Investigated initial temperatures and pressures of CF_4 hydrate formation.

Initial Temperature (K)	Initial Pressure (MPa)
275.3	7.08
275.3	7.92
275.3	9.11
275.3	11.83
276.1	11.47
276.6	11.47

The driving force suggested by Skovborg and Rasmussen (1994) (Skovborg and Rasmussen, 1994) is based on the difference between the mole fraction of the guest at the vapour-liquid water interface and that in the bulk. In Figure 6-17, the driving force or the degree of subcooling for hydrate growth was defined as the difference between the three-phase equilibrium pressure (at the constant temperature) and the experimental (bulk) pressure according to Vysniauskas and Bishnoi (Vysniauskas and Bishnoi, 1983). As shown in Figure 6-17, an increase in the initial pressure of CF_4 leads to a higher degree of subcooling.

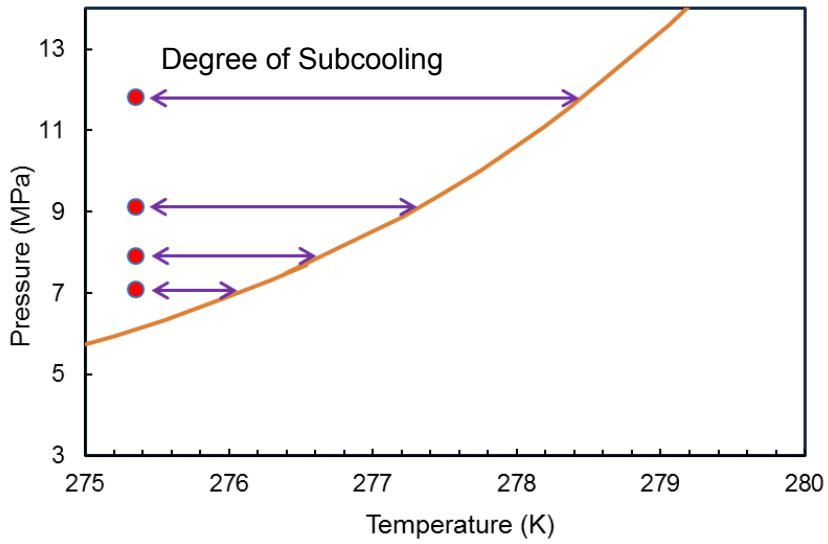

Figure 6-17. The driving force or degree of subcooling between the initial pressure conditions (●) and CF_4 hydrate equilibrium line (solid line) at a constant temperature of 275.3 K.

6.3.2. Induction time

The induction time is the period of time that the hydrate crystals required to form stable nuclei and to grow to a noticeable size. The induction time is often named the hydrate nucleation or lag time which is the time taken for hydrates to be detected macroscopically (Sloan and Koh, 2008). Two methods have been used by several researchers to measure the induction time of clathrate hydrate formation. The first method, or the super cooling point, represents the temperature of spontaneous freezing of a solution subjected to a constant cooling rate, such as in the work of Wilson et al. (2005) (Wilson et al., 2005). The other method which was used in this study, involves holding the sample at a constant temperature and pressure within the hydrate stability zone and waiting for appearance of a detectable volume of hydrate phase (Natarajan et al., 1994). The value of induction time is dependent on the surface area, cell volume, rate of mixer, temperature and pressure condition, gas consumption and rate of heat and mass transfer (Sloan and Koh, 2008). Figure 6-18 displays the induction time for CF_4 hydrate formation at a temperature and pressure of 275.3 K and 7.08 MPa, respectively.

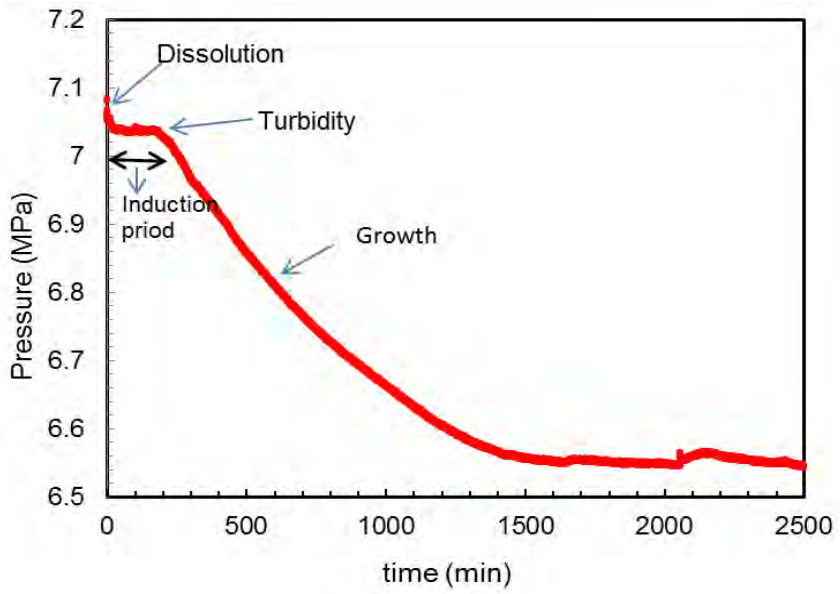

Figure 6-18. The pressure of the system during the hydrate formation of CF_4 at an initial temperature 275.3 K and pressure of 7.08 MPa.

As seen in Figure 6-18, three distinct regions can be determined during the CF_4 hydrate formation. The first region is the dissolution stage. During this period, some of the CF_4 gas present in the vapour phase diffuses across the vapour-liquid water interface and dissolves in the aqueous phase. The rate at which CF_4 gas diffuses across the interface is a function of the interfacial area and mass transfer coefficient, both intensely dependent on the agitation within the system. During the second period or induction period, CF_4 hydrate crystals form and decompose until they form a stable nucleus (nucleation) and grow to a detectable size. The turbidity point in Figure 6-18 marks the beginning of the growth stage, which corresponds to the last period shown in Figure 6-18. In the growth stage, CF_4 molecules are trapped inside the cavities of hydrate and the pressure of the system decreases significantly to a constant value.

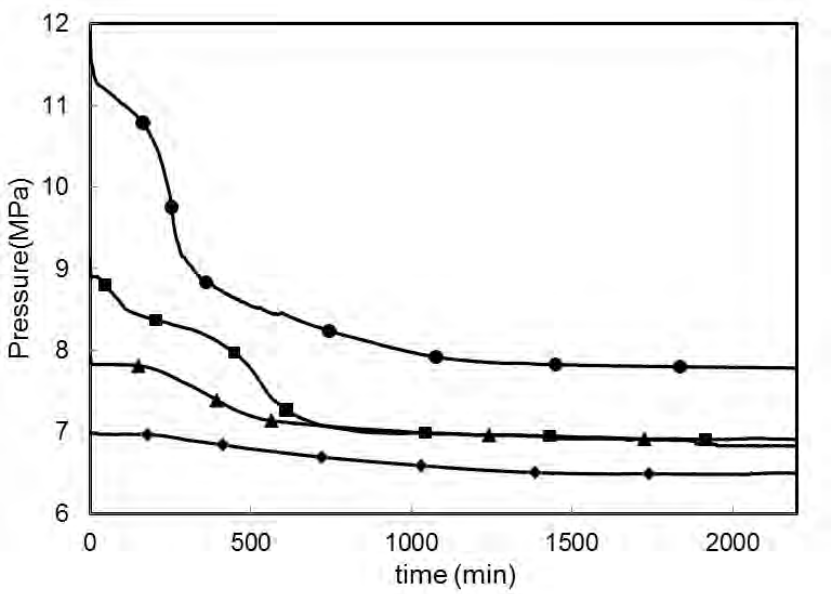

Figure 6-19. The pressure of the system during the hydrate formation of CF_4 at an initial temperature 275.3 K and initial pressure of —♦—, 7.08 MPa; —▲—, 7.92 MPa; —■—, 9.11 MPa; —●—, 11.83 MPa.

Figure 6-19 compares the induction time for CF_4 hydrate at constant temperature of 275.3 K and four initial pressures of 7.08, 7.92, 9.11 and 11.83 MPa. The induction time at a constant temperature of 275.3 K and pressure of 7.08 MPa was about 166 min. Though, this amount at a constant temperature of 275.3 K and the initial pressures of 7.92, 9.11, 11.83 MPa, were about 96, 19 and 1.5 min, respectively.

Table 6-20. The values of Induction time at different initial temperatures and pressures for CF_4 hydrate formation.

Initial Temperature (K)	Initial Pressure(MPa)	Induction time (min)
275.3	7.08	166
275.3	7.92	96
275.3	9.11	19
275.3	11.83	1.5
276.1	11.47	2.8
276.6	11.47	5.8

As observed in Figure 6.19, with an increase in the initial pressure at constant temperature, there is a decrease in the induction time. Similar results are found with a decrease in the initial temperature at a constant pressure. Therefore, at two initial temperatures of 276.1 K and 276.6 K and constant pressure of 11.47 MPa, the induction time were about 2.8 and 5.8 min, respectively. Table 6-20 summarises the induction time obtained in this kinetic measurements.

6.3.3. Gas consumption

As mentioned earlier in Chapter 3, the model proposed by Englezos et al. (Englezos et al., 1987) was used to estimate the number of gas molecules consumed during hydrate formation at different conditions of initial pressures and temperatures. Figure 6-20 represents the CF_4 consumptions during hydrate formation at an initial temperature of 275.35 K and initial pressure of 7.08 MPa.

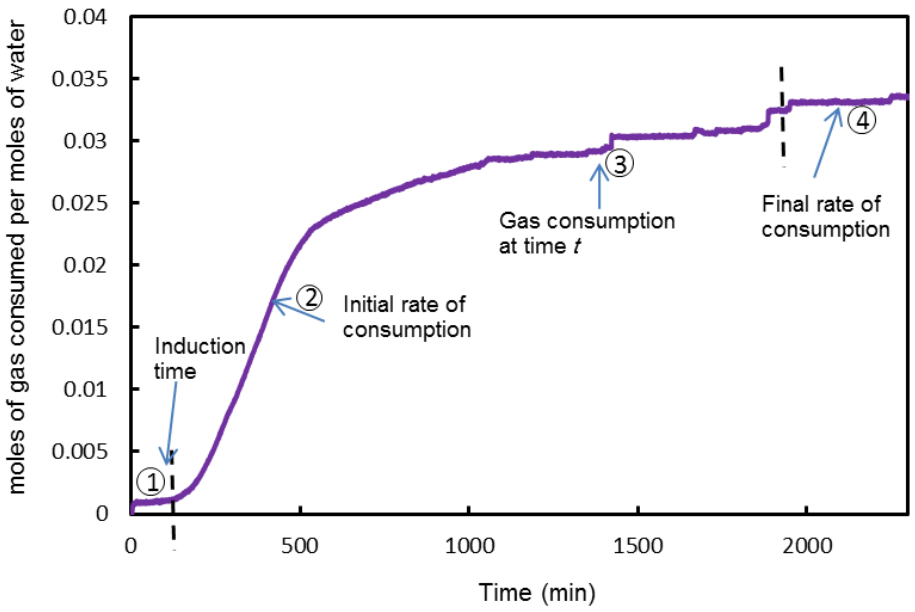

Figure 6-20. Number of moles of CF_4 consumed per mole of water during the hydrate formation at an initial temperature 275.35 K and initial pressure of 7.08 MPa.

As shown in Figure 6-20, gas consumption during hydrate formation is divided into four regions. During the first region or induction period, the gas consumption was approximately zero because hydrates did not form in this region. The CF_4 hydrate formed rapidly in the growth

region (second region). During this period, CF_4 molecules were concentrated and packed inside the hydrate cavities more than those in the vapour phase. The rate of hydrate formation as well as the slope of the gas consumption curve versus time decreased in region 3 because of water consumption during the hydrate formation and the effects of mass and heat transfer. In region 4, the CF_4 consumption reaches a constant value and the hydrate formation was complete.

Figure 6-21 compares the consumption of CF_4 hydrate during the hydrate formation at an initial temperature of 275.35 K and different pressures of 7.08, 7.92, 9.11 and 11.83 MPa. As observed in this figure, with an increase in the initial pressure at a constant temperature, CF_4 consumption increased. Figure 6-22 shows the consumption of CF_4 hydrate during the hydrate formation at an initial pressure of 11.47 MPa and two different temperatures of 276.1 and 276.6 K. As can be seen in this figure, CF_4 consumption decreased with an increase in the initial temperature.

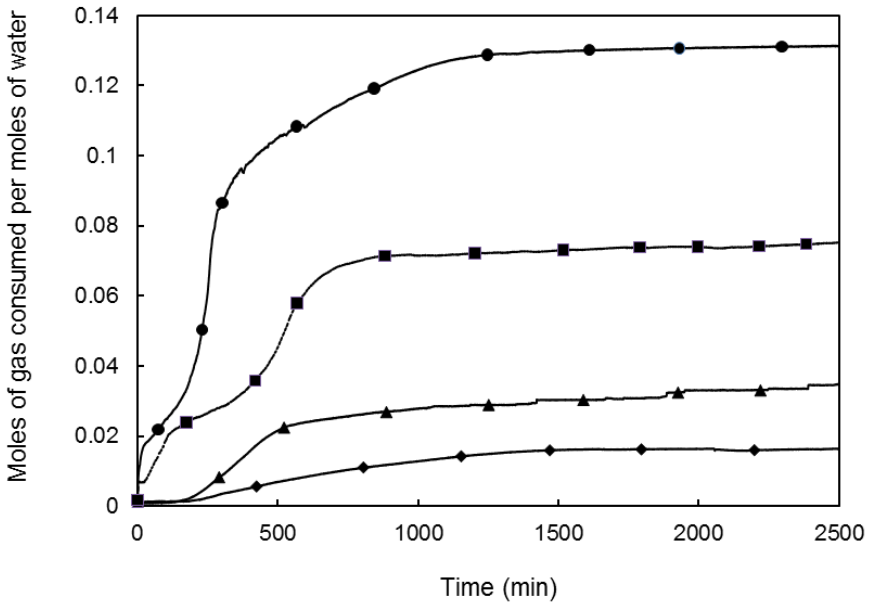

Figure 6-21. Number of moles of CF_4 consumed per mole of water during the hydrate formation at an initial temperature 275.35 K and different pressures: —♦—, 7.08 MPa; —▲—, 7.92 MPa; —■—, 9.11 MPa; —●—, 11.83 MPa.

Table 6-21 summarises the final values of CF_4 consumed at the end of experiment at different conditions of initial pressure and temperatures.

Table 6-21. Final moles of CF_4 consumed per moles of water at different initial temperatures and pressures conditions.

Initial Temperature (K)	Initial Pressure(MPa)	Final moles of gas consumed per moles of water
275.3	7.08	0.016
275.3	7.92	0.035
275.3	9.11	0.077
275.3	11.83	0.132
*276.1	*11.47*	*0.105*
276.6	*11.47*	*0.066*

*The italic format shows the effect of initial temperature at the pressure of 11.47 MPa.

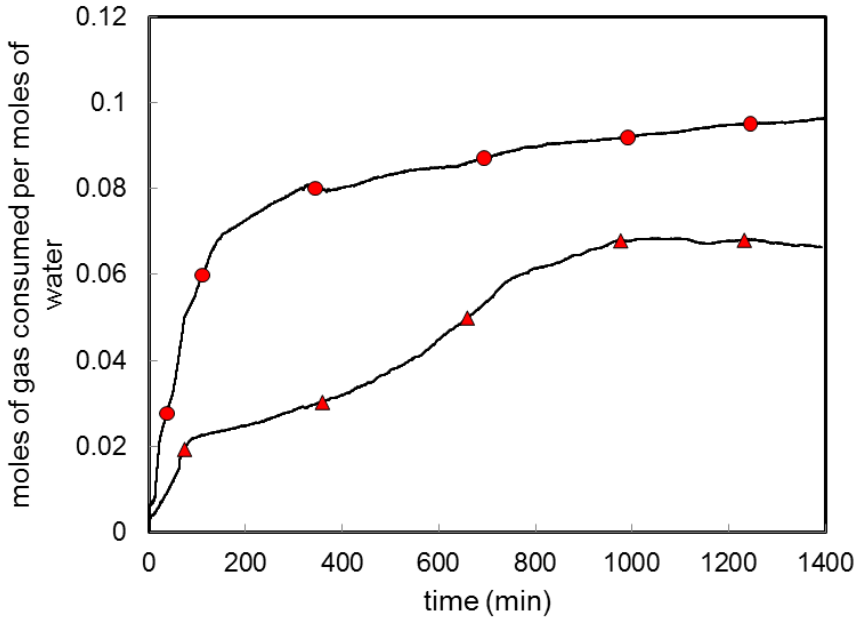

Figure 6-22. Number of moles of CF_4 consumed per mole of water during the hydrate formation at an initial pressure of 11.47 MPa and two initial temperatures of: —▲—, 276.6 K; —●—, 276.1 K.

As observed in Table 6-21, the maximum amount of gas consumed per moles of water is 0.132 which is related to the initial temperature and pressure of 275.3 K and 11.83 MPa, respectively. With an increase in the initial pressure from 9.11 to 11.83 MPa (ΔP = 2.72 MPa) at a constant temperature of 275.3 K, the final amount of gas consumed per moles of water increased by almost 71% which shows the initial pressure has a significant effect on the CF_4 consumption. As shown in Table 6-21, with an increase in the initial temperature from 276.1 K to 276.6 K (ΔT = 0.5 K) at a constant pressure of 11.47 MPa, the final amount of gas consumed per moles of water decreased by nearly 59%. The results of this study indicated that the initial temperature has an important effect on the CF_4 consumption.

6.3.4. Water to hydrate conversion

The amount of water converted to hydrate was named as "water to hydrate conversion". Figure 6-23 represents a diagram for water to hydrate conversion at the initial temperature and pressure conditions of 275.3 K and 7.08 MPa, respectively. As shown in this figure, the amount of water converted to hydrate increased rapidly after the hydrate nucleation (after the induction time). As water was consumed during the hydrate formation, the slope of the water converted to hydrate curve decreased gradually until no change in the slope was observed at the end of the hydrate formation.

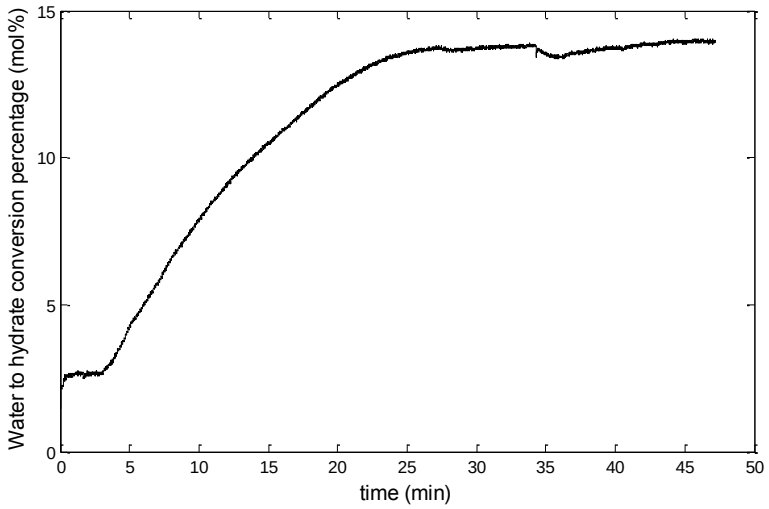

Figure 6-23. Water to hydrate conversion percentage versus time at the initial temperature and pressure conditions of 275.3 K and 7.08 MPa, respectively.

Table 6-22 reports the final amount of water converted to hydrate at the different conditions of pressure and temperature at the end of the experiment.

Table 6-22. Final moles of CF_4 consumed per moles of water at different initial temperatures and pressures conditions.

Initial Temperature (K)	Initial Pressure(MPa)	Final water to hydrate conversion percentage (mole %)
275.3	7.08	12.4
275.3	7.92	25.2
275.3	9.11	51.1
275.3	11.83	80.6
276.1	11.47	67.2
276.6	11.47	45.3

As observed in Table 6-22 and depicted in Figure 6-24, with an increase in the initial pressure at a constant temperature of 275.3 K, the final amount of water converted to hydrate increased. Similar results were obtained by decreasing the initial temperature at a constant pressure of 11.47 MPa.

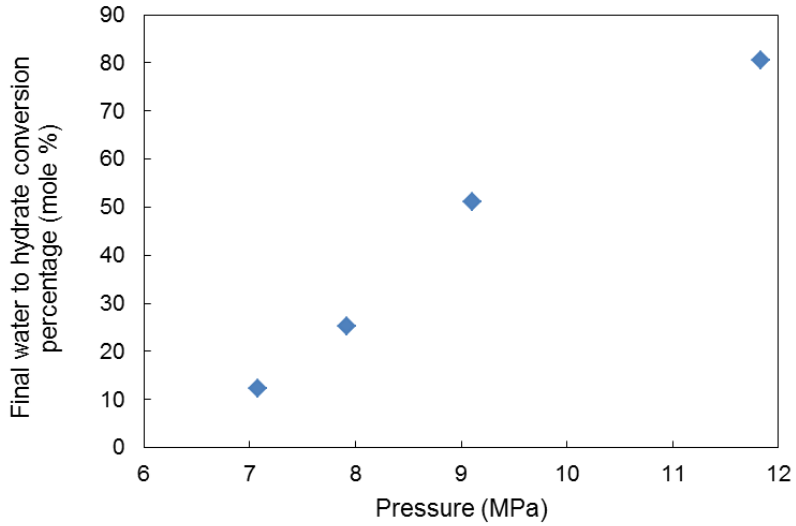

Figure 6-24. Final moles of CF_4 consumed per moles of water at the constant temperature of 275.3 and different initial pressures.

As shown in Table 6-22, the maximum final water converted to hydrate was about 80.6 mol % at the initial temperature and pressure conditions of 275.3 K and 11.83 MPa, respectively. With an increase in the initial pressure from 7.08 to 11.83 MPa at a constant temperature of 275.3 K, the final value of the water converted to hydrate increased from 12.4% to 80.6% which indicates the initial pressure has a significant effect on the value of water converted to hydrate. As shown in Table 6-22, with an increase in the initial temperature from 276.1 K to 276.6 K (ΔT = 0.5 K) at a constant pressure of 11.47 MPa, the water converted to hydrate decreased from 67.2% to 45.3%.

6.3.5. Storage Capacity (SC)

The storage capacity (SC) of gas hydrates is expressed as the volume of gas stored in a volume of gas hydrate at the STP (standard temperature pressure) conditions. Figure 6-25 illustrates the amount of storage capacity at a constant initial temperature of 275.3 K and four initial pressures of 7.08 MPa, 7.92 MPa, 9.11 MPa, and 11.83 MPa. As seen in this figure, the storage capacity increased with an increase in the initial pressure.

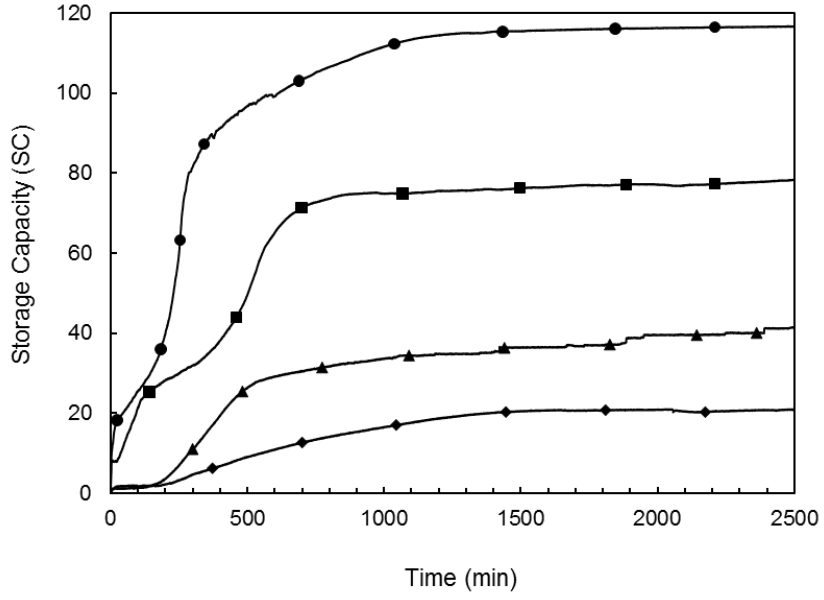

Figure 6-25. CF_4 storage capacity during hydrate formation at an initial temperature 275.35 K and different pressures: —♦—, 7.08 MPa; —▲—, 7.92 MPa; —■—, 9.11 MPa; —●—, 11.83 MPa.

Figure 6-26 shows the amount of storage capacity at a constant initial pressure of 11.47 MPa and two initial temperatures of 276.1 and 276.6 K. It can be observed in Figure 6-26 that an increase in the initial temperature has a reverse effect on the storage capacity. Thus, storage capacity decreased with an increase in the initial temperature.

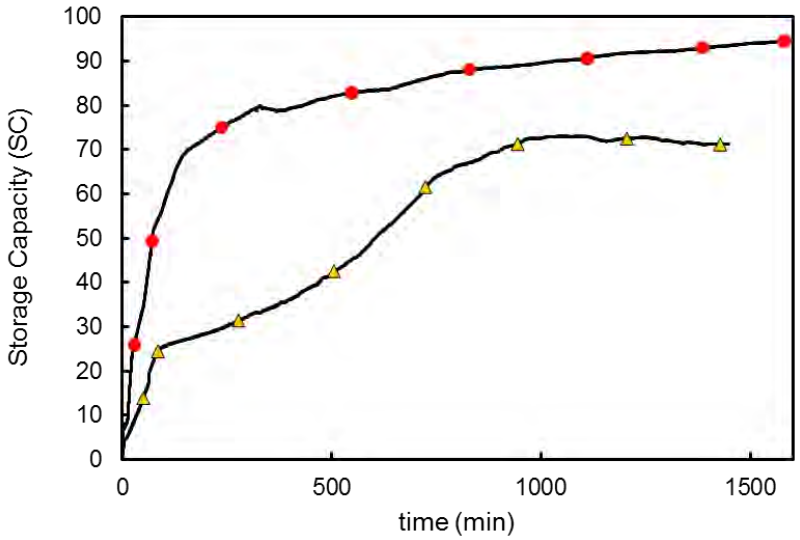

Figure 6-26. CF_4 Storage capacity during hydrate formation at an initial pressure of 11.47 MPa and different temperatures: —▲—, 276.6 K; —●—, 276.1 K.

The final storage capacity at different initial conditions, at the end of each experiment, is presented in Table 6-23.

Table 6-23. The final storage capacity at different initial temperatures and pressures conditions.

Initial Temperature (K)	Initial Pressure(MPa)	[a] SC (V/V)
275.3	7.08	21.14
275.3	7.92	41.4
275.3	9.11	78.3
275.3	11.83	116.92
276.1	11.47	100.35
276.6	11.47	71.18

[a] Storage capacity

The maximum and minimum amount of storage capacity was 21.14 and 116.92 (v/v), respectively which are related to initial conditions of (T=275.3 K, P=11.83 MPa) and (T=275.3 K, P=7.08 MPa), respectively. The maximum amount of storage capacity at the constant temperature of 275.3 K is related to the maximum pressure of 11.83 MPa. As can be observed in Table 6-23, the final storage capacity was 100.35 and 71.18 v/v at the constant pressure of 11.47 MPa and two initial temperatures of 276.1 K and 276.6 K, respectively.

6.3.6. Rate of hydrate formation

According to the kinetic model proposed by Englezos et al. (1987) (Englezos et al., 1987), hydrate formation consists of three stages. At the first stage, gas molecules move from the vapour phase to the liquid bulk. Thereafter in the second step, gas molecules diffuse from the liquid bulk to the boundary and finally at the third stage, molecules of gas encapsulate inside the hydrate cavities (Sloan and Koh, 2008). With these assumptions, the rate of growth per particle was achieved using the differences between the fugacity of gas molecule in the bulk liquid and that in the liquid at the hydrate interface. Using this model, the rate of growth for CF_4 hydrate was modelled in this study. The rate of hydrate formation is shown in Figures 6-27 and 6-28, with the highest rate peak obtained at 11.83 MPa (at a constant temperature of 275.3 K) which occurred at 250 min after the induction time (Figure 6-27). As shown in these figures, the rate of hydrate formation increased significantly to reach to the maximum value. During this period, CF_4 molecules were concentrated and packed inside the hydrate cavities more than those in the vapour phase. Due to the water consumption during the hydrate formation and the effects of mass and heat transfer, the rate of hydrate formation gradually decreased until it reached zero at the end of each experiment. As can be observed in Figure 6-27 with an increase in the initial pressure, the hydrate formation rate increased. As observed in Figure 6-28, an increase in the initial temperature has the reverse effect on the rate of hydrate formation. The maximum rate of CF_4 formation was 0.0009 (mol of CF_4 / (mol of water .min)) which is related to initial conditions of (T=276.1 K, P=11.47 MPa).

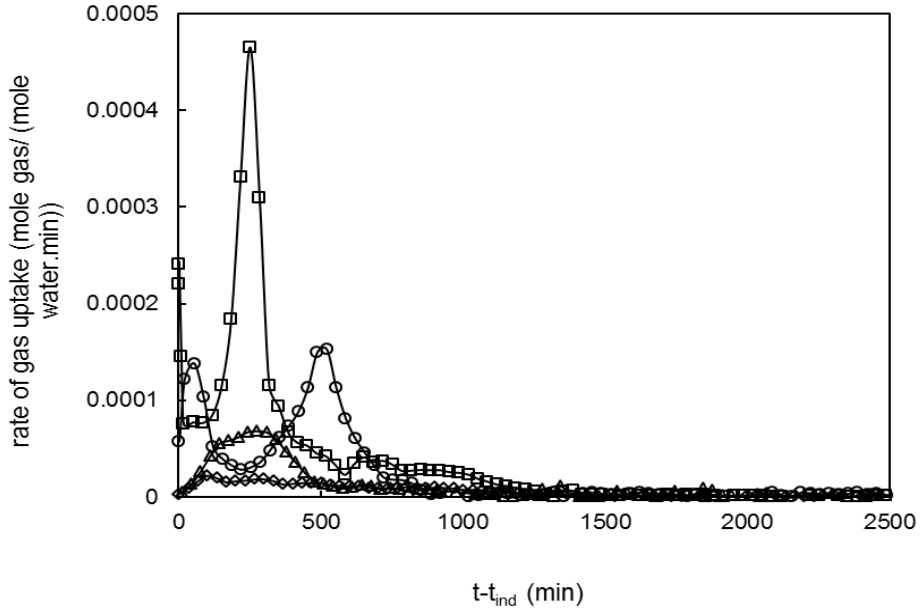

Figure 6-27. Rate of CF_4 consumption during the hydrate formation at an initial temperature of 275.35 K and different pressures: —◊—, 7.08 MPa; —Δ—, 7.92 MPa; —○—, 9.11 MPa; —□—, 11.83 MPa.

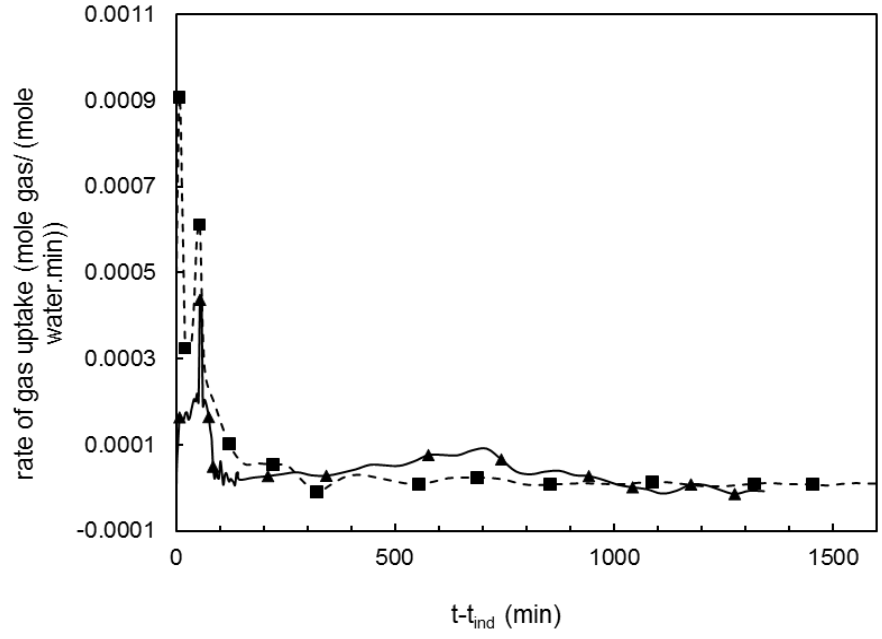

Figure 6-28. Rate of CF_4 consumption during the hydrate formation at an initial pressure of 11.47 MPa and different temperatures: ---■---, 276.11 K; —▲—, 276.60 K.

6.3.7. Apparent rate constant (K_{app})

The apparent rate constant (K_{app}) during hydrate formation at a constant temperature of 275.3 K and an initial pressure of 7.08, 7.92, 9.11 and 11.83 MPa is reported in Figure 6-29. In addition the maximum apparent rate constant for CF_4 hydrate formation at the different initial conditions is presented in Figures 6-30 and 6-31 and Table 6-24. It is observed in Figure 6-30 that with an increase in the initial pressure, the maximum apparent rate constant was increased. As observed in Figure 6-31, an increase in the initial temperature has the reverse effect on the apparent rate constant. In addition as shown in these figures, the maximum amount of the apparent rate constant of $2.458\times10^{-9}\left(\frac{moleG}{moleW.Pa.\min}\right)$ was detected at a constant initial temperature of 275.3 K and an initial pressure of 11.83 MPa.

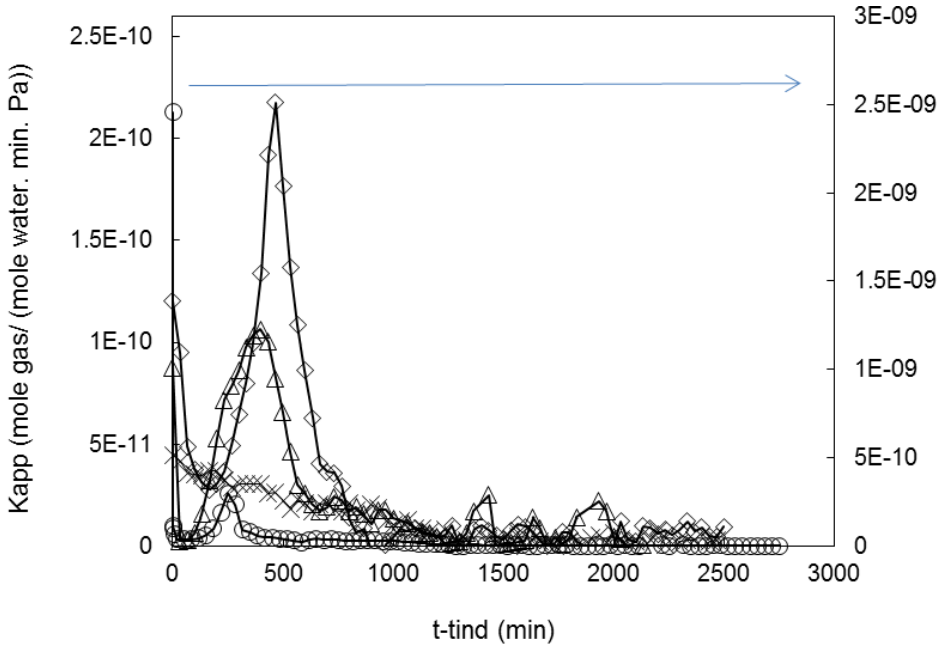

Figure 6-29. The apparent rate constant (K_{app}) of CF_4 hydrate formation at a temperature of 275.35 K and different pressures: —×—, 7.08 MPa; —Δ—, 7.92 MPa; —◊—, 9.11 MPa; —○—, 11.83 MPa, (K_{app} values for 11.83 MPa is related to secondary axes (right side axes)).

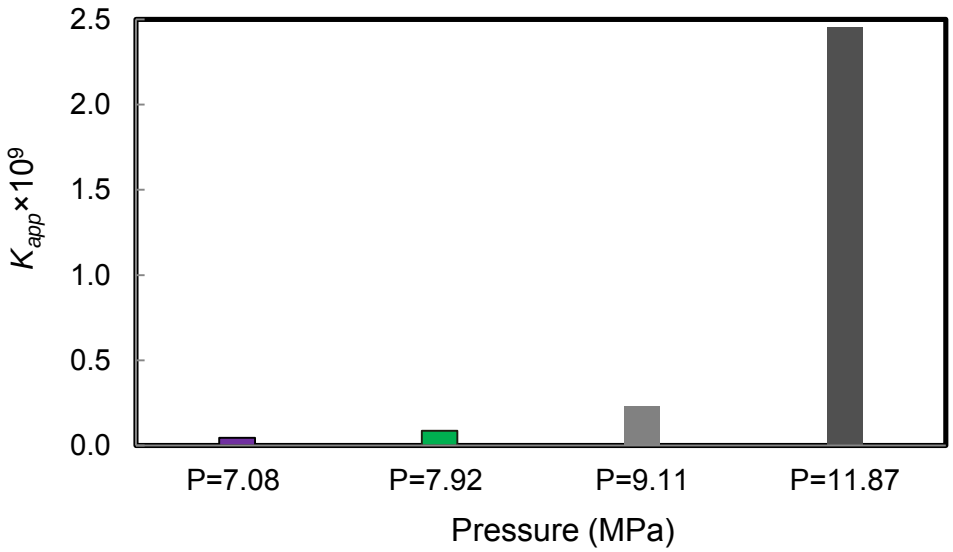

Figure 6-30. The effect of initial pressure on the maximum apparent rate constant of CF_4 hydrate formation at T=275.36 K.

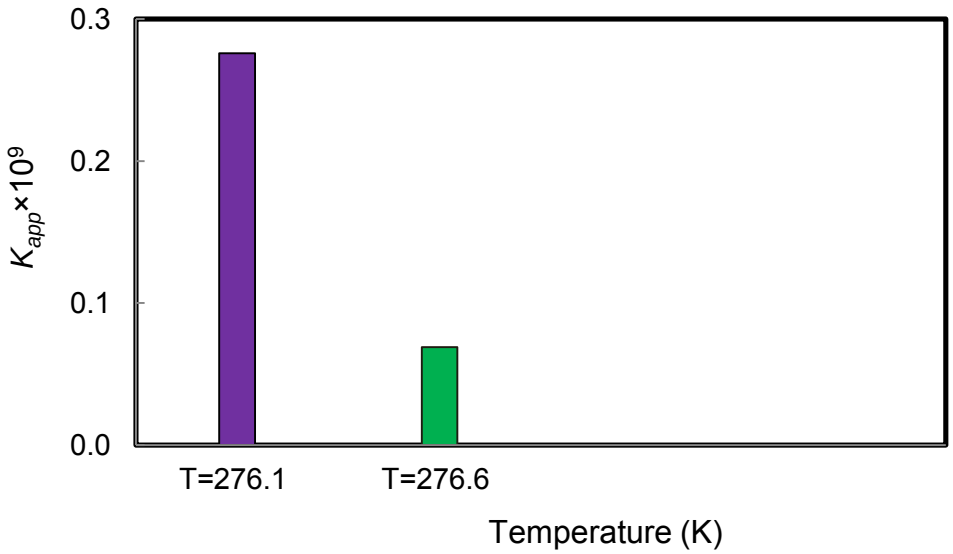

Figure 6-31. The effect of initial temperature on the maximum apparent rate constant of CF_4 hydrate formation at P=11.47 MPa.

Table 6-24. The maximum apparent rate constant of CF_4 hydrate formation at different initial temperatures and pressures conditions.

Initial Temperature (K)	Initial Pressure(MPa)	${}^{e}K_{app\times10}{}^{9}$ $\left(\frac{mole\,G}{(mole\,W).\,min.\,Pa}\right)$
275.3	7.08	0.044
275.3	7.92	0.087
275.3	9.11	0.230
275.3	11.83	2.458
276.1	11.47	0.276
276.6	11.47	0.069

The aim of this study was to find an initial condition of CF_4 hydrate formation with the high apparent rate constant and also discover a systematic trend between the initial conditions and the rate of CF_4 hydrate formation. As observed in Figure 6-29, the apparent rate constant increased significantly to reach to the maximum value and then it decreased gradually to zero at the end of each experiment. As shown in Table 6-24, with an increase in the initial pressure from 9.11 to 11.83 MPa (ΔP = 2.72 MPa) at a constant temperature of 275.3 K, the value of apparent rate constant increased from 0.23×10^{-9} $\left(\frac{mole\,G}{(mole\,W).\,min.\,Pa}\right)$ to 2.458×10^{-9} $\left(\frac{mole\,G}{(mole\,W).\,min.\,Pa}\right)$. As shown in Table 6-24, with an increase in the initial temperature from 276.1 K to 276.6 K (ΔT = 0.5 K) at a constant pressure of 11.47 MPa, apparent rate constant decreased from 0.276×10^{-9} $\left(\frac{mole\,G}{(mole\,W).\,min.\,Pa}\right)$ to 0.069×10^{-9} $\left(\frac{mole\,G}{(mole\,W).\,min.\,Pa}\right)$. The results showed that the initial temperature has a significant effect on the apparent rate constant of CF_4 hydrate formation. The maximum apparent rate constant was 2.458×10^{-9} $\left(\frac{mole\,G}{(mole\,W).\,min.\,Pa}\right)$ which is related to the initial conditions of T=275.36 K and P=11.87 MPa.

6.4. Kinetic results for the semi-clathrate hydrate of Ar + aqueous TBAB solution + SDS

To the best of our knowledge, there is no kinetic study in the literature on the systems of semi-clathrate hydrate of Ar + water + TBAB + SDS and the kinetics behaviours for these systems. The aim of this study was to investigate the effect of initial temperature, initial pressure, aqueous TBAB solution concentration, and sodium dodecyl benzene sulfonate (SDS) concentration on the kinetic of the semi-clathrate hydrate of Ar + aqueous TBAB solutions. The model which was used in this study for the kinetic of semi-clathrate hydrate for the system of Ar + water + TBAB is presented in Appendix D.

6.4.1. Effect of initial temperatures and pressures

For investigation of the effect of initial pressure on the semi-clathrate hydrate for the system of Ar + aqueous TBAB solution, experimental measurements were performed at a constant temperature of 285 K and the initial pressures of 6.1 MPa, 8.1 MPa, and 10.1 MPa. The initial pressures and temperatures were selected inside the hydrate stability zone with different degree of sub cooling. The changes in the initial conditions make change in the driving force of hydrate formation. Figure 6-32 shows the degree of subcooling for the semi-clathrate hydrate formation for the system of Ar + 0.1 TBAB + 0.9 water (concentrations are in mass fractions) for different initial pressures. As shown in Figure 6-32, an increase in the initial pressure leads to a higher degree of subcooling. Table 6-25 shows the investigated initial temperatures and pressures performed in this study for the semi-clathrate hydrate formation for the system of Ar + 0.1 TBAB + 0.9 water.

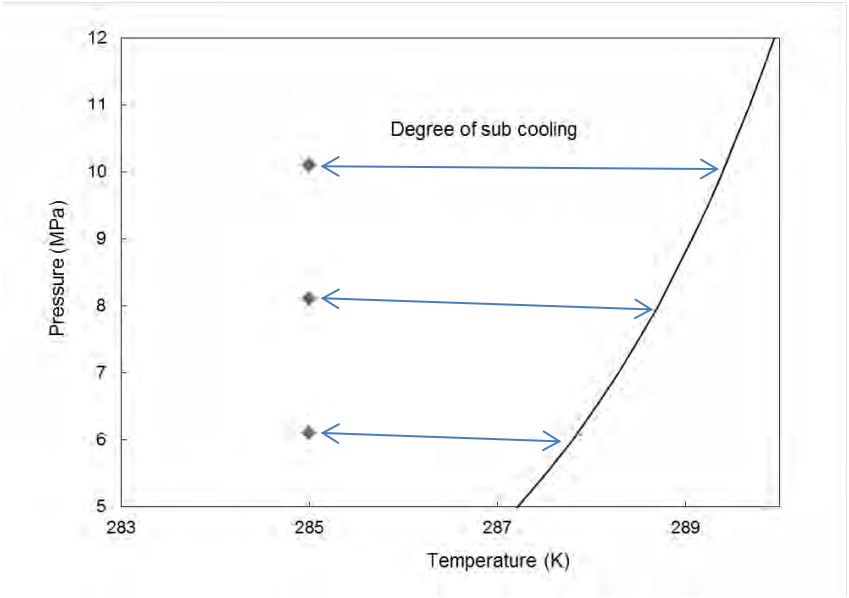

Figure 6-32. The degree of subcooling between the initial pressure conditions (♦) and the semi-clathrate hydrate of Ar + 0.1 TBAB + 0.9 water equilibrium line (solid line) at a constant temperature of 285 K and initial pressures of 6.1 MPa, 8.1 MPa and 10.1 MPa.

Table 6-25. The values of induction time, final mole of Ar consumed and maximum kinetic constant at different initial temperatures and pressures for the semi-clathrate hydrate formation of Ar + 0.1 TBAB + 0.9 water.

Initial Temperature (K)	Initial Pressure (MPa)	Induction time (min)	Final moles of Ar consumed (mole)	Maximum Intrinsic rate constant $\times 10^7$ (mol/(J.min))
285.0.0	6.1	58.0	0.0063	1.6
285.0.0	8.1	27.0	0.0066	2.5
285.0.0	10.1	20.0	0.0112	2.3
*281.0.0	*8.1*	*0.3*	*0.0085*	9.4
285.0.0	*8.1*	*26.2*	*0.0066*	2.5
287.5	*8.1*	*595.7*	*0.0058*	1.8

* The italic format shows the effect of initial temperature at the pressure of 8.1 MPa.

Figure 6-33 presents the pressure changes during the semi-clathrate hydrate formation of Ar + 0.1 TBAB + 0.9 water at an initial temperature of 285 K and different initial pressures of 6.1 MPa, 8.1 MPa and 10.1 MPa. As mentioned earlier, three regions can be determined during the

hydrate formation: 1) dissolution stage, 2) induction period and 3) growth stage. At the first stage, some of Ar gas in the vapour phase dissolves in the aqueous TBAB solutions. During the second period or induction period, semiclathrate hydrate crystals form and decompose until they form a stable nucleus (nucleation) and grow to a detectable size. In the growth period, Ar gas molecules are trapped inside the TBAB semi-clathrate hydrate cavities and the pressure of the system significantly decreases until it reaches to a constant value. As seen in Figure 6-33 and Table 6-25, the induction time for the semi-clathrate hydrate formation for the system of Ar + 0.1 TBAB + 0.9 water at a constant temperature of 285 K and initial pressures of 6.1 MPa, 8.1 MPa and 10.1 MPa are equal to 58 min, 27 min, and 20 min, respectively. For design of an economic hydrate based process, the initial temperature and pressure with a short induction time is desired. As can be observed in Figure 6-33, with an increase in the pressure form 6.1 MPa to 10.1 MPa, the induction time decreases. The minimum induction time between these three conditions is related to the initial pressure and temperature of 10.1 MPa and 285 K, respectively.

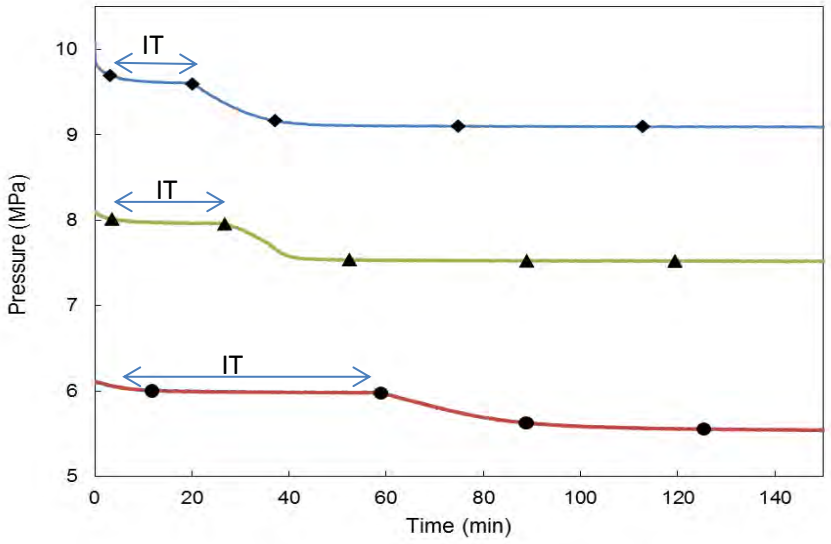

Figure 6-33. The pressure changes during the semi-clathrate hydrate formation for the system of Ar + 0.1 TBAB + 0.9 water at an initial temperature of 285 K and different initial pressures: —♦—, 10.1 MPa; —▲—, 8.1 MPa; —●—, 6.1 MPa.

Figure 6-34 presents the effect of the initial temperature on the semi-clathrate hydrate for the system of Ar + 0.1 TBAB + 0.9 water, at a constant pressure of 8.1 MPa and the initial temperatures of 281 K, 285 K and 287.5 K. As shown in Figure 6-34, with an increase in the temperature from 281 K to 287.5 K, the induction time decreases, significantly. As shown in Table 6-25, with an increase the initial temperature from 285 K to 287.5 K (ΔT = 2.5 K), the induction time decreases 569.5 min which shows the importance of the effect of the initial temperature on the semi-clathrate of Ar + aqueous TBAB solutions. As observed in Table 6-25, the minimum and maximum induction time for the investigated initial temperatures and pressures are 0.3 min (for the initial conditions of T = 281 K, P = 8.1 MPa) and 595.7 min (for the initial conditions of T = 287.5 K, P = 8.1 MPa), respectively. As seen in Figure 6-34, with a decrease in the initial temperature, the pressure drop during the semi-clathrate hydrate formation increases resulting in the increasing gas consumption. For instance, at the initial temperature of T = 281 K, the pressure of the system changed from 8.1 MPa to 7.4 MPa (ΔP = 0.7 MPa) while at the initial temperature of 287.5 K the pressure drops from 8.1 MPa to 7.6 MPa (ΔP = 0.5 MPa).

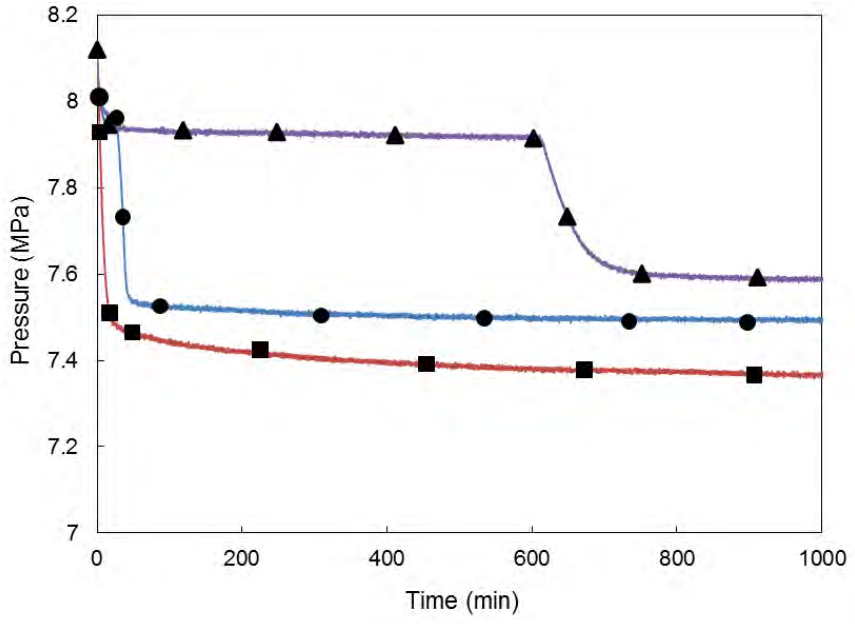

Figure 6-34. The pressure of the system during the semi-clathrate hydrate formation for the system of Ar + 0.1 TBAB + 0.9 water at an initial pressure of 8.1 MPa and different temperatures —■—, 281 K; —●—, 285K, —▲—, 287.5 K.

Figure 6-35 compares the consumption of Ar during the semi-clathrate hydrate formation for the system of Ar + 0.1 TBAB + 0.9 water at an initial temperature 285.0 K and different pressures of 6.1, 8.1 and 10.1 MPa.

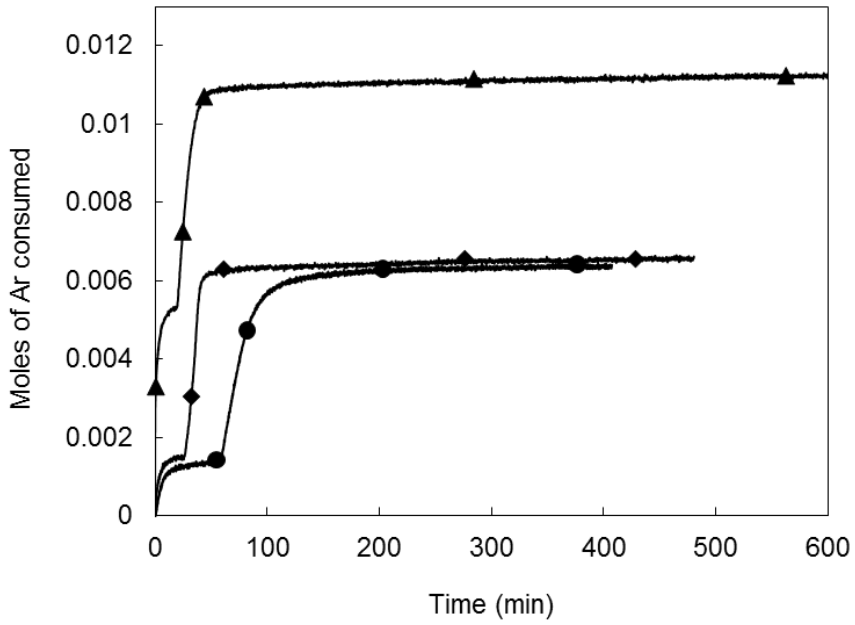

Figure 6-35. Number of moles of Ar consumed during the hydrate formation at an initial temperature 285.0 K and different pressures: —●—, 6.1 MPa; —♦—, 8.1 MPa; —▲—, 10.1 MPa.

As observed in Figure 6-35 and Table 6-25, with an increase in the initial pressure from 6.1 to 8.1 MPa, the amount of gas consumed does not increase significantly. In addition, with an increase in the initial pressure from 8.1 to 10.1 MPa at a constant temperature of 285.0 K, the final amount of gas consumed increased by almost 84% which shows higher initial pressures has a significant effect on the Ar consumption. Figure 6-36 shows the consumption of Ar during the semi-clathrate hydrate formation for the system of Ar + 0.1 TBAB + 0.9 water at an initial pressure of 8.1 MPa and temperatures of 281.0, 285.0, and 276.6 K.

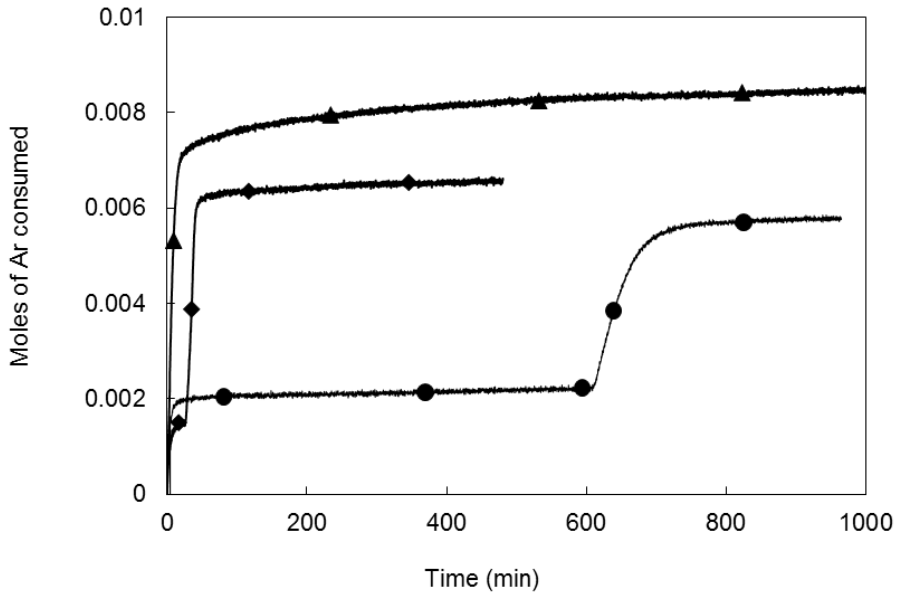

Figure 6-36. Number of moles of Ar consumed during the semi-clathrate hydrate formation for the system of Ar + 0.1 TBAB + 0.9 water at an initial pressure of 8.1 MPa and different temperatures: —▲—, 281.0 K, —♦—, 285.0 K; —●—, 287 K.

As can be seen in this Figure, Ar consumption decreased with an increase in the initial temperature. As shown in Table 6-25, with an increase in the initial temperature from 281.0 K to 287 K (ΔT = 6 K) at a constant pressure of 8.1 MPa, the final amount of gas consumed decreased by nearly 47%. The results of this study indicated that the initial temperature has an important effect on the Ar consumption. As observed in Table 6-25, the maximum amount of number of argon molecules consumed is 0.0112 mole which is related to the initial temperature and pressure of 285.0 K and 10.1 MPa. Figure 6-37 shows the kinetic constant, ak_f, during the semi-clathrate hydrate formation for the system of Ar + 0.1 TBAB + 0.9 water at an initial pressure of 8.1 MPa and different temperatures of 285.0 and 287 K.

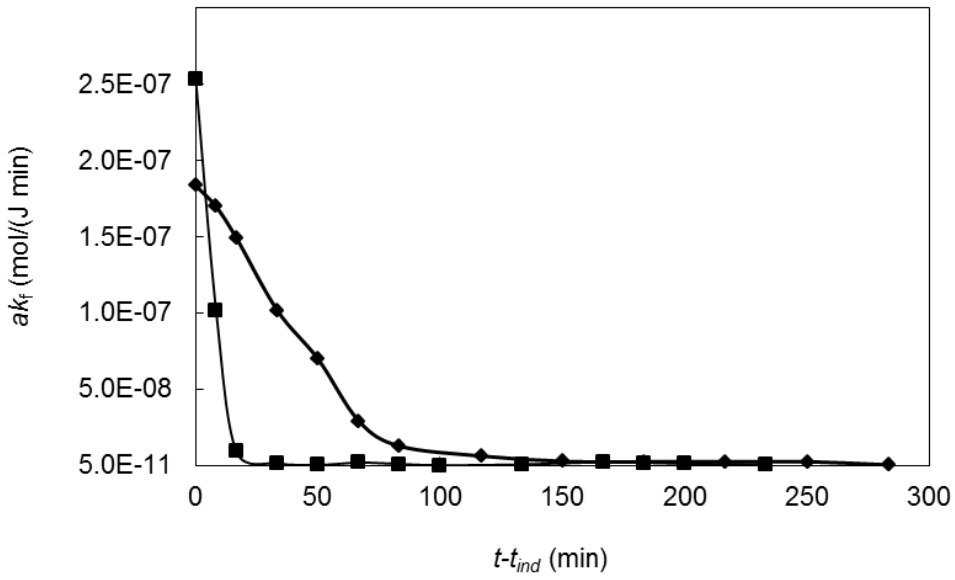

Figure 6-37. Kinetic constant, ak_f, during the semi-clathrate hydrate formation for the system of Ar + 0.1 TBAB + 0.9 water at an initial pressure of 8.1 MPa and different temperatures: —♦—, 287 K; —■—, 285.0 K.

As observed in Figure 6-37, the kinetic constant reaches to its maximum value at the start of hydrate formation and then decreases to reach to a constant value which shows a steady state condition of hydrate formation. It is observed in Figure 6-37 that with an increase in the initial temperature, the maximum kinetic constant is decreased. In addition the maximum kinetic constant for the semi-clathrate hydrate formation for the system of Ar + 0.1 TBAB + 0.9 water at different initial conditions is presented in Figures 6-38 and Table 6-25. As observed in Table 6-25, with an increase in the initial pressure, the kinetic constant increases. In addition as shown in Figure 6-38, the maximum amount of the kinetic constant of $9.4\times10^{-7}\left(\frac{molG}{molW.Pa.\min}\right)$ was detected at a constant initial temperature of 281.0 K and an initial pressure of 8.1 MPa.

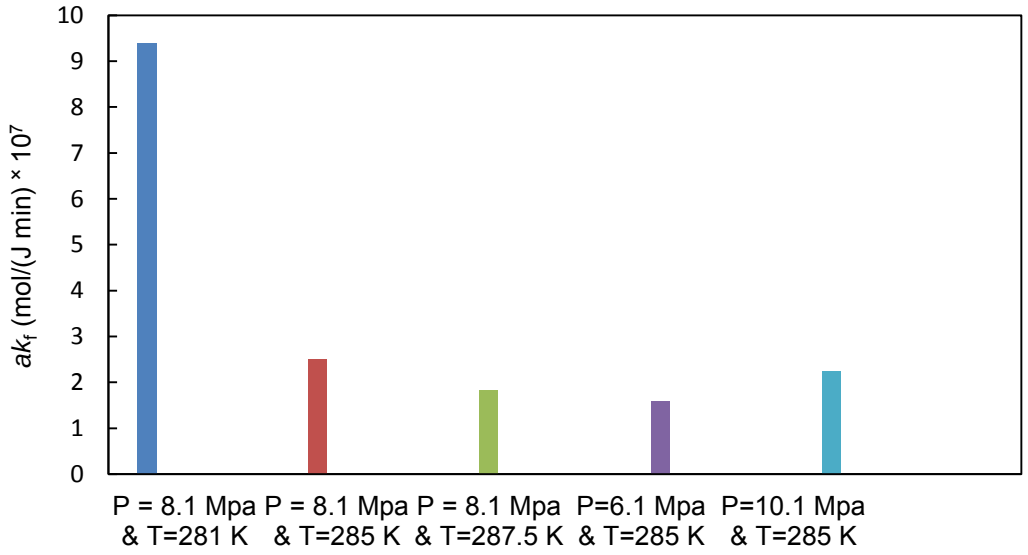

Figure 6-38. The effect of initial pressure and temperature on the maximum kinetic constant for the semi-clathrate hydrate formation for the system of Ar + 0.1 TBAB + 0.9 water.

6.4.2. Effect of SDS

In order to design a cost effective separation process based on clathrate/semi-clathrate hydrate formation, it is crucial to work at low pressures. One solution to this problem is the application of the TBAB solutions to decrease the pressure of the hydrate formation. Additionally the rate of the hydrate formation has a significant effect on the economics of the process. Consequently the influence of some kinetic additives on the semi-clathrate hydrate formation rate is also investigated in this study. Several studies indicated that sodium dodecyl sulfate (SDS), as a surfactant, can accelerate the growth rate of clathrate hydrates such as methane and carbon dioxide and decrease the induction time (Zhang et al., 2007, Partoon and Javanmardi, 2013, Hashemi et al., 2015). However, there is no kinetic study in the literature on the effect of SDS on the rate of semi-clathrate hydrate formation and the behaviour of these systems.

The aim of this study was to clearly understand the effect of SDS concentration on the semi-clathrate hydrate formation for the system of Ar + aqueous TBAB solution. Figure 6-39 presents the pressure of the system during the semi-clathrate hydrate formation for the system of Ar + 0.1 TBAB + 0.9 water + SDS at an initial temperature of 285 K at different SDS concentrations of 0 ppm, 100 ppm, 200 ppm and 400 ppm and different initial pressures of 6.1 MPa, 8.1 MPa and 10.1 MPa. The values of the induction times for the aforementioned system

are shown in Table 6-26. As seen in Figure 6-39 part *(a)* and Table 6-26, the addition of SDS (in the concentration of 100, 200, 400 ppm) increases the induction time, at initial temperature and pressure of 285 K and 6.1 MPa, respectively. As seen in Table 6-26, the induction time in the presence of 400ppm SDS is about eight times greater than that without SDS, at initial temperature and pressure of 285 K and 6.1 MPa, respectively.

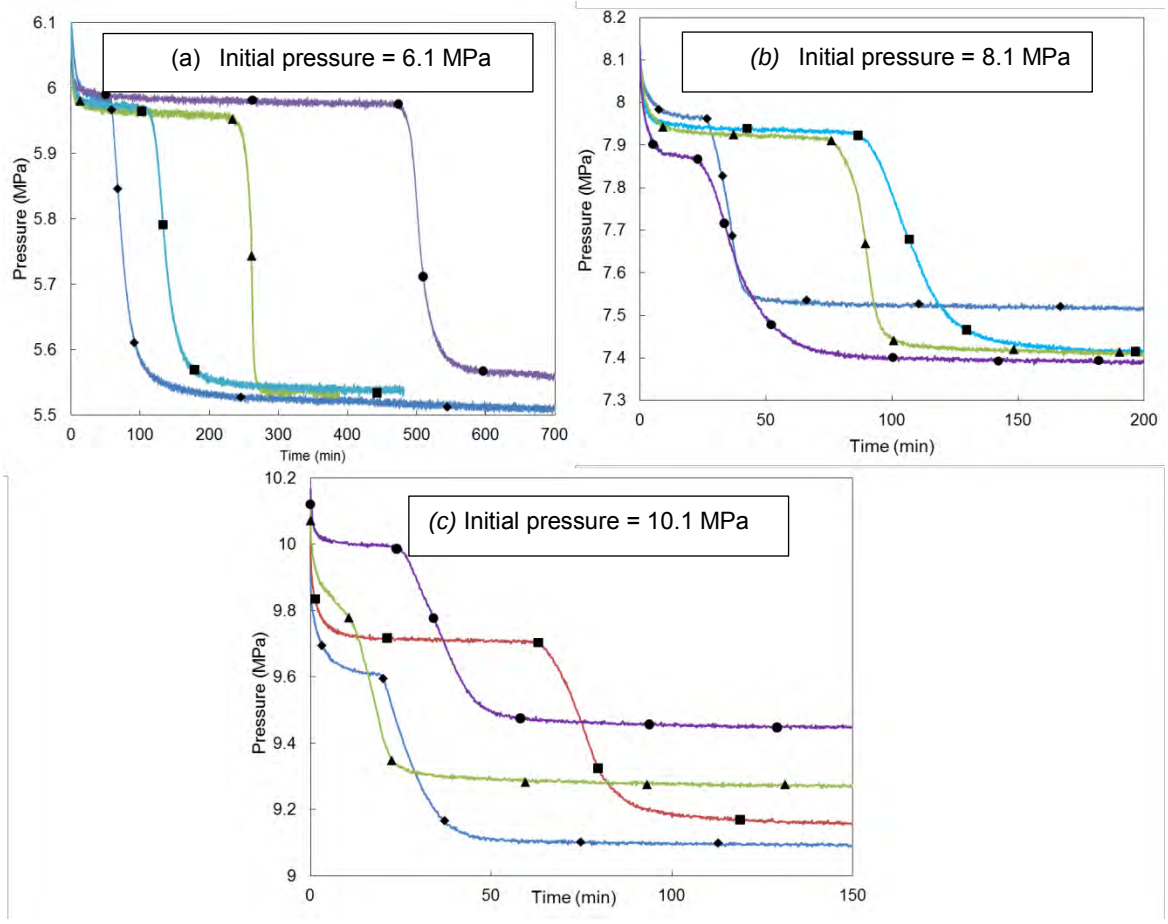

Figure 6-39. The pressure change during the semi-clathrate hydrate formation for the system of Ar + 0.1 TBAB + 0.9 water + SDS at an initial temperature of 285 K and different SDS concentrations: —♦—, 0 ppm SDS; —▲—, 100 ppm SDS; —■—, 200 ppm SDS; —●—, 400 ppm SDS.

Figure 6-39 part *(c)* shows the effect of SDS at a higher initial pressure of 10.1 MPa on the semi-clathrate hydrate of Ar + 0.1 TBAB + 0.9 water. As can be seen in this Figure, the presence of SDS has no positive effect on the decreasing the induction time. As shown in

Figure 6-39 part *(b)* and Table 6-26, 200 ppm SDS increase the induction time about three times greater than without SDS.

As seen in Figure 6-39 part *(c)*, 100 ppm SDS decreases the induction time to ten minutes compared with the solution without SDS at 10.1 MPa. As observed in Table 6-26, two concentrations of 200 ppm and 400 ppm have no positive effect on the decreasing the induction time for the aforementioned system. There is no systematic trend between induction times and the SDS concentrations for this system. The results showed an unusual behaviour of SDS on the semi-clathrate hydrate formation for the system of Ar + water + TBAB. Hence the SDS solution did not increase the rate of hydrate nucleation and an alternative kinetic promoter should be explored for the semi-clathrate hydrate of Ar + aqueous TBAB solutions.

Table 6-26. The values of induction time , at different SDS concentrations and initial pressures for the semi-clathrate hydrate formation for the system of Ar + 0.1 TBAB + 0.9 water.

SDS concentration (ppm)	Initial Pressure (MPa)	Induction time (min)
0	6.1	58.0
100	6.1	233.4
200	6.1	109.8
400	6.1	474.0
0	8.1	27.0
100	8.1	73.9
200	8.1	84.8
400	8.1	22.3
0	10.1	20.0
100	10.1	11.2
200	10.1	61.0
400	10.1	24.4

6.4.3. Effect of TBAB

The aim of this experimental work was to discover the effect of aqueous TBAB solution on the kinetics of argon hydrate formation. For this purpose, the effect of three TBAB concentrations of 0.1, 0.2, and 0.3 mass fractions on the argon hydrate were examined. Figure 6-40 shows the pressure change during the semi-clathrate hydrate formation of Ar + aqueous TBAB solutions at TBAB concentrations of 0.1, 0.2 and 0.3 mass fractions. Table 6-27 presents the values of induction time for this system.

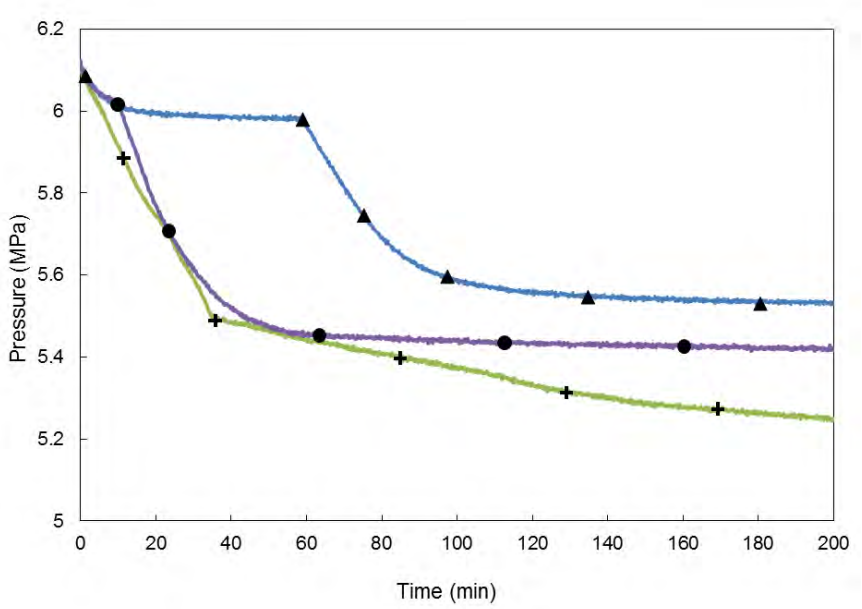

Figure 6-40. The pressure change during the semi-clathrate hydrate formation for the system of Ar + TBAB + water at an initial temperature of 285 K and pressure of 6.1 MPa and different TBAB concentrations: —▲—, 0.1 mass fraction aqueous TBAB solution; —●— 0.2 mass fraction aqueous TBAB solution; — + —, 0.3 mass fraction aqueous TBAB solution.

As observed in Figure 6-40, with an increase in the TBAB concentration form 0.1 to 0.3 mass fraction, the rate of semi-clathrate hydrate nucleation increases and the induction time decreases, significantly. As seen in Table 6-27, the induction time for the semi-clathrate hydrate formation for the system of Ar + 0.3 TBAB + 0.7 water is 0.1 min which is 580 times smaller than of that for the system of Ar + 0.1 TBAB + 0.9 water. As observed in Figure 6-40, with an

increase in the TBAB concentration from 0.1 to 0.3 mass fraction, the amount of the pressure drop increases, resulting in more gas consumption during the semi-clathrate hydrate formation.

Table 6-27. The values of induction time and final moles of gas consumed for the semi-clathrate hydrate of Ar + TBAB + water at an initial temperature of 285.0 K and pressure of 6.1 MPa and different TBAB concentrations.

TBAB concentration (mass fraction)	Induction time (min)	Final moles of gas consumed
0.1	58.0	0.0065
0.2	9.3	0.0093
0.3	0.1	0.0105

Figure 6-41 shows the Ar consumed during the semi-clathrate hydrate formation for the system of Ar + TBAB + water at the initial conditions of 285.0 K and 6.1 MPa and different TBAB concentrations of 0.1, 0.2, and 0.3 mass fractions.

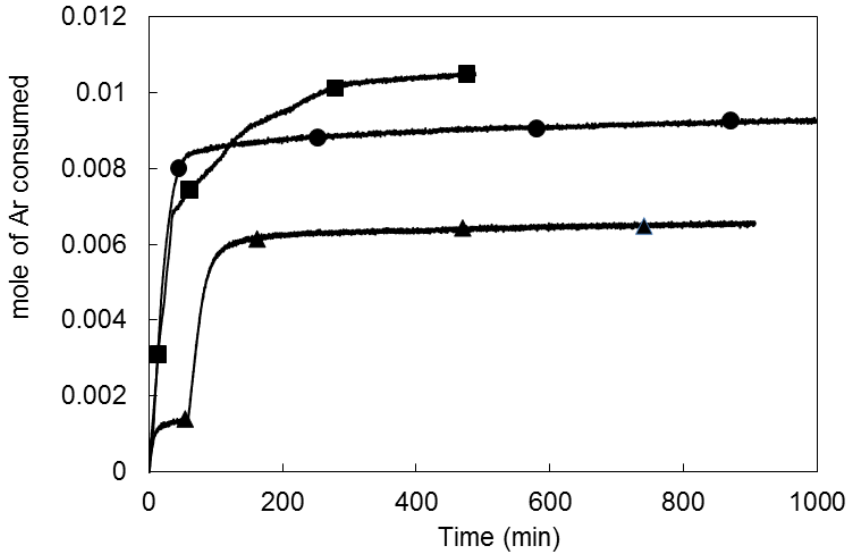

Figure 6-41. Number of moles of Ar consumed during the semi-clathrate hydrate formation for the system of Ar + TBAB + water at the initial conditions of 285.0 K and 6.1 MPa and different TBAB concentrations (mass fraction): —▲—, 0.1 TBAB, —●—, 0.2 TBAB; —■—, 0.3 TBAB.

As can be seen in this Figure, Ar consumption increased with an increase in the concentration of TBAB aqueous solutions. The amount of final consumption of Ar at the end of experiment was shown in Table 6-27. As shown in Table 6-27, with an increase in the TBAB concentration from 0.1 to 0.2 mass fraction, the final amount of gas consumed increased by approximately 43%. Figure 6-42 shows the rate of Ar consumed during the semi-clathrate hydrate formation for the system of Ar + TBAB + water at an initial conditions of 285.0 K.

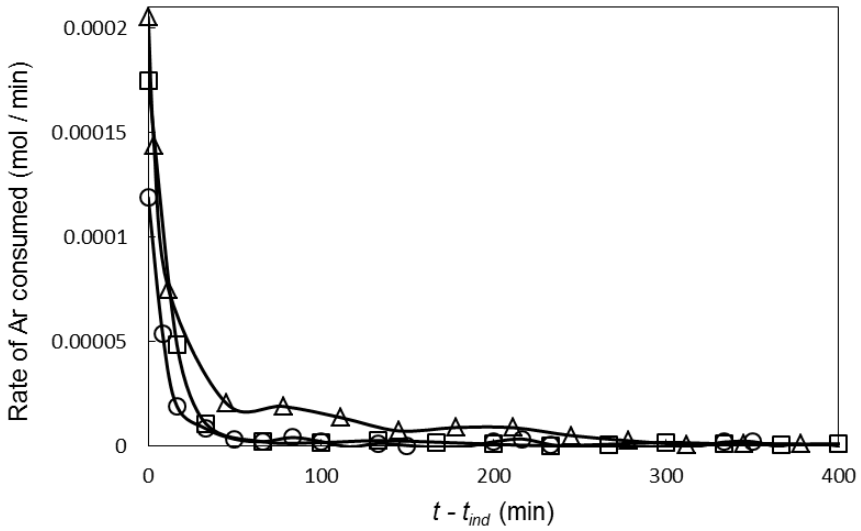

Figure 6-42. Rate of Ar consumed during the semi-clathrate hydrate formation for the system of Ar + TBAB + water at an initial conditions of 285.0 K and 6.1 MPa and different TBAB concentrations (mass fraction): ―○―, 0.1 TBAB, ―□―, 0.2 TBAB; ―Δ―, 0.3 TBAB.

As observed in Figure 6-42, the maximum rate of Ar consumed occurred at the start of hydrate formation and then the rate of hydrate formation decreases to reach to a constant value which shows a steady state condition of hydrate formation. It is observed in Figure 6-42 that with an increase in the TBAB concentration, the maximum rate of Ar consumed increases. The results show the positive kinetic behaviour of TBAB for the semi-clathrate hydrate formation for the system of Ar + TBAB aqueous solution. The results show the positive kinetic behaviour of TBAB for the semi-clathrate hydrate formation for the system of Ar + aqueous TBAB solution.

According to the findings in this study, TBAB is a reliable promoter to decrease the pressure of argon hydrate formation and increase the rate of argon hydrate formation.

6.5. Application of this study

Separation and purification of expensive gases such as Ar, Kr, Xe and CF_4 are an important issue as high purities of these gases are required in industries. As mentioned earlier, current technologies for gas separation consist of cryogenic distillation (Kerry, 2010), zeolite adsorbent (Branken et al., 2014, Fujii et al., 1991), methal-organic framework (MOF) (Rowsell and Yaghi, 2004, Férey, 2008, Kitagawa et al., 2004) and membranes (Branken et al., 2014). In a comparison of the separation methods mentioned above for the gas purification and separation, cryogenic distillation is a costly and energy intensive process owing to the required low temperature for gas liquefaction. However, separation of gases with close boiling point using distillation method is impossible (Branken et al., 2014). It is shown in the literature that adsorbents such as zeolite can adsorb approximately 20% of their pore volumes. As a result, a large amount of zeolite is needed for the adsorption of the main component in a gas mixture which is not economical. Other separation methods such as membranes have not been proven to be economical (Hnatow M.A. and Happel, 1995). Gas hydrates one of the new method for gas purification, has captured the attention of scientists in recent decades (Vorotyntsev and Malyshev, 2011). Gas hydrate method in separation have lower costs in comparison to the cryogenic distillation because gas hydrates can form and dissociate at ambient temperatures and not very high pressures (compared to cryogenic distillation which are based on gas liquefaction at very low temperatures). One of the other advantages of the application of gas hydrate method in the gas separation is its simplicity because gas hydrate can form and dissociate easily with cooling and heating of the system.

In general, hydrate formation requires a high pressure condition. However, there are methods to decrease the hydrate pressure by use of a promoter such as tetra butyl ammonium (TBAB) or tetrahydrofuran (THF) during hydrate formation and dissociation. Prior to designing the hydrate based process for separation of gas mixtures, precise knowledge of the pure gas hydrate formation/dissociation conditions as well as the kinetic rate of hydrate formation is essential.

The investigated gases in this study (Ar, Kr, Xe, and CF_4) form the gas hydrate at high pressures which makes them difficult to handle and limits their applications in the gas separation. The major aim of this study was to investigate the effect of aqueous TBAB solution as a hydrate promoter on the gas hydrates of Ar, Kr, Xe and CF_4. For this purpose, the hydrate measurements were performed on the systems of: 1) Ar + 0, 0.05, 0.10, 0.20, and 30 mass fraction of aqueous TBAB solution; 2) Kr + 0, 0.05, 0.10, and 0.20 mass fraction of aqueous TBAB solution 3) Xe + 0, 0.10, 0.20, and 0.30 mass fraction of aqueous TBAB solution; 4) CF_4 + 0, 0.05, 0.10, 0.20, and 0.30 mass fraction of aqueous TBAB solution. The results showed that aqueous TBAB solutions have a drastic promotion effect on the Ar and Kr hydrates. Also, with an increase in the concentration of TBAB, the promotion effects of TBAB on the Ar and Kr hydrate formation increase significantly. This promotion effect is an advantage for the practical application of gas hydrate in gas separation technologies compared with processes using only the conventional clathrate hydrate method which is in the presence of pure water. The results indicate that the TBAB aqueous solutions with mass fractions of 0.1, 0.2 and 0.3 TBAB show a promotion effect with regard to the xenon hydrate equilibrium dissociation conditions at pressures lower than 0.73 MPa, 1.40 MPa, and 1.57 MPa, respectively. At higher pressures, the TBAB aqueous solutions show no effect on the xenon hydrate phase equilibrium. The results showed 0.05, 0.10, and 0.20 mass fraction of aqueous TBAB solutions has no promotion effect on the CF_4 hydrate. However, the aqueous TBAB solution with 0.30 mass fraction showed a significant promotion effect on the CF_4 hydrate formation.

Three thermodynamic models based on the fugacity approach (Approach 1) (Mohammadi et al., 2005, Javanmardi et al., 2012), the model proposed by Chen and Guo (Approach 2) (Chen and Guo, 1998) and a simple method based on the vapour pressure calculations (Approach 3) (Parrish and Prausnitz, 1972, Eslamimanesh et al., 2011c) were used to predict the hydrate phase equilibria for the argon, krypton, xenon and CF_4. The maximum value for AAD% was about 0.3% which indicates these three approaches can predict the hydrate dissociation conditions, accurately.

The results from this kinetic study indicated that that increasing the initial pressure at constant temperature decreases the induction time, while hydrate formation rate, the apparent rate constant of reaction, storage capacity, and water to hydrate conversion increase. The same trends were observed with a decrease in the initial temperature at constant pressure.

From the literature survey performed, there is no kinetic study in the literature on the systems of semi-clathrate hydrate and the kinetic behaviours for these systems are unknown. In this study, a kinetic study was performed on the semi-clathrate hydrate for the system of Ar + aqueous TBAB solutions to investigate the effect of initial temperature, initial pressure, aqueous TBAB solution concentration, and sodium dodecyl benzene sulfonate (SDS) concentration. The results showed that with an increase in the initial pressure from 6.1 MPa to 10.1 MPa, the induction time decreases significantly which means the rate of hydrate nucleation increases. The same trends were detected with a decrease in the initial temperature from 285.7 K to 281 K at a constant pressure of 8.1 MPa. In addition, with a decrease in the initial temperature, the amount of the pressure drop during the semi-clathrate hydrate formation increases resulting in the increase of gas consumption. The results indicated that with an increase in the TBAB concentration form 0.1 to 0.3 mass fraction, the rate of semi-clathrate hydrate nucleation increases and the induction time decreases, significantly. In addition, with an increase in the TBAB concentration, the amount of the pressure drop increases resulting in more gas consumption during the semi-clathrate hydrate formation. The results show the positive kinetic and thermodynamic effect of TBAB on Ar hydrate which makes TBAB as a reliable promoter to decrease the pressure of argon hydrate formation and increase the rate of argon hydrate formation. The results for the addition of SDS (in the concentration of 100, 200, 400 ppm) indicated that SDS increases the induction time of the semi-clathrate hydrate formation for the system of Ar + TBAB + water. The addition of SDS (in the concentration of 100, 200, 400 ppm) to the TBAB solution, increased the induction time of the semi-clathrate hydrate formation for the system of Ar + TBAB + water. An alternative kinetic promoter should be explored for the semi-clathrate hydrate of Ar + aqueous TBAB solutions. Due to the high price of Kr and Xe in the high pressures, the kinetic measurements were not performed for these two gases in this study.

The result shows Xe hydrate in the presence of aqueous TBAB solution has much lower pressure conditions compared with Kr, and Ar + aqueous TBAB solutions. Table 6-28 shows the hydrate dissociation pressure for the system of Ar/ Kr/ or Xe + 0.2 mass fraction of aqueous TBAB solutions at 293.6 K.

Table 6-28. Hydrate dissociation pressure for the system of Ar/ Kr/ or Xe + 0.2 mass fraction of aqueous TBAB solutions at 293.6 K.

Gas	Hydrate dissociation pressure (MPa)
Xe	1.34
Kr	3.06
Ar	11.55

As observed in Table 6-28, the hydrate dissociation pressure for the system of Xe + 0.2 mass fraction of aqueous TBAB solutions at the temperature of 293.6 K is approximately 8.6 times smaller than that of Ar + 0.2 mass fraction of aqueous TBAB and 2.3 times smaller than that of Kr + 0.2 mass fraction of aqueous TBAB solutions. These differences of the gas hydrate dissociation pressure confirm the capability of the separation of the mixture of Ar + Kr + Xe in the presence of aqueous TBAB solution using the hydrate method. In addition as seen in Table 6-28, xenon in the presence of TBAB can form hydrate at ambient temperatures and very low pressures which decreases the cost of separation with the hydrate method compared to the cryogenic distillation which is costly and quite energy intensive. The findings in this study indicate that TBAB is a reliable promoter to decrease the pressure of the hydrate formation and increase the rate of hydrate formation which can be used in the separation of noble gases mixtures. In order to design a hydrate based process for noble gas separation and estimate the number of stages, further experimental work on the hydrate phase equilibria for the system of Ar + Kr + Xe + aqueous TBAB solution, considering the equilibrium composition data in liquid, gas and hydrate phases, and a thermodynamic model based on the mass balance are required.

Dabrowski et al. (2009) proposed the gas hydrate method for the separation of CO_2 from the mixture of N_2 +CO_2 (Dabrowski et al., 2009). In this study, this process is suggested for the separation of Xe from the mixture of Xe + Kr + Ar. A schematic diagram of the proposed Xe separation from a mixture of Ar, Kr, and Xe, using the gas hydrates method is presented in Figure 6-43 (Dabrowski et al., 2009).

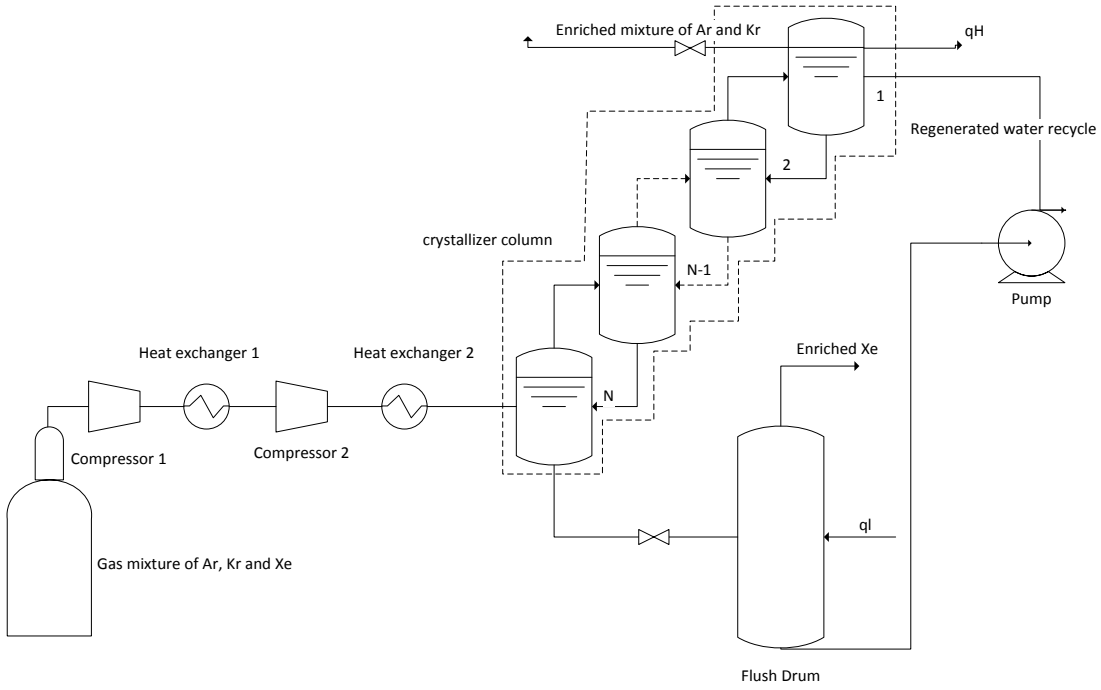

Figure 6-43. A schematic diagram of the gas hydrate process for Xe separation from the mixture of Kr, Xe and Ar using a multi-staged crystallizer (Dabrowski et al., 2009).

As shown in this figure the main part of the process consists of N-staged continuously stirred tank reactors, which are also known as a multi-staged crystallizer column (CC). As observed in Figure 6-43, before the gas mixture enters to the first stage of separation, it is needed to pressurize it to the desired equilibrium pressure condition using a two-staged compressor. The temperature of the gas mixture is decreased using a cooler after each compressor. As observed in Figure 6-43, at each stage of separation, for the formation of gas hydrate, the gas stream and the slurry are coming from the stages (N-1) and (N + 1) respectively. As the hydrate equilibrium pressure of Xe is much lower than Ar and Kr hydrates, Xe can be extracted from this mixture during the N-stages of gas hydrate crystallization. As shown in Figure 6-43, the hydrate slurry produced in the N^{th} reactor is flashed using a flash drum to produce enriched Xe and water. This water is pumped to the first reactor to regenerate the process water. The gas mixture which comes from the first stage is enriched Ar and Kr. It can be assumed that each stage of the gas hydrate crystallization performs as an ideally stirred equilibrium stage. The temperature in each stage is dependent on the pressure and vapour phase composition. Then using the vapour phase composition data and the pressure at each individual stage, the hydrate

equilibrium temperature can be calculated. Fully stirred of gas, liquid and hydrate phases as well as an adequate residence times are required to achieve a thermodynamic equilibrium condition at each step. From a microscopic perspective, to calculate the equilibrium temperature at each stage, the equilibrium hydrate temperature of the vapour phase within the stage and the melting point of the hydrate entering from the stage above are required. As shown in Figure 6-43, crystallization heat is required to be withdrawn at the top stage of the crystallizer column using an external refrigerator, while the regeneration heat is provided using an external heat source to the flash drum. The minimum number of crystallizer stages can be obtained using the equilibrium curve and the operating line in McCabe-Thiele graphical method. To plot the equilibrium diagram, the equilibrium compositions in vapour and hydrate phases are required. Calculation of the power consumption in the compressors, refrigeration, water pump, and heat exchanger are needed to evaluate the energy required in the gas separation using the hydrate method. The advantages of the gas hydrate application in the gas separation are including the simpilicity of the process, the moderate working temperature, capability to acheive more than 99% (dependenting of the number of stages) of purification, enviromentally friendly and comparatively low cost of the process. However, cryogenic distillation is a costly and energy intensive and other separation methods such as membranes and adsorbents have not been proven to be economical. In addition prior to separation using the cryogenic distillation process, other separation methods should be applied to remove water from the gas mixture (Aaron and Tsouris, 2005).

7

CHAPTER SEVEN: CONCLUSIONS

Reliable gas hydrate equilibrium experimental data plays an essential role in the design of a hydrate based process. In this study, a non-visual isochoric-pressure search method, designed and built in-house, was used to measure the gas hydrate equilibrium conditions. The important reason for choosing the mentioned experimental procedure was the accuracy and reliability of this method especially at high pressure conditions.

The major aim of this study was to investigate the effect of aqueous TBAB solution as a promoter on the argon (Ar)/ krypton (Kr)/ xenon (Xe) or tetrafluoromethane (CF_4) hydrate phase equilibria. The hydrate measurements were performed on the systems of: 1) Ar + 0, 0.05, 0.10, 0.20, and 30 mass fraction of aqueous TBAB solution; 2) Kr + 0, 0.05, 0.10, and 0.20 mass fraction of aqueous TBAB solution 3) Xe + 0, 0.10, 0.20, and 0.30 mass fraction of aqueous TBAB solution; 4) CF_4 + 0, 0.05, 0.10, 0.20, and 0.30 mass fraction of aqueous TBAB solution. The Overall Standard Uncertainty, containing calibration and manufacturer uncertainty, was found to be ±0.1 K and ±0.01 MPa for temperature and pressure, respectively.

The results indicated that the TBAB solution has a drastic promotion effect on the Ar and Kr hydrates, i.e., with an increase in the concentrations of aqueous TBAB solutions from 0.05 to

0.20 mass fractions, the promotion effect of TBAB on the Ar and Kr hydrate phase equilibria increases.

The results obtained for the hydrate dissociation data related to the system of Xe + TBAB + water showed that aqueous TBAB solutions, depending on the pressure range, have a twofold effect on the Xe gas hydrate phase equilibria. So, at pressures below 0.73 MPa, the aqueous TBAB solution with a concentration of 0.1 mass fraction, has a drastic promotion effect on the xenon hydrate dissociation conditions. A similar behaviour was observed for the semi-clathrate hydrate dissociation conditions for the system of xenon + 0.2 and 0.3 mass fraction of aqueous TBAB solution in which, aqueous TBAB solutions with concentrations of 0.2 and 0.3 mass fraction, showed a promotion effect for xenon hydrate dissociation conditions at pressures below (1.4 and 1.57) MPa respectively. The results indicated that the promotion effect of TBAB on Ar hydrate is greater than on the Kr and Xe hydrate.

Obtained results of hydrate dissociation data for the CF_4 + water system revealed a discrepancy between the experimental data reported in literature. The possible reason for such discrepancies may be attributed to some parameters such as a small gas leak, fast heating, error in the calibration and low-accuracy of the measurements. The results showed that 0.05, 0.10, and 0.20 mass fractions of aqueous TBAB solutions have no promotion effect on the CF_4 hydrate phase equilibrium. The aqueous TBAB solution with 0.30 mass fraction showed a significant promotion effect on the CF_4 hydrate formation with a temperature difference, ΔT, approximately equal to 10 K. Some crystallographic studies such as H-NMR, Raman Spectrometry, C13-NMR or X-Ray Diffraction are needed to explain the strange behaviour of this hydrate system.

The maximum value for average absolute deviation percentage (AAD%) between the experimental and the results of three thermodynamic models (namely fugacity approach (Approach 1), Chen and Guo approach (Approach 2) and a simple method based on vapour pressure calculations (Approach 3)) was approximately 0.3% which confirms the accuracy of the used thermodyamic models. The binary interaction parameters (BIPs) of the VPT EoS combined with the NDD mixing rules for Ar/Ke/Xe/ or CF_4 + water, new Kihara parameters, Antonine constants, and Langmuir constants for Ar, Kr, Xe and CF_4 were derived.

A thermodynamic model based on Joshi et al's work was extended in this work for representation of semi-clathrate hydrates dissociation conditions for the systems of Ar/ Kr/ Xe and CF_4 + TBAB +water. A reasonable agreement between the measured data and the model results with the maximum AAD% of 0.3% was observed.

The kinetic study on the CF_4 hydrate demonstrated that with an increase in the initial pressure from 7.08 MPa to 11.83 MPa, the induction time decreases, consequently the CF_4 hydrate formation rate, the apparent rate constant of reaction, storage capacity, and water to hydrate conversion increase. Similar results were found with decreasing the initial temperature at a constant initial pressure. The values obtained for the apparent rate constants, rate of hydrate formation, water to hydrate conversion and gas consumption can be useful to design a cost effective separation process based on clathrate/semi-clathrate hydrate formation.

The kinetic results on the semi-clathrate hydrate of Ar + TBAB + water showed that with an increase in the initial pressure, the induction time decreases significantly which means the rate of hydrate nucleation increases. The same trends were detected with a decrease in the initial temperature. With a decrease in the initial temperature, the amount of the pressure drop during the semi-clathrate hydrate formation increases resulting in the increase of the gas consumption. With an increase in the TBAB concentration form 0.1 to 0.3 mass fraction, the rate of semi-clathrate hydrate nucleation increases and the induction time decreases, significantly. With an increase in the TBAB concentration, the amount of the pressure drop increases resulting in more gas consumption during the semi-clathrate hydrate formation. The results show the positive kinetic and thermodynamic effect of TBAB on Ar hydrate which makes TBAB as a reliable promoter to decrease the pressure of argon hydrate formation and increase the rate of argon hydrate formation. The results indicated that SDS in the concentration of 100, 200, 400 ppm increases the induction time of the semi-clathrate hydrate formation for the system of Ar + TBAB + water. Therefore, the recommendation from this study is not to use SDS for the separation of noble gases. An alternative kinetic promoter should be explored for the semi-clathrate hydrate of Ar + aqueous TBAB solutions.

The results demonstrated that Xe hydrate in the presence of aqueous TBAB solution has much lower pressure conditions compared with Kr, and Ar + aqueous TBAB solutions. These differences of the gas hydrate dissociation pressure confirm the capability of the separation of the mixture of Ar + Kr + Xe using gas hydrate method. Semi-clathrate hydrate of Xe + TBAB + water form at ambient temperatures and very low pressures which decreases the cost of separation with hydrate method compared to the cryogenic distillation which is costly and quite energy intensive. In order to design a hydrate based process for gas separation (Kr, Xe, Ar) and estimate the number of stages necessary, further studies considering the equilibrium composition data in liquid, vapour and hydrate phases are required.

8

CHAPTER EIGHT: RECOMMENDATIONS

Separation and purification of expensive gases such as Ar, Kr, Xe and CF_4 are an important issue in industries. Gas hydrate method is considered as a new method for the separation of mixtures of noble gases such as Ar, Kr and Xe and also expensive gases such as CF_4. However, further hydrate measurements for systems containing mixture of argon, krypton and xenon are recommended. Additionally, hydrate systems consisting of a mixture of CF_4 and NF_3 and also pure NF_3 should be investigated.

As concluded in this study, TBAB can promote the hydrate phase equilibria to the lower pressures and higher temperatures conditions. However for the future work, the measurement of the hydrate phase equilibria for the mixture of noble gases in the presence of aqueous TBAB solution with various TBAB concentrations are recommended. In addition, the investigation of the effect of other promoters such as THF, TBAC, TBAF, $TBANO_3$, and TBPB as well as the mixture of these promoters on the hydrate dissociation conditions for the mixture of noble gases are suggested.

To design a separation process using the hydrate method, the mole fraction of the compounds in the vapour, liquid and hydrate phases are needed to determine the number of separation steps. Consequently, a set-up equipped with the gas chromatography and also a thermodynamic model based on the mass balance equations are recommended to determine the mole fraction of the compounds in gas, liquid and hydrate phases.

As mentioned earlier, the semi-clathrate structure of TBAB has two structures of type A and type B. These structures can change from one structure to other during the hydrate formation

and dissociation. It is not possible to distinguish the hydrate structure from the phase equilibrium measurements by PVT studies only. It is consequently recommended using molecular experimental methods such as solid-state NMR spectroscopy, Raman spectroscopy crystallography and X-ray diffraction to determine the TBAB semi-clathrate structures. On a mesoscopic level, laser scattering and particle video microscope can be applied to distinguish the hydrate crystal size through the hydrate formation and dissociation.

The effect of the mixture of sodium dodecyl sulfate (SDS) and THF on the kinetic of Ar, Kr and Xe gas hydrates are suggested.

The promotion effect of water insoluble promoters consist of heavy hydrocarbon such as methyl cyclohexane, cyclopentane and cylcohexane on the hydrate dissociation conditions for the mixture of noble gases are suggested.

REFERENCES

AARON, D. & TSOURIS, C. 2005. Separation of CO2 from flue gas: a review. *Separation Science and Technology,* 40**,** 321-348.

ABBOTT, M., SMITH, J. & VAN NESS, H. 2001. *Introduction to chemical engineering thermodynamics*, McGraw-Hill.

ABE, K., HOSAKA, J., IIDA, T., IKEDA, M., KOBAYASHI, K., KOSHIO, Y., MINAMINO, A., MIURA, M., MORIYAMA, S., NAKAHATA, M., NAKAJIMA, Y., NAMBA, T., OGAWA, H., SEKIYA, H., SHIOZAWA, M., SUZUKI, Y., TAKEDA, A., TAKEUCHI, Y., UESHIMA, K., YAMASHITA, M., KANEYUKI, K., EBIZUKA, Y., KIKUCHI, J., OTA, A., SUZUKI, S., TAKAHASHI, T., HAGIWARA, H., KAMEI, T., MIYAMOTO, K., NAGASE, T., NAKAMURA, S., OZAKI, Y., SATO, T., FUKUDA, Y., SATO, T., NISHIJIMA, K., SAKURAI, M., MARUYAMA, T., MOTOKI, D., ITOW, Y., OHSUMI, H., TASAKA, S., KIM, S. B., KIM, Y. D., LEE, J. I., MOON, S. H., URAKAWA, Y., UCHINO, M. & KAMIOKA, Y. 2009. Distillation of liquid xenon to remove krypton. *Astroparticle Physics,* 31**,** 290-296.

ADISASMITO, S., FRANK III, R. J. & SLOAN JR, E. D. 1991. Hydrates of carbon dioxide and methane mixtures. *Journal of Chemical and Engineering Data,* 36**,** 68-71.

ALAGAPPAN, B. 2013. *Assessing Different Zeolitic Adsorbents for their Potential Use in Kr and Xe Separation.* Master of Science (MS), University of Nevada, USA.

ARJANG, S., MANTEGHIAN, M. & MOHAMMADI, A. 2013. Effect of synthesized silver nanoparticles in promoting methane hydrate formation at 4.7 MPa and 5.7 MPa. *Chemical Engineering Research and Design,* 91**,** 1050-1054.

ARJMANDI, M., CHAPOY, A. & TOHIDI, B. 2007. Equilibrium Data of Hydrogen, Methane, Nitrogen, Carbon Dioxide, and Natural Gas in Semi-Clathrate Hydrates of Tetrabutyl Ammonium Bromide. *Journal of Chemical & Engineering Data,* 52**,** 2153-2158.

AVLONITIS, D., DANESH, A. & TODD, A. 1994. Prediction of VL and VLL equilibria of mixtures containing petroleum reservoir fluids and methanol with a cubic EoS. *Fluid Phase Equilibria,* 94**,** 181-216.

AVLONITIS, D. & VAROTSIS, N. 1996. Modelling gas hydrate thermodynamic behaviour: theoretical basis and computational methods. *Fluid phase equilibria,* 123**,** 107-130.

BABAEE, S., HASHEMI, H., JAVANMARDI, J., ESLAMIMANESH, A. & MOHAMMADI, A. H. 2012. Thermodynamic model for prediction of phase equilibria of clathrate hydrates of hydrogen with different alkanes, alkenes, alkynes, cycloalkanes or cycloalkene. *Fluid Phase Equilibria,* 336**,** 71-78.

BABAEE, S., HASHEMI, H., MOHAMMADI, A. H., NAIDOO, P. & RAMJUGERNATH, D. 2015. Kinetic and thermodynamic behaviour of CF 4 clathrate hydrates. *The Journal of Chemical Thermodynamics,* 81**,** 52-59.

BACHER, P. 2002. Meeting the energy challenges of the 21st century. *International journal of energy technology and policy,* 1**,** 1-26.

BARRER, R. & RUZICKA, D. 1962. Non-stoichiometric clathrate compounds of water. Part 2.—Formation and properties of double hydrates. *Transactions of the Faraday Society,* 58**,** 2239-2252.

BARRER, R. M. & EDGE, A. V. J. 1967. Gas hydrates containing argon, krypton and zerlon : kinetics and energetics of formation and equilibria. *Proceding of the Royal Society of London Series A- Mathematical and Physical Science,* 300**,** 1-24.

BELANDRIA, V., MOHAMMADI, A. H., ESLAMIMANESH, A., RICHON, D., SANCHEZ-MORA, M. F. & GALICIA-LUNA, L. A. 2012. Phase equilibrium measurements for semi-clathrate hydrates of the (CO_2+ N_2 + tetra-n-butylammonium bromide) aqueous solution systems: Part 2. *Fluid Phase Equilibria,* 322**,** 105-112.

BEN-ISRAEL, A. 1966. A Newton-Raphson method for the solution of systems of equations. *Journal of Mathematical analysis and applications,* 15**,** 243-252.

BENESH, M. E. 1942. The use of gas hydrates in improving the load factor of gas supply systems. US Patent 2,270,016.

BERGERON, S., BELTRÁN, J. G. & SERVIO, P. 2010. Reaction rate constant of methane clathrate formation. *Fuel,* 89**,** 294-301.

BERNABEI, R., BELLI, P., MONTECCHIA, F., INCICCHITTI, A., PROSPERI, D., DAI, C. J., ANGELONE, M., BATISTONI, P. & PILLON, M. 1998. New limits on particle

dark matter search with a liquid Xenon target-scintillator. *Physics Letters B,* 436**,** 379-388.

BIRCH, K. 2003. Estimating uncertainties in testing. *Measurement Good Practice Guide,* 36**,** 1-40.

BOUCHEMOUA, A., BRANTUAS, P. & HERRI, J.-M. Equilibrium data of CO_2-based semi-clathrates from quaternary ammonium solutions. Proceedings of the 7th International Conference on Gas Hydrates (ICGH 2011), 2011a.

BOUCHEMOUA, A., BRANTUAS, P. & HERRI, J. M. 2011b. Thermodynamic stability and self-preservation properties of semi-clathretes in the methane+ tetra-n-butyl ammonium bromide + water system. *Proceedings of the 7th International Conference on Gas Hydrates (ICGH 2011).* Edinburgh, Scotland, United Kingdom.

BRAIBANTI, A., FISICARO, E., DALLAVALLE, F., LAMB, J., OSCARSON, J. & RAO, R. S. 1994. Molecular thermodynamic model for the solubility of noble gases in water. *The Journal of Physical Chemistry,* 98**,** 626-634.

BRANKEN, D. J., KRIEG, H. M., LE ROUX, J. P. & LACHMANN, G. 2014. Separation of NF3 and CF4 using amorphous glassy perfluoropolymer Teflon AF and Hyflon AD60 membranes. *Journal of Membrane Science,* 462**,** 75-87.

BRUUSGAARD, H., BELTRÁN, J. G. & SERVIO, P. 2010. Solubility measurements for the CH_4 + CO_2 + H_2O system under hydrate–liquid–vapor equilibrium. *Fluid Phase Equilibria,* 296**,** 106-109.

BRYANT, E. 1997 Climate Process and Change. *Cambridge University Press.* Cambridge, UK.

BYK, S. S. & FOMINA, V. 1968. Gas hydrates. *Russian Chemical Reviews,* 37**,** 469-491.

BYK, S. S., MAKOGON, Y. F. & FOMINA, V. I. 1980. *Gazovye gidraty (Gas Hydrates),* Moscow: Khimiya.

CARROLL, J. 2009. *Natural gas hydrates: a guide for engineers*, Gulf Professional Publishing.

CARSON, D. B. & KATZ, D. L. 1942. Natural gas hydrates. *Transactions of the AIME,* 146**,** 150-158.

CHAPOY, A., MOKRAOUI, S., VALTZ, A., RICHON, D., MOHAMMADI, A. H. & TOHIDI, B. 2004. Solubility measurement and modeling for the system propane–water from 277.62 to 368.16 K. *Fluid Phase Equilibria,* 226**,** 213-220.

CHATTI, I., DELAHAYE, A., FOURNAISON, L. & PETITET, J.-P. 2005. Benefits and drawbacks of clathrate hydrates: a review of their areas of interest. *Energy Conversion and Management,* 46**,** 1333-1343.

CHEN, G.-J. & GUO, T.-M. 1998. A new approach to gas hydrate modelling. *Chemical Engineering Journal,* 71**,** 145-151.

CHUN, M.-K., LEE, H. & RYU, B.-J. 2000. Phase equilibria of R22 ($CHClF_2$) hydrate systems in the presence of NaCl, KCl, and $MgCl_2$. *Journal of Chemical & Engineering Data,* 45**,** 1150-1153.

CLARKE, M. & BISHNOI, P. R. 2001a. Determination of the activation energy and intrinsic rate constant of methane gas hydrate decomposition. *The Canadian Journal of Chemical Engineering,* 79**,** 143-147.

CLARKE, M. A. & BISHNOI, P. 2004. Determination of the intrinsic rate constant and activation energy of CO2 gas hydrate decomposition using in-situ particle size analysis. *Chemical engineering science,* 59**,** 2983-2993.

CLARKE, M. A. & BISHNOI, P. R. 2001b. Measuring and modelling the rate of decomposition of gas hydrates formed from mixtures of methane and ethane. *Chemical Engineering Science,* 56**,** 4715-4724.

COLLABORATION, X., ANGLE, J., APRILE, E., ARNEODO, F., BAUDIS, L., BERNSTEIN, A., BOLOZDYNYA, A., BRUSOV, P., COELHO, L. C. C., DAHL, C. E., DEVIVEIROS, L., FERELLA, A. D., FERNANDES, L. M. P., FIORUCCI, S., GAITSKELL, R. J., GIBONI, K. L., GOMEZ, R., HASTY, R., KASTENS, L., KWONG, J., LOPES, J. A. M., MADDEN, N., MANALAYSAY, A., MANZUR, A., MCKINSEY, D. N., MONZANI, M. E., NI, K., OBERLACK, U., ORBOECK, J., PLANTE, G., SANTORELLI, R., DOS SANTOS, J. M. F., SHAGIN, P., SHUTT, T., SORENSEN, P., SCHULTE, S., WINANT, C. & YAMASHITA, M. 2008. First Results from the XENON10 Dark Matter Experiment at the Gran Sasso National Laboratory. *Physical Review Letters,* 100**,** 021303.

COLLETT, T. S. & KUUSKRAA, V. A. 1998. Hydrates contain vast store of world gas resources. *Oil and Gas Journal,* 96**,** 90-94.

DABROWSKI, N., WINDMEIER, C. & OELLRICH, L. R. 2009. Purification of natural gases with high CO2 content using gas hydrates. *Energy & Fuels,* 23**,** 5603-5610.

DAIMARU, T., YAMASAKI, A. & YANAGISAWA, Y. 2007. Effect of surfactant carbon chain length on hydrate formation kinetics. *Journal of Petroleum Science and Engineering,* 56**,** 89-96.

DARBOURET, M., COURNIL, M. & HERRI, J.-M. 2005. Rheological study of TBAB hydrate slurries as secondary two-phase refrigerants. *International Journal of Refrigeration,* 28**,** 663-671.

DAVIDSON, D. W. 1973. *Gas hydrates in water: a comprehensive treatise,* Frank F. Ed; Plenum Press: New York.

DE FORCRAND, R. 1902. Sur la composition des hydrates de gaz. 135**,** 959-961.

DELAHAYE, A., FOURNAISON, L., MARINHAS, S. & MARTÍNEZ, M. C. 2008. Rheological study of CO2 hydrate slurry in a dynamic loop applied to secondary refrigeration. *Chemical engineering science,* 63**,** 3551-3559.

DESCHAMPS, J. & DALMAZZONE, D. 2009. Dissociation enthalpies and phase equilibrium for TBAB semi-clathrate hydrates of N2, CO2, N2+ CO2 and CH4+ CO2. *Journal of thermal analysis and calorimetry,* 98**,** 113-118.

DESCHAMPS, J. & DALMAZZONE, D. 2010. Hydrogen storage in semiclathrate hydrates of tetrabutyl ammonium chloride and tetrabutyl phosphonium bromide. *Journal of Chemical & Engineering Data,* 55**,** 3395-3399.

DHARMAWARDHANA, P. B., PARRISH, W. R. & SLOAN, E. D. 1980. Experimental Thermodynamic Parameters for the Prediction of Natural Gas Hydrate Dissociation Conditions. *Industrial & Engineering Chemistry Fundamentals,* 19**,** 410-414.

DUC, N. H., CHAUVY, F. & HERRI, J.-M. 2007. CO2 capture by hydrate crystallization – A potential solution for gas emission of steelmaking industry. *Energy Conversion and Management,* 48**,** 1313-1322.

DYADIN, Y. A., LARIONOV, E., MIRINSKIJ, D., MIKINA, T., ALADKO, E. Y. & STAROSTINA, L. 1997a. Phase diagram of the Xe–H2O system up to 15 kbar. *Journal of inclusion phenomena and molecular recognition in chemistry,* 28**,** 271-285.

DYADIN, Y. A., LARIONOV, E. G., MIKINA, T. V. & STAROSTINA, L. I. 1996. Clathrate hydrate of xenon at high pressure. *Mendeleev communications,* 6**,** 44-45.

DYADIN, Y. A., LARIONOV, E. G., MIKINA, T. V. & STAROSTINA, L. I. 1997b. Clathrate formation in Kr-H 2 O and Xe-H 2 O systems under pressures up to 15 kbar. *Mendeleev communications,* 7**,** 74-76.

DYADIN, Y. A., LARIONOV, E. G., MIRINSKI, D. S., MIKINA, T. V. & STAROSTINA, L. I. 1997c. Clathrate formation in the Ar-H 2 O system under pressures up to 15000 bar. *Mendeleev communications,* 7**,** 32-34.

DYADIN, Y. A. & UDACHIN, K. A. 1984. Clathrate Farmation in Water-Peralkylonium Salts Systems. *J. Inclus. Phenomena,* 2**,** 61.

ENGLEZOS, P. & BISHNOI, P. 1991. Experimental study on the equilibrium ethane hydrate formation conditions in aqueous electrolyte solutions. *Industrial & Engineering Chemistry Research,* 30**,** 1655-1659.

ENGLEZOS, P., KALOGERAKIS, N., DHOLABHAI, P. D. & BISHNOI, P. R. 1987. Kinetics of formation of methane and ethane gas hydrates. *Chemical Engineering Science,* 42**,** 2647-2658.

ESLAMIMANESH, A., GHARAGHEIZI, F., MOHAMMADI, A. H. & RICHON, D. 2011a. Phase Equilibrium Modeling of Structure H Clathrate Hydrates of Methane + Water "Insoluble" Hydrocarbon Promoter Using QSPR Molecular Approach. *Journal of Chemical & Engineering Data,* 56**,** 3775-3793.

ESLAMIMANESH, A., MOHAMMADI, A. H. & RICHON, D. 2011b. Thermodynamic Consistency Test for Experimental Data of Sulfur Content of Hydrogen Sulfide. *Industrial & Engineering Chemistry Research,* 50**,** 3555-3563.

ESLAMIMANESH, A., MOHAMMADI, A. H. & RICHON, D. 2011c. Thermodynamic model for predicting phase equilibria of simple clathrate hydrates of refrigerants. *Chemical Engineering Science,* 66**,** 5439-5445.

ESLAMIMANESH, A., MOHAMMADI, A. H. & RICHON, D. 2012a. Thermodynamic modeling of phase equilibria of semi-clathrate hydrates of CO2, CH4, or N2+tetra-n-butylammonium bromide aqueous solution. *Chemical Engineering Science,* 81**,** 319-328.

ESLAMIMANESH, A., MOHAMMADI, A. H., RICHON, D., NAIDOO, P. & RAMJUGERNATH, D. 2012b. Application of gas hydrate formation in separation processes: A review of experimental studies. *The Journal of Chemical Thermodynamics,* 46**,** 62-71.

EWING, G. J. & IONESCU, L. G. 1974. Dissociation pressure and other thermodynamic properties of xenon-water clathrate. *Journal of Chemical and Engineering Data,* 19**,** 367-369.

FAZLALI, A., KAZEMI, S.-A., KESHAVARZ-MORAVEJI, M. & MOHAMMADI, A. H. 2013. Impact of Different Surfactants and their Mixtures on Methane-Hydrate Formation. *Energy Technology,* 1**,** 471-477.

FÉREY, G. 2008. Hybrid porous solids: past, present, future. *Chemical Society Reviews,* 37**,** 191-214.

FOWLER, D., LOEBENSTEIN, W., PALL, D. & KRAUS, C. A. 1940. Some unusual hydrates of quaternary ammonium salts. *Journal of the American Chemical Society,* 62**,** 1140-1142.

FREDENSLUND, A., JONES, R. L. & PRAUSNITZ, J. M. 1975. Group-contribution estimation of activity coefficients in nonideal liquid mixtures. *AIChE Journal,* 21**,** 1086-1099.

FROST, E. & DEATON, W. 1946. Gas hydrate composition and equilibrium data. *Oil Gas J,* 45**,** 170-178.

FUJII, T., KOBAYASHI, Y. & SUENAGA, T. 1991. Method of refining nitrogen trifluoride gas. Google Patents.

GAPONENKO, L., SOLODOVNIKOV, S. F., DYADIN, Y. A., ALADKO, L. S. & POLYANSKAYA, T. N. 1984. Crystallographic Study of Tetra-n-butylammonium Bromide Polydrates. *J. Struct. Chem.,* 25**,** 157−159.

GARCIA, M. & CLARKE, M. 2014. Equilibrium Conditions for TBAB and TBAC Semiclathrates of Xenon and Argon. *Journal of Chemical & Engineering Data*.

GARG, S. K., GOUGH, S. R. & DAVIDSON, D. W. 1975. A wide-line NMR study of reorientation of some spherical-top molecules enclathrated in water. *The Journal of Chemical Physics,* 63**,** 1646-1654.

GHOLINEZHAD, J., CHAPOY, A., HAGHIGHI, H. & TOHIDI, B. Determination of intrinsic rate constant for hydrate formation in the methane–TBAB–water system. Proceedings of the 7th International Conference on Gas Hydrates, 2011. 17-21.

GORMAN, S. 2009. [Online], As hybrid cars gobble rare metals, shortage looms, DOI [http://www.reuters.com/article/2009/08/31/us-mining-toyota-idUSTRE57U02B20090831].

HALL, C., THARAKAN, P., HALLOCK, J., CLEVELAND, C. & JEFFERSON, M. 2003. Hydrocarbons and the evolution of human culture. *Nature,* 426**,** 318-322.

HAMMERSCHMIDT, E. 1934. Formation of gas hydrates in natural gas transmission lines. *Industrial & Engineering Chemistry,* 26**,** 851-855.

HAPPEL, J., HNATOW, M. A. & MEYER, H. 1994. The Study of Separation of Nitrogen from Methane by Hydrate Formation Using a Novel Apparatusa. *Annals of the New york Academy of sciences,* 715**,** 412-424.

HASHEMI, H., BABAEE, S., MOHAMMADI, A. H., NAIDOO, P. & RAMJUGERNATH, D. 2015. Experimental study and modeling of the kinetics of refrigerant hydrate formation. *The Journal of Chemical Thermodynamics,* 82**,** 47-52.

HERRI, J.-M., BOUCHEMOUA, A., KWATERSKI, M., FEZOUA, A., OUABBAS, Y., CAMEIRÃO, A. & BRANTUAS, P. Gas hydrate equilibria for CO2-N2 and CO2-CH4 gas mixtures, experiments and modelling. Proceedings of the 7th International Conference on Gas Hydrates (ICGH 2011), 2011.

HERSLUND, P. J., THOMSEN, K., ABILDSKOV, J. & VON SOLMS, N. 2012. Phase equilibrium modeling of gas hydrate systems for CO_2 capture. *The Journal of Chemical Thermodynamics,* 48**,** 13-27.

HNATOW M.A. & HAPPEL, J. 1995. *Process and Apparatus for Separation of Constituents of Gases Using Gas Hydrates*.

HOLDER, G. D., CORBIN, G. & PAPADOPOULOS, K. D. 1980. Thermodynamic and Molecular Properties of Gas Hydrates from Mixtures Containing Methane, Argon, and Krypton. *Industrial & Engineering Chemistry Fundamentals,* 19**,** 282-286.

HYNE, J. B. 1983. Controlling sulfur deposition in sour gas wells. *Journal Name: World Oil; (United States); Journal Volume: 197:2***,** Medium: X; Size: Pages: 35-39, 46.

ILANI-KASHKOULI, P., BABAEE, S., GHARAGHEIZI, F., HASHEMI, H., MOHAMMADI, A. H. & RAMJUGERNATH, D. 2013. An assessment test for phase equilibrium data of water soluble and insoluble clathrate hydrate formers. *Fluid Phase Equilibria,* 360**,** 68-76.

ILLBEIGI, M., FAZLALI, A. & MOHAMMADI, A. H. 2011. Thermodynamic Model for the Prediction of Equilibrium Conditions of Clathrate Hydrates of Methane + Water-Soluble or -Insoluble Hydrate Former. *Industrial & Engineering Chemistry Research,* 50**,** 9437-9450.

JAVANMARDI, J., BABAEE, S., ESLAMIMANESH, A. & MOHAMMADI, A. H. 2012. Experimental Measurements and Predictions of Gas Hydrate Dissociation Conditions in the Presence of Methanol and Ethane-1,2-diol Aqueous Solutions. *Journal of Chemical & Engineering Data,* 57**,** 1474-1479.

JAVANMARDI, J. & MOSHFEGHIAN, M. 2003. Energy consumption and economic evaluation of water desalination by hydrate phenomenon. *Applied thermal engineering,* 23**,** 845-857.

JAVANMARDI, J., NASRIFAR, K., NAJIBI, S. & MOSHFEGHIAN, M. 2005. Economic evaluation of natural gas hydrate as an alternative for natural gas transportation. *Applied Thermal Engineering,* 25**,** 1708-1723.

JAVANMARDI, J., PARTOON, B. & SABZI, F. 2011. Prediction of hydrate formation conditions based on the vdWP-type models at high pressures. *The Canadian Journal of Chemical Engineering,* 89**,** 254-263.

JEFFREY, G. A. & MCMULLAN, R. K. 1967. Clathrate hydrates. *Prog. Inorg. Chem.,* 8**,** 43-108.

JIN, Y., KIDA, M. & NAGAO, J. 2012. Phase Equilibrium Conditions for Clathrate Hydrates of Tetra-n-butylammonium Bromide (TBAB) and Xenon. *Journal of Chemical & Engineering Data,* 57**,** 1829-1833.

JOSHI, A., MEKALA, P. & SANGWAI, J. S. 2012. Modeling phase equilibria of semiclathrate hydrates of CH_4, CO_2 and N_2 in aqueous solution of tetra-n-butyl ammonium bromide. *Journal of Natural Gas Chemistry,* 21**,** 459-465.

KAMATA, Y., OYAMA, H., SHIMADA, W., EBINUMA, T., TAKEYA, S., UCHIDA, T., NAGAO, J. & NARITA, H. 2004. Gas separation method using tetra-n-butyl ammonium bromide semi-clathrate hydrate. *Japanese journal of applied physics,* 43**,** 362.

KAMATA, Y., YAMAKOSHI, Y., EBINUMA, T., OYAMA, H., SHIMADA, W. & NARITA, H. 2005. Hydrogen sulfide separation using tetra-n-butyl ammonium bromide semi-clathrate (TBAB) hydrate. *Energy & Fuels,* 19**,** 1717-1722.

KANG, S.-P. & LEE, H. 2000. Recovery of CO_2 from flue gas using gas hydrate: thermodynamic verification through phase equilibrium measurements. *Environmental science & technology,* 34**,** 4397-4400.

KATZ, D. L. 1945. Prediction of conditions for hydrate formation in natural gases. *Transactions of the AIME,* 160**,** 140-149.

KELLAND, M. A., MOI, N. & HOWARTH, M. 2013. Breakthrough in Synergists for Kinetic Hydrate Inhibitor Polymers, Hexaalkylguanidinium Salts: Tetrahydrofuran Hydrate Crystal Growth Inhibition and Synergism with Polyvinylcaprolactam. *Energy & Fuels,* 27**,** 711-716.

KERRY, F. G. 2010. *Industrial gas handbook: gas separation and purification*, CRC Press.

KHOKHAR, A., GUDMUNDSSON, J. & SLOAN, E. 1998. Gas storage in structure H hydrates. *Fluid Phase Equilibria,* 150**,** 383-392.

KIHARA, T. 1953. Virial coefficients and models of molecules in gases. *Reviews of modern physics* 25 (4)**,** 831-843.

KINNEY, P. J. & KAHRE, L. C. 1963. *Helium Recovery from Natural Gas, US Patent 3 097 924*. US patent application.

KITAGAWA, S., KITAURA, R. & NORO, S. I. 2004. Functional porous coordination polymers. *Angewandte Chemie International Edition,* 43**,** 2334-2375.

KLAUDA, J. B. & SANDLER, S. I. 2000. A Fugacity Model for Gas Hydrate Phase Equilibria. *Industrial & Engineering Chemistry Research,* 39**,** 3377-3386.

KOJIMA, R., YAMANE, K. & AYA, I. Dual nature of CO2 solubility in hydrate forming region. Fourth international conference on gas hydrates, 2002. 286-9.

KOMAI, T., KAWAMURA, T. & YAMAMOTO, Y. 2000. *Reformation and Replacement of CO_2 and CH_4 Gas Hydrates*. National Institute for Resources and Environment, Japan patent application.

KROON, M. C., SHARIATI, A., COSTANTINI, M., VAN SPRONSEN, J., WITKAMP, G.-J., SHELDON, R. A. & PETERS, C. J. 2005. High-pressure phase behavior of systems with ionic liquids: Part V. The binary system carbon dioxide+ 1-butyl-3-methylimidazolium tetrafluoroborate. *Journal of Chemical & Engineering Data,* 50**,** 173-176.

KUJI, Y., YAMASAKI, A. & YANAGISAWA, Y. 2006. Effect of cyclodextrins on hydrate formation rates. *Energy & fuels,* 20**,** 2198-2201.

KVENVOLDEN, K. A. 1988. Methane hydrate—a major reservoir of carbon in the shallow geosphere? *Chemical Geology,* 71**,** 41-51.

LE PARLOUËR, P., DALMAZZONE, C., HERZHAFT, B., ROUSSEAU, L. & MATHONAT, C. 2004. Characterisation of gas hydrates formation using a new high pressure MICRO-DSC. *Journal of Thermal Analysis and Calorimetry,* 78**,** 165-172.

LEE, S., LEE, Y., PARK, S. & SEO, Y. 2010. Phase equilibria of semiclathrate hydrate for nitrogen in the presence of tetra-n-butylammonium bromide and fluoride. *Journal of Chemical & Engineering Data,* 55**,** 5883-5886.

LI, S., FAN, S., WANG, J., LANG, X. & WANG, Y. 2010. Semiclathrate hydrate phase equilibria for CO2 in the presence of tetra-n-butyl ammonium halide (bromide, chloride, or fluoride). *Journal of Chemical & Engineering Data,* 55**,** 3212-3215.

LI, X.-S., ZHANG, Y., LI, G., CHEN, Z.-Y., YAN, K.-F. & LI, Q.-P. 2008. Gas hydrate equilibrium dissociation conditions in porous media using two thermodynamic approaches. *The Journal of Chemical Thermodynamics,* 40**,** 1464-1474.

LIPKOWSKI, J., KOMAROV, V. Y., RODIONOVA, T. V., DYADIN, Y. A. & ALADKO, L. S. 2002. The Structure of Tetrabutylammonium Bromide Hydrate $(C_4H_9)_4NBr \cdot 2\ ^{1/3}H_2O$. *Journal of Supramolecular Chemistry,* 2**,** 435-439.

LIU, J., THALLAPALLY, P. K. & STRACHAN, D. 2012. Metal–Organic Frameworks for Removal of Xe and Kr from Nuclear Fuel Reprocessing Plants. *Langmuir,* 28**,** 11584-11589.

MAKOGON, T. Y., MEHTA, A. P. & SLOAN, E. D. 1996. Structure H and structure I hydrate equilibrium data for 2, 2-dimethylbutane with methane and xenon. *Journal of Chemical & Engineering Data,* 41**,** 315-318.

MAKOGON, Y. 1998. Natural gas hydrates: the state of study in the ussr and perspectives for its use. *Third chemical congress of North America.* Toronto, Canada.

MANTEGHIAN, M., MOUSAVI SAFAVI, S. M. & MOHAMMADI, A. 2013. The equilibrium conditions, hydrate formation and dissociation rate and storage capacity of ethylene hydrate in presence of 1,4-dioxane. *Chemical Engineering Journal,* 217**,** 379-384.

MARINHAS, S., DELAHAYE, A., FOURNAISON, L., DALMAZZONE, D., FÜRST, W. & PETITET, J.-P. 2006. Modelling of the available latent heat of a CO 2 hydrate slurry in an experimental loop applied to secondary refrigeration. *Chemical Engineering and Processing: Process Intensification,* 45**,** 184-192.

MARSHALL, D. R., SAITO, S. & KOBAYASHI, R. 1964. Hydrates at high pressures: Part I. Methane-water, argon-water, and nitrogen-water systems. *AIChE Journal,* 10**,** 202-205.

MARTINEZ, M., DALMAZZONE, D., FÜRST, W., DELAHAYE, A. & FOURNAISON, L. 2008. Thermodynamic properties of THF+ CO2 hydrates in relation with refrigeration applications. *AIChE journal,* 54**,** 1088-1095.

MCMULLAN, R. & JEFFREY, G. A. 2004. Hydrates of the Tetra n-butyl and Tetra i-amyl Quaternary Ammonium Salts. *The Journal of Chemical Physics,* 31**,** 1231-1234.

MCMULLAN R. & G.A., J. 1959. Hydrates of the tetra n-butyl and Tetra i-amyl Quaternary Ammonium Salts. .*Journal of Chemical Physics,* 31 (5)**,** 1231-1234.

MOHAMMADI, A., MANTEGHIAN, M., HAGHTALAB, A., MOHAMMADI, A. H. & ABKENAR, M. R. 2014. Kinetic Study of Carbon Dioxide Hydrate Formation in

Presence of Silver Nanoparticles and SDS. *Chemical Engineering Journal,* 237**,** 387–395.

MOHAMMADI, A., MANTEGHIAN, M. & MOHAMMADI, A. H. 2013. Dissociation Data of Semiclathrate Hydrates for the Systems of Tetra-n-butylammonium Fluoride (TBAF)+ Methane+ Water, TBAF+ Carbon Dioxide+ Water, and TBAF+ Nitrogen+ Water. *Journal of Chemical & Engineering Data,* 58**,** 3545-3550.

MOHAMMADI, A. H., ANDERSON, R. & TOHIDI, B. 2005. Carbon monoxide clathrate hydrates: Equilibrium data and thermodynamic modeling. *AIChE Journal,* 51**,** 2825-2833.

MOHAMMADI, A. H., ESLAMIMANESH, A., BELANDRIA, V. & RICHON, D. 2011. Phase equilibria of semiclathrate hydrates of CO2, N2, CH4, or H2+ Tetra-n-butylammonium bromide aqueous solution. *Journal of Chemical & Engineering Data,* 56**,** 3855-3865.

MOHAMMADI, A. H., ESLAMIMANESH, A., BELANDRIA, V., RICHON, D., NAIDOO, P. & RAMJUGERNATH, D. 2012. Phase equilibrium measurements for semi-clathrate hydrates of the (CO_2+ N_2+ tetra-n-butylammonium bromide) aqueous solution system. *The Journal of Chemical Thermodynamics,* 46**,** 57-61.

MOHAMMADI, A. H. & RICHON, D. 2008a. Estimating Sulfur Content of Hydrogen Sulfide at Elevated Temperatures and Pressures Using an Artificial Neural Network Algorithm. *Industrial & Engineering Chemistry Research,* 47**,** 8499-8504.

MOHAMMADI, A. H. & RICHON, D. 2008b. Thermodynamic Model for Predicting Liquid Water−Hydrate Equilibrium of the Water−Hydrocarbon System. *Industrial & Engineering Chemistry Research,* 47**,** 1346-1350.

MOHAMMADI, A. H. & RICHON, D. 2009. Development of predictive techniques for estimating liquid water-hydrate equilibrium of water-hydrocarbon system. *Journal of Thermodynamics, Hindawi Publishing Corporation,* 2009**,** 1-12.

MOHAMMADI, A. H., TOHIDI, B. & BURGASS, R. W. 2003. Equilibrium data and thermodynamic modeling of nitrogen, oxygen, and air clathrate hydrates. *Journal of Chemical & Engineering Data,* 48**,** 612-616.

MOOIJER-VAN DEN HEUVEL, M. M., SAWIRJO, N. M. & PETERS, C. J. 2006. Influence of fluoroalkanes on the phase behaviour of methane gas hydrate systems. *Fluid Phase Equilibria,* 241**,** 124-137.

MOOIJER-VAN DEN HEUVEL, M. M., WITTEMAN, R. & PETERS, C. J. 2001. Phase behaviour of gas hydrates of carbon dioxide in the presence of tetrahydropyran, cyclobutanone, cyclohexane and methylcyclohexane. *Fluid Phase Equilibria,* 182**,** 97-110.

MORK, M. & GUDMUNDSSON, J. S. 2002. Hydrate formation rate in a continuous stirred tank reactor: experimental results and bubble-to-crystal model. *Proceedings of the Fourth International Conference on Gas Hydrates, Yokohama*.

NATARAJAN, V., BISHNOI, P. & KALOGERAKIS, N. 1994. Induction phenomena in gas hydrate nucleation. *Chemical Engineering Science,* 49**,** 2075-2087.

NG, H.-J. & ROBINSON, D. B. 1985. Hydrate formation in systems containing methane, ethane, propane, carbon dioxide or hydrogen sulfide in the presence of methanol. *Fluid Phase Equilibria,* 21**,** 145-155.

NIKITIN, B. A. 1956. *Selected Works (Akad. Nauk SSSR),* Russian, Moscow.

OELLRICH, L. Natural gas hydrates and their potential for future energy supply. Proceedings of the 6th ISHMT/ASME Heat and Mass Transfer Conference, 2004. 5-7.

OHGAKI, K., SUGAHARA, T., SUZUKI, M. & JINDAI, H. 2000. Phase behavior of xenon hydrate system. *Fluid phase equilibria,* 175**,** 1-6.

OHGAKI, K., TAKANO, K., SANGAWA, H., MATSUBARA, T. & NAKANO, S. 1996. Methane exploitation by carbon dioxide from gas hydrates. Phase equilibria for CO2-CH4 mixed hydrate system. *Journal of chemical engineering of Japan,* 29**,** 478-483.

OHNO, M., OZAKI, O., SATO, H., KIMURA, S. & MIYAUCHI, T. 1977. Radioactive rare gas separation using a separation cell with two kinds of membrane differing in gas permeability tendency. *Journal of Nuclear Science and Technology,* 14**,** 589-602.

OYAMA, H., SHIMADA, W., EBINUMA, T., KAMATA, Y., TAKEYA, S., UCHIDA, T., NAGAO, J. & NARITA, H. 2005. Phase diagram, latent heat, and specific heat of TBAB semiclathrate hydrate crystals. *Fluid Phase Equilibria,* 234**,** 131-135.

PACK, D. J. 2003. Paper presented at the 14th Biennal Joint Technical Meeting on Pipelines Research. Berlin.

PANG, W., CHEN, G., DANDEKAR, A., SUN, C. & ZHANG, C. 2007. Experimental study on the scale-up effect of gas storage in the form of hydrate in a quiescent reactor. *Chemical engineering science,* 62**,** 2198-2208.

PAPADIMITRIOU, N. I., TSIMPANOGIANNIS, I. N., STUBOS, A. K., MARTÍN, A., ROVETTO, L. J., FLORUSSE, L. J. & PETERS, C. J. 2011. Experimental and Computational Investigation of the sII Binary He−THF Hydrate. *The Journal of Physical Chemistry B,* 115**,** 1411-1415.

PARRISH, W. R. & PRAUSNITZ, J. M. 1972. Dissociation Pressures of Gas Hydrates Formed by Gas Mixtures. *Industrial & Engineering Chemistry Process Design and Development,* 11**,** 26-35.

PARTOON, B. & JAVANMARDI, J. 2013. Effect of mixed thermodynamic and kinetic hydrate promoters on methane hydrate phase boundary and formation kinetics. *Journal of Chemical & Engineering Data,* 58**,** 501-509.

PENG, P. & ZHUANG, Y. 2012. The evaluation and comparison of carbon dioxide capture technologies applied to FCC flue gas. *Advanced Materials Research,* 347**,** 1479-1482.

RAAL, J. & MU˙ LBAUER, A. 1998. Phase equilibria—measurement and computation, . *Taylor & Fraccis, London***,** 302-309.

RAEISSI, S. & PETERS, C. 2001. Bubble-point pressures of the binary system carbon dioxide+ linalool. *The Journal of Supercritical Fluids,* 20**,** 221-228.

RICHON, D. 1996. New experimental developments for phase equilibrium measurements. *Fluid phase equilibria,* 116**,** 421-428.

RIPMEESTER, J. & RATCLIFFE, C. 1990. Xenon-129 NMR studies of clathrate hydrates: new guests for structure II and structure H. *Journal of Physical Chemistry,* 94**,** 8773-8776.

ROEBUCK, J. R., MURRELL, T. A. & MILLER, E. E. 1942. The Joule-Thomson Effect in Carbon Dioxide. *Journal of the American Chemical Society,* 64**,** 400-411.

ROWSELL, J. L. & YAGHI, O. M. 2004. Metal–organic frameworks: a new class of porous materials. *Microporous and Mesoporous Materials,* 73**,** 3-14.

RYAN, J. & HILLS, V. 2012. *Metal Organic Frameworks for Xe/Kr Separation*. US 2012/0073438 A1.

SABIL, K. M. 2009. *Phase behaviour, thermodynamics and kinetics of clathrate hydrate systems of carbon dioxide in presence of tetrahydrofuran and electrolytes.* PhD thesis.

SABIL, K. M., WITKAMP, G. J. & PETERS, C. J. 2010. Phase equilibria in ternary (carbon dioxide+tetrahydrofuran+water) system in hydrate-forming region: Effects of carbon dioxide concentration and the occurrence of pseudo-retrograde hydrate phenomenon. *The Journal of Chemical Thermodynamics,* 42**,** 8-16.

SANDER, R. 1999. Germany: Compilation of henry's law constants for inorganic and organic species of potential importance in environmental chemistry, Air Chemistry Department, Max-Planck Institute of Chemistry, PO Box 3060, 55020 Mainz.

SCHARLIN, P. & BATTINO, R. 1995. Solubility of CCl2F2, CClF3, CF4, and CH4 in Water and Seawater at 288.15-303.15 K and 101.325 kPa. *Journal of Chemical and Engineering Data,* 40**,** 167-169.

SCHROETER, J., KOBAYASHI, R. & HILDEBRAND, M. 1983. Hydrate decomposition conditions in the system hydrogen sulfide-methane-propane. *Industrial & engineering chemistry fundamentals,* 22**,** 361-364.

SEO, Y. & LEE, H. 2001. A new hydrate-based recovery process for removing chlorinated hydrocarbons from aqueous solutions. *Environmental science & technology,* 35**,** 3386-3390.

SHARIATI, A. & PETERS, C. J. 2003. High-pressure phase behavior of systems with ionic liquids: measurements and modeling of the binary system fluoroform+ 1-ethyl-3-methylimidazolium hexafluorophosphate. *The Journal of supercritical fluids,* 25**,** 109-117.

SHIMADA, W., EBINUMA, T., OYAMA, H., KAMATA, Y., TAKEYA, S., UCHIDA, T., NAGAO, J. & NARITA, H. 2003. Separation of gas molecule using tetra-n-butyl ammonium bromide semi-clathrate hydrate crystals. *Japanese Journal of Applied Physics,* 42**,** L129.

SHIMADA, W., SHIRO, M., KONDO, H., TAKEYA, S., OYAMA, H., EBINUMA, T. & NARITA, H. 2005. Tetra-n-butyl-ammonium bromide–water (1/38). *Acta Crystallographica Section C,* 61**,** o65-o66.

SIKORA, B. J., WILMER, C. E., GREENFIELD, M. L. & SNURR, R. Q. 2012. Thermodynamic analysis of Xe/Kr selectivity in over 137000 hypothetical metal–organic frameworks. *Chemical Science,* 3**,** 2217-2223.

SINNOT, R. K. 2005. *Coulson & Richardson's Chemical Engineering*, Elsevier.

SINNOTT, R. K. 2005. *Coulson & Richardson's Chemical Engineering*, Elsevier.

SKOVBORG, P. & RASMUSSEN, P. 1994. A mass transport limited model for the growth of methane and ethane gas hydrates. *Chemical Engineering Science,* 49**,** 1131-1143.

SLOAN, E. D. & KOH, C. A. 2008. *Clathrate Hydrates of Natural Gases*, CRC Press, Taylor & Francis Group, Boca Raton.

SMITH, J. M., VAN NESS, H. & ABBOTT, M. 2001. *Introduction to Chemical Engineering Thermodynamics,* Mcgraw-Hill New York.

STACKELBERG, M. V. 1970. Solid gas hydrates. DTIC Document.

STACKELBERG, M. V. & MEUTHEN, B. 1958. Solid Gas-Hydrate VII. Water-Soluble Ether. *Z. Electrochem,* 62**,** 130-131.

STROBEL, T. A., HESTER, K. C., KOH, C. A., SUM, A. K. & SLOAN JR, E. D. 2009a. Properties of the clathrates of hydrogen and developments in their applicability for hydrogen storage. *Chemical Physics Letters,* 478**,** 97-109.

STROBEL, T. A., KOH, C. A. & SLOAN, E. D. 2009b. Thermodynamic predictions of various tetrahydrofuran and hydrogen clathrate hydrates. *Fluid Phase Equilibria,* 280**,** 61-67.

STRYJEK, R. & VERA, J. 1986. PRSV: An improved Peng—Robinson equation of state for pure compounds and mixtures. *The canadian journal of chemical engineering,* 64**,** 323-333.

SUGAHARA, K., SUGAHARA, T. & OHGAKI, K. 2005. Thermodynamic and Raman spectroscopic studies of Xe and Kr hydrates. *Journal of Chemical & Engineering Data,* 50**,** 274-277.

SUGAHARA, K., YOSHIDA, M., SUGAHARA, T. & OHGAKI, K. 2004. High-Pressure Phase Behavior and Cage Occupancy for the CF4 Hydrate System. *Journal of Chemical & Engineering Data,* 49**,** 326-329.

SUGINAKA, T., SAKAMOTO, H., IINO, K., TAKEYA, S., NAKAJIMA, M. & OHMURA, R. 2012. Thermodynamic properties of ionic semiclathrate hydrate formed with tetrabutylphosphonium bromide. *Fluid Phase Equilibria,* 317**,** 25-28.

TAJIMA, H., NAGATA, T., ABE, Y., YAMASAKI, A., KIYONO, F. & YAMAGIWA, K. 2010. HFC-134a hydrate formation kinetics during continuous gas hydrate formation with a kenics static mixer for gas separation. *Industrial & Engineering Chemistry Research,* 49**,** 2525-2532.

TAJIMA, H., YAMASAKI, A. & KIYONO, F. 2004. Energy consumption estimation for greenhouse gas separation processes by clathrate hydrate formation. *Energy,* 29**,** 1713-1729.

TAYLOR, B. N. 2009. *Guidelines for Evaluating and Expressing the Uncertainty of NIST Measurement Results (rev*, DIANE Publishing.

TOHIDI, B., ØSTERGAARD, K., DANESH, A., TODD, A. & BURGASS, R. 2001. Structure-H gas hydrates in petroleum reservoir fluids. *The Canadian Journal of Chemical Engineering,* 79**,** 384-391.

TUMBA, K., HASHEMI, H., NAIDOO, P., MOHAMMADI, A. H. & RAMJUGERNATH, D. 2013. Dissociation Data and Thermodynamic Modeling of Clathrate Hydrates of Ethene, Ethyne, and Propene. *Journal of Chemical & Engineering Data,* 58**,** 3259-3264.

VALDERRAMA, J. O. 1990. A generalized Patel-Teja Equation of State for polar and nonpolar Fluids and their Mixtures. *Journal of chemical engineering of Japan,* 23**,** 87-91.

VAN DER WAALS, J. & PLATTEEUW, J. 1959. Clathrate solutions. *Adv. Chem. Phys,* 2**,** 1-57.

VILLARD, P. 1888. Sur quelques nouveaux hydrates de gaz. *Compt. Rend. ,* 106**,** 1602-1603.

VILLARD, P. 1890. Sm quelques noiiveaux hydrates de gaz. *Compt. Rend,* 111**,** 302.

VOROTYNTSEV, V. M. & MALYSHEV, V. M. 1998. Gas Hydrates: A New Class of Impurities in Ultrapure Gases and Gas–Vapor Mixtures. *Usp. Khim. ,* 67**,** 87.

VOROTYNTSEV, V. M. & MALYSHEV, V. M. 2011. Calculating the Separation Coefficients in Argon, Krypton and Xenon Gas Mixture Separation by Gas Hydrate Crystallization. *Russ. J. phys. Chem. A,* 85**,** 1990-1994.

VYSNIAUSKAS, A. & BISHNOI, P. R. 1983. A kinetic study of methane hydrate formation. *Chemical Engineering Science,* 38**,** 1061-1072.

WAALS, J. D. 1873. *Over de continuiteit van den gas-en vloeistoftoestand*, AW Sijthoff.

WILSON, P., LESTER, D. & HAYMET, A. 2005. Heterogeneous nucleation of clathrates from supercooled tetrahydrofuran (THF)/water mixtures, and the effect of an added catalyst. *Chemical engineering science,* 60**,** 2937-2941.

YARYM-AGAEV, N. L. 1999. Vapor-Liquid Equilibrium and Volumetric Properties of the Liquid Phase of the gamma-Butyrolactone-Carbon Dioxide System at Increasing Pressures. *Zh.Prikl.Khim.,* 72**,** 1085-1089.

YE, Y. & LIU, C. 2012. *Natural Gas Hydrates: Experimental Techniques and Their Applications*, Springer.

YUCELEN, B. & KIDNAY, A. J. 1999. Vapor−Liquid Equilibria in the Nitrogen + Carbon Dioxide + Propane System from 240 to 330 K at Pressures to 15 MPa. *Journal of Chemical & Engineering Data,* 44**,** 926-931.

ZHANG, C., FAN, S., LIANG, D. & GUO, K. 2004. Effect of additives on formation of natural gas hydrate. *Fuel,* 83**,** 2115-2121.

ZHANG, J., LEE, S. & LEE, J. W. 2007. Kinetics of methane hydrate formation from SDS solution. *Industrial & Engineering Chemistry Research,* 46**,** 6353-6359.

ZHONG, Y. & ROGERS, R. 2000. Surfactant effects on gas hydrate formation. *Chemical Engineering Science,* 55**,** 4175-4187.

APPENDIX A

VPT EOS AND NDD MIXING RULE

It has been believed that VPT EoS (Valderrama, 1990) and NDD mixing rule (Avlonitis et al., 1994) are the strong tools for modelling the phase equilibria of the systems containing polar compounds such as water (Mohammadi et al., 2005, Javanmardi et al., 2012). Valdrrama in 1990 (Valderrama, 1990) proposed a three parameter EoS as follows:

$$P = \frac{RT}{v-b} - \frac{a}{v^2 + (b+c)v - bc} \qquad \text{A-1}$$

In which, P, T, v and R present pressure, temperature, molar volume and gas universal constant, respectively. In this EoS, the a, b, c constants for pure component are introduced as below:

$$a_i = \frac{\Omega_a R^2 T_c^2}{P_c}\alpha(T_r) \qquad \text{A-2}$$

$$b_i = \frac{\Omega_b R T_c}{P_c} \qquad \text{A-3}$$

$$c_i = \frac{\Omega_c R T_c}{P_c} \qquad \text{A-4}$$

where T_c and P_c are the critical temperature and pressure respectively. The $\alpha(T_r)$ function in Equation A-2 is defined as follows:

$$\alpha(T_r) = \left[1 + F\left(1 - T_r^{\Psi}\right)\right]^2 \qquad \text{A-5}$$

$$\Psi = 0.5 \qquad \text{A-6}$$

The constants, F and Ψ for water are considered 0.72318 and 0.52084 respectively (Avlonitis et al., 1994). The parameters used in equations A-2 to A-5 are defined in the following equations:

$$\Omega_a = 0.66121 - 0.76105 Z_c \qquad \text{A-7}$$

$$\Omega_b = 0.02207 + 0.20868 Z_c \quad \text{A-8}$$

$$\Omega_c = 0.57765 - 1.87080 Z_c \quad \text{A-9}$$

$$F = 0.46286 + 3.58230(\omega Z_c) + 8.19417(\omega Z_c)^2 \quad \text{A-10}$$

where ω and Z_c are the acentric factor and critical compressibility factor, respectively. There are different types of mixing rules in the literatures for applying EoS in mixtures. van der Waals (1873) (Waals, 1873) proposed the first mixing rule named "classical quadratic mixing rule" which is defined as follows:

$$a = \sum_i \sum_j x_i x_j a_{ij} \quad \text{A-11}$$

$$b = \sum_i x_i b_i \quad \text{A-12}$$

where,

$$a_{ij} = \sqrt{a_i a_j}\left(1 - k_{ij}\right) \quad \text{A-13}$$

where k_{ij} is the binary interaction parameter which is used for estimating the attractive energy parameter between the binaries. The classical mixing rule can be extended to incorporate the three parameters EoS, using equations A-11 to A-13 and the following equation:

$$c = \sum_i x_i c_i \quad \text{A-14}$$

It is well established that the accuracy of the classical mixing rules for modelling of the phase equilibria of the systems containing polar components such as water is poor. Avlonitis et al. (Avlonitis et al., 1994) developed the NDD mixing rules which can be applied for modelling of the phase equilibria of systems containing polar components, as follow:

$$a = a^C + a^A \quad \text{A-15}$$

in which a^C is estimated from the classical mixing rule and asymmetric collisions between polar-polar and polar-non-polar molecules can be corrected using parameter a^A as follows:

$$a^A = \sum x_p^2 \sum x_i a_{pi} l_{pi} \quad \text{A-16}$$

$$a_{pi} = \sqrt{a_p a_i} \quad \text{A-17}$$

where, l_{pi} is the binary interaction parameter between polar- polar and polar- nonpolar molecules and introduced as follow:

$$l_{pi} = l_{pi}^{0} - l_{pi}^{1}\left(T - T_0\right) \quad \text{A-18}$$

The values of *b* and *c* in the EoS are defined by the classical mixing rules. The fugacity coefficient for component *i* in the VPT EoS is presented by the following equation:

$$\ln \varphi_i^{EoS} = -\ln\left(Z-B\right) + \frac{B_i' B}{Z-B} + \frac{A}{\sqrt{U^2+4W^2}}\left[A_i' - \frac{U_i' U^2 + 4W_i' W^2}{U^2+4W^2}\right] \times \ln\left[\frac{2Z+U-\sqrt{U^2+4W^2}}{2Z+U+\sqrt{U^2+4W^2}}\right] - A\left[\frac{2\left(2Z+U\right)W_i' W^2 + \left(UZ-2W^2\right)U_i' U}{\left(Z^2+UZ-W^2\right)\left(U^2+4W^2\right)}\right] \quad \text{A-19}$$

where the compressibility factor is defined as below:

$$Z^3 - \left(1+B-U\right)Z^2 + \left(A-BU-U-W^2\right)Z - \left(AB-BW^2-W^2\right) \quad \text{A-20}$$

In Equations A-19 and A-20, the *A*, *B*, *U*, and *W* parameters are defined as follows:

$$A = \frac{Pa}{(RT)^2} \quad \text{A-21}$$

$$B = \frac{Pb}{RT} \quad \text{A-22}$$

$$U = \frac{Pu}{RT} \quad \text{A-23}$$

$$W = \frac{Pw}{RT} \quad \text{A-24}$$

where *a* and *b* are the parameters for the classical mixing rule and *u* and *w* in the equations A-23 and A-24 are defined as follows:

$$u = b + c \quad \text{A-25}$$

$$w = \sqrt{bc} \quad \text{A-26}$$

The other parameters in Equation A-19 are defined in the following equations:

$$A_i' = \frac{1}{na}\left[\frac{\partial n^2 a}{\partial n_i}\right]_{T,n_j} \quad \text{A-27}$$

$$B_i' = \frac{1}{nb}\left[\frac{\partial nb}{\partial n_i}\right]_{T,n_j} \quad \text{A-28}$$

$$U_i' = \frac{1}{nu}\left[\frac{\partial nu}{\partial n_i}\right]_{T,n_j} \quad \text{A-29}$$

$$W_i' = \frac{1}{nw}\left[\frac{\partial nw}{\partial n_i}\right]_{T,n_j} \quad \text{A-30}$$

The fugacity of the compound in the liquid and vapour phases are determined using the VPT EoS and NDD mixing rule

Using the VPT EoS (Valderrama, 1990) and the NDD mixing rule (Avlonitis et al., 1994), the fugacity of the liquid and vapour phases are calculated as follows:

$$f_i = x_i \phi_i P \quad \text{A-31}$$

where, x_i is the molecular composition in the liquid or vapour phases.

APPENDIX B

FUGACITY OF WATER IN THE HYDRATE PHASE

In the fugacity approach, the fugacity of water in the hydrate phase, f_w^H, is defined as follows (Klauda and Sandler, 2000):

$$f_w^H = f_w^\beta \exp\left(\frac{-\Delta\mu_w^{\beta-H}}{RT}\right) \qquad \text{B-1}$$

where, $\Delta\mu_w^{\beta-H}$ is the chemical potential difference between the empty hydrate lattice and the hydrate phase which is determined using the following equation:

$$\Delta\mu_w^{\beta-H} = RT\sum_{m=1}^{NC}\bar{\nu}_m \ln\left(1+\sum_{i=1}^{nc}C_{mi}f_i\right) \qquad \text{B-2}$$

where R and T show the universal gas constant and temperature respectively. The superscripts NC and nc in Equation B-2 symbolize the number of cavity and the number of component respectively. Other symbols in Equation B-2 are explained as follows:

$\bar{\nu}_m$: The number of cavities of type m per water molecule in a unit cell of hydrate crystal lattice.

C_{mi}: Langmuir constant of the guest molecule i in the m cavity.

f_i: Fugacity of the i^{th} guest molecule in the gas phase which is obtained using an appropriate equation of state (EoS).

The Lenard-Jones Devonshire theory is used to calculate the Langmuir constant (C_{mi}) in Equation B-2 as follow (van der Waals and Platteeuw, 1959, Klauda and Sandler, 2000):

$$C_{mi} = \frac{4\pi}{kT}\int_0^{r/2}\exp\left[-\frac{\omega(r)}{kT}\right]r^2\,dr \qquad \text{B-3}$$

where k and T represent the Boltzmann's constant and temperature, respectively. *w(r)* shows spherically symmetric cell potential function to define the interaction between the water and hydrate former, and finally r is labelled as the distance between the cavity centre and molecule. As it can be seen in Equation B-3, the Langmuir constant is only a function of temperature. To estimate the cell potential function, *w (r),* the Kihara potential energy function (1953) can be used as follow (Kihara, 1953):

$$\Gamma(r)=4\varepsilon\left[\left(\frac{\sigma}{r-2a}\right)^{12}-\left(\frac{\sigma}{r-2a}\right)^{6}\right] \qquad \text{B-4}$$

where, σ represents the collision diameter, and a and ε show the hard core radius and the depth of energy well, respectively. Equation B-4 represents the interaction energy between a guest molecule and one water molecule. If the interaction between the guest molecule and all the water molecules in a unit cell is assumed, *w (r)* is defined as follow:

$$w(r)=2z\varepsilon\left[\frac{(\sigma^{*})^{12}}{\overline{R}^{11}r}\left(\delta^{10}+\frac{\alpha}{\overline{R}}\delta^{11}\right)-\frac{(\sigma^{*})^{6}}{\overline{R}r}\left(\delta^{4}+\frac{\alpha}{\overline{R}}\delta^{5}\right)\right] \qquad \text{B-5}$$

in which, Z indicates the coordination number for each cavity (the number of oxygen molecules around the cavity) and $\overline{R}$ is the average radius of the cavity. In addition, $\sigma^{*}=\sigma-2\alpha$, and the δ^{N} values are obtained from the following equation:

$$\delta^{N}=\frac{1}{N}\left[\left(1-\frac{r}{\overline{R}}-\frac{a}{\overline{R}}\right)^{-N}-\left(1+\frac{r}{\overline{R}}-\frac{a}{\overline{R}}\right)^{-N}\right] \qquad \text{B-6}$$

where N is an integer equal to 4, 5, 10 or 11 (Sloan and Koh, 2008). Parrish and Prausnitz (1972), for simplicity in the calculations, provided an empirical correlation estimating the Langmuir constant of the hydrate formers as below: (Parrish and Prausnitz, 1972)

$$C_{ij}=\frac{A_{ij}}{T}\exp\left[\frac{B_{ij}}{T}\right] \qquad \text{B-7}$$

The values for A_{ij} and B_{ij} for different hydrate formers have been reported in the open literature (Sloan and Koh, 2008, Parrish and Prausnitz, 1972).

In addition in Equation B-1, f_{w}^{β} is used to the fugacity of water in the empty hydrate lattice which is determined using the following equation (van der Waals and Platteeuw, 1959):

$$f_w^{\beta} = f_w^{l^o} \exp(\frac{-\Delta\mu_w^{\beta-l/\alpha}}{RT}) \quad \text{B-8}$$

in which, $f_w^{l^o}$ represents the fugacity of pure water in the liquid or ice phase. The following equation is used to calculate the chemical potential difference between empty hydrate lattice and liquid or ice phase , $\Delta\mu_w^{\beta-l/\alpha}$, as below:

$$\frac{\Delta\mu_w^{\beta-l/\alpha}}{RT} = \frac{\Delta\mu_w^0}{RT} - \int_{T_0}^{T} \frac{\Delta h_w^{\beta-l/\alpha}}{RT} dT + \int_{P_0}^{P} \frac{\Delta v_w^{\beta-l/\alpha}}{RT} dP \quad \text{B-9}$$

where:

T_0: the freezing point of water (273.15 K).

$\Delta\mu_w^0$: The difference in the chemical potential of water in the empty hydrate lattice and the liquid phase at the temperature of 273.15 K.

$\Delta h_w^{\beta-l/\alpha}$: The molecular enthalpy difference between the empty hydrate lattice and liquid water or ice.

$\Delta v_w^{\beta-l/\alpha}$: The molecular volume difference between the empty hydrate lattice liquid water or ice.

$\Delta h_w^{\beta-l/\alpha}$ in Equation B-9 is obtained from the following equation:

$$\Delta h_w^{\beta-l/\alpha} = \Delta h_w^0 + \int_{T_0}^{T} \Delta C_{pw} dT \quad \text{B-10}$$

where Δh_w^0 shows the enthalpy difference between the empty hydrate lattice and liquid water.

For temperatures below the freezing point of water, the specific heat capacity difference is assumed to be zero. Table B-1 represents the phase transition parameters, Δh_w^0, $\Delta\mu_w^0$ and $\Delta v_w^{\beta-L}$, for the different hydrate structures of sI, sII and sH (Sloan and Koh, 2008).

Table B-1. Phase transition parameters for different hydrate structures. (Sloan and Koh, 2008)

Hydrate structure	sI	sII	sH
$\Delta\mu_w^0(J/mol)$	1263	937	1187.33
$\Delta h_w^0(J/mol)$	1389*	10.25*	846.57
$\Delta v_w^0(cm^3/mol)$	3**	3.4**	3.85

*When liquid water is present, subtract 6009.5 J/mol from Δh_w^0.

**When liquid water is present, subtract 1.601 cm^3/mol from Δv_w^0.

APPENDIX C

FUGACITY OF WATER IN THE EMPTY HYDRATE LATTICE

The following equation is used for the calculation of the fugacity of water in the empty hydrate lattice, f_w^{β} : (Sloan and Koh, 2008, Mohammadi and Richon, 2008b, Mohammadi and Richon, 2009, Eslamimanesh et al., 2012a)

$$f_w^{\beta} = P_w^{sat,MT}\varphi_w^{sat,MT}\exp\int_{P_w^{MT}}^{P}\frac{v_w^{MT}dP}{RT} \qquad \text{C-1}$$

where, $P_w^{sat,MT}, \varphi_w^{sat,MT}$ and v_w^{MT} are the vapour pressure, fugacity coefficient, and molar volume of water in the empty hydrate lattice respectively. The fugacity coefficient of water in the empty hydrate lattice ($\varphi_w^{sat,MT}$) in Equation C-1 is assumed to be unity because of the low vapour pressure of water. In addition, v_w^{MT} is considered to be independent of the pressure. The above equation is therefore simplified to the following equation (Eslamimanesh et al., 2012a, Sloan and Koh, 2008, Mohammadi and Richon, 2008b, Mohammadi and Richon, 2009)**:**

$$f_w^{\beta} = P_w^{sat,MT}\exp\left(\frac{v_w^{MT}\left(P-P_w^{sat,MT}\right)}{RT}\right) \qquad \text{C-2}$$

Klauda and Sandler (Klauda and Sandler, 2000) and Dharmawardhana et al. (Dharmawardhana et al., 1980) proposed the following equation for computing the molar volume (v_w^{MT}) and vapour pressure of water ($P_w^{sat,MT}$) in the hypothetic empty hydrate lattice for structure I, respectively (Eslamimanesh et al., 2011c, Mohammadi and Richon, 2008b, Mohammadi and Richon, 2009, Eslamimanesh et al., 2012a):

$$v_w^{MT}\left(m^3/mol\right)=\left(11.835+2.217\times10^{-5}T+2.242\times10^{-6}T^2\right)^3\frac{10^{-30}N_A}{46}-8.006\times10^{-9}P+ \quad \text{C-3}$$

$5.448\times10^{-12}P$ [T in K, P in MPa]

$$P_w^{MT}\left(MPa\right)=0.1\exp\left(17.440-\frac{6003.9}{T}\right) \quad \text{C-4}$$

N_A in Equation C-3 is Avogadro's number.

APPENDIX D

KINETICS MODEL FOR THE SEMICLATHRATE HYDRATES

Englezos et al. (Englezos et al., 1987) developed the first kinetic model for the growth of methane and ethane hydrates, based on the differences between the fugacity of the guest molecule in the vapor and hydrate phase. Tajima et al. (Tajima et al., 2010) used the model proposed by Daimaru et al. (Daimaru et al., 2007) and Kuji et al. (Kuji et al., 2006) which was based on the chemical potential difference in the vapor and hydrate phase as a driving force to study the hydrate formation kinetics of HFC-134a. The kinetic model applied in this study was based on the Tajima et al.'s work (Tajima et al., 2010) as the following equation(Gholinezhad et al., 2011):

$$r_f = \left(-\frac{dn}{dt}\right) = aK^*\left(\mu_g - \mu_{eq}\right) \qquad \text{D-1}$$

where, r_f is the rate of hydrate formation, n and t show the number of gas molecule and time, respectively. In addition, in Equation D-1, a indicates the interfacial area, K^* is the overall kinetic constant and μ_g and μ_{eq} show the chemical potentials of the guest molecules in the vapor and hydrate phases, respectively. The following equation is used to estimate the overall kinetics constant, K^* (Tajima et al., 2010, Gholinezhad et al., 2011):

$$\frac{1}{K^*} = \frac{1}{k_L} + \frac{1}{k_f} \qquad \text{D-2}$$

where, k_L and k_f are the mass transfer coefficient and the hydrate crystal growth constant, respectively. Mass transfer constant, k_L, is an increasing function of the stirring rate, while the crystal growth constant, k_f, is independent of the stirring rate. Consequently, the amount of $1/k_f$ is much bigger than $1/k_L$ and then the contribution the term of $1/k_l$ can be eliminate from the overall kinetic constant as follow (Tajima et al., 2010, Gholinezhad et al., 2011):

$$K^* = k_f \qquad \text{D-3}$$

With replacing $\mu = RT\ln(f)$ in Equation D-1 and also using Equation D-3, the hydrate formation rate can be rewritten as follow (Tajima et al., 2010, Gholinezhad et al., 2011):

$$r_f = ak_f RT \ln\left(\frac{f_g}{f_{eq}}\right) \quad \text{D-4}$$

where f_g and f_{eq} show the fugacity of the gas molecules in the gas and the hydrate phases, respectively. In addition R and T are the universal gas constant and temperature, respectively. The number of gas consumed during the hydrate formation is calculated according to the real gas law as follow (Tajima et al., 2010, Gholinezhad et al., 2011, Babaee et al., 2015):

$$\Delta n_g = \frac{P_0 V_0}{Z_0 RT_0} - \frac{P_t V_t}{Z_t RT_t} \quad \text{D-5}$$

where P, V and Z indicate the pressure, volume and compressibility factor of the gas molecule. Subscripts "0" and "t" in Equation D-5 shows conditions of equilibrium cell at time=0 and time=t, respectively (Babaee et al., 2015). In this study it was assumed that the phase volume change is negligible and then the volume of the gas phase remains constant during the hydrate formation (Gholinezhad et al., 2011). The compressibility factor and fugacity of gas during the hydrate formation is calculated using the Valderrama, Patel-Teja equation of state (VPT EoS) (Valderrama, 1990)